JUNE 1960

VOLUME 7 (1960) No. 3

GREGG M. SINCLAIR LIBRARY
UNIVERSITY OF HAWAII
8-7-63

NUCLEAR INSTRUMENTS & METHODS

A JOURNAL ON ACCELERATORS, INSTRUMENTATION AND TECHNIQUES IN NUCLEAR PHYSICS

EDITOR: K. SIEGBAHN - UPPSALA

LAST NUMBER OF THIS VOLUME

CONTENTS

G. A. DORAN, E. A. FINLAY, H. R. SHAYLOR and M. M. WINN, Extraction of protons from the Birmingham 1000-MeV synchrotron 225
W. LOTZ und A. SITTKUS, Elektronische Geräte hoher Konstanz für die Registrierung der Nukleonenkomponente der kosmischen Strahlung 237
T. K. FOWLER and W. M. GOOD, A theory on obtaining short bursts of ions from a beam of ions 245
W. E. FRAHN, W. L. RAUTENBACH and L. WÅHLIN, The electromagnetic isotope separator in Pretoria 253
L. WÅHLIN, Improvements of the collector system for a laboratory isotope separator. . . . 269
BO SJÖRGEN, Cyclotron instrumentation for nuclear reaction studies by magnetic analysis 274
E. P. GRIGORYEV and A. V. ZOLOTAVIN, The spectral sensibility of a magnetic gamma-spectrometer in a photoelectric method 289
E. H. BELLAMY, W. R. HOGG and D. MILLER, A thin liquid hydrogen or deuterium target . . . 293

(contined on p. 3 of cover)

NORTH-HOLLAND PUBLISHING COMPANY - AMSTERDAM

NUCLEAR INSTRUMENTS AND METHODS

A journal on accelerators, instrumentation and techniques in nuclear physics

EDITOR: K. SIEGBAHN, UPPSALA

EDITORIAL BOARD:

J. B. ADAMS (CERN)
F. A. ALSINA (Buenos Aires)
E. AMALDI (Rome)
H. L. ANDERSON (Chicago)
K. T. BAINBRIDGE (Cambridge, Mass.)
P. R. BELL (Oak Ridge)
R. E. BELL (Montreal)
A. BERTHELOT (Saclay)
H. BRINKMAN (Groningen)
E. H. COOKE–YARBOROUGH (Harwell)
S. DE BENEDETTI (Pittsburgh)
M. DE HEMPTINNE (Louvain)
A. DE-SHALIT (Rehovoth)
M. DEUTSCH (Cambridge, Mass.)
S. DU TOIT (Pretoria)
B. S. DŽELEPOV (Leningrad)
W. GENTNER (Heidelberg)
P. C. GUGELOT (Amsterdam)
H. HALBAN (Paris)
O. HAXEL (Heidelberg)
P. HUBER (Basel)
S. KIKUCHI (Tokyo)
J. KOCH (Copenhagen)
M. S. KOZODAEV (Moscow)
S. LIVINGSTON (Cambridge, Mass.)
E. M. MCMILLAN (Berkeley)
M. G. MEŠČERJAKOV (Moscow)
P. B. MOON (Birmingham)
M. L. OLIPHANT (Canberra)
W. PAUL (Bonn)
A. S. RAO (Bombay)
G. SALVANI (Rome)
P. SAVIĆ (Belgrade)
P. SCHERRER (Zürich)
CH. SCHMELZER (CERN)
R. TANGEN (Oslo)
D. TAYLOR (Northampton)
V. I. VEKSLER (Moscow)
G. VON DARDEL (CERN)
O. WERNHOLM (Stockholm)
R. R. WILSON (Cornell)
S. D. WINTER (Saclay)

INSTRUCTIONS FOR CONTRIBUTORS

Contributions may be sent to the Editor, Professor K. Siegbahn, Institute of Physics, University of Uppsala, Sweden, either directly or through the intermediation of one of the members of the Editorial Board. Contributions may be written in English, French or German but should always, except for very short papers, be supplied with a brief abstract in English. Figures should be in inked original drawings or glossy prints and they should be sufficiently large. Contributors should make sure that important details in drawings and photographs will show up clearly in the diminished copy used by the publisher.

Books for review should be sent to Professor Siegbahn.

Objective and descriptive material on endeavours and product developments from the industry for the section "Spotlight on Industry" should be sent directly to the publishers, North-Holland Publishing Company, P.O. Box 103, Amsterdam.

Nuclear Instruments and Methods is published monthly. The subscription price of a volume of 360 pages is $ 17.00 (130 s), postage free.

Subscriptions should be sent to the publishers, North-Holland Publishing Company, P.O. Box 103, Amsterdam or to any subscription-agent.

No part of this issue may be reproduced in any form, by print, photoprint, microfilm or any other means without written permission from the publisher.

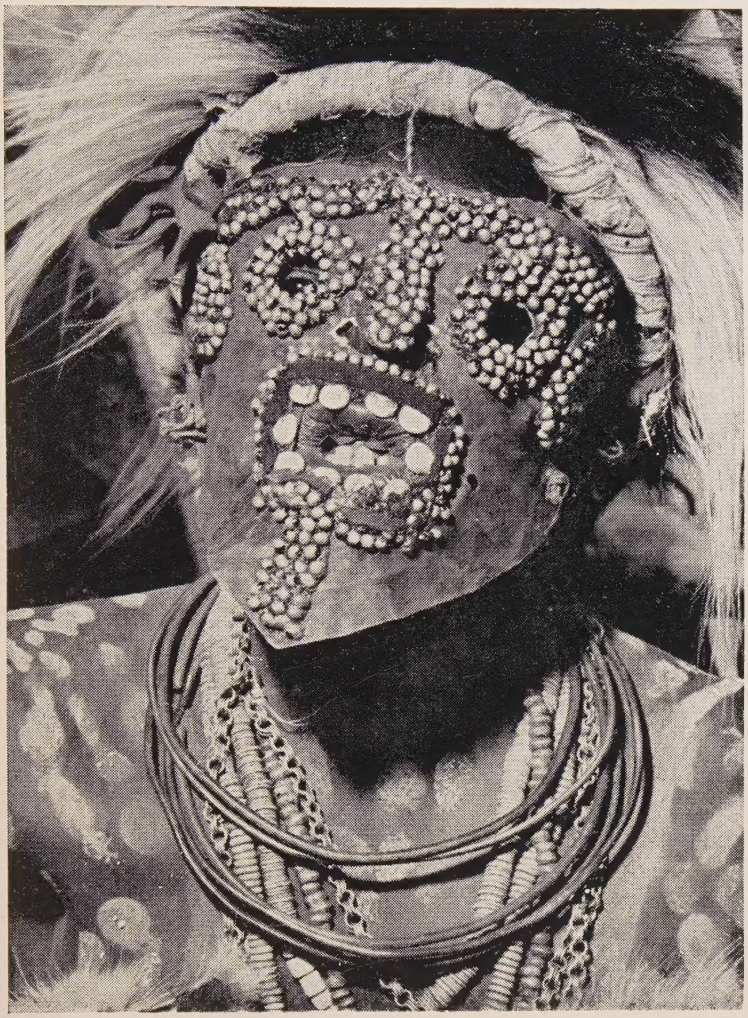

PHILIPS

NRO

Even against the seemingly mysterious threats to human life which radioactivity can entail, health physics does not make use of the magic invariably resorted to by the witch doctor.

For the detection and measurement of radioactive radiation a great variety of methodically developed equipment is available to provide an effective health protection service.

The increasing application of radioactive sources in industrial processes and the growing number of nuclear reactors which are coming into use, call for constantly intensified care on the part of Health Physics Officers in their efforts to protect the growing numbers of people coming daily into close contact with ionizing radiation.

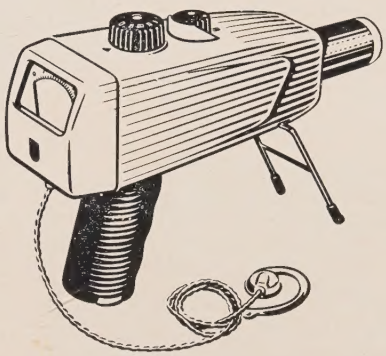

modern witchcraft

Philips produce indispensable aids in a range extending from small monitors and dosimeters for the protection of individual workers to permanent monitoring, multi-channel installations for the coverage of buildings and surroundings of reactors, nuclear research laboratories or "hot labs".

N.V. PHILIPS' GLOEILAMPENFABRIEKEN - EINDHOVEN - HOLLAND

PHILIPS
nuclear equipment

Particle accelerators ● Reactor control instrumentation ● Health protection and monitoring equipment ● Radiation measuring and detection equipment ● Geiger counter tubes ● Photomultipliers ● Radio-active isotopes ● Vacuum measuring equipment ● Air and gas liquefiers.

Eldorado

DECIMAL SCALERS
FOR THE NUCLEAR PHYSICIST

100% SOLID STATE

...and Fast

Eldorado solid state all-electronic scalers count random events at a maximum rate of over one million counts per second. Resolving time is less than 1.0 microsecond. Especially well-suited for accelerator counting room service, these compact instruments weigh just 13 pounds and use ⅓ fewer transistors than comparable models. They can be used wherever the advantages of complete transistorization are important.

Eldorado offers three standard models in the SC-750 series, each with built-in regulated power supply. Two models provide full electronic storage of 10^7 and 10^8 counts. The third has 3 decades of electronic storage and a 4-digit mechanical register. Special versions can be furnished with other counting combinations and provisions for readout to a printer or tape punch.

KEY SPECIFICATIONS

SCALER	
Resolution	Better than 1.0 microsecond
Max. Counting Rate	Greater than 1 megacycle
AMPLIFIER (optional)	
Minimum Input Signal	10 millivolts
Overload Recovery	100 X, 7 microsecond
DISCRIMINATOR TYPE	Integral
RANGE	1 to 11 volts
SIZE	19 x 3¼ x 10½ inches

Eldorado can furnish scalers and counters to fit your specific application. For more details, please address Dept. 79

Eldorado Electronics

2821 Tenth Street

Berkeley 10, California

PRACTICAL ACCURACY

The portable CN-110 256-channel pulse analysis system — can be changed from pulse height analysis to time-of-flight to pulsed neutron measurement — or to some special program — simply by interchanging the compact plug-in logic units in the front panel. The basic computer with plug-in weighs only 30 lbs., and can be bench or rack-mounted or carried anywhere in a portable case for laboratory or field work. Power consumption is only 25 watts — needs no auxiliary cooling . . . can be set up for analog, digital or binary readout of various methods.

. . . new portability in TMC instruments

These new instruments from TMC, with completely transistorized circuits and efficient, straightforward design, are the most practical answer to the need for portable yet accurate pulse measurement instruments. Whether in a laboratory or in the field, the extreme reliability, accuracy and compactness of these instruments combine to provide convenient, dependable operation wherever they are set up.

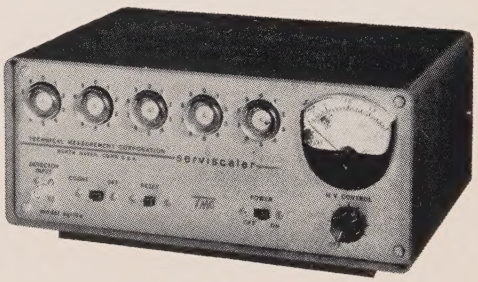

The SG-10A Serviscaler is an extremely economical and portable instrument designed for training or general laboratory use. All-transistor circuits are housed in a 12 lb., 12¾" x 9" x 5⅞" package. Continuous high voltage, adjustable from 600 to 1600 volts; resolving time better than 200 μsec; power consumption of only 20 watts. Price is $350.

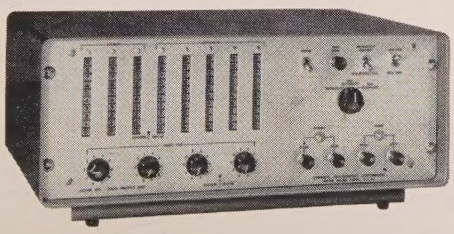

The No. 220 Data Handling Unit — a logical companion to the CN-110, is both a timer and data-handling unit. During the CN-110's accumulation cycle the 220 can be used for true or live timing, then instantly switched to a manual, semi-, or fully-automatic digital readout cycle (destructive or non-destructive). The compact 220 may be used with various paper tape punching and printing machines.

TMC also manufactures a complete line of single instruments, systems and related equipment for radiation measurement. Complete details are available on request.

TMC

TECHNICAL MEASUREMENT CORPORATION

441 WASHINGTON AVENUE, NORTH HAVEN, CONNECTICUT

This NMC Gamma Spectrometer Eliminates "Dark Current" Defect

Combines Better Resolution. With Greater Precision Over Wider Range Than Any Other System At Any Price.

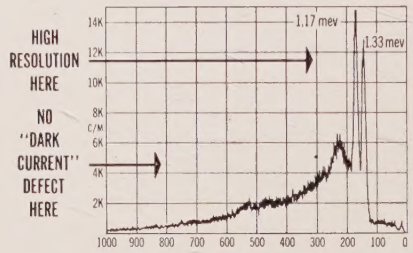

Actual spectrogram of Cobalt-60 made with a GSS-1. Window No. 3 Time constant: 2 sec.

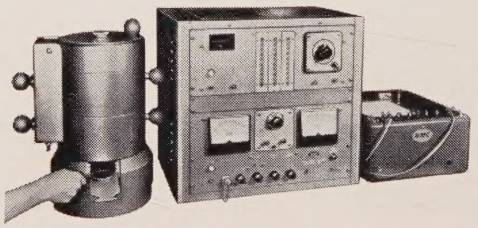

A complete gamma spectrometer system NMC model GSS-1

This greatly simplified system features regulated high voltage supply as part of the counting ratemeter auto-scan system... all-transistorized probe amplifier and spectrometer circuits... and solid or well-type crystal. These points and the actual spectograms shown here tell only part of the story. For full details, write.

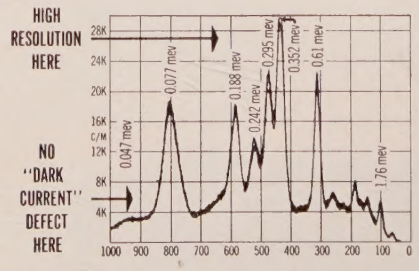

Actual spectrogram of Radium made with a GSS-1. Four runs over a period of 20 hours with no adjustment of instrument between runs, demonstrating utmost stability. Range: 30.000 C/M. Time constant: 3 sec.

NMC

NUCLEAR MEASUREMENTS CORP.

International Office: 13 E. 40th Street,
New York 16, N.Y.

NEW EH 130 PULSE GENERATOR

DOES ALMOST EVERY PULSER JOB BETTER!

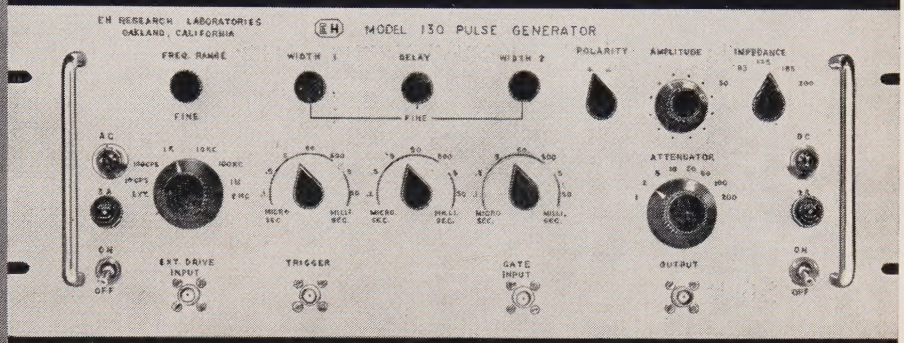

EH Model 130, f.o.b. Oakland, California, $1175

SPECIFICATIONS

REPETITION RATE
10 cps to 2 Mc

RISE AND FALL TIME
Less than 10 millimicroseconds

RELATIVE PULSE DELAY
200 millimicroseconds to 50 milliseconds

JITTER (Pulse widths, relative delay, rep rate)
0.1 percent

TRIGGER OUTPUT
Positive 25 volt pulse

EXTERNAL DRIVE
3 volts rms required (0.1 volt or 2 mμsec equivalent jitter referenced to Pulse Output)

ELECTRONIC GATE
10 volts required

OUTPUTS
Two Pulses at one output connector, independently variable in width and relative delay

PULSE WIDTHS
100 millimicroseconds to 50 milliseconds

PULSE AMPLITUDE
0 to 50 volts maximum
0 to 500 ma maximum

POLARITY
Positive or Negative Pulses available

DUTY FACTOR
50 percent

OUTPUT IMPEDANCE
50, 93, 125, 185 or 200 ohms available (selected by front panel switch)

OUTPUT ATTENUATOR
1:1 to 200:1 coarse selector, 3 to 1 vernier control

Here at last is a pulse generator which can shoulder a broad range of applications . . . a flexible, reliable pulser whose fast rise and low jitter features make it the most advanced instrument of its kind. With its provisions for external drive and electronic gating, its enormous range in pulse widths and delays, and the arbitrary cable impedance feature, you'll find the E-H 130 indispensable for almost any pulser job. Call, write or wire E-H for more information today.

E-H RESEARCH LABORATORIES, INC.
163 ADELINE STREET • TEMPLEBAR 4-3030 • OAKLAND 20, CALIFORNIA

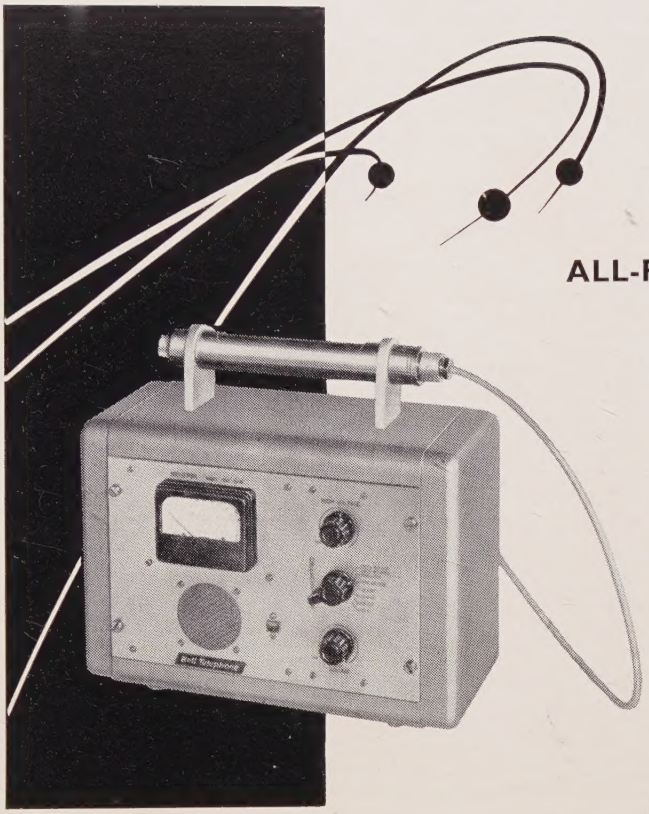

ALL-ROUND, LOW PRICED MONITOR

Typically developed as a laboratory equipment the monitor 111-A1 combines quality and high performance with low cost.

- Completely transistorized
- Designed as portable type
- Very low count rate: 0 to 5 c.p.s. full scale
- Highest count rate: 0 to 5000 c.p.s. full scale
- Equalizing accumulators
- Automatically recharged from A.C. mains
- Priced $ 410 F.O.B. Antwerp

For further information on this and other applications in the field of "Electronics for Nucleonics" ask :

AN ITT ASSOCIATE

Bell Telephone Mfg Co

"NUCLEAR ENERGY DIVISION"
33, Berkenrodelei
HOBOKEN-Antwerp
Belgium

NON-OVERLOADING

LINEAR PULSE AMPLIFIER NE 5202 of the Fairstein type.

Designed for scintillation spectrometry and pulse height analysis studies, this new wide band amplifier features high gain, high gain stability, good linearity, low noise, excellent non-overloading characteristics, and operation at high duty cycles. Based on a double delay line differentiated system, it consists of three high gain feedback groups and a white cathode follower output. Premium tubes and the highest workmanship are used throughout.

Check these data;

Overload performance: Fastest recovery of any available amplifier (5 microseconds for 100 times overload).
Maximum Voltage Gain: 50,000.

Gain Control Range: 1,200: 1 with coarse & fine controls.

Gain Drift: Better than 0.25% per week with stabilised supply

Gain Stability: Better than 1% for 10% change in mains voltage.

Input noise rms:	40 microvolts
Output voltage:	± 100 volts
Output rise time:	0.2 microseconds
Output pulse width:	1.2 microseconds
Integral linearity:	0.15%
Output impedence:	17 ohms

Also available, the following companion units:

Pre-amplifier and cathode follower NE 5202A; Single-channel pulse height selector NE 5102; Highly stabilised EHT supply NE 5302; Scanning Scintillation spectrometer NE 8601; Ratemeter NE 5401; Complete assembly for C14 and H3 counting.

Write for Bulletins and New Illustrated Price List

Nuclear Enterprises (G.B.) Ltd.

BANKHEAD MEDWAY, SIGHTHILL, EDINBURGH, 11, SCOTLAND - TEL.: CRA 5262

Associate Company: Nuclear Enterprises Ltd., 1750 Pembina Highway, Winnipeg, Canada.

One of a series of discussions on topics of particular interest to those employing radioisotopes and tracer techniques.

LIQUID SCINTILLATION COUNTERS

If you plan to buy a Liquid Scintillation Counting System, the *only* important criteria are:

1. The counting efficiency and background;
2. The number of samples to be counted;
3. The cost of the system and,
4. The reputation and experience of the manufacturer

As you know, the first commercial Liquid Scintillation Counting System was produced at Tracerlab back in 1954, and we believe that our newest system, the LSC-10, is the most economical and practical ever designed.

The Tracerlab system consists of a console for the scaler and associated circuitry, and a freezer containing the sample changer and detectors. The unique detection system is a coincidence type with two photomultiplier tubes mounted at right angles to each other. The freezer, an 11 cubic foot unit, is only 38″ wide, and has a capacity of forty-20 ml. samples with an in-freezer storage rack for 40 more. Yet it is compact enough to be practical even for crowded laboratories. Phototubes are fully protected against accidental light exposure by means of a freezer mounted interlock.

Here's another point to consider: In the LSC-10 system, you don't have to open the freezer to transfer samples. External controls are provided—samples remain dark adapted—you get uniform counting conditions. Incidentally, the LSC-10 can be readily converted, *in your laboratory* to fully automatic operation (by means of standard accessories) if and when your volume of work requires it.

Experts agree that both low temperature and coincidence circuitry are an absolute necessity for low background and stable operation when counting tritium or low concentrations of carbon-14. Tritium compounds are among the most difficult to assay, particularly when in aqueous solutions. A look at the final test records made on five typical units, in series shows the following efficiencies and backgrounds for counting aqueous tritium.

And, remember, these units can perform even better when installed in your laboratory with settings optimized for your counting requirements.

Unit	Efficiency and Background
A	9.0% at 95 cpm
B	6.2% at 70 cpm
C	7.6% at 73 cpm
D	6.2% at 83 cpm
E	5.3% at 64 cpm

Naturally, much higher efficiencies are obtained when counting non-aqueous tritium or carbon-14 compounds. Greater than 75% efficiency can be expected when counting C-14 samples and greater than 25% efficiency when counting tritium compounds in hydrocarbon solution.

Further facts about the LSC-10.

THE COST? The lowest for any fine system.

DELIVERY? Currently less than 30 days.

INSTALLATION? Usually completed in a matter of hours.

SERVICE? It's world-wide, with more than 100 qualified representatives.

INTERESTED? *Write for a quotation and full details.*

Tracerlab first in radiation measurement

TRACERLAB, INC., 1610 Trapelo Rd., Waltham 59, Massachusetts · 2030 Wright Ave., Richmond, California

NORTH-HOLLAND BOOKS

Paul Ehrenfest

COLLECTED SCIENTIFIC PAPERS

XII + 632 pages

Guilders 45,00 (90s.)

This volume makes widely scattered publications readily available. All Dutch articles appear here in English; the German publications are in the original language.

Sole Agency for U.S.A.:

Interscience Publishers Inc. — New York

NORTH-HOLLAND PUBLISHING COMPANY - AMSTERDAM

MODEL 412 MERCURY RELAY

PRECISION SLIDING PULSER

for Precise Calibration of Single & Multi-Channel Pulse Height Analyzers

Determines Window Widths Using Principle of *Constant Angular Velocity*

AUTOMATICALLY
10 × more accurately
40 × faster than conventional pulsers

Incorporates Both Manual Control and Precision Motor Drive

Simulates Pulses from Scintillation, Proportional or Geiger Counters

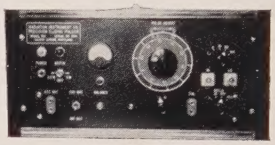

MERCURY PULSER, Model 401

Featuring Versatility and Precision

Specifically designed for the Nuclear Physics Laboratory

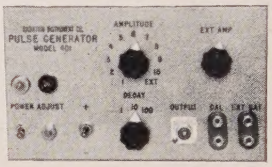

Fast rise and exponential decay simulates scintillation, proportional or geiger counter pulses for test and calibration of amplifiers, pulse height analyzers, scalers, etc.

MODEL 412 . . . $ 450.00 — MODEL 401 . . . $ 125.00

RADIATION INSTRUMENT CO.

P. O. BOX 733, SILVER SPRING, MARYLAND, U.S.A.

NORTH-HOLLAND BOOKS

Analytical and Canonical Formalism in Physics

by

ANDRÉ MERCIER

Head of the Department of Theoretical Physics, University of Berne

6 × 9″ VIII + 222 pages Guilders 20.00 (40 s.)

THE CONTENTS

i LAGRANGIAN FORMALISM
ii LAGRANGIAN DENSITY
iii CANONICAL FORMALISM
iv CANONICAL FORM OF ELECTRODYNAMICS
v HAMILTONIAN DENSITIES
vi TRANSFORMATIONS
vii CANONICAL FORMALISM WITH VANISHING JACOBIAN DETERMINANT

Sole Agency for U.S.A.: Interscience Publishers Inc. – New York

NORTH-HOLLAND PUBLISHING COMPANY — AMSTERDAM

STANDARD FUNCTIONNAL UNITS . . .

FRENCH ATOMIC ENERGY COMMISSION SYSTEM

. . . master-key to nuclear instrumentation

Standard functional units are assembled in cabinets in order to be used as complete assemblies : scales for counting, amplitude selectors, ratemeters, etc...

REGISTER UNIT TYPE TND.1
Function :
counting (registering)
Dekatron divider

IMER UNIT (SLOW RESPONSE)
YPE TAL.2
ntended
or
utomatic
re-set
ounting

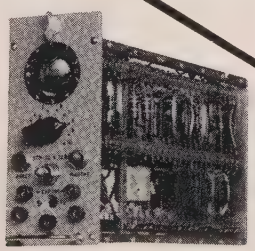

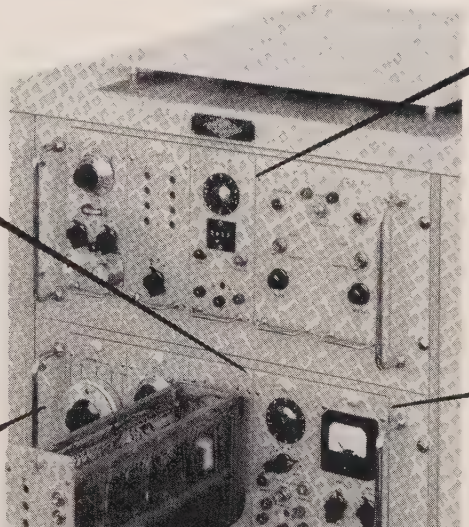

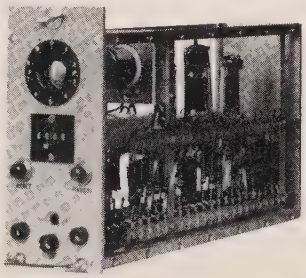

VERY HIGH TENSION UNIT

ATEMETER TYPE TIS.1
pplies a tension
r a current
roportionnal
o the number
f counts
eceived

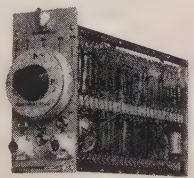

TYPE THT.4

Supplies a very high stabilised tension for detectors, pre-amplifiers

L'ÉLECTRONIQUE APPLIQUÉE

96/100, rue Maurice Arnoux • MONTROUGE • ALE 45-20, 83-20
25, rue du Docteur Finlay • PARIS 15e • TÉL. SÉGUR 14-75

INTERNATIONAL

advertise

YOUR NUCLEAR PRODUCTS IN

sell

YOUR NUCLEAR PRODUCTS

reap

YOUR NUCLEAR SALES REWARDS

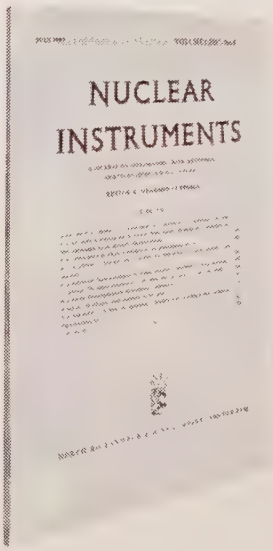

world wide

KEY NUCLEAR MANAGEMENT
NUCLEAR SCIENTISTS
NUCLEAR ENGINEERS
NUCLEAR PRODUCTION PERSONNEL

SUBSCRIBE TO

you reach

THE WHOLE NUCLEAR SALES WORLD IN

Entirely international in scope Nuclear Instruments and Methods is the one nuclear scientific journal that has an established subscription clientele throughout the whole world-where-ever nuclear men are at work—they want your nuclear products—they need your nuclear products—advertise in Nuclear Instruments and tell them WHAT – HOW – WHERE they can get your nuclear products

GO INTERNATIONAL WITH YOUR SALES PROGRAM TODAY WRITE

WILLIAM F. BAARS - ADVERTISING MANAGER NORTH-HOLLAND PUBLISHING COMPANY

P.O. BOX 103 – AMSTERDAM, HOLLAND

INTERNATIONAL

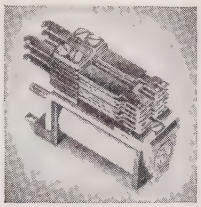

customer evidence...

8

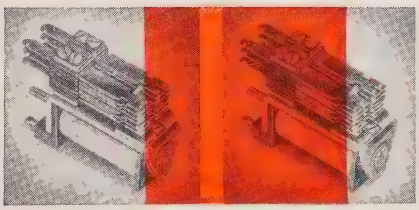

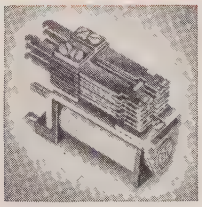

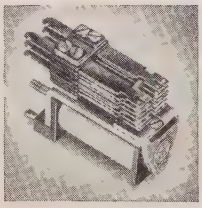

operations

Modestly we claim that under suitable conditions this new miniature will give service in excess of 10 million operations but 100 millions leaves us breathless and not a little proud. Capable of handling springset arrangements of up to 12 springs normal duty loading and switching at speeds of better than 10 m.s. when required, the G.P.S.T. is a natural for computers and similar applications.

See us on Stand D.153 at the I.E.A. Exhibition, Grand Hall, Olympia, London, from May 23rd — May 28th.

ETELCO

For more details please write to the
TECHNICAL SERVICES DEPT.
ELECTROMECHANICAL DIVISION
BEESTON · NOTTINGHAM

TELCO LIMITED · HEAD OFFICE · 22 LINCOLN'S INN FIELDS LONDON W.C.2

The place of the Particle Accelerator in Basic Research...

Accelerators at the Research Frontier — XII

The needs of science for charged particles in the nuclear binding-energy range continue to create a dynamic and demanding interest in Van de Graaff and microwave linear accelerators. In the last of this series, typical requirements will be considered regarding higher energy, greater intensity, and more exacting specifications of stability and pulsing. The uses for such advanced accelerator techniques are not clearly known. It is felt that a consideration of attainable performance from accelerators may stimulate action on research programs now lying dormant because of a lack of appropriate apparatus. The advanced characteristics outlined below, although not exhibited by standard equipment, can be contemplated now, due to recent technical advances in the design of accelerator components.

Energy: The successful performance of the tandem Van de Graaff has already demonstrated the availability of 45-Mev oxygen ions.[1] By utilizing 3- or 4-stage ion-exchange and acceleration systems, heavy ions in the 100-Mev realm are not inconceivable. The normal Van de Graaff criteria of energy-homogeneity and low dispersion would be maintained.

The new modular design concept for the microwave linear accelerator extends the availability of high-energy electron beams to hundreds of Mev, limited primarily by budgetary considerations. Microwave power tubes and flexible design techniques can now be utilized to provide more versatile laboratory apparatus.

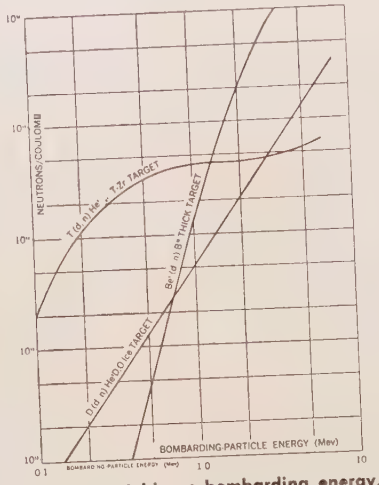

Neutron yields vs bombarding energy.

Intensity: Electron or ion-beam currents in the one-ampere range, at a few Mev, can now be considered seriously. Pulsed beams with these instantaneous intensities are closer to realization than continuous beams of the same order of magnitudes.

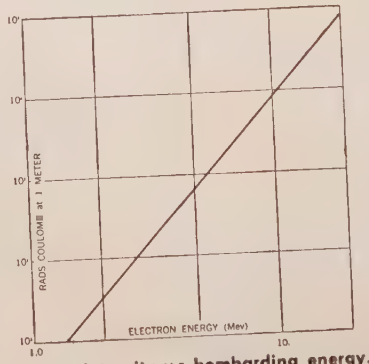

X-ray intensity vs bombarding energy.

The x-ray and neutron outputs from these beams are indeed heroic.

X-rays — millions of rads per minute at a few centimeters distance.

Neutrons — 10^{15} neutrons per second, from a "point" source.

Pulsing: New techniques now enable Van de Graaffs to be pulsed in the range from a few millimicroseconds up to a millisecond. Instantaneous intensities as described above make feasible the consideration of hundreds of rads per pulse, or more than 10^{11} neutrons per burst.

Energy Stability: It is now possible to consider stabilizing systems to a limit imposed primarily by the thermal motion of nuclear targets. With little effort, continuous particle-energy stabilities of a few tens of electron-volts can be provided.

Among the research fields in which it is believed these particle-accelerator characteristics may make a considerable contribution, are the following: nuclear physics, biology, solid-state, radiation damage, plasma physics, the ignition of thermonuclear systems, and space-environment studies.

A great variety of fruitful research can clearly be covered by existing accelerators now considered by HIGH VOLTAGE ENGINEERING to be standard items. Physicists and radiation chemists at HIGH VOLTAGE are prepared to explore on an individual basis, long-range and immediate problems that could utilize our accelerator systems.

[1] *Chalk River Laboratories, Atomic Energy of Canada, Ltd., reported at Am. Phys. Soc. Meeting, Vancouver (Aug. 1958)*

High Voltage Servicing Company, Ltd.
London, England

High Voltage Engineering (Europa) N.V.
Amersfoort, The Netherlands

HIGH VOLTAGE ENGINEERING CORPORATION

BURLINGTON MASSACHUSETTS

NUCLEAR INSTRUMENTS AND METHODS 7 (1960) 225–236; NORTH-HOLLAND PUBLISHING CO.

EXTRACTION OF PROTONS FROM THE BIRMINGHAM 1000-MeV SYNCHROTRON

G. A. DORAN, E. A. FINLAY, H. R. SHAYLOR and M. M. WINN†

Physics Department, The University Edgbaston, Birmingham 15

Received 18 January 1960

An electromagnetic deflecting channel for protons is described. This is moved close to the circulating beam in the synchrotron vacuum box after the accelerating cycle has commenced. Protons are induced to enter the deflector by Coulomb scattering through a very small angle, and when the current flowing through the deflector is ~ 35 kA the protons are deflected through an angle ~ 0.03 radians and escape from the synchrotron. The number of protons available per pulse in the experimental area has been increased by a factor ~ 1000 from that obtained previously by nuclear scattering from internal targets.

1. Introduction

The external beam of the Birmingham synchrotron has hitherto been produced by nuclear scattering of the internal beam through an angle of 4° by a carbon target. The beam so produced, measured at a distance of 5 metres from the exit port after passing through a quadrupole lens, contained only about 10^5 protons per pulse, less than 1 part in 10^4 of the internal beam[1]). A much more intense external beam has now been produced, using an air-core electro-magnet as a deflector. The protons are caused to enter this by Coulomb scattering through a very small angle.

To extract particles efficiently from circular accelerators, it is usual to induce them to enter a deflecting system in which they receive a single deflection large enough to eject them from the machine. The deflector will have either a material wall or a transition region of reduced deflecting power on the side facing the undisturbed beam. In either case, a substantial fraction of the circulating particles must pass from the undisturbed guide field of the accelerator into the region of full deflecting power without encountering the intervening region if an intense external beam of well-defined direction is to be produced. In conventional fixed-frequency cyclotrons the separation of successive orbits is such that no special provision is required to induce the beam to enter the deflector efficiently. Electrostatic deflectors having very thin walls are used. In the larger machines employing the synchrotron principle, the turn-to-turn separation is much too small to be of assistance in entering any conceivable deflector structure. In the Birmingham synchrotron, for example, a rate of orbit expansion greater than about 10^{-4} cm per rev. cannot normally be produced. In most large synchro-cyclotrons the necessary orbit separation is obtained by inducing radial betatron oscillations by the method suggested by Tuck and Teng[2]).

It has been shown by Cohen and Crewe[3]) that this method may be modified to suit such a machine as the Birmingham synchrotron, and it seems that a suitable "peeler" should cause a large fraction of the internal beam to enter the deflector. However, synchrotron magnets provide stronger vertical focusing than synchro-cyclotron magnets, and this fact favours the use of Coulomb scattering in beam extraction from synchrotrons. Preliminary experiments showed the feasibility of this approach, and on the ground of simplicity it was adopted in preference to the method of Cohen and Crewe.

† Now at the University of Sydney, Australia.

[1]) H. B. van der Raay, Nuclear Instruments 1 (1957) 351.
[2]) J. L. Tuck and L. C. Teng, Phys. Rev. 81 (1951) 305.
[3]) S. Cohen and A. V. Crewe, Proceedings of the C.E.R.N. Symposium on High Energy Accelerators at Geneva, 1956, Vol. 1.

The Birmingham extraction project has been beset throughout by mechanical difficulties arising from the fact that the synchrotron has no field-free straight sections, a circumstance attributable to its early inception date. All apparatus placed within its vacuum chamber must be capable of operating in a field of 12 000 gauss. The vacuum chamber (a) (fig. 1) is made entirely of porcelain, and access to it is restricted.

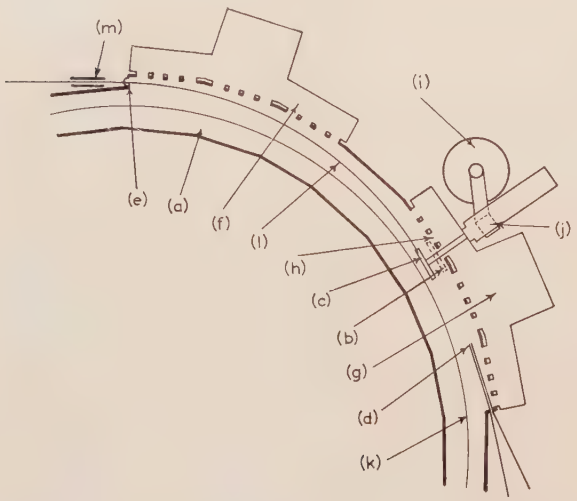

Fig. 1. Extractor in relation to synchrotron. (a) vacuum chamber; (b) deflector, withdrawn; (c) deflector in operating position; (d) inflector plates of injector; (e) exit port; (f), (g) pumping manifolds; (h) port used in assembly; (i) pulse transformer; (j) contactor; (k) nominal orbit; (l) path of extracted beam; (m) "self-excited quadrupole".

In particular, these features led to the rejection of the method of extraction which has proved very satisfactory in the Brookhaven Cosmotron[4]). Since the synchrotron magnet encloses the vacuum chamber on three sides, it was not considered practicable to support or to supply with current a magnet located near the inner wall of the vacuum chamber, as required by this method.

It was therefore decided that the deflector used in the Birmingham synchrotron must lie outside the nominal orbit. Hence it must withdraw beyond the radius of the inflector (to position (b), fig. 1) to permit injection to take place, and move in to its operating position (c) when the envelope of the beam has contracted sufficiently. The provision of these movements is taken for granted when small targets are involved, but adds greatly to the complexity of heavy apparatus which must be supplied with a large current.

A list of machine parameters relevant to the extraction problem is given in table 1.

Table 1

Parameters of the Birmingham 1000 MeV Proton Synchrotron

Peak magnetic field	12500	gauss
Time of rise of magnetic field	1.1	sec
Nominal orbit radius	450	cm
Inflector tip radius	466	cm
Radius of circle circumscribing inner wall of vacuum chamber	435	cm
Height of vacuum chamber	10	cm
Radius of exit port centre	481	cm
Diameter of exit port hole	5.0	cm
Azimuthal separation of deflector and exit port	1.01	radian
n value of magnetic field	0.68	
Interval between synchrotron pulses	10	sec

2. Deflecting Power Required

Since it was difficult to predict in advance the value of the loop radius which would give most efficient extraction, particularly as the outer radius at which the beam is stable is not known with certainty for high values of field, the angular deflection required to bring the protons to the exit port (e) (fig. 1) was calculated for a number of deflector radii assuming that their path was normal to a machine radius on entering the deflector. The paths of the deflected protons were computed by integrating the linear approximation to the equation for radial betatron oscillations in the fringing field of the synchrotron by a step-by-step method, giving the results shown in table 2. Owing to the presence of betatron oscillations of amplitude of the order of 1 cm in the undisturbed beam, together with the occurrence of energy loss in the scatterer, the radii of the instantaneous circles of the extracted protons will be somewhat smaller than the radius of the scatterer.

[4]) O. Piccioni, D. Clark, R. Cool, G. Friedlander and D. Kassner, Rev. Sci. Inst. **26** (1955) 232.

From the figures of table 2, a deflection of 0.033 radian appeared to be a typical requirement. In view of the large uncertainty in this figure, all components of the extraction apparatus were designed to permit it to be exceeded by a factor of two when extracting at the time of peak magnetic field.

TABLE 2

Radius of instantaneous circle R (cm)	Radius entry to channel (cm)	Deflection (radian)	Radius after 1.01 radians (cm)
460.5	462.0	0.0375	481.5
462.0	463.5	0.0333	480.8
462.0	465.5	0.0367	489.7
464.0	465.5	0.0275	480.5

The bracketed sets of figures refer to the same values of deflector radius and current. The significance of the difference between them is discussed in Section 8.

3. Design of the Deflector

The principal choice lay between an iron channel, as used in synchro-cyclotrons, and an electromagnet. An electrostatic deflector of reasonable length would require the use of a prohibitively high voltage. The use of an iron channel was rejected on the following grounds: when finally shimmed, it would be heavy and unwieldy; it would be inflexible as far as operation at different energies is concerned, owing to variation of the degree of saturation of the iron; if the mechanism for moving it were to develop a fault which allowed it to tilt, disastrous effects would follow. Hence an electro-magnet containing no iron has been chosen. Since the conductors must withstand considerable forces, the adoption of a single-turn loop seemed essential.

Considerations of stresses in the conductors and economy of power suggest that the length of the deflector loop should be as great as possible. A value of 46 cm has been chosen as the greatest length compatible with ease of assembly (see Section 4).

The shapes of the conductors have been chosen so as to make the external field of the loop adjacent to conductor (a) (fig. 2(a)) as small as possible. The conductors may be regarded as an

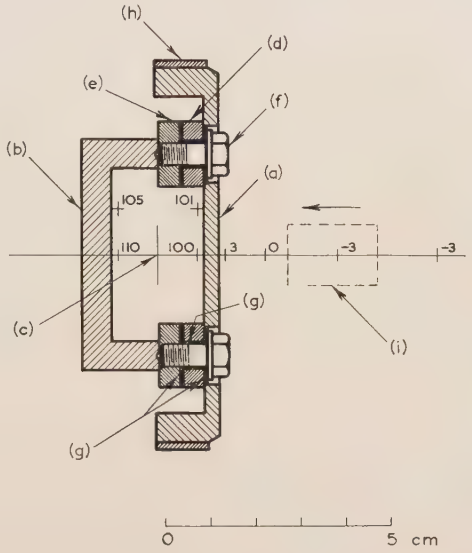

Fig. 2a. Construction of deflector loop. (a) inner conductor; (b) outer conductor; (c) mid-point of aperture; (d), (e) stainless steel spacers; (f) clamping bolts; (g) insulation; (h) correcting strips; (i) beam cross-section. The numbers on the diagram give relative values of the magnetic field produced by the loop.

adaptation of the simple arrangement of fig. 2(b), in which the ratio of the lengths of the conductors may be chosen to make the magnetic

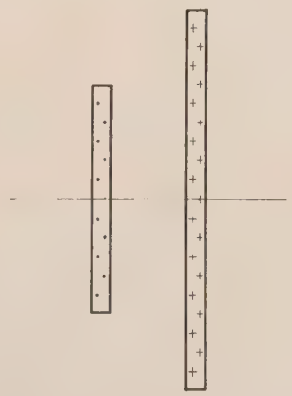

Fig. 2b. Basic cross-section of extractor loop conductors.

field intensity vanish at any one external point on the median plane on the side facing the wider conductor.

In computing the conductor shapes, it was assumed that the direct-current distribution would be established, and that the conductors could be regarded as equivalent to current sheets coincident with their central planes. End effects were not taken into account. On this basis it was calculated that the field intensity on the median plane at the outer face of conductor (a) (fig. 2a) would be 3% of the field at the inner face of (a) and in the same direction as the latter, and that at a distance of 8 mm from the outer face of (a) the corresponding value would be 1% in the opposite direction. The calculated value of the field due to the loop (gauss) at the mid point (c) was 0.11 I, where I is the current in amperes. Thus it was expected that the loop would deflect full energy protons through an angle of 0.00094 radian when carrying a current of 1000 A.

In order to calculate the current required and the resulting forces, a figure of 0.033 radian was taken as the most likely value of the required deflection, and this implied a current of 35 kA. For reasons discussed in Section 2, the loop was designed to carry 70 kA safely. The interaction of this current with the field of the synchrotron will produce an attractive force between conductors of 86 kg per cm of length, which places the spacing strips (d) and (e) in compression. These strips are hard soldered to (a) and (b) respectively. If 70 kA were passed through the loop in the absence of the synchrotron's field, a repulsive force between conductors of approximately 40 kg per cm length would be set up. This force would be resisted by the bolts (f).

Since wall (a) must be as thin as practicable, it is essential that the loop should be made of the strongest available material which is non-magnetic and which possesses a reasonably high electrical conductivity. Beryllium copper was chosen. The strips (d) and (e) are made of stainless steel so that they do not carry an appreciable fraction of the current. The steel is non-magnetic. The front and back portions of the loop are insulated from each other, except at the ends, by strips, bushes and washers (g) of glass tape impregnated with an epoxy resin.

In choosing conductor shapes to give a small external field, it is unavoidable that the internal field should vary across the aperture in such a way as to cause appreciable radial defocusing of the extracted beam, unless a design of greater complexity than the above is attempted. It was calculated that the conductors of fig. 2(a) would produce a field which varied by 12% across the aperture in the median plane, being weakest near conductor (a) and strongest near conductor (b).

4. Mechanical Features

The extraction system is shown in relation to the vacuum chamber of the synchrotron in fig. 1. Access to the vacuum chamber is provided by 9.5 cm diameter ports spaced 22 cm apart on the periphery. Until the project was nearly completed, the interval between the pumping manifolds (f) and (g) was occupied by narrow porcelain sectors, and so it was necessary to install the deflector in the sector covered by manifold (f). The layout of the vacuum chamber has since been modified, and fig. 1 shows the existing arrangement.

Fig. 3 is a schematic assembly drawing of the extraction system. The deflector loop (a) is supported and supplied with current by the coaxial conductor (b), in which considerable electrical losses occur. The length of (b), determined in part by the need to traverse the manifold, is 108 cm. Its diameter is 7.6 cm, which was considered the largest value compatible with adequate mechanical clearances. It is desirable that all moving parts should be arranged symmetrically about the axis of (b) in view of the fact that they are subjected to large accelerations. Hence the end of (b) is attached to the centre of the loop. The loop is closed at each end by a pair of straps (c), one above and one below the median plane, so as to leave the central region unobstructed.

As explained in Section 1, the loop must move in and out once during each synchrotron cycle. The movement at present provided is 6.3 cm. The assembly slides in the bearings (d) and (e),

which are widely spaced since the overhung weight is considerable. In order to reduce the voltage drop in (b) as much as possible, the current feed flanges ((f) and (g) in fig. 3 and (d) deflector with current, the heavy current circuit is completed by a contactor. The time of rise of the magnetic field of the synchrotron is 1.1 sec, and it is desirable that the time

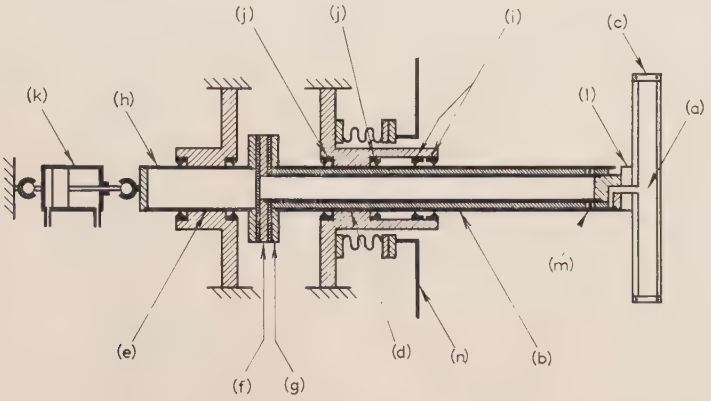

Fig. 3. Schematic diagram of extractor loop assembly. (a) deflector loop; (b) coaxial conductor; (c) loop end connector; (d) main bearing; (e) outboard bearing; (f), (g) current feed flanges; (h) extension shaft; (i) vacuum seals; (j) oil-retaining and vacuum seals; (k) pneumatic cylinder; (l) loop connecting block; (m) vacuum seal; (n) synchroton pump manifold.

in fig. 5) have been placed between the bearings, and the extension shaft (h) (fig. 3) fitted. Shaft (h) and the outer member of (b) are coated with polished chromium, which presents a suitable surface to (d) and (e) and to the vacuum seals (i) and (j).

The design of (i) and (j) was based on the moving targets already in use in the synchrotron, though the diameter of (b) is very much greater than the diameter of the target shafts. The sealing elements are made of synthetic rubber and are spring loaded and metal reinforced†. Each seal contains two elements, and the space between these is filled with oil, degassed diffusion pump oil in the case of (i), and a lubricating oil in the case of (j), since the latter also performs the function of retaining the oil in which bearing (d) is immersed. The distance between (i) and (j) is greater than the longest stroke contemplated and the space between them is pumped to a rough vacuum, so that occluded air cannot be carried across both seals when the shaft moves.

Since it is not practicable to move the heavy transformer (see Section 5) which supplies the

† Geo. Angus and Co. Ltd., Type MIM 7595/12.

occupied by the movement of the deflector and the closing of the contactor should be considerably less than this in order that protons of intermediate energies may be extracted. The return stroke may be very slow, and presents no difficulty.

The total mass of the moving parts is 46 kg. They are driven inwards by the pneumatic cylinder (k) (fig. 3), and brought to rest against a buffer which provides a sufficiently defined rest position. Cylinder (k) is double acting, and provides cushioning by trapping air during the forward stroke and releasing it at the end of the stroke through a valve coupled to the piston rod. The exact piston rod positions at which the valve closes and opens are adjusted to eliminate bounce when the moving parts strike the buffer, which contains rubber springs.

The closing of the contactor is initiated by the deflector assembly as it comes to rest in its operating position. The opening of the contactor initiates the return stroke of the deflector. The forward stroke of the deflector occupies an interval of 0.18 sec, and the operation of control relays and the closing of the contactor at present require a further 0.25 sec. These times set a

lower limit to the energy of the extracted protons.

When assembling the extractor, the concentric conductor is first mounted in its bearings and inserted through the appropriate port of the vacuum chamber. The deflector loop is then inserted through the adjacent port (h) (fig. 1) by means of a long rod attached at one end by a hinged joint. When inside the vacuum chamber, the loop is turned through a right angle and brought up against the end of (b) (fig. 3), to which it is secured from the inside by bolts, using a long spanner. The inserting rod is then removed. This method of assembly limits the length of the loop to less than the radial depth of the wide sections of the vacuum chamber (49.7 cm), and a value of 46 cm was chosen. It may be possible to assemble a deflector consisting of two or more pieces each 46 cm long by an extension of this method, but the additional complication was not considered to be warranted.

Small pipes inside the inner member of (b) carry cooling water to the loop and cooling air for (b) itself.

5. Energising the Loop

It was decided to adapt the familiar radar technique involving a pulse forming network, ignitron switch, and pulse transformer for the purpose of energising the deflector loop. Of these components, the transformer promised to present the most serious difficulties in the form of excessive winding resistance, leakage reactance, and eddy current losses in the secondary winding, all of which were circumvented at the expense of introducing considerable constructional difficulties by adopting a toroidal form.

The transformer core consists of two coils of steel strip together forming a ring of cross section 25 cm by 20 cm and weighing 360 kg (fig. 4). The primary is wound on the core and the single turn secondary enfolds the primary and core and forms a large diameter concentric pair of output conductors. A short length of the outer member of this concentric pair is made of brass and serves as a current-measuring resistor. Its measured value is $2.01 \pm 0.04\ \mu\Omega$. The transformer is immersed in oil and enclosed in a steel box 3.2 cm thick to screen it from the leakage field of the synchrotron magnet.

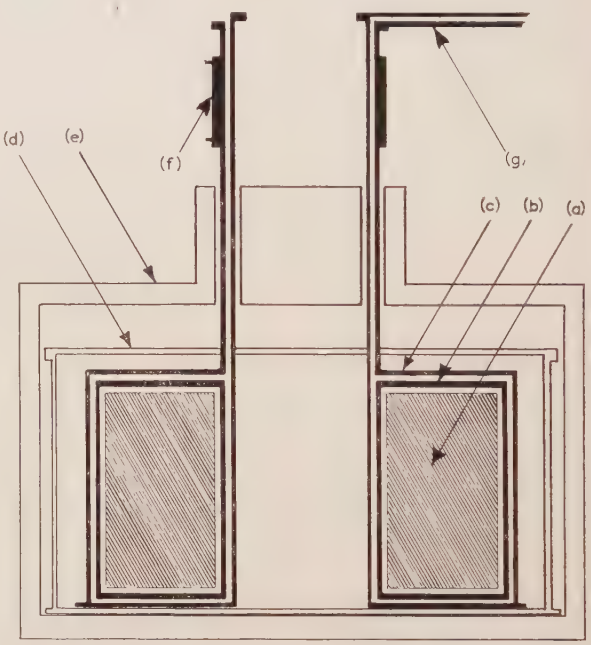

Fig. 4. Toroidal pulse transformer. (a) core; (b) primary; (c) secondary; (d) oil tank; (e) magnetic screen; (f) current measuring resistor; (g) secondary connections.

The voltage pulse applied to the transformer primary is unidirectional, and so it is necessary to reverse the remanent magnetism of the core during the interval between pulses. This is done by passing a small current for a short time in the reverse direction through the primary from an auxiliary circuit.

The primary is wound in four sections which alternate in sense so that a ratio of 60:1 may be obtained without stressing the insulation between sections, and ratios of 120:1 and 240:1 may be obtained without the voltage between sections exceeding one half of the terminal voltage.

As explained in Section 4, the secondary circuit is completed by a contactor after the deflector has moved to its operating position. The contactor is not required either to make or to break current. Although both the feed to the deflector and the output of the transformer take the form of coaxial conductors, it did not appear

practicable to retain this form for the intermediate conductors. These consist of thin, wide, closely spaced parallel strips, and the contactor is inserted in this portion. Its arrangement, which is largely dictated by inductance considerations, is shown in fig. 5. Each pole contains eight spherical copper contacts (a) which close on the moving blade (b), also of copper. Pneumatic cylinders (c) apply to each contact a force of 45 kg, which must counteract the "blow off" force due to the current in addition to providing sufficient pressure at the area of contact. Tests showed that when a single contact was operated under these conditions its destruction by welding or burning would occur only if a current greater than about 20 kA passed through it. Hence eight contacts should carry 70 kA with a considerable margin of safety. In normal operation an interlock ensures that the proper contact pressure is applied before current passes.

The question of designing the switch in such a way that the contacts would tend to "blow on" was investigated, but the mechanical complexity arising from the severe inductance requirements appeared to outweigh the advantage gained. The use of flexible connectors or sliding contacts as an alternative to the contactor was also considered, but was rejected after a brief investigation.

The transformer and switch are shown in relation to the whole extraction system in fig. 1 ((i) and (j)).

Preliminary mechanical and electrical tests of the extractor were carried out at a time when the vacuum system of the synchrotron was dismantled. Fig. 6 is a photograph taken during these tests showing the principal components located at the synchrotron magnet.

The pulse forming network is an eight-section low pass filter. Details of its construction and performance are given in table 3. Alternative inductance values of 2.6 and 0.16 mH per section are available, and in conjunction with the choice of transformer ratio these give considerable flexibility should changes in operating conditions be desired. The principal circuit components are shown in fig. 7.

An oscillogram of the transformer secondary current (a) and the magnetic field (b) developed by the deflector loop is reproduced in fig. 8. It

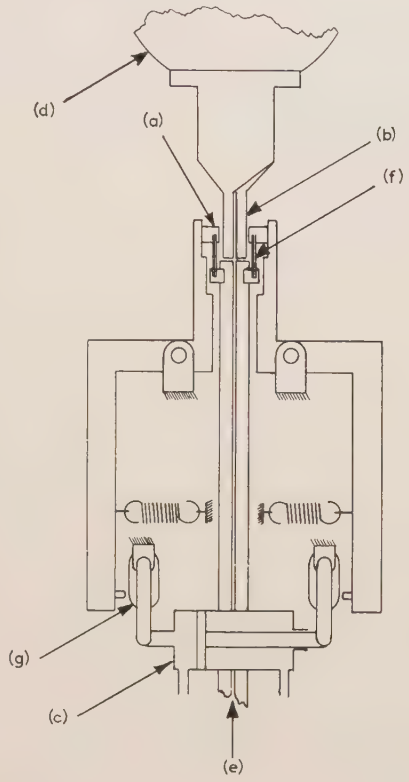

Fig. 5. Schematic diagram of contactor. (a) spherical contacts; (b) moving blade; (c) pneumatic cylinder; (d) current feed flanges; (e) incoming conductors; (f) flexible strap; (g) crankshaft.

will be seen that the leading edges of the two waveforms differ considerably.

This behaviour makes it seem doubtful whether a much shorter pulse of magnetic field of satisfactory waveform could be produced in this loop if ever it were desired to do so. An interval of the top of the magnetic field pulse 3.5 m sec long is flat to within $\pm$ 1%. It was necessary to trim individual capacitors of the pulse forming network to obtain this result.

When the loop was first constructed, the field outside conductor (a) (fig. (2a)) was considerable, the departure from the calculated performance being attributed mainly to the presence of the terminals (1) and end straps (c)

TABLE 3
The Pulse Forming Circuit (References are to fig. 7)

Quantity		Design or calculated value	Measured value
Total capacitance 8 × C	(μF)	2000	
Maximum working voltage of capacitors	(kV)	2.5	
Number of sections		8	
Inductance per section L	(mH)	0.65	
Final inductance L_0	(mH)	0.16	
Pulse length	(msec)	6.5	6.4 at half height
Characteristic impedance	(Ω)	1.6	
Ignitron V	Type	BK66	
Primary current when correctly matched	(A)	780	
Ratio of transformer T		60:1	
Load Z on secondary of T	($\mu\Omega$)	450 (match)	340
Available secondary current when $Z = 340\ \mu\Omega$	(kA)	54 ± 3	47 ± 3
Deflecting power of loop for 1000-MeV protons	(radian/kA)	9.4×10^{-4}	$(8.2 \pm 1.3) \times 10^{-4}$

(fig. 3). The external field was reduced by modifying (c) and by adding the brass strips (h) (fig. 2(a)) until it had the relative values shown on fig. 2(a). These values were obtained with the aid of a long, narrow search coil so aligned that they represent average values taken over the path of a proton. During the rise time of the current pulse, eddy currents produce a "spike" of field of 1.4 msec. duration at the outer face of (a) equal in magnitude to 8% of the useful field and opposite in direction. If the rise of the current pulse is slowed down by increasing L_0 (fig. 7) to 2.6 mH, the amplitude of the spike is halved, though at some sacrifice of the useful length of the pulse. It is conceivable that, under some operating conditions, this spike might deflect the protons and cause them to strike the wall of the loop, or an auxiliary

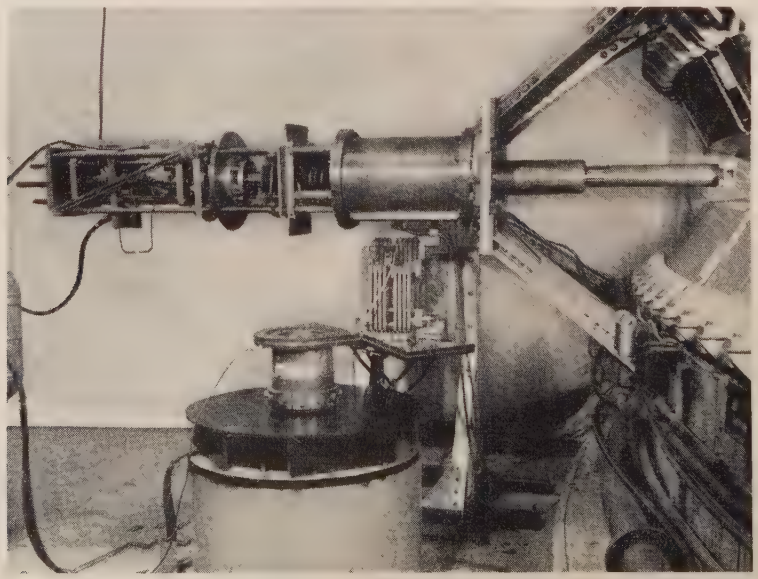

Fig. 6. Extractor loop assembly, contactor and pulse transformer in position at synchrotron magnet during tests.

scattering target if used, before the field within the loop has reached its proper value.

The long search coil referred to above was used to measure the variation of field intensity across the aperture of the loop, and the relative values are shown in fig. 2(a). After the coil had been calibrated by rotating it about its long axis in a known uniform magnetic field, the deflecting power of the loop was calculated (see table 3).

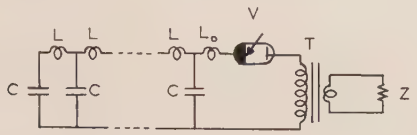

Fig. 7. Pulse forming circuit. Values of components are given in table 3.

6. Timing the Current Pulse

The beam of protons circulating in the synchrotron may be brought to a target located outside the normal orbit by suitably programming the frequency of the accelerating voltage or, at full energy only, by switching off the accelerating voltage and allowing the orbits to expand as the magnetic field decreases[5]). The second method produces much the shorter pulse of protons, 1—4 msec duration at radii permitted by existing adjustments of the extractor, and was therefore used in the tests of the extraction system described in Section 8, since the shorter pulse could be made to occur during the flat portion of the deflector field pulse without overlapping the rising and falling edges.

A firing pulse must be applied to the ignitron V (fig. 7) in advance of the time of arrival of the beam at the front edge of the deflector and there should be as little fluctuation in time between the two events as possible. This pulse was provided by the beam itself as it impinged on an auxiliary target which was thrust in to a position of smaller radius than that occupied by the inner face of the deflector. The target was offset below the median plane by an adjustable amount of the order of one centimetre so that it did not destroy more than a small fraction of the circulating beam. A scintillation counter placed near the synchrotron provided a convenient means of producing a pulse when the beam struck the target, and this pulse fired the ignitron after an adjustable delay.

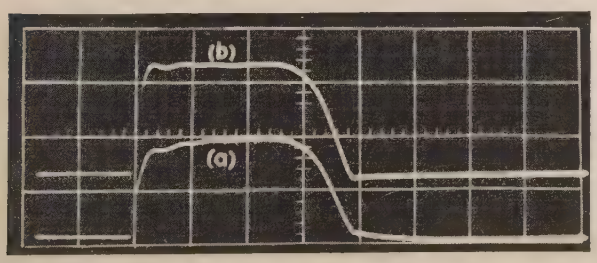

Fig. 8. Deflector waveforms: (a) current, (b) magnetic field. One horizontal graticule division represents 2.0 m sec.

7. Coulomb Scattering by Targets

When protons strike the edge of a thin target situated at a radius nearly equal to that of the inflector, they lose energy in it by ionization, and so the majority of them ultimately strike the inner wall of the vacuum chamber after repeated encounters with the target, having suffered an energy loss of approximately 16 MeV if the synchrotron is operating at full energy. Coulomb scattering makes a comparatively small contribution to the oscillation induced by the target, but this contribution is important in that it causes the protons to swing out beyond the radius at which they strike the target by amounts which are typically of the order of 1 cm. Further, if the target consists of a material of high atomic number, and if its thickness is of the order of 0.1 g cm^{-2}, the probability of a proton extending its outward excursion by 1 cm in one encounter is quite high. Hence protons may be caused to enter the deflecting field of the loop without striking wall (a) (fig. 2(a)).

Preliminary trials of the efficacy of this process were carried out with the aid of a model of the deflector consisting of a block of Perspex fitted with a brass plate to simulate wall (a). When traversed by protons, the Perspex block gave off Čerenkov radiation, the intensity of which was a measure of their number. A thin platinum target placed 150° before the "de-

[5]) P. B. Moon, L. Riddiford and J. L. Symonds, Proc. Roy. Soc. A **230** (1955) 204.

flector" increased the amount of radiation when the radius of the front edge of the "deflector" was less than 462 cm. At larger radii the separate scattering target produced no improvement, probably because the "deflector" itself was situated at a more favourable azimuth for a scattering target, and was acting as such. By comparison with the radiation emitted when the brass plate was removed and all the protons were allowed to impinge directly on the Perspex, it was estimated that a fraction of the order of 10% of the circulating protons could be induced to enter the "deflector" by this method. It was expected that the efficiency of collection of light from the Perspex block would vary considerably with the distribution of protons within the block, and therefore results obtained by this method were treated with reserve.

8. Performance of the Extraction System

At the time of writing, all tests of the extraction system have been carried out when the synchrotron was operating at full energy, and the deflector loop itself has been allowed to act as the scattering target. To obtain a short pulse (see Section 6) the protons were allowed to spiral outwards to the deflector after the radio-frequency accelerating voltage had been switched off. A sufficient number of protons was ejected in one synchrotron pulse to produce an opaque image on a sensitive X-ray film† placed normal to the beam at the exit port.

The image on the film consisted of a well defined, nearly horizontal line. The vertical dimension varied a little from pulse to pulse, lying between 0.5 and 0.7 cm. The width appeared to be of the order of 10 cm, but the walls of the vacuum chamber interfered with the outer edges of the image. Images obtained with less sensitive film gave more information as to the distribution of protons over the profile of the beam. They showed a high concentration of protons close to the edge of the image nearer the synchrotron, where the edge was relatively sharp, and a gradual fall off in intensity towards the outer edge of the image. The height of the image was much smaller on the less sensitive film, and the edges were more diffuse showing that the distribution in height was non uniform also. The long axes of the images were inclined at an angle of 3° to the horizontal. The beam can be moved radially across the exit port by varying the deflecting current, which can be adjusted to cause the maximum number of protons to pass through the 5.0 cm diameter port. The appearance of the image on an X-ray film of low sensitivity gives a satisfactory indication as to when this has been achieved. Values of current so determined are shown in table 4, with the corresponding measured deflecting powers of the loop.

A quantitative estimate of the horizontal distribution of the extracted beam was obtained by counting the C^{11} β-activity induced in polyethylene sheet. Four pieces 1.25 cm wide were arranged to cover the 5.0 cm diameter exit port, together with an X-ray film which confirmed that the beam was correctly placed with respect to the polyethylene. Histograms of

† Kodirex, by Kodak Ltd., London, England.

Table 4

Operating conditions

Radius of front edge of loop †† (cm)	Pulseforming network charging voltage (V)	Loop current (kA)	Deflection produced (radian)	Reference to fig. 9
461.5	2070	39	0.032 ± 0.005	Histogram (a)
462.5	1820	34	0.028 ± 0.005	Histogram (b)
463.5	1650	31	0.025 ± 0.004	

†† Measured by interruption of beam at injection, and subject to an uncertainty of $\pm$ 0.6 cm. Values are self-consistent.

two horizontal distributions so obtained are shown in fig. 9. Each irradiation consisted of five pulses, and each histogram represents the

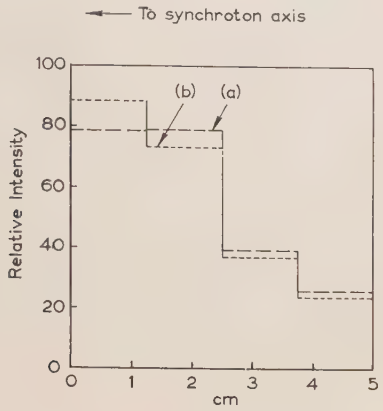

Fig. 9. Distribution of extracted beam across exit port. Radius of inner edge of extractor loop: (a) 461.5 cm, (b) 462.5 cm.

mean of two irradiations. The operating conditions under which they were taken are given in table 4.

The histograms, taken in conjunction with the film images, suggest that approximately three-quarters of the protons passing through the deflector can be brought through the exit port.

The factors contributing to the horizontal width of the emerging beam at the exit port are thought to be variation of the field of the deflector across its aperture, the energy spread of the protons entering it, and the strong defocusing action of the fringing field of the synchrotron magnet. The accompanying vertical focusing brings the beam to a line focus close to the exit port. Most of the protons will enter the deflector when close to an antinode of their betatron oscillations, and hence their angular spread at entry will be small. The two sets of figures given in table 2 for protons of instantaneous circle of radius 462.0 cm show the effect of entering the deflector at different radii, taking into account the variation of the deflecting power of the loop over its aperture. This alone is sufficient to account for the observed beam width.

An absolute measurement of the number of protons emerging from the exit port was obtained from the two irradiations of polyethylene referred to in table 4, since the efficiencies of the counters used to monitor them were known. The number was the same in both cases, namely 3×10^8 protons per pulse. The intensity of the circulating beam was at the time slightly below normal, being estimated from electrostatic induction on an internal electrode[6]) as about 2×10^9 protons per pulse.

On this occasion approximately one third of the circulating beam was lost as a result of striking the auxiliary target (Section 6).

9. The Behaviour of the External Beam

After leaving the exit port, where the magnetic field reaches a maximum value of 8750 gauss, the protons continue to traverse a region of the fringing field of the magnet in which the radial gradient of flux density is very high. Consequently the angular divergence of the beam in the horizontal plane increases rapidly. Two markers placed 2.5 cm apart at the exit port cast shadows which are spaced 15 cm apart at a distance of 2.9 m from the port. The vertical divergence is comparatively small. At a distance of 3.4 m from the exit port the height of the image produced on a film was approximately 3.5 cm.

It was clear that a lens capable of providing radial focusing should be placed close to the exit port. The "self-excited quadrupole" previously used for focusing the 4°-scattered beam[1]) was increased in strength and placed in position (m) (fig. 1).

Since the quadrupole is not far removed from the position of the vertical focus, it was expected that it would not produce serious vertical defocusing. When the inner face of the extractor loop was at a radius of 463.0 cm and the current in the loop was 33 kA the profile of the beam at a distance of 5.2 m from the exit port approximated to a rectangle 9 cm wide by 3 cm high. By passing this beam through a pair of quadrupole electromagnets, it was then concentrated

[6]) L. Riddiford, H. B. van der Raay and R. F. Coe, Proc. Phys. Soc. A **68** (1955) 489.

to an approximately circular focal spot of diameter 5 cm at a distance of 2.0 m from the exit of the last quadrupole magnet. By irradiating polyethylene sheet, it was found that the focal spot contained 8×10^7 protons per pulse.

The number of particles available per pulse in the experimental area has been increased by the combination of the new extraction apparatus and additional focusing magnets by a factor of the order of 10^3. The size of the focal spot is approximately equal to that previously obtained, though the angular divergence is now somewhat greater.

Acknowledgements

The authors are grateful to Professor P. B. Moon for many helpful suggestions. Mr. G. Guest prepared the mechanical design of the heavy current contactor. Members of the staff of the General Electric Company, Witton, gave valued assistance with some aspects of the construction. This project depended heavily on the staff of the workshop of the Physics Department; in particular, the authors wish to thank Messrs. V. J. Brady and J. Harling for much accurate and painstaking work. The focusing of the extracted beam was carried out by Dr. H. B. van der Raay.

NUCLEAR INSTRUMENTS AND METHODS 7 (1960) 237–244; NORTH-HOLLAND PUBLISHING CO.

ELEKTRONISCHE GERÄTE HOHER KONSTANZ FÜR DIE REGISTRIERUNG DER NUKLEONENKOMPONENTE DER KOSMISCHEN STRAHLUNG

W. LOTZ† und A. SITTKUS

Physikalisches Institut der Universität Freiburg im Breisgau

Eingegangen am 23. Februar 1960

A discription is given of a full set of electronic instruments for a Neutron Intensity Monitor. The obtained stability in time for 10^4h amounts to 6% for the sensitivity of the amplifier and discriminator; 2% for the dead time; 0.5% for 300 V d.c., 0.25% for high voltage. The probable error of the annual mean of the neutron intensity may be reduced to 0.1%. A ratemeter with logarithmic scale has been constructed by using a voltage dependent resistor.

1. Einführung

Auf dem Schauinsland bei Freiburg im Breisgau wurde 1957 ein Blei-Paraffin-Messblock zur Registrierung der Nukleonenkomponente der kosmischen Strahlung errichtet[1]). Durch den Einbau van 72 Zählrohren konnte die statistische Schwankung gegenüber der Simpson'schen Standard-Anordnung um den Faktor 1.6 verkleinert werden.

Damit die Messergebnisse auch über lange Zeit vergleichbar bleiben[2]), müssen die Messgeräte eine hohe zeitliche Konstanz besitzen. Aus diesem Grunde wurden einerseits die verwendeten Schaltelemente sorgfältig auf Langzeitkonstanz hin ausgewählt und andererseits die verwendeten Schaltungen möglichst unempfindlich gegen Alterung der Schaltelemente, insbesondere der Elektronenröhren, gemacht.

2. Die verwendeten Schaltelemente

Als Widerstände wurden in der Anlage fast ausschliesslich 1 Watt-Typen von Kohleschichtwiderständen der Klasse 0.5 mit 5% Toleranz benutzt. Widerstände der Klasse 0.5 ändern ihren Wert bei halber Nennlast nur um maximal 0.5% im Jahr, bei einem Zehntel der Nennlast nur um etwa 0.1%.

Als Kondensatoren wurden solche der Klasse 1 und 2 mit 5% Toleranz verwendet, die also genügend unempfindlich gegen Luftfeuchtigkeit sind. Bis zu einer Kapazität von 1 μF betrug die Nennspannung 400 V. Bei höherer Kapazität wurden Metallpapierkondensatoren mit 160 V Nennspannung und 400 V Spitzenspannung eingesetzt, die ohne weiteres mit Dauerspannungen von 300 V = betrieben werden konnten.

Zur Wechselspannungsgleichrichtung wurden ausschliesslich Selen- oder Siliziumgleichrichter eingesetzt.

In zwei ein halb Betriebsjahren trat kein Ausfall an Widerständen, Kondensatoren und Gleichrichtern auf.

Für die Röhrenbestückung wurden Langlebensröhren benutzt. Eine Ausnahme bildet lediglich die ECC 83, da die äquivalenten Typen E 83 CC und E 283 CC erst seit kurzem auf dem Markt sind. Die Langlebensröhren sind in den angegebenen Schaltungen im Mittel mindestens zwei Jahre lang brauchbar, d.h. der Anodenstrom beträgt bei der Kontrolle im Prüfgerät ohne Gleichstromgegenkopplung noch mehr als 50% des Sollwertes. Es wurden nur keramische Röhrenfassungen verwendet.

3. Übersicht über die Anlage

Die Anlage besteht aus zwei (bzw. drei) identischen, völlig von einander getrennten

† Jetzt im Max-Planck-Institut für Physik und Astrophysik, München.

[1]) W. Lotz, A. Sittkus und W. Hassler, Nuclear Instruments and Methods **6** (1960) 296.

[2]) S. E. Forbusch, J. Geophys. Res. **63** (1958) 651.

Teilen. Das Blockschaltbild einer Einheit ist in Fig. 1 dargestellt.

In den Verteilerkästen werden die Zählrohrimpulse von den parallel liegenden Bortrifluoridzählrohren gesammelt, im Vor- und Hauptverstärker verstärkt und anschliessend diskriminiert. Der Diskriminator gibt die Impulse weiter an ein logarithmisch anzeigendes Ratemeter mit Tintenschreiber und an den Vorwahluntersetzer. Der Vorwahluntersetzer betätigt mechanische Zählwerke, die alle viertel Stunden fotografiert und zur vollen Stunde auf Null zurückgestellt werden.

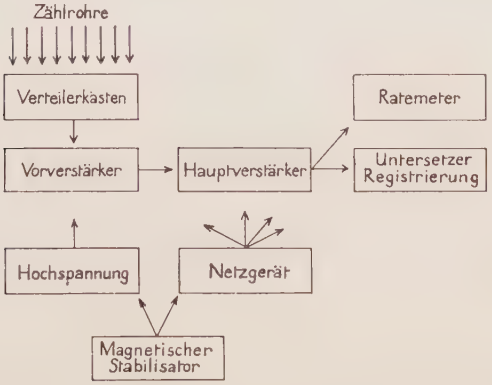

Fig. 1. Blockschaltbild der Apparatur.

Der Gleichspannungsversorgung dient ein Netzgerät für 300 V und ein Hochspannungsgerät für 0.7 bis 3.0 kV. Der Netzteil enthält ferner einen käuflichen magnetischen Spannungskonstanthalter für Wechselstrom und ein Verzögerungsrelais, das die Anodenspannungstransformatoren verzögert aufschaltet, um die Röhren zu schonen.

4. Vorverstärker, Hauptverstärker, Diskriminator

Der Vorverstärker (Fig. 2) enthält eine Gegenkopplung über drei Verstärkerröhren, die linke Hälfte der Doppeltriode dient gleichzeitig zur Phasenumkehr, die rechte Hälfte arbeitet als Kathodenfolger. Durch die Gegenkopplung wird die Verstärkung auf 100-fach festgelegt und die Bandbreite auf etwa 2 MHz begrenzt.

Am Eingang des Hauptverstärkers (Fig. 3) kann die Gesamtverstärkung in Stufen von 10% geregelt werden. Die Grobregelung der Verstärkung geschieht im Gegenkopplungsweg, sodass bei jeder gewählten Verstärkung die Gegenkopplung dem maximal erreichbaren Wert entspricht. Dabei werden die jeweils nicht benötigten Widerstände für Hochfrequenz kapazitiv kurzgeschlossen, für Niederfrequenz und für Gleichstrom ist die Gegenkopplung dagegen immer voll wirksam. Die Verstärkung kann auf diese Weise um einen Faktor 100 variiert werden.

Der zur Impulshöhensortierung notwendige Diskriminator wurde im Hauptverstärkerchassis eingebaut. Seine Empfindlichkeit beträgt nach Kandiah[3]) in erster Näherung $E = IR$. (I = gesamter Diodenstrom der zweifachen Doppeldiode, $R = 1/S_1 + 1/S_2$, S_i = Anodenstromsteilheit der beiden Penthoden.) In unserem Falle ist $I = 1.4$ mA, $S_1 = S_2 = 3$ mA/V, $R = 0.67$ kOhm und also $E = 0.94$ V.

Um eine hohe Konstanz der Ansprechschwelle dieses Diskriminators zu erreichen, erwiesen sich einige Änderungen an der Schal-

[3]) K. Kandiah, Proc. Inst. Electr. Engineers II, **101** (1954) 239.

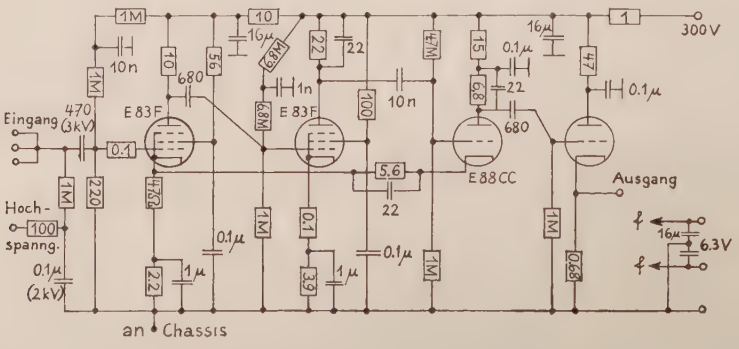

Fig. 2. Schaltschema des Vorverstärkers. In den Schaltschemen sind alle nicht näher gekennzeichneten Werte in kOhm bzw. pF angegeben mit 5% Toleranz. Es handelt sich um 1-Watt-Widerstände und 400-V-Kondensatoren.

tung von Kandiah als notwendig. Die Ansprechschwelle wurde von anfänglich 100 mV auf 0.9 V heraufgesetzt, der Gitterwiderstand der rechten Penthode parallel zur (Halbleiter-)-Diode gelegt und zwei parallele Doppeldioden dioden am Eingang des Hauptverstärkers abschneiden.

Nach den ersten 100 Stunden ändert sich E_e noch um maximal 2% in 10^3 h und um maximal 6% in 10^4 h. Diese Änderungen sind fast aus-

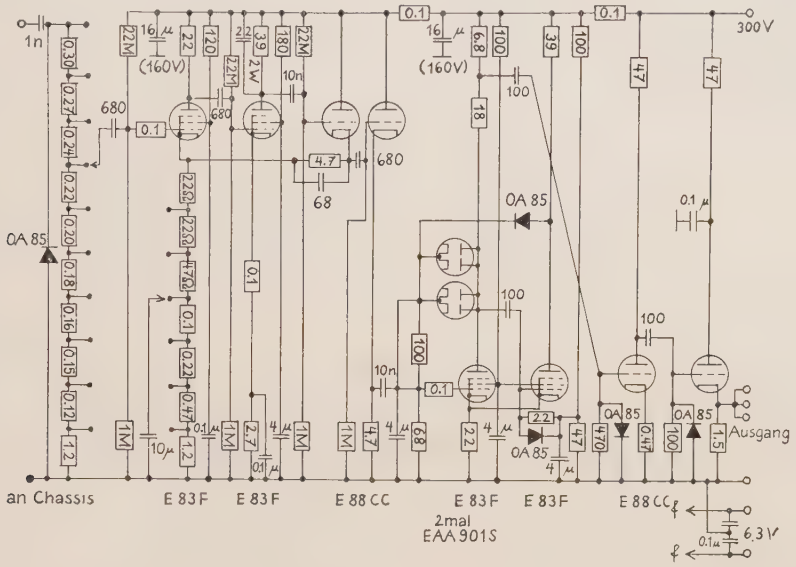

Fig. 3. Schaltschema des Hautpverstärkers und Diskriminators.

Daten des Impulsverstärkers und des Diskriminators.

Bandbreite	0.7 MHz	Empfindlichkeit des Diskriminators	0.9 V
Anstiegszeit	0.5 μs	Maximale Impulsfrequenz	10 kHz
Differentielle Zeitkonstante	3 μs	Totzeit des Diskriminators	10 μs
Eingangsempfindlichkeit E_e für negative Impulse	0.07 bis 12 mV	Schwellenunsicherheit	$< 0.5\%$
Verstärkung	70 bis 10^4-fach	Übersteuerungsfestigkeit	$> 200\, E_e$
HF-Gegenkopplung je Verstärker	> 20 fach	Heizspannungsänderung	$d \ln E_e / d \ln U_f = 0.2$
Rauschen am Eingang	$< 10\, \mu V_{eff}$	Anodenspannungsänderung	$d \ln E_e / d \ln U_a = 0.8$

mit langer Lebensdauer eingesetzt. Die den Zählverlust bestimmende Totzeit wurde in den Vorwahluntersetzer verlegt, da dort eine hohe Konstanz der Totzeit gewährleistet ist.

Der Kandiah-Diskriminator hat bei gleicher Konstanz eine um etwa einen Faktor 20 niedrigere Ansprechschwelle als ein Schmitt-Diskriminator. Dadurch können Verstärkerröhren eingespart und der vorgeschaltete Verstärker um diesen Faktor 20 übersteuerungsfester gemacht werden. Extrem hohe Impulse, die den Verstärker trotzdem zum Blockieren bringen würden, lassen sich bequem durch Halbleiterschliesslich auf den Diskriminator zurückzuführen, die Verstärkung ändert sich nur um etwa 1% in 10^4 h.

5. Vorwahluntersetzer

Die Schaltung (Fig. 4) entspricht Vorschlägen des Herstellers der dekadischen Zählröhre E 1 T[4]). Um Langzeitkonstanz zu erzielen, erwiesen sich jedoch verschiedene Änderungen als notwending.

[4]) Valvo GmbH, Technische Informationen für die Industrie Heft 2S und 4S (Valvo GmbH, Hamburg, 1953);
R. Kretzmann, Handbuch der industriellen Elektronik, (Verlag für Radio-, Foto-, Kinotechnik, Berlin, 1954).

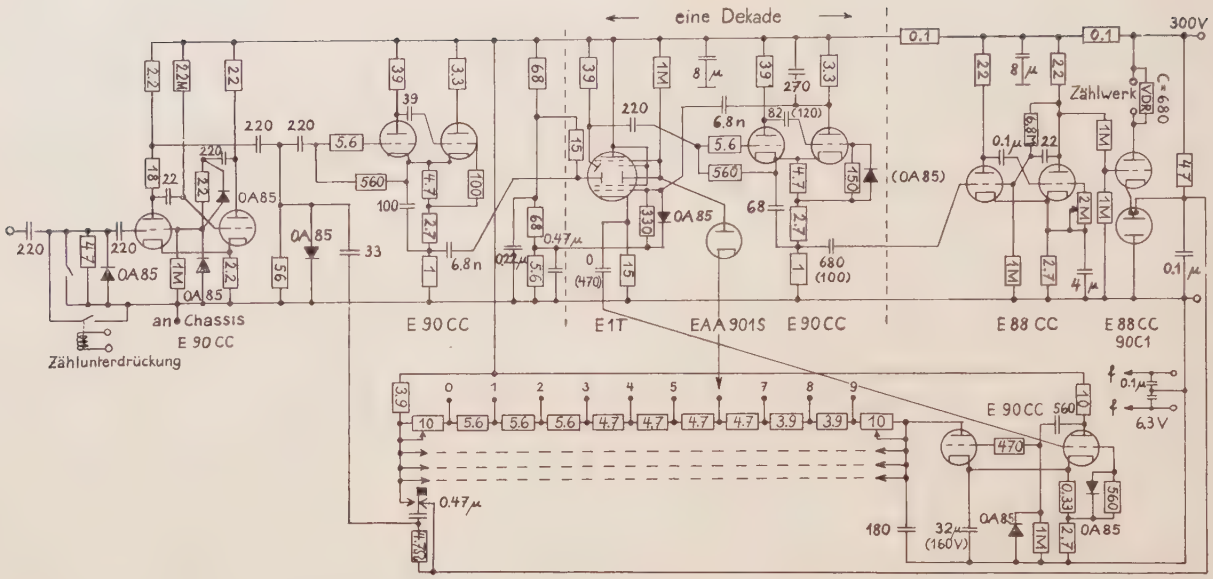

Fig. 4. Schaltschema des Vorwahluntersetzers. Gezeigt ist die 1. Dekade, die 2. und 3. Dekade sind identisch mit der 1., eingeklammerte Werte gelten für die 4. Dekade. Die Zählwerkendstufe ist in Wirklichkeit doppelt vorhanden, damit zwei Zählwerke parallel laufen können. (Widerstände in kOhm, Kondensatoren in pF, Toleranz überall 5%.)

Kenndaten der Schaltung

Untersetzungsfaktor ganzzahlig	von 1 bis 10^4	Eingangsempfindlichkeit für positive Impulse	20 V
Totzeit	28 μs	bei 20 kHz	25 V
Totzeitkonstanz	2%/10^4h	Zählwerkimpuls bis	200 V, bzw. 40 mA
Obere Grenzfrequenz	20 kHz	einstellbar von	1 ms bis 1 s

Eine Eingangsstufe mit einer wohldefinierten Totzeit wurde hinzugefügt. Die Kippzeiten der Univibratoren der einzelnen Dekaden wurden verkleinert, um den Rückstellvorgang und die Vorwahl zu beschleunigen. Die Zählwerk-Endstufe wurde neu konstruiert, um schnelle Zählwerke zuverlässig betreiben zu können. Die Vorwahlstufe wurde neu dimensioniert und arbeitet bis 20 kHz auch mit gealterten Zählröhren einwandfrei.

Die Potentiometer von 10 kOhm im Vorwahlspannungsteiler müssen mehrmals jährlich etwas nachjustiert werden. Die Anodenspannung kann um 50 V variiert werden, ohne dass Zählfehler

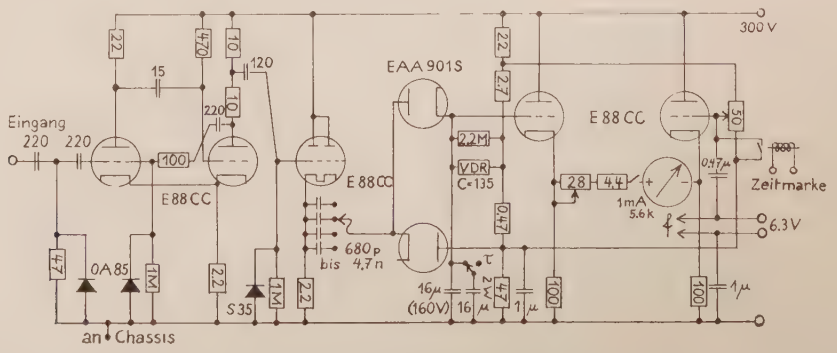

Fig. 5. Schaltschema des Integrators. Der Koppelkondensator G kann variiert werden von z.B. 470 pF bis 4.7 nF, entsprechend einer normalen Intensität von etwa 100 s^{-1} bzw. 10 s^{-1}.

auftreten. Wird für die erste Dekade auf Vorwahl verzichtet, so kann die Totzeit mit einigem Aufwand auf 1 μs herabgesetzt werden[5]).

6. Ratemeter

Nach Ultrastrahlungsausbrüchen auf der Sonne muss kurzzeitig mit etwa dem 100-fachen der normalen Neutronenintensität gerechnet werden. Mit Hilfe eines spannungsabhängigen Widerstandes ist es gelungen ein Ratemeter (Fig. 5) zu konstruieren, das einen entsprechenden Bereich logarithmisch überstreicht.

Unter gewissen Voraussetzungen ist die Spannungsdifferenz U an den Gittern der Elektrometer-Doppeltriode[6])

$$U = N\,G\,E\,R$$

(N = Zählrate, G = Koppelkapazität, E = Höhe des Rechteckimpulses vom Univibrator, R = Gitterableitwiderstand, 2.2 MOhm parallel zu einem spannungsabhängigen Widerstand).

Bei nicht zu kleiner Spannung gilt für einen spannungsabhängigen Widerstand (VDR)

$$R = C^a\ U^{(1-a)},$$

dabei sind C und a für den betreffenden VDR charakteristische Konstanten. C liegt zwischen 10 und 10^3, a zwischen 3 und 6, wenn R in Ohm und U in Volt gemessen werden.

Damit ergibt sich $U \propto N^{1/a}$. Diese Näherung ist umso besser logarithmisch, je grösser a ist. Es hat sich herausgestellt, dass bei kleinen Spannungen $U \ll C$ die Grössen a und C keine Konstanten der obigen Gleichung mehr sind: lässt man U gegen 0 gehen, geht a gegen 1 (ohmscher Widerstand) und C gegen einen hohen Grenzwert.

Um bei hohen Spannungen (a und C konstant) ein zu starkes Ansteigen von U mit wachsendem N zu verhindern, wurden zwei der oben erwähnten Voraussetzungen nicht streng erfüllt: Der Strom durch das Messinstrument ist nicht klein gegen den Kathodenstrom der Elektrometer-Doppeltriode und E ist nicht gross gegen U, Fig. 6 zeigt das Ergebnis. Durch Variation des "Innenwiderstandes" des Messinstrumentes kann der nutzbare logarithmische Bereich in weiten Grenzen auseinandergezogen oder zusammengedrängt werden.

Zwischen Univibrator und Koppelkondensator ist ein Kathodenfolger als Impedanzwandler eingeschaltet, um Totzeit und Erholungszeit klein zu halten. Zu jeder vollen Stunde wird über

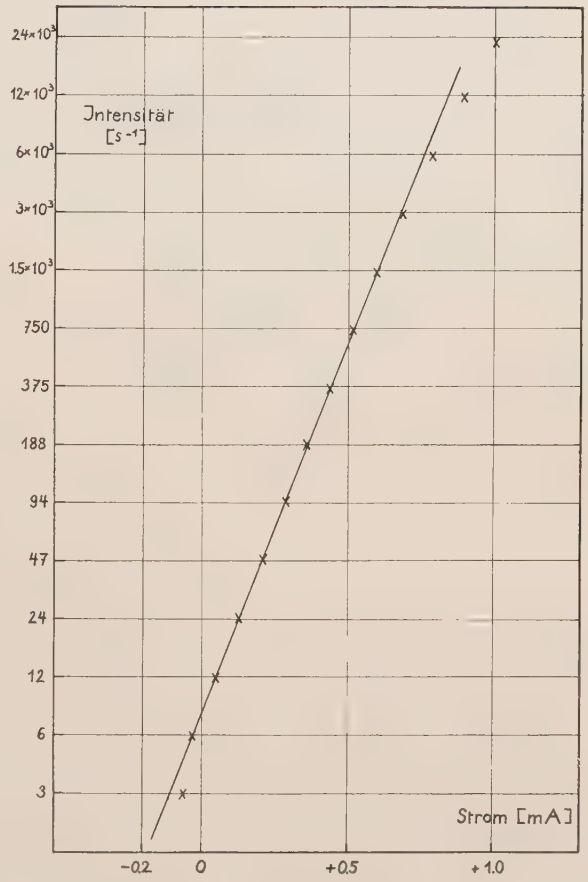

Fig. 6. Anzeige des Messinstruments im Ratemeter in Abhängigkeit von der Impulsfrequenz mit einem Koppelkondensator $G = 4.7$ nF und einem Messinstrument-"Innenwiderstand" von 46 kOhm. (Logarithmischer Massstab, unterdrückter Nullpunkt.)

Kenndaten der Schaltung

Messbare Zählraten von etwa	5 bis 10^5 s^{-1}
Bereichsumfang bis etwa	1 : 10^3 (logarithmisch)
Totzeit	5 μs
Erholungszeit je nach Koppelkapazität	3 bis 20 μs
Eingangsempfindlichkeit	20 V (positiv)
Langzeitkonstanz etwa	5%/10^4 h durch Nullpunktdrift

[5]) D. J. Porat, Rev. Sci. Instr. **27** (1956) 150.

[6]) W. C. Elmore and M. Sands, Electronics, Experimental Techniques (McGraw-Hill Book Company, New York, 1949).

ein Relais eine Zeitmarke auf das Gitter der rechten Doppeltriode gegeben. Da sich R mit der Intensität ändert, ist auch die Integrationszeitkonstante von der Intensität abhängig.

7. Netzgerät für 300 V Gleichspannung

Die Schaltung (Fig. 7) entspricht etwa dem Model 50 von Elmore[6]). Für ein universell verwendbares Netzgerät muss von der Regelröhre gefordert werden:

1. Bei 100 V Schirmgitter-, Bremsgitter- und Anodenspannung und 0 V Steuergitterspannung soll der Kathodenstrom möglichst gross sein (kleine Verlustleistung!).

2. Das Verhältnis von Steilheit zu Kathodenstrom soll möglichst gross sein (kleiner Innenwiderstand!).

3. Bei 300 V Schirmgitter-, Bremsgitter und Anodenspannung und 1 mA Kathodenstrom soll die negative Steuergitterspannung kleiner als 80 V sein (Leerlauf!).

4. Die zulässige Verlustleistung muss gross genug sein. Unter den auf ihre Eignung untersuchten Röhren El 34, EL 38, EL 152, EL 156, E 130 L, E 235 L, PL 36, TB 2.5/400, 6 BG 6, 6 Y 6, 12 E 1, 5881/6 L 6 und 6080/6 AS 7 erfüllten nur die E 130 L und die EL 34 die gestellten Forderungen.

Nach 1 min ist die Ausgangsspannung auf 100 mV (3×10^{-4}) über Stunden konstant. Nach den ersten 10^3 h ändert sie sich noch um

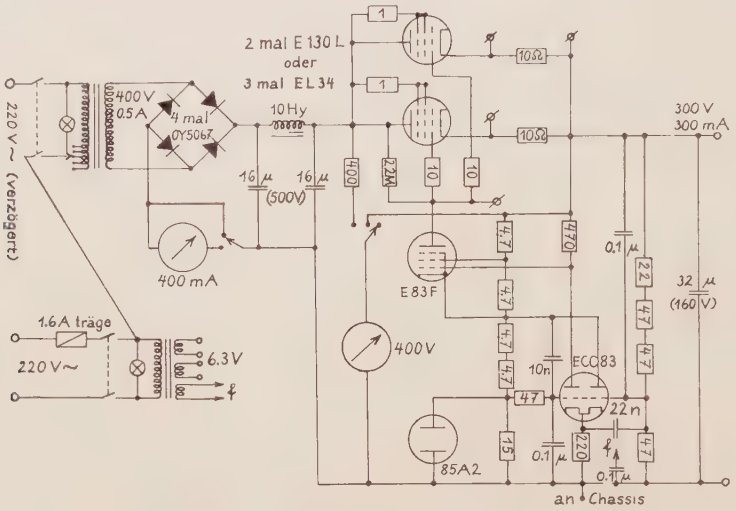

Fig. 7. Schaltschema des 300 V Netzgerätes.

Kenndaten der vorliegenden Schaltung

Netzspannungsbereich	180 bis 240 V	Innenwiderstand für Gleichstrom	< 0.1 Ohm
Belastbarkeit	0 bis 300 mA	Störspannungen einschliesslich Brumm	< 0.5 mV_{eff}
Stabilisationsfaktor für Netzschwankungen	$> 3 \times 10^3$		

maximal 0.5%/10^4 h. Die Schwankungen sind fast ausschliesslich auf die Vergleichsspannungsröhre 85 A 2 zurückzuführen. Die Störspannungen lassen sich noch weiter verkleinern[7]).

Durch Messung des Spannungsabfalls an den Kathodenwiderständen von 10 Ohm kann die gleichmässige Stromverteilung kontrolliert werden. Die Kondensatoren von 10 nF, 22 nF und 0.1 μF und die Dämpfungswiderstände von 1 und 10 kOhm an den Gittern der Regelröhren unterdrücken ein selbsttätiges Schwingen der Schaltung.

[7]) D. W. W. Rogers, Electronic and Radio Engineer **34** (1957) 320.

8. Netzgerät für Zählrohrspannung

Die Schaltung (Fig. 8) entspricht der des 300 V-Netzgerätes. Für ein universell verwendbares Hochspannungsgerät muss von der Regelröhre gefordert werden:

1. Bei 500 V Anodenspannung, 0 V Brems-, Schirm- und Steuergitterspannung soll der Anodenstrom möglichst gross sein (kleine Verlustleistung!).

2. Die zulässige Anodenverlustleistung muss gross genug sein (mindestens 20 W).

3. Die Spannungsfestigkeit muss ausreichend sein. Unter den auf ihre Eignung untersuchten Röhren EL 34, EL 38, EL152, E 130 L, PL 36, PL 81, TB 2.5/400 und 6 BG 6 war die E 130 L am besten geeignet. Wenn höhere Ströme entnommen werden sollen, sind auch die TB 2.5/400[8]) und die EL 152 brauchbar.

Auch als Penthode im Verstärkerteil ist die E 130 L am besten geeignet, da sie ausreichende Spannungsfestigkeit und einen hohen Penthoden verstärkungsfaktor besitzt.

Nach 1 min ist die Ausgangsspannung auf etwa 0.1 V (5×10^{-5}) über Stunden konstant. Nach den ersten 10^3 h ändert sie sich noch um maximal 0.25 %/10^4h bei 2 kV Ausgangsspannung. Die Schwankungen sind fast ausschliesslich auf die Vergleichsspannungsröhren 85 A 2 zurückzuführen; die Konstanz wird umso besser, je mehr Röhren 85 A 2 für die Vergleichsspannung in Serie geschaltet werden. Die Ausgangsspannung lässt sich in Stufen von etwa 4 V reproduzierbar einstellen. Die Kondensatoren von 330 pF, 22 nF und 47 nF verhindern zusammen mit den drei Anodenwiderständen von 1 kOhm ein selbsttätiges Schwingen der Schaltung, ihre optimale Grösse muss bei einer Neukonstruktion durch Versuche ermittelt werden.

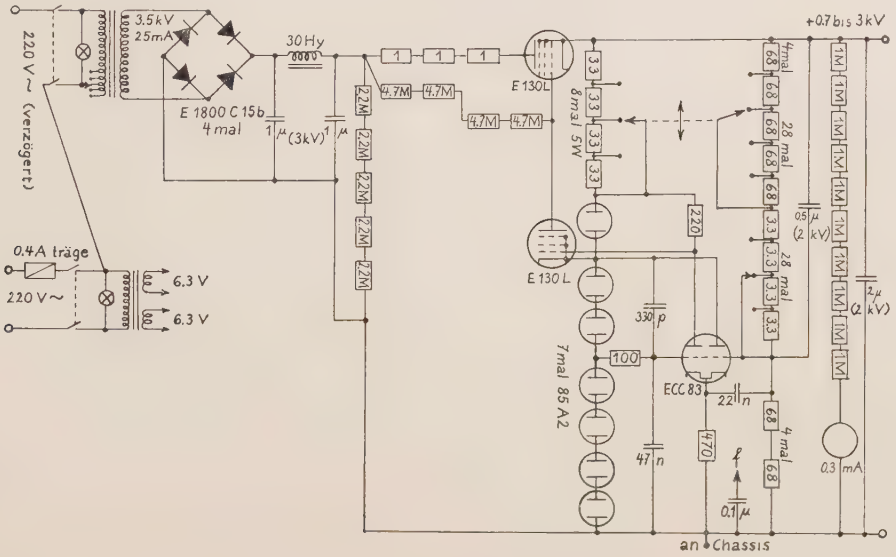

Fig. 8. Schaltschema des Hochspannungsgerätes.

Kenndaten der vorliegenden Schaltung

Netzspannungsbereich	180 bis 240 V	Stabilisationsfaktor für Netzschwankungen	$> 1 \times 10^3$
Ausgangsspannung regelbar von	0.7 bis 3.0 kV	Innenwiderstand für Gleichstrom	ca. 20 Ohm
Belastbarkeit	0 bis ca. 10 mA	Störspannungen einschliesslich Brumm	< 0.5 mV$_{eff}$

9. Zuverlässigkeit der Messergebnisse

In der Tabelle 1 sind die zu erwartenden dreifachen Standard-Abweichungen für die

[8]) P. Perilhou und J. Cayzac, Philips technische Rundschau **14** (1952) 113.

Tabelle 1

Zu erwartende dreifache Standard-Abweichung der zeitlichen Mittelwerte der Neutronenintensität, die durch die verschiedenen Fehlerquellen verursacht wird. Angaben in % der Intensität für eine Hälfte der Apparatur mit 6 Messingzählrohren mit einer mittleren Neutronenintensität von 33×10^3/h.

Fehlerquelle	Zeitmittel über			
	1 Stunde	1 Tag	1 Monat	1 Jahr
Statistik	2.0	0.4	0.08	0.02
Baromeetereffekt	0.2	0.5	0.2	0.03
Störuntergrund	0.05	0.05	0.05	0.05
Röhrenausfälle			0.1	0.4
Eingangsempfindlichkeit der Verstärker			0.03	0.10
Totzeit			0.03	0.08
Hochspannung			0.01	0.03
Niederspannungen				0.01
Zählrohre				0.02
Wurzel aus der Summe der Fehlerquadrate	2.0	0.7	0.2	0.4
Beide Apparaturhälften zusammengenommen	1.4	0.6	0.2	0.3

meistbenutzten zeitlichen Mittelwerte der Neutronenintensität zusammengestellt. Zugrundegelegt wurde die Standard-Anordnung nach Simpson[9]) mit 2 mal 6 Messingzählrohren und 2 mal 33×10^3 Imp/h. Die Unsicherheit des Barometereffektes wurde mit 0.02%/mb angesetzt[1]). Durch Hinzunahme einer dritten unabhängigen Elektronik würden sich die Fehler durch Röhrenwechsel fast völlig vermeiden lassen, die Unsicherheit des Jahresmittels der Intensität sollte sich damit also auf etwa 0.1% herabdrücken lassen.

[9]) H. Elliot and J. A. Simpson, Cosmic Radiation Neutron Intensity Monitor (University of Chicago, 1955).

Wir danken Herrn Prof. W. Gentner für seine freundliche Unterstützung. Die Anlage wurde aus Mitteln der Deutschen Forschungsgemeinschaft errichtet.

NUCLEAR INSTRUMENTS AND METHODS 7 (1960) 245–252; NORTH-HOLLAND PUBLISHING CO.

A THEORY ON OBTAINING SHORT BURSTS OF IONS FROM A BEAM OF IONS

T. K. FOWLER and W. M. GOOD

Oak Ridge National Laboratory, Oak Ridge, Tennessee

Received 7 February 1960

Many modern-day experiments in nuclear physics, particularly neutron physics, require short duration bursts of ions whose definition in energy and angle correspond to an ion beam of rather high quality. This paper treats the problem of producing bursts of ions by beam sweeping across an aperture. By considering several examples of electric-field sweeping, it is shown that (a) an essential equivalence exists between different time-varying wave forms that may be employed, (b) that the beam quality, as measured by energy and/or angular spread, is necessarily diminished in the process of burst production. In a general way it is shown that if a steady "monoenergetic" beam, characterized by y-component of momentum spread Δp_y and object size Δy, is chopped by beam sweeping, then there is a relation which in its simplest form is given by $\Delta E \Delta t = \Delta p_y \Delta y$. In this relation ΔE is the energy that must be introduced into a monoenergetic beam in order to produce bursts as short as Δt. Finally, it is shown that beam bunching results in diminished beam quality. An example is klystron bunching of a nearly parallel pulsed beam. In this case there is a relation, the simplest form of which is

$$\Delta E_a \Delta t_a = \Delta E_b \Delta t_b$$

relating the product $\Delta E \Delta t$ before bunching to that which exists after bunching.

1. Introduction

The idealized steady beam of particles almost always assumed in nuclear reaction physics can usually be provided to good approximation by d.c. accelerators such as the Van de Graaff. In recent years, the use of the time-of-flight method to measure neutron energy has, for experiments involving neutrons, come to require not only an ideal beam on target but also a beam localized in time, a beam consisting of ion bursts. Since the precision of neutron energy measurement depends upon the shortness of burst time, it follows that ion bursts arbitrarily shorter than the presently available 2 mμs are desired. However, it is essential that the pulsing mechanism not alter too greatly the ideal character of the beam.

It is the purpose of this paper to point out a complementary relationship between beam quality and pulse duration such that shortness of burst duration is always obtained at some cost in beam quality, for example, energy spread. To be more specific, we shall show that all methods of producing pulses by "sweeping" a steady beam past a stationary aperture introduce an energy spread which in turn places qualifications on further shortening the pulses by leading them through "bunching" fields. All results are obtained subject to two assumptions. First, it is assumed that in order to obtain clean bursts of ions with no ions between bursts it is necessary to "chop" a steady beam. Second, only "optical", or single-particle, effects are considered, which is to say that collective effects such as space charge, which admittedly may become critical factors, are not considered. The results presented are contained implicitly in many papers on ion optics, but they do not seem to have been extracted explicitly heretofore[1]).

For definiteness, we begin by describing several methods of chopping a beam. Next we show by specific calculation that for each of these methods burst duration and beam quality, particularly energy spread, are complementary. Then, motivated by these particular cases, we explore a general formulation of the problem in terms of a well-known differential invariant applicable to the motion of any particle acted upon by Hamiltonian forces. Finally, the general result is reapplied to the specific cases as examples of its use.

[1]) E. D. Courant and H. S. Snyder, Theory of Alternating Gradient Synchrotron, Annals of Physics 3 (1958) 1.

2. Chopping a Beam of Ions

"Beam chopping" seems the most apt term to apply to the process of extracting bursts of ions from a steady beam which for convenience we will assume monoenergetic. A supplementary

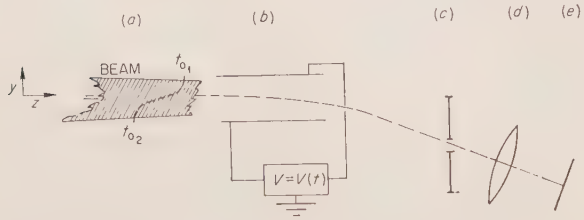

Fig. 1. Schematic representation of a beam chopper showing: (a) incident beam with profile of the beam that escapes a point aperture as a result of applying an arbitrary field $E(t_0)$; (b) deflector plates across which is applied a sweep field $(E)t = V(t)/d$; (c) burst defining aperture; (d) optical system which may include the Van de Graaff; (e) target.

term is needed to distinguish how a given ion beam is chopped. The method of beam chopping considered here which employs a time-varying electric field is figuratively-speaking one of "sweeping" the beam across an aperture. Fig. 1 shows schematically a typical sweeping system consisting of (a) a steady ion beam prior to chopping, (b) a set of parallel plates to which is applied a time-varying voltage $V = V(t)$ to sweep the beam, (c) an aperture which in practice is chosen equal in size to the beam diameter, (d) a system of ion optics including the Van de Graaff, and (e) the target.

The shortest burst obtainable by sweeping a given beam corresponds to sweeping it across an infinitesimal aperture. For simplicity, we restrict attention to this case. On account of the time-varying nature of the sweep field each ordinal point of the incident steady beam has to enter the sweep field at some characteristic time, say t_0, in order to arrive at the screen aperture point y. Thus, an instantaneous snapshot of the profile of that part of the unchopped steady beam that is able to exit through the aperture at ordinate y of the screen might look like that indicated in fig. 1(a). It is important to note that the "duration of sweep" as measured by $(t_{0_1} - t_{0_2})$ is not necessarily equal to $(t_{\text{screen}_2} - t_{\text{screen}_1})$, which is the burst duration measured at the screen.

We shall describe two practicable sweeping configurations, to be distinguished as impulse sweeping and differential impulse sweeping. The basic differences between these are shown in fig. 2. In impulse sweeping, the more literal version of the sweeping idea, the beam as a whole is given a sideways kick to cause it to pass over an aperture displaced from the original beam path. That is, each ion which manages to reach the aperture has received the same impulse, the same increase in velocity perpendicular to the original beam direction. Differential impulse sweeping differs from impulse sweeping in that each ion that manages to exit through the screen aperture has received a different impulse, depending on its time of arrival at the deflector plates, and the beam at the aperture does not have a net sideways velocity. Most systems actually used employ the latter technique for reasons that will presently appear.

Impulse sweeping, though it is the most difficult to execute, is the simplest to discuss. Consider, then, fig. 2(a). Let it be assumed, to be exact, that the beam to be chopped is imaged, i.e., focused, on a screen and that at the proper ordinate on this screen is located an infinitesimal aperture. The beam is imaged with

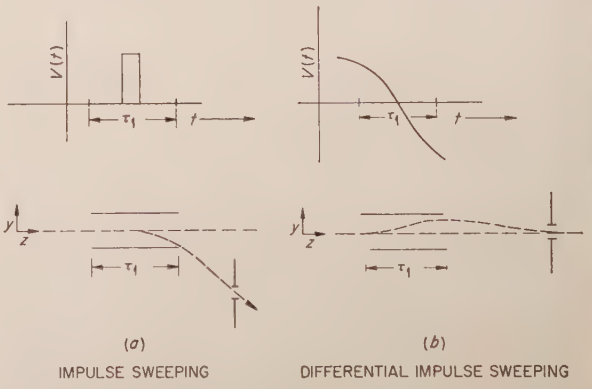

Fig. 2. Schematic representation of two distinct classes of beam sweepers identified as: (a) impulse sweeper; (b) differential impulse sweeper.

a certain size Δy and a certain angular divergence $\Delta\theta$ characteristic of the beam. Let the beam be given a component of velocity v_y or, in other words, let every particle which manages

to escape through the infinitesimal aperture be given an impulse which changes its original y-component of velocity by the amount v_y. Under these conditions, beam will emerge from the infinitesimal aperture for a time duration

$$\Delta t_{\text{screen}} = \frac{\Delta y_{\text{screen}}}{v_y} . \tag{1}$$

The component of velocity v_y arises from the impulse

$$\frac{eV_0}{md}\,\Delta t$$

and is given by

$$v_y = \frac{eV_0}{md}\,\Delta t . \tag{2}$$

The deflector plate spacing, d, must be sufficiently large to insure that the plates do not intercept deflected ions. That is, we must have

$$d > \tfrac{1}{2}\left(\frac{eV_0}{md}\right) \times (\Delta t)^2 . \tag{3}$$

For example, if a deflecting field of 20 kV/cm which accelerates protons at $\frac{1}{50}$ cm/mμs^2, is applied to a proton beam for 10 mμs, then, from (2), $v_y = \frac{1}{5}$ cm/mμs and from (1) there obtains a burst of 1 mμs from a beam focused to $\frac{1}{5}$ cm diameter. The physical requirements to produce this pulse are now a pair of deflector plates of 1 cm spacing, a plate length several cm long to insure a parallel field inside the plates, and a 10 mμs square voltage pulse exceeding 20 kV peak voltage. In addition, the burst-defining aperture must be located at such a position off axis as to accept only those ions that have received the same impulse. This approach to ion burst production is both difficult and inconvenient from the standpoint of producing the required timevarying voltage and the geometrical configuration.

For the most part, ion burst production has been accomplished in practice either by means of case (b), fig. 2, or with case (b) as the first step to be followed by bunching. In virtually all such cases the time-varying voltage has been sinusoidal with a period many times the deflector plate transit time. The theory for the deflector plate action subject to an impressed sinusoidal voltage has been given several times, and only the result will be stated here. We shall also give corresponding results for a number of other waveforms, viz.: (a) step function, (b) saw tooth, (c) ramp, in addition to (d) sinusoidal. We have discussed sweeping in terms of finite beams and point apertures. However, what will actually be calculated to compare these waveforms is a quantity called the writing speed, defined

$$\text{w.s.} = \text{writing speed} = \Delta y_{\text{screen}}/\Delta t_0 , \tag{4}$$

where Δt_0 is the difference in the times of entrance into the deflector plates of two particles, initially following the paths of an axial ray, which arrive at the screen a distance Δy_{screen} apart. It can be shown to good approximation that the writing speed, calculated for sweeping a point beam across a finite aperture Δy, can be taken as an estimate of the time Δt_0 to sweep a beam of width Δy at the screen across a point aperture.

Since the sweep voltage is continuously varying, w.s. is a function of the time t_0 when particles enter the deflector plates. It is usually defined at t_0 such that the aperture Δy lies on the original beam axis. If $y(t_0,\tau_1)$ is the y-position on emerging from the plates of a ray which enters at t_0 and crosses the plates in time τ_1, $\dot{y}$ is its velocity, a constant in the fieldfree region beyond the plates, and τ_2 is the transit time from plates to screen (see fig. 2(b)), then the position of the particle on arriving at the screen is

$$y_{\text{screen}} = y\,(t_0, \tau_1) + \tau_2 \dot{y}\,(t_0, \tau_1) \tag{5}$$

and since to good approximation τ_2 is independent of small changes in t_0, the writing speed is

$$\text{w.s.} = \frac{\mathrm{d}y_{\text{screen}}}{\mathrm{d}t_0} = \frac{\mathrm{d}y\,(t_0, \tau_1)}{\mathrm{d}t_0} + \tau_2 \frac{\mathrm{d}\dot{y}\,(t_0, \tau_1)}{\mathrm{d}t_0} . \tag{6}$$

Table 1 gives for the four waveforms listed previously a summary of the writing speeds for (a) arbitrary screen position and for (b) the screen position chosen so as to make $y(t_0, \tau_1) \approx 0$. This latter situation corresponds to having the aperture located on axis but far away from the deflector plates.

It is useful before proceeding further to

summarize in different terms what has been said so far. First, ion burst production by "beam sweeping" can be classified as to two general types (a) impulse sweeping in which the burst duration is related to the beam cross section and the velocity $\Delta y_{\text{screen}}/\Delta t_{\text{screen}}$ at the burst-defining aperture, and (b) differential impulse sweeping in which the ion burst duration is related to the beam cross section and a quantity, writing speed, which is $\Delta y_{\text{screen}}/\Delta t_0$, where t_0 is the time of entry of an ion into the deflector plates. For a beam of given diameter at the infinitesimal aperture the formulae for the ion burst duration for these two classes of "sweepers" can, at least for large distances between sweeper plates and aperture, be made to look formally alike, viz.:

$$\Delta t \begin{pmatrix} a \\ b \end{pmatrix} = \frac{\text{beam diameter at screen}}{\left(\frac{eV_0}{md}\right) \times \begin{matrix}\text{(duration of applied voltage)} \\ \text{(twice the plate-aperture transit time)}\end{matrix}} . \quad (7)$$

Second, basically there is no great advantage in the choice of one sweep voltage waveform over another. For arbitrary periods of the impressed sweep voltage, the square wave and saw tooth waveforms fully utilize the peak voltage. The ramp and sinusoidal voltages, on the other hand, develop higher voltages than are actually used unless the period is correctly related to the deflector plate transit time. These superficial differences in the type of waveform employed can be utilized to satisfy various practical aspects of the problem.

3. Burst Duration versus Beam Quality

The results of the previous section, indicating the possibility of arbitrarily short bursts of ions, would hold for a beam whose physical dimensions were sufficiently small. It will now be shown by applying the previous results in an elementary way to special situations that the

TABLE 1

Writing speed of beam sweeper as a function of transit times in deflector plates and beyond, and as a function of the amplitude V_0 and period T of the sweep voltage

Wave form $V(t)$	Writing speed aperture at arbitrary distance and on axis	Writing speed, aperture far away and on axis
(a) 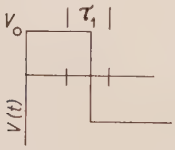	$\frac{eV_0}{md}\sqrt{2\tau_1^2 + 4\tau_1\tau_2 + 4\tau_2^2}$	$2\frac{eV_0}{md}\tau_2$
(b) 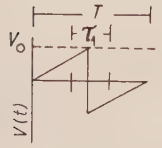	$\frac{eV_0}{md}\sqrt{\left[2(\tau_1+\tau_2) - \frac{\tau_1}{2T}(\tau_1+2\tau_2)\right]^2 - 4\left[\frac{1}{2}\tau_1^2 - \frac{1}{6}\frac{\tau_1^3}{T} + \tau_1\tau_2 - \frac{1}{2}\tau_1^2\frac{\tau_2}{T}\right]}$	$2\frac{eV_0}{md}\left[\tau_2 - \frac{1}{2}\left(\frac{\tau_1}{T}\right)\tau_2\right]$
(c) 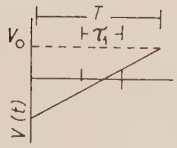	$\frac{eV_0}{md}\frac{1}{2}\left(\frac{\tau_1}{T}\right)(\tau_1+2\tau_2)$	$\frac{eV_0}{md}\left(\frac{\tau_1}{T}\right)\tau_2$
(d) 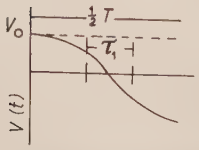	$\frac{eV_0}{md}\sqrt{\frac{T^2}{2\pi^2} + \tau_1^2 + 2\tau_2\tau_1 + 2\tau_2^2 - 2\left[\frac{T^2}{4\pi^2} + \tau_2\tau_1 + \tau_2^2\right]\cos 2\pi\frac{\tau_1}{T} - \frac{T\tau_1}{\pi}\sin 2\pi\frac{\tau_1}{T}}$	$\frac{eV_0}{md}(\omega\tau_1)\tau_2$ for $\omega\tau_1 \ll 1$

beam finiteness has a bearing upon the following important question: What is the shortest ion burst that can be produced at (a) the burst-defining aperture and (b) beyond? If the time of transit between the aperture and the target is τ, then, as is well-known, there will be superimposed upon the ion burst duration a time-spread given by

$$\Delta t(\tau) = \tfrac{1}{2}\frac{\Delta E}{E}\tau \tag{8}$$

where ΔE is the energy spread in the beam. Thus, the question just posed can better be stated in the form of two questions: What is the shortest burst that can be "chopped" from a beam? And, what energy spread is introduced by this process?

Consider the case of burst production by impulse sweeping. From eqs. (1) and (2)

$$\Delta t_{\text{burst}} = \frac{\Delta y_{\text{beam}}}{\frac{eV_0}{md}\Delta t} = \frac{\Delta y_{\text{beam}}}{v_y} \tag{9}$$

where Δt is the time duration of the voltage V_0.

In this system the shortest bursts are achieved if $v_y \gg v_z$, i.e., if the beam is bent through 90°, in which case the deflector has actually defined the ion velocity,

$$v_y \cong v \equiv \text{velocity of ion burst emerging from aperture,} \tag{10}$$

and the minimum burst duration achievable is

$$\Delta t_{\text{min}} = \frac{\Delta y_{\text{beam}}}{v}. \tag{11}$$

An important relation between burst time and energy spread is obtained by multiplying numerator and denominator of (9) by the momentum spread across the beam related to the divergence $\Delta\theta$ by

$$\Delta p_{\text{beam}} = mv_Z \Delta\theta, \tag{12}$$

which gives

$$\Delta t_{\text{burst}} = \frac{\Delta y_{\text{beam}} \Delta p_{\text{beam}}}{\Delta E_{\text{beam}}}. \tag{13}$$

The energy spread ΔE is the difference in energy of two extreme rays having y-momenta $mv_y \pm \frac{1}{2}\Delta p$, it being assumed that the beam is originally monoenergetic so v_z is the same for each.

Eq. (13) expresses a complementary relation between Δt and ΔE which, as will be seen, has a counterpart in any other sweeping system. For impulse sweeping, since the quantity $\Delta y_{\text{beam}}\,\Delta p_{\text{beam}}$ is the same wherever the beam is focused (the impulse only gives the beam a sideways velocity without altering its divergence), the conclusion is that irrespective of what is done to a beam a certain energy spread must be introduced to produce a certain burst duration.

Consider differential impulse sweeping. From (4), for the case of a ramp sweep voltage, $V(t) = V_0\, t/T$,

$$\Delta t_0 = \frac{\Delta y_{\text{screen}}}{\text{writing speed}} = \frac{\Delta y_{\text{screen}}}{\frac{eV_0}{md}\frac{\tau_1}{T}\tau_2} \tag{14}$$

where we have assumed that the aperture to deflector plate distance is large in evaluating the writing speed. Consider now fig. 3. We have from (14) for the rays in the beam designated 1, 2, 3,

$$\Delta t_{0_{12}} = \frac{0}{\text{w.s.}} = 0$$
$$\Delta t_{0_{13}} = \frac{\Delta y_{\text{screen}}}{\text{w.s.}} \tag{15}$$

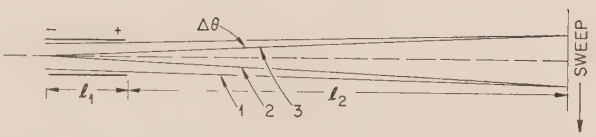

Fig. 3. Configuration of a differential impulse sweeper such that corresponding rays to two different focal points of a steady beam image are made by means of a sweep voltage to arrive at a single point simultaneously.

A little reflection will show that, since the aperture is at a large distance from the deflector plates, an axial ray must enter at approximately $-\frac{1}{2}\tau_1$ and leave at approximately $+\frac{1}{2}\tau_1$ with respect to the voltage in order to pass through the aperture. Thus, there exists voltage differences across parts of the beam as it enters and leaves the deflector plates. In particular, consider rays 1, 2, 3 of fig. 3. Between rays 1, 2 and 1,3 there exists on leaving the plates a net energy difference of order

$$\Delta E = \frac{w}{d}\frac{\tau_1}{T}\mathrm{eV}_0 \tag{16}$$

where

$$w = l_2\Delta\theta = v_Z\tau_2\Delta\theta\,. \tag{17}$$

For the situation in fig. 3, the direction of sweep is such that ions are bunched. That is, ions entering the plates last receive the greatest kinetic energy so that they tend to catch up with the ions emerging first, and the time spread due to ΔE given by (8) subtracts from the initial time difference Δt_0. Then, recalling (4), we have at the screen

$$\Delta t_{\mathrm{screen}_{12}} = \frac{0}{\text{w.s.}} - \tfrac{1}{2}\frac{\Delta E}{E}\tau_2$$

$$\Delta t_{\mathrm{screen}_{13}} = \frac{\Delta y_{\mathrm{screen}}}{\text{w.s.}} - \tfrac{1}{2}\frac{\Delta E}{E}\tau_2\,. \tag{18}$$

Now we can evidently arrange that $\Delta t_{\mathrm{screen}} = 0$, in which case, using (14),

$$\Delta t_{\mathrm{screen}_{12}} = \frac{\Delta y_{\mathrm{screen}}}{\text{w.s.}} = \frac{\Delta y_{\mathrm{screen}}}{\dfrac{eV_0}{md}\dfrac{\tau_1}{T}\tau_2}\,. \tag{19}$$

Using (16) and (17), (19) becomes

$$\Delta t_{\mathrm{screen}_{12}} = \frac{\Delta y_{\mathrm{screen}} wm}{\Delta E\tau_2} = \frac{\Delta y_{\mathrm{screen}}\Delta p_y}{\Delta E}\,. \tag{20}$$

Then, as before,

$$\Delta t_{\mathrm{screen}}\Delta E_{\mathrm{screen}} = (\Delta p_y \Delta y)_{\mathrm{screen}}\,.$$

Alternatively, (20) can be transformed to

$$\Delta t_{\mathrm{screen}_{12}} = \tfrac{1}{2}\frac{\Delta y_{\mathrm{screen}}\, wm/E}{\tfrac{1}{2}\dfrac{\Delta E}{E}\tau_2} = \frac{\Delta y_{\mathrm{screen}}\, w/v_z^2}{\Delta t_{\mathrm{screen}_{12}}}$$

or

$$\Delta t_{\mathrm{screen}_{12}} = \frac{\sqrt{\Delta y_{\mathrm{screen}} w}}{v_z} = \frac{\sqrt{l_2\Delta y_{\mathrm{screen}}\Delta\theta}}{v_z}\,. \tag{21}$$

This burst duration is the minimum that can be achieved. In setting $\Delta t_{13} = 0$, we have chosen circumstances to utilize to best advantage the energy spread in that, due to ΔE, certain rays are brought into coincidence. However, we have done this only to find that other rays then necessarily arrive at the aperture with a time difference depending on the finiteness of the beam. The minimum duration (21) for differential impulse sweeping can be compared with (11) for impulse sweeping.

4. General Formulation

We turn now to a general formulation of the problem of changes in beam quality introduced by chopping, focusing, and bending fields, which we denote collectively as an optical system. Since rays are close together on entering the optical system and on emerging to a focus, we can treat differential relations among them which are quite insensitive to the details of the optical system in question. Specifically, we shall employ the differential constant of motion which Whittaker calls a bilinear covariant[2]).

The bilinear covariant relates the coordinates of particles traversing two physically-realizable, adjacent orbits, or rays, to those of a particle traveling along a third nearby ray used as reference.

The three rays are chosen to encompass the extreme conditions in the beam. For example, to describe a steady beam we might take the three rays of fig. 4 with 2 as the reference ray. Ray 3, parallel to 2 initially, is as far from 2 as it can be and thus introduces the beam width without divergence, while ray 1, originating at the same point as 2, makes an angle with 2 taken equal to the greatest divergence[3]).

The derivation of the bilinear covariant demands only that coordinates q and momenta p be canonical conjugates, therefore satisfying

$$\frac{\mathrm{d}\boldsymbol{p}}{\mathrm{d}t} = \frac{-\partial H}{\partial \boldsymbol{q}}\,,\quad \frac{\mathrm{d}\boldsymbol{q}}{\mathrm{d}t} = \frac{\partial H}{\partial \boldsymbol{p}} \tag{22}$$

for some Hamiltonian $H(\boldsymbol{p},\boldsymbol{q},t)$. The invariant is obtained on taking successively two independent variations of Hamilton's characteristic function

$$V = \int_{t_a}^{t_b}\left(\boldsymbol{p}\cdot\frac{\mathrm{d}\boldsymbol{q}}{\mathrm{d}t} - H\right)\mathrm{d}t \tag{23}$$

where the integration is a line integral between initial and final times t_a and t_b along a real ray satisfying (22). The two variations of path pass from points on the reference ray 2 to

[2]) E. T. Whittaker, Analytical Dynamics (Dover Publications, 1944) Ch. XI.

[3]) Three-ray analyses of the sort used here are employed throughout P. A. Sturrock, Static and Dynamic Electron Optics (Cambridge University Press, 1955), See especially Ch. 2.

points on adjacent real rays 1 and 3 at the same time. Simultaneous differences in coordinates of particles on 2 and 1 will be denoted by δ; on 2 and 3, by Δ. Endpoint times t_a and t_b are not varied. Then, because (22) holds,

$$\delta V = \int_{t_a}^{t_b} \frac{\mathrm{d}}{\mathrm{d}t} (\boldsymbol{p}\cdot\delta\boldsymbol{q})\, \mathrm{d}t \tag{24}$$

and

$$\Delta\delta V = (\Delta\boldsymbol{p}\cdot\delta\boldsymbol{p} + \boldsymbol{p}\cdot\Delta\delta\boldsymbol{q})\Big|_{t_a}^{t_b}. \tag{25}$$

Now, since Δ and δ are independent, we can set $\Delta\delta V = \delta\Delta V$, terms in $\Delta\delta\boldsymbol{q}$ and $\delta\Delta\boldsymbol{q}$ drop out and we are left with

$$(\Delta\boldsymbol{p}\cdot\delta\boldsymbol{q} - \delta\boldsymbol{p}\cdot\Delta\boldsymbol{q})\Big|_{t_a}^{t_b} = 0\,. \tag{26}$$

Eq. (26) says that the differential quantity in parentheses, the bilinear covariant, has the same value at any two times along the path. More precisely, it says that, whenever particles traversing three given rays are sufficiently close together to apply differential relations, their bilinear covariant will have the same value. Between times, the rays may diverge greatly; nevertheless, if they are refocused, (26) again applies.

Since (26) applies to any canonical set of coordinates and momenta, we shall introduce orthogonal curvilinear coordinates with the reference ray as one axis, to be called z, and the other two coordinates x and y lying in a plane perpendicular to z†. For simplicity, we shall in fact restrict attention to two dimensions by assuming that the optical system applies no force in the x-direction so that x can be dropped. Furthermore, since we are interested in comparing beam quality at definite positions along the path rather than at definite times, we swap the roles of z and t, p_z and $-H$. This is a canonical transformation, being nothing more than a relabeling of variables. Finally, we obtain as the working form of (26)

$$(\Delta p_y\delta y - \delta p_y\Delta y - \Delta E\delta t + \delta E\Delta t)\Big|_{z_a}^{z_b} = 0\,. \tag{27}$$

† If we imagine the problem stated in Cartesian coordinates, any coordinate transformation, a point transformation, is canonical.

Here the notational change $E = H$ takes note of the fact that, in general, the Hamiltonian, the negative of which is the momentum canonically conjugate to t, is the energy.

Of course, with the roles of t and z reversed, the variations Δ and δ in (27) now pass from one ray to another at constant z rather than constant t. This interchange of z and t is simply a change as to which of the three parameters y, z, t is used to clock particle progress. With t as the clock, the orbit is taken to be a ray in y, z space. Now, with z as the clock, orbits are rays in y, t space. It should be noted that, being insensitive to the nature of the optical system, the bilinear covariant (27) makes no distinction between systems employing time-dependent and time-independent fields. In the d.c. case, the facts that energy is conserved and that variations involving translations in time alone are trivial must be supplied as extra conditions.

A simple example of the use of (27) is the derivation of Abbe's law. Given a monochromatic beam, so that ΔE and δE are zero, and taking for the three rays those of fig. 4, for which δy and Δp_y are zero, we get immediately the constancy of $\delta p_y \Delta y$ relating spot size to divergence[4]).

An example already treated in this paper and one of general significance for methods of pulsing beams is the case of three rays starting out simultaneously and later focusing to a point. As has been pointed out in Section 2, this is the situation, shown in fig. 5(a), pertaining to the first of the two simplifying pictures of beam sweeping whereby we treat either (1) a beam of finite width sweeping a point aperture or (2) a point beam sweeping a finite aperture. In the first instance, since time differences are zero at z_a and space differences are zero at the aperture, z_b, (27) yields

$$\delta p_y \Delta y\,|_{z_a} = (\Delta E\delta t - \delta E\Delta t)\,|_{z_b}\,. \tag{28}$$

Since the left side is not zero, one or both terms on the right are also not zero. Thus, the divergence in the beam at a shows up as an energy spread at the point aperture, as in the special case eq. (13). From the second point of view of

[4]) P. A. Sturrock, op. cit., pp. 39–45.

sweeping, shown in fig. 5(b), a result similar to (28) is again obtained. Now the bilinear covariant at a is zero, so that the inevitable divergence at the aperture must be compensated by energy spread there; in this case, (27) gives

$$(\delta p_y \Delta y - \delta E \Delta t + \Delta E \delta t)\,|_{z_b} = 0\,, \qquad (29)$$

of which (20) is a special case. For an initially monoenergetic beam, the requirement that the

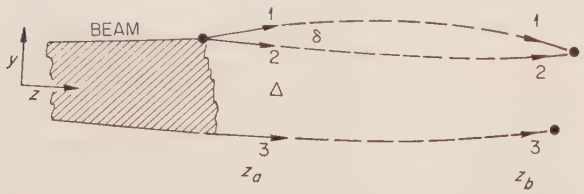

Fig. 4. Representation of a beam by means of three extreme rays from the beam.

rays be initially simultaneous is not necessary to the derivation of (28) and (29) since initially δE and ΔE are zero. In the monoenergetic case, then, the rays of fig. 5 obey (28) and (29) if they are able to converge to a point or emerge from a point.

From either viewpoint, then, it appears that chopping a beam by sweeping introduces energy spread at the aperture. In seeking counter-examples to this general maxim, one might wonder about sweeping with a magnetic field since, for d.c. fields, magnetic fields bend orbits without imparting energy spread to the particle. However, chopping demands time variation. Granting our assumption that the beam to be chopped is itself steady, it is the sweeping field which must be time-varying. Presumably it is the time-dependence of a magnetic sweeping field which introduces the energy spread predicted by (29). The only exceptions to (28) and (29) must involve non-Hamiltonian forces, such as mechanical chopping by rotating a slit past a steady beam.

So far it has only been shown that at the sweeping aperture the beam has energy spread introduced by the chopping mechanism. The further history of the beam can also be traced by the use of the bilinear covariant. Once chopped, to what extent can the beam pulse duration be shortened? How effective is the method called "bunching", whereby an applied field is programmed to decelerate the leading particles in a pulse and accelerate the trailing particles so that all emerge from the bunching field simultaneously?

To treat bunching subsequent to burst production we again take for the three rays those shown in fig. 4, where 1 and 2 introduce the divergence, but now, in order to take the pulse length into account, we take 3, still parallel to 2, as far away as possible with respect to both y and t. That is, 1 and 2 start at the same y and t at the front and upper edge of the pulse, while 3 is delayed in time to start at the rear at the lower edge. Initially, then, δt, δy and Δp_y, ΔE are all zero, but not the other differentials, in particular not δE, since the pulse was produced by chopping. All rays start at the same z_a, of course, since z is the clock. No generality is lost; the extreme beam conditions are represented.

Now, we assume that the bunching field causes 3 and 2 to emerge simultaneously, optimum bunching, accomplished in the formalism by setting $\Delta t = 0$ at the terminal point z_b. Then (27) yields

$$(\delta p_y \Delta y - \delta E \Delta t)\,|_{z_a} = (\delta p_y \Delta y + \Delta E \delta t)\,|_{z_b}\,. \qquad (30)$$

Since in practical cases it turns out that terms in E and t dominate, (30) says that the initial time spread Δt_a between rays 2 and 3, the initial pulse duration, is diminished to zero at the

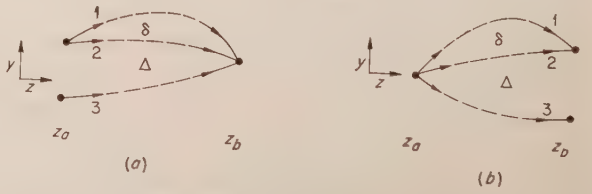

Fig. 5. Representation for applying bilinear invariant to the problem of beam sweeping showing: (a) sweeping a beam of finite width across a point apertures; (b) sweeping a point beam across a finite aperture.

expense of introducing a time spread δt_b between rays 1 and 2 which were initially simultaneous. Even if bunching accomplishes shorter times, it will be at the expense of larger energy spreads, for if $\delta t_b \ll \Delta t_a$, then also $\Delta E_b \gg \delta E_a$.

NUCLEAR INSTRUMENTS AND METHODS 7 (1960) 253–268; NORTH-HOLLAND PUBLISHING CO.

THE ELECTROMAGNETIC ISOTOPE SEPARATOR IN PRETORIA

W. E. FRAHN†, W. L. RAUTENBACH and L. WÅHLIN

Nuclear Physics Division, National Physical Research Laboratory, C.S.I.R., Pretoria, South Africa

Received 19 January 1960

A technical description is given of the electromagnetic isotope separator in Pretoria. This machine is a laboratory separator of the "Scandinavian" type using a 90° magnetic sector field of mean radius 180 cm, a maximum acceleration voltage of 80 kV, an electrostatic lens system with two-directional focussing, and magnetic arc sources with end extraction. Special design features make the instrument suitable for the performance of certain nuclear experiments. Particular attention has been given to ion beam formation in the separator in order to obtain optimum resolving power and good transmission at high ion currents.

1. Introduction

For work in nuclear spectroscopy it is desirable and, in fact, in many cases indispensable to use separated isotopes in reasonable quantities, either in the preparation of sources for β- and γ-ray spectrometry or as targets for accelerator irradiation. Among the separators employing magnetic mass analysis, a special category of machines, particularly suited for this type of work, has been developed during the past two decades. These laboratory separators are characterized by the fact that they permit a rapid and nearly complete separation of isotopes of all elements, both stable and radioactive, in quantities necessary and sufficient for nuclear spectroscopical purposes (up to about 1 microgramme-atom per hour). The ion currents required are in the region between one and several hundred microampères. The laboratory separator thus occupies an intermediate position between mass spectrometers and large-scale machines of the Calutron type[1]).

After a visit by one of the authors to several European separator groups early in 1955, it was decided to build a laboratory separator of the "Scandinavian" type, which was to be used in connection with the cyclotron, beta-spectrometers and other equipment (then under construction) in the Nuclear Physics Laboratory in Pretoria. The Scandinavian type of separator, originated by J. Koch in Copenhagen[2]), uses a 90° magnetic sector field and a high acceleration voltage. At present there are four separators of this type, working under very similar conditions, in Copenhagen[3–6]), Stockholm[7–10]), Uppsala[11,12]) and Gothenburg[13,14]). The operational experience gained with these machines up to 1955 suggested a number of improvements, advantage of which was taken in the design of the Pretoria separator, and which in the meantime

† Now at the Department of Physics, University of Stellenbosch, Cape Province.

[1]) A comprehensive review of laboratory separators has been given by J. Koch in: J. Koch (editor), R. H. Dawton, M. L. Smith and W. Walcher, "Electromagnetic Isotope Separators and Application of Electromagnetically Enriched Isotopes" (North-Holland Publishing Co., Amsterdam, 1958).

[2]) J. Koch, thesis, Copenhagen 1942.

[3]) J. Koch and B. Bendt-Nielsen, Mat. Fys. Medd. Dan. Vid. Selsk. **21**, No. 8 (1944).

[4]) J. Koch, in "Mass Spectroscopy in Physics Research", National Bureau of Standards Circular 522 (Government Printing Office, Washington D.C., 1953), p. 165.

[5]) K. O. Nielsen and O. Skilbreid, Nuclear Instruments 2 (1958) 15.

[6]) K. O. Nielsen, thesis, Copenhagen 1958.

[7]) I. Bergström, S. Thulin, N. Svartholm and K. Siegbahn, Arkiv Fysik **1** (1949) 281.

[8]) I. Bergström, Arkiv Fysik **5** (1952) 191.

[9]) S. Thulin, Arkiv Fysik **9** (1954) 107.

[10]) T. Alväger and J. Uhler, Arkiv Fysik **13** (1958) 145.

[11]) G. Andersson, Phil. Mag. (7) **45** (1954) 621.

[12]) G. Andersson, Arkiv Fysik **12** (1957) 331.

[13]) O. Almén and A. Lundén, Arkiv Fysik **8** (1954) 2.

[14]) O. Almén, G. Bruce and A. Lundén, Nuclear Instruments **2** (1958) 249.

were also included in the further development and reconstruction of the Scandinavian separators[5,10]). Apart from these improvements, this separator was to have special design features which would make it suitable for the performance of certain experiments. The principles of design are discussed in section 2, and a technical description of the separator is given in section 3.

Construction of the separator started early in 1956, and by the end of 1957 the first separated ion beams were collected on a provisional collector screen near the exit boundary of the magnet. After completion of the collector system proper, the machine went into full operation early in 1958. Since then some routine separations have occasionally been carried out, but the separator has mainly been used for the investigation of ion beam formation and the study of operational characteristics (section 4). As an example of work with radioisotopes, the separation of radio-phosphorus is described in section 5.

A separate investigation on ion sources started in the end of 1957, first with an auxiliary testing installation and later in conjunction with the separator itself. The results of these investigations will be reported in detail elsewhere[15]).

2. Design Principles

2.1. GENERAL REQUIREMENTS

The basic requirements for a laboratory separator are (i) the complete separation of the isotopes of even the heaviest elements, and (ii) the production, within a sufficiently short time, of such quantities of these isotopes as are necessary and sufficient for nuclear spectroscopical purposes. The second condition implies a collection rate in the region 10^{-2} to 1 microgramme-atoms per hour. From the production formula (Faraday's law)

$$m = \frac{A}{eN} It \tag{1}$$

(m = separated mass, I = ion current, t = separation time, A = mass number, N = Avogadro's number) it follows that the separator should be able to handle ion currents between one and several hundred micro-ampères. Condition (i) requires the distance between neighbouring mass lines to be larger than twice the half-width of the lines for all mass numbers up to $A = 240$. The implications of this condition follow from the well-known ion optical properties of magnetic sector fields[16]).

An ion of mass M, moving in a homogeneous magnetic field B under the acceleration voltage V, describes a circular path of radius

$$R = \frac{1}{B}\left(\frac{2MV}{e}\right)^{1/2}, \tag{2}$$

and ions of different masses are focussed at different positions on an image surface. The mass dispersion

$$D = \frac{1}{2}\frac{\Delta M}{M} K \tag{3}$$

gives the distance between the images of the masses M and $M + \Delta M$ in a plane perpendicular to the central ray for ions of constant energy. The dispersion coefficient K for a 90° sector field and normal entrance and exit is given by

$$K = R + l, \tag{4}$$

where l denotes the ion path length between image and exit boundary of the magnet.

The resolving power is defined by

$$P = \frac{M}{(\Delta M)_0},$$

where $(\Delta M)_0$ is obtained from the condition $D_0 = b$ = half-width of the mass line M (measured in a plane perpendicular to the central ray). Hence

$$P = \frac{K}{2b} = \frac{D}{b}\frac{A}{\Delta A}. \tag{5}$$

Therefore, to satisfy condition (i), a resolving power of at least 480 is required.

The finite line width b is caused by a number

[15]) W. L. Rautenbach, thesis, to be published.

[16]) See e.g. H. Ewald and H. Hintenberger, "Methoden und Anwendungen der Massenspektroskopie" (Weinheim, 1953).

of contributions b_i[9]) which arise from: (1) fluctuations of the acceleration voltage

$$b_1 = \frac{1}{2}\frac{\Delta V}{V} K ,$$

of the magnetic field

$$b_2 = \frac{\Delta B}{B} K ,$$

and the spread of thermal energies of the ions from the ion source

$$b_3 = \frac{1}{2}\frac{\Delta E}{V} K ;$$

(2) aberrations of the magnetic sector field ($b_4 = R\alpha^2$, α = entrance angle of the beam), of the electrostatic lens system (b_5), and the angular spread caused by the thermal velocity components normal to the accelerating field near the emitting aperture (b_6); (3) interactions of the ions with residual gas molecules (b_7) and with their own electrostatic field (space charge broadening, b_8).

High isotopic purity of the separated samples requires high resolving power P. The mass dispersion can be increased by increasing the size of the separator. However, since the contributions to the line width are approximately proportional to the radius R, the resolving power is very nearly independent of the size of the separator†. Therefore it is necessary to minimize the line width b for a given radius R.

The contributions from fluctuations can be made negligible by beam position stabilization. The aberrations can either be corrected (e.g. by a suitable shape of the magnet boundaries) or by using small beam angles only. The main contributions to the line width then arise from the interaction of the ion beam with the residual gas and from space charge effects. The former contribution is mainly due to small-angle elastic scattering and ionization, and is of the form

$$b_7 = \text{const.}\,\frac{R}{(MV)^{1/2}} . \qquad (6)$$

The line broadening due to space charge is given by

$$b_8 = \text{const.}\, M^{1/2}\frac{I}{V^{3/2}}\frac{R^2}{d} , \qquad (7)$$

where d is the diameter of the beam at the entrance to the magnetic field. For high ion currents this space charge contribution is predominant. It can be reduced by space charge compensation, i.e. neutralization by electrons or negative ions arising from ionization of the residual gas molecules and charge exchange, or by secondary electrons liberated from the walls of the vacuum chamber[17]). Space charge neutralization takes place mainly inside the region of the magnetic field, and is still effective at such low pressures as are necessary to keep b_7 sufficiently small. The beam broadening outside the magnetic field can be counteracted by an electrostatic lens which corrects the negative lens action of space charge.

For a given ion current and constant geometry, both b_7 and b_8 can be reduced by increasing V. Therefore, the main requirement for high resolution is the use of a high acceleration voltage.

2.2. SPECIAL REQUIREMENTS

Apart from its normal use for the separation of stable and radioactive isotopes, it is intended to perform certain experiments with the Pretoria separator. The special design features required by these experiments will now be discussed.

One of the projects is to use the separated ion beams for the study of the interaction of ions with matter in the region 10—50 keV. A laboratory separator is particularly suited for the investigation of ionic impact phenomena, since it provides geometrically well-defined monoenergetic beams of ions of uniform mass. Energy and mass number of the ions can easily be varied, and different target materials used.

† When space charge effects are taken into consideration, the size-independence of P is only valid if for similar machines the beam diameter d scales proportional to the radius R (see eq. (7) below). This is a consequence of the general similarity laws for the motion of charged particles in electromagnetic fields under the influence of space charge.

[17]) W. Walcher, in "Electromagnetic Isotope Separators and Applications of Electromagnetically Enriched Isotopes" (North-Holland Publishing Co., Amsterdam 1958).

These experiments require an unusually large collector chamber in order to accomodate the target arrangement and measuring equipment. By these means it is possible to measure angular distributions of the secondary particles. For this purpose the distance between neighbouring mass lines has to be large, i.e. it is essential to have a high mass dispersion. Furthermore, two-directional focussing is required to concentrate the beam on a small target area.

Our main objective is to operate the isotope separator in conjunction with the cyclotron[18]) and a beta spectrometer for nuclear spectroscopical studies of very short-lived beta-active isotopes. In this experiment, the activity will be produced by cyclotron irradiation of a target inside the ion source of the separator†. By continuous production and mass separation of the short-lived reaction products, an equilibrium amount of activity can be collected on a small area of a thin collector foil which at the same time serves as the source of a lens-type beta spectrometer. In this way it should be possible to investigate the spectra of pure isotopic samples of beta emitters with half-lives too short (< 15 min) for the usual procedure of nuclear spectroscopy with separated activities.

This experiment requires the construction of a special ion source with the following properties: (1) The activity produced in the surface layers of the internal target has to be transported efficiently into the discharge chamber for ionization. A promising method is sputtering by the ions of the gas discharge[19]). (2) The lower limit of half-lives in this method is essentially given by the average time spent by an ion in the source. To keep this as short as possible, the time between condensation and re-evaporation of charge material on the walls of the discharge chamber has to be shortened by sufficiently high temperatures. A new type of ion source combining both properties, the "high temperature sputtering ion source", has been constructed and tested with satisfactory results[15]).

Since the equilibrium activity on the collector should be as high as possible, and the specific activity in the target is proportional to the half-life, the maximum total ion currents which can be handled by the separator have to be used. Losses of useful ions from the beam should be kept at a minimum, i.e. a high transmission is required. Again it is essential to achieve high mass dispersion, and two-directional beam focussing is necessary to form an image sufficiently small to serve as a source for the lens spectrometer.

2.3. DESIGN FEATURES

The mass dispersion is determined by the size of the separator. Since the spacing between neighbouring lines of mass number A and $A + 1$ is given by $D_{(\Delta A = 1)} = K/2A$, a high dispersion is obtained by chosing a fairly large radius R. Because of eq. (4), the mass dispersion can be further increased by focussing at a distance l from the exit boundary of the magnet. At the distance $l = R$ the dispersion is doubled, but it is necessary to ensure that the resolving power P remains at least unchanged under these conditions. An inspection of the influence of l on the line width[9]) gives the following results: No change in P results from the fluctuation contributions since they are proportional to K. The aberration and interaction contributions are approximately independent of l, thus entering P with a factor $K/R = 1 + l/R$. Since the latter contributions are predominant, an increase of P by approximately a factor 2 can be expected at the distance $l = R$. Focussing at this distance has the further advantage of leaving sufficient space for a large collector system, and for appropriate shielding necessary in the experiment on short-lived activities.

The total ion currents which can be handled in

† This type of experiment has been discussed for some time among the Scandinavian separator groups, especially by J. Koch at a meeting in Uppsala in January 1955. See also J. Koch, Proc. Conf. on Electromagnetically Enriched Isotopes and Mass Spectrometry, Harwell, 1955 (Butterworth's Scientific Publications, London 1956).

[18]) J. J. Burgerjon, S. J. du Toit and C. A. J. Kritzinger, Nuclear Instruments **3** (1958) 323.

[19]) J. Druaux and R. Bernas, Proc. Conf. on Electromagnetically Enriched Isotopes and Mass Spectrometry, Harwell, 1955 (Butterworth's Scientific Publications, London 1956) p. 30.

laboratory separators are limited by space charge effects. From general similarity principles, and in particular from eq. (7), it can be seen that the total current is connected with the acceleration voltage by the relation $I \propto V^{3/2}$. Therefore, the maximum ion current can be increased by using a high acceleration voltage V. As previously mentioned, high acceleration voltages are essential to obtain high resolution and, in addition, space charge neutralization becomes more effective with increasing V.

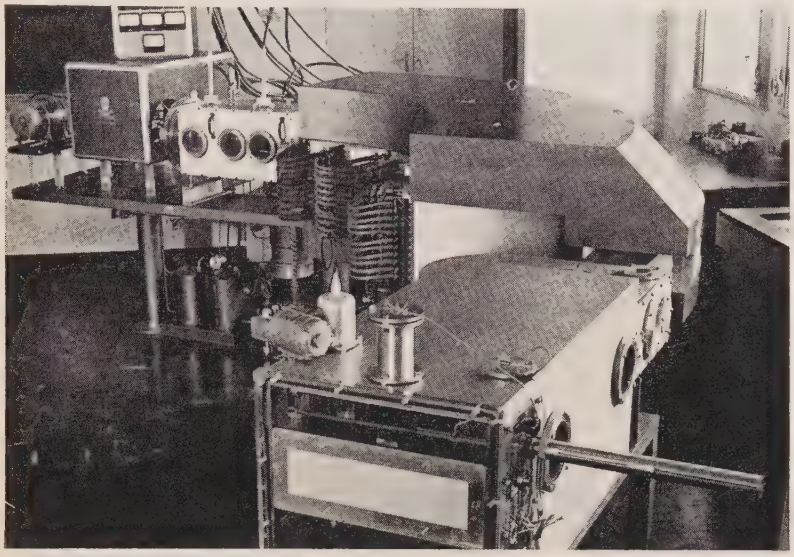

Fig. 1. General view of isotope separator.

The focussing condition for an image distance $l = R$ requires the virtual object to be situated at the same distance R from the entrance boundary of the magnet. For practical reasons it appeared advisable to place the ion source at a shorter distance (0.6 R) and to use a unipotential electrostatic converging lens to comply with the condition for symmetrical focussing. By means of the lens system, the entrance angle and width of the beam can be altered, and different focussing conditions realized by changing the distance between lens and ion source and by variation of the lens voltage during operation. Even in the case of a symmetrical arrangement, a lens system is necessary to correct the aberration due to the negative lens action of space charge.

Since the magnetic sector field acts as a cylinder lens, there is no focussing in axial direction. In order to obtain focussing in both radial and axial directions, a system of horizontal plates with an adjustable DC voltage is situated before the entrance to the magnet. Over other possible methods of line height reduction (e.g. magnetic double-focussing by a negative radial magnetic field gradient or oblique entrance and exit of the beam), this has the advantage that the line height is continuously variable during operation, and all mass lines are equally reduced in height without appreciable radial defocussing[10]).

The final choice of the main parameters was made as follows: Mean radius $R = 180$ cm. This gives a spacing $D = R/A = 0.75$ cm between neighbouring mass lines at $A = 240$ and, from the minimum resolving power required $P = 500$, a maximum allowable line width $b_{\max} = 3.6$ mm. The maximum acceleration voltage is $V_{\max} = 80$ kV. The necessary maximum magnetic field then follows from eq. (2): $B_{\max} = 3500$ gauss. The pole gap h_m should be smaller than 10% of the radius; we chose $h_m = \frac{1}{15} R = 12$ cm and a pole width $w_m = 40$ cm.

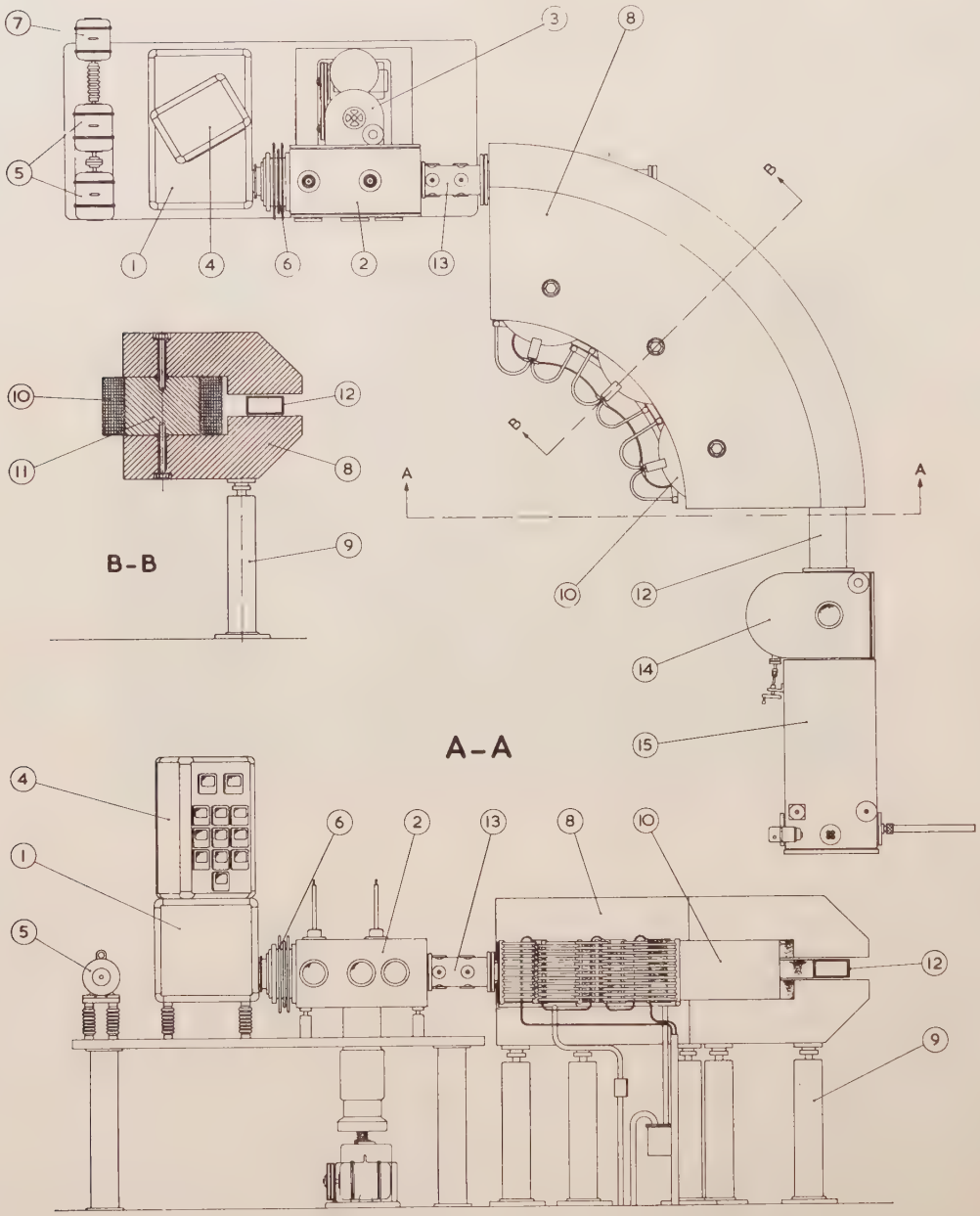

Fig. 2. Assembly drawing of isotope separator.

3. Technical Description

3.1. GENERAL

A general view of the separator is shown in fig. 1, and an assembly drawing is given in fig. 2. The ion source and accessories are housed in an aluminium cabinet (1). The acceleration and focussing systems are mounted in a steel chamber (2), to which a pump chamber (3) is attached. The ion source unit, consisting of cabinet (1) with an instrument case (4) placed on top of it, and two DC generators (5), rests on perspex insulators. The ion source is connected to the acceleration chamber by a cylindrical perspex insulator (6). The whole system, together with a synchro-motor (7) driving the DC generators by an insulating shaft, is

mounted on a large steel table supported by three steel pillars. The magnet (8) rests on five steel columns (9) which are fitted with jacking screws and thrust bearings for vertical adjustment. The magnet is excited by three coils (10) with separate cores (11). The stainless steel deflection chamber (12) is on one side connected to the acceleration chamber by a brass tube (13) containing the x- and y-deflection plates, and on the other side by a pump chamber (14) to the collector unit (15). All components of the separator can easily be disconnected and reassembled in a short time.

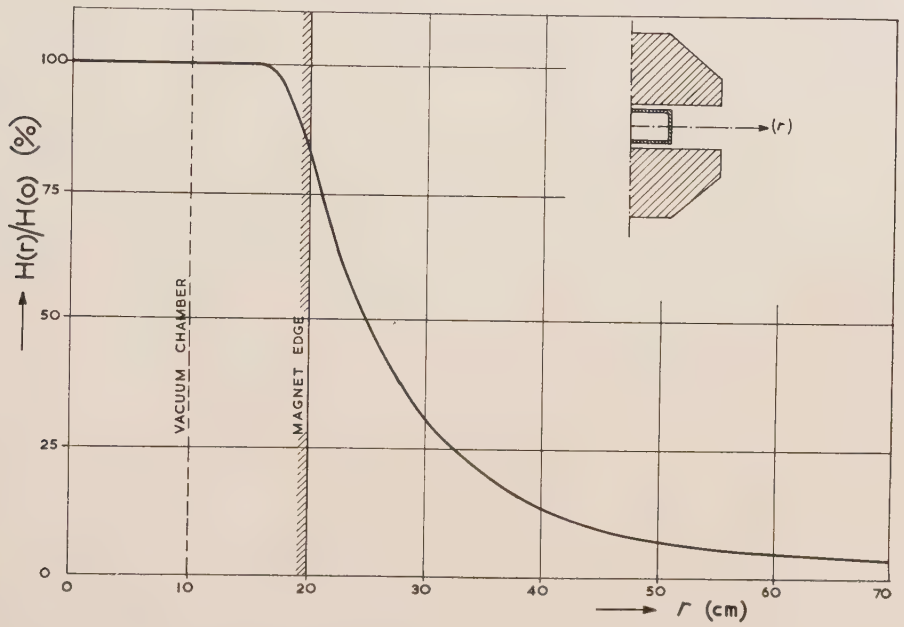

Fig. 3. Radial magnetic field distribution.

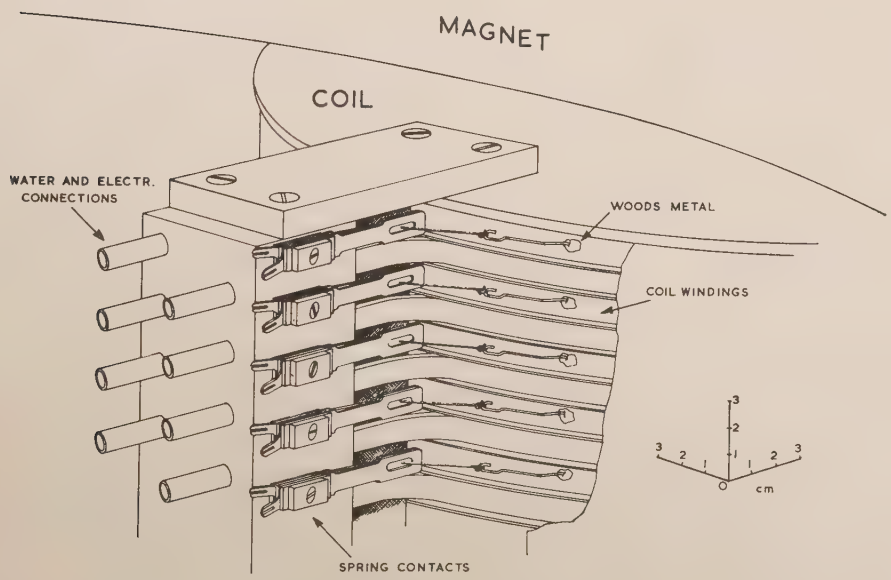

Fig. 4. Magnet coil with safety device.

3.2. MAGNET AND POWER SUPPLY

The magnet is of 90° sector type with mean radius $R = 180$ cm, pole gap $h_m = 12$ cm and pole width $w_m = 40$ cm. It is made of mild steel with a carbon content less than 0.1%, provided by ISCOR at Pretoria and machined by VECOR at Vanderbijl Park. The distance between the pole faces is constant within 0.025 mm. The maximum magnetic field is 3500 gauss, and the field homogeneity is better than 0.2% within 5 cm from the pole face edges. The field distribution along the optical axis in the vicinity of the magnet boundaries is practically identical with the radial field distribution given in fig. 3.

The field is produced by three series-connected coils wound on steel bobbins. Each coil consists of 22 sections with altogether 638 turns of flattened $\frac{3}{8}''$ copper tubing with an inner cross-sectional area of 1×11 mm² for water cooling.

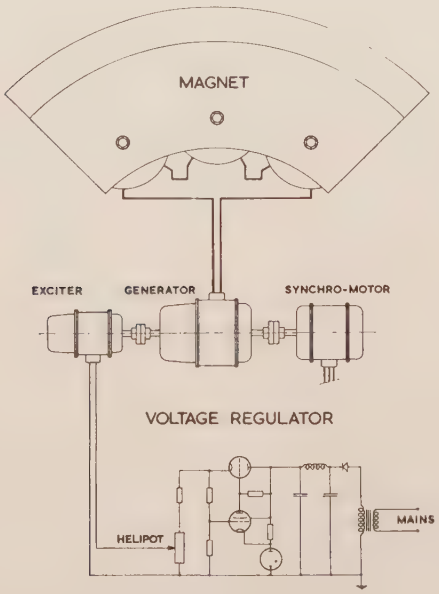

Fig. 5. Magnet power supply.

The coil sections are electrically in series, but are pairwise parallel connected in the cooling circuit. The total water flow through the recirculating system is 18.5 l/min at a pressure of 5 atm. Thermofuses on the coil sections (fig. 4), water flow and excess pressure relays protect against failures in the cooling circuit.

The magnet current is supplied by a 180 V × 70 A Siemens & Halske motor-generator with exciter. It is controlled by varying the current through the field coils of the exciter. A schematic diagram of the power supply unit is given in fig. 5.

3.3. VACUUM SYSTEM

The vacuum system is shown in fig. 6. The total volume is 455 l. It consists of the following parts: steel acceleration chamber (1), brass connecting tube (2), stainless steel deflection chamber (3), steel collector chamber (4), and two steel pump chambers (5). The vacuum is produced by two oil diffusion pumps type Balzers 1000 (6), each with a pumping speed of 1000 l/sec at 10^{-4} mm Hg. These are backed by one fore vacuum pump type Balzers Duo 25 (7) Another backing pump of the same type is used for rough pumping of the collector chamber (8). Each pump chamber is provided with a liquid air trap (9). Each oil diffusion pump has a high vacuum valve (10) and a motor-driven fore vacuum valve (11). The collector chamber can be closed off from the main system by a sliding shutter of Siegbahn type (12), and air can be let in by a valve (13). The collector and acceleration chambers can be opened by removing the perspex window (14) and the steel front plate (15), respectively. The high vacuum is measured at both the acceleration and collector chambers by Penning ionization gauges (16), and the fore vacuum by compensation-type thermocouples at the main backing pump and at the collector chamber.

The minimum pressure obtainable in the system is 3×10^{-6} mm Hg. The pressure during operation is in the region $6–8 \times 10^{-6}$ mm Hg depending on the total ion current. For high ion currents it proved advantageous to connect another oil diffusion pump type Balzers 1000 (17), complete with high and fore vacuum valves, Penning gauge and liquid air trap, to the deflection chamber. All three diffusion pumps are connected to the backing pump (7) by a brass tube (18).

Each oil diffusion pump is provided with a

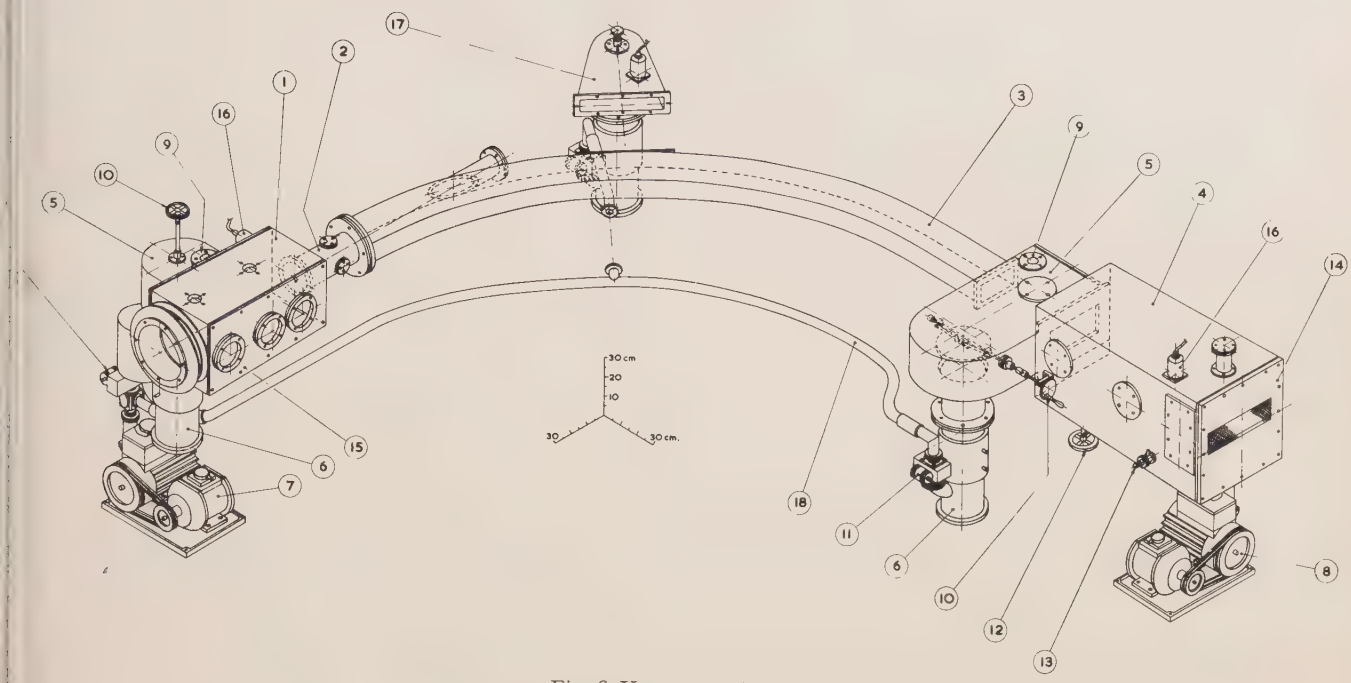

Fig. 6. Vacuum system.

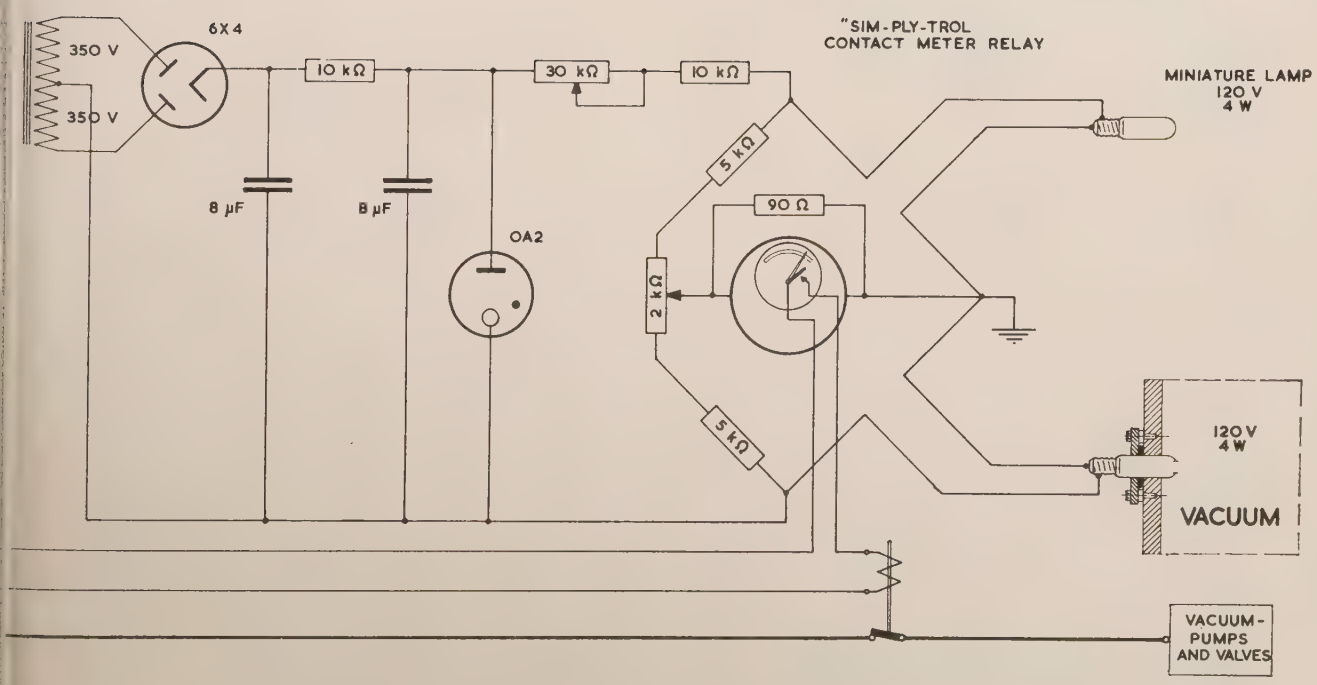

Fig. 7. Vacuum safety device.

water flow and a thermo-relay which cuts off the power in the event of cooling failure. A vacuum relay (fig. 7) is connected to the fore

The motors are fed from a 12 V battery system to be able to operate in the event of main power failure.

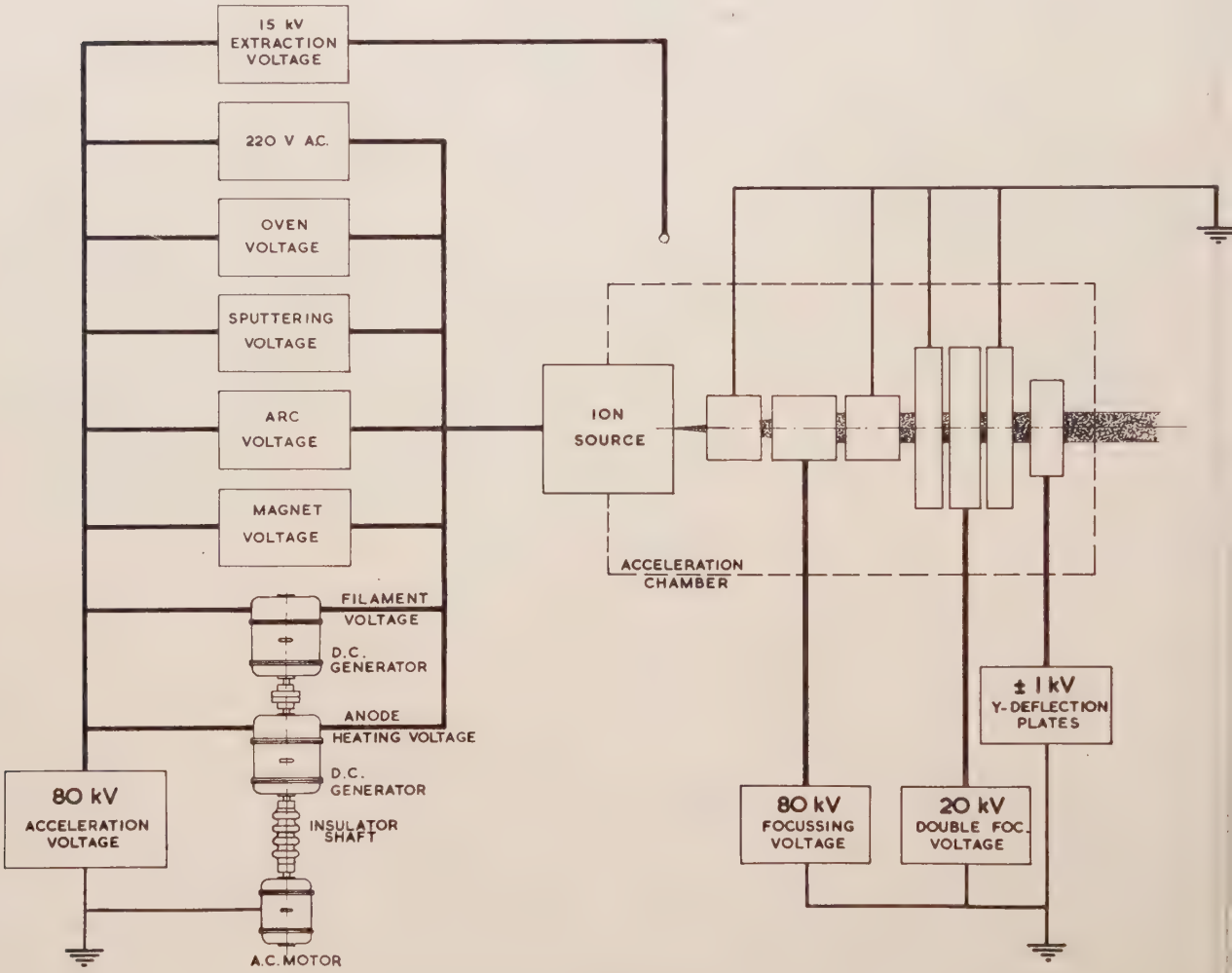

Fig. 8. High tension system.

vacuum system to protect the oil diffusion pumps against pressure rise caused by sudden air leaks. The vacuum relay is an electronic device based on the Pirani principle. Two glowlamps, one in a fixed vacuum and the other exposed to the vacuum system, are connected in a bridge circuit. The contacts on the meter relay can be set to switch off the pumps at any given pressure in the region 10^{-2} — 2 mm Hg. The motor-driven valves close automatically when the power for the pumps is switched off.

3.4. HIGH TENSION SUPPLIES

A block diagram of the high tension system is given in fig. 8. The 80 kV acceleration voltage, the focussing voltage and all voltages for the ion source (except for filament and anode heating) are provided by a Beta Electric model 2080-2P-C2 power supply, in which all components are under oil for corona-free operation. All voltages mentioned above (except the auxiliary 220 V AC) are variable by means of variacs. Insulating transformers are used to

supply the ion source voltages at high voltage level. The line voltage is stabilized to 1 part in 1000 by means of a Sorensen regulator.

The filament and the anode heating element of the ion source are supplied by two DC generators. These generators operate on high voltage level and are driven by a synchro-motor on earth potential via an insulating shaft. The field excitation is regulated by means of resistors operated by servo-mechanisms via insulating rods. The high voltage supply for the double-focussing plates is of radio-frequency type.

The specifications for the different power supplies are given in the following table.

Power supplies	Voltage	Max. current	Internal resistance	Ripple
Acceleration	0–80 kV + DC	2 mA	4.5 MΩ	< 0.1%
Focussing voltage	0–80 kV + DC	1 mA	4.5 MΩ	< 0.1%
Extraction voltage	0–16 kV + DC	1 mA	0.9 MΩ	< 0.1%
Magnet	0–500 V DC	0.4 A	800 Ω	< 2 %
Anode supply	0–200 V + DC	5 A	35 Ω	< 2 %
Oven heating	0– 25 V AC	25 A	—	—
Filament	0– 30 V DC	25 A	—	—
Auxiliary	220 V AC	4 A	—	—
Anode heating	0– 30 V DC	25 A	—	—
Sputtering	0–500 V DC	300 mA	—	—
Double focussing	0– 20 kV DC	100 μA	—	—
Vertical deflection	— 1– + 1 kV	1 mA	—	—

3.5. CONTROL CIRCUIT

All meters (except the meters for the ion source) and controls for the isotope separator are mounted on a control cabinet situated near the collector chamber (fig. 9). The controls for the ion source and the focussing voltages are within comfortable reach while focussing the mass lines on the fluorescent screen. The meters for the ion source operate at high voltage level and are mounted in an aluminium case on top of the ion source cabinet. The motor-generator and the pump for water cooling of the magnet are started by a press button. Pilot lamps indicate blown thermofuses on the magnet coils or failure in the cooling system. Meters show magnet voltage and current and the temperature of the cooling water. The vacuum pumps can be switched on or off by means of press buttons. Instruments show the current and the temperature of the cooling water through the diffusion pumps, and pilot lamps indicate the position of the motor-driven fore vacuum valves. A Balzers KV 313 vacuum meter is used to measure the fore and high vacuum. A spot galvanometer-type radiometer GVM 23 measures the ion current at the collector, and a chopper-stabilized DC amplifier is used as ion current integrator. A Dumont type 241 oscilloscope is used for line scanning, and a Honeywell Brown 0–10 mV chart recorder for the automatic recording system[20]).

3.6. ION SOURCES

Three different types of ion sources are used: (1) a conventional gas ion source mainly for testing purposes, (2) a high temperature ion source of Nielsen type[21,22]), and (3) a newly developed high temperature sputtering ion source. A detailed description of the latter and its characteristics is given elsewhere[15]).

All ion sources fit into the same magnet holder and can easily be interchanged. Since the ion source is kept at high tension, it is connected to the acceleration chamber by a large cylindrical perspex insulator. The position of the

[20]) L. Wåhlin, Nuclear Instruments **7** (1960) 269.
[21]) K. O. Nielsen, Nuclear Instruments **1** (1957) 289.
[22]) O. Almén and K. O. Nielsen, Nuclear Instruments **1** (1957) 302.

source on this insulator can be adjusted by means of setting screws. The ion source is centered with respect to the acceleration and focussing system by viewing through an extension tube of the deflection chamber with the aid of a telescope. The ion source is cooled by paraffin oil obtained from a recirculating system, with the pump and water heat exchanger operating on earth potential. Insulating plastic pipes connect the ion source to the recirculating system.

A gas battery consisting of four glass containers in parallel, filled with neon, argon, krypton and xenon, respectively, is connected to the ion source by a needle valve. These gases are used for mass reference and for stabilizing the discharge in case of solid charge material. The needle valve is controlled from the control board. The fore vacuum pump for the collector chamber is used for evacuating the ion source system. A vacuum relay ensures that the high tension is switched off during evacuation.

Fig. 10 shows the inside of the ion source cabinet. The high temperature sputtering ion source is seen in position, with the vacuum lock system for exchange of sputtering electrodes.

3.7. ACCELERATION AND FOCUSSING SYSTEM

For ion beam formation studies (see section 4), several different types of electrostatic lens systems have been used. However, for most applications a lens system is employed which is similar to that of the Stockholm separator[10]). This system forms a unipotential retarding lens, consisting of two concentrical steel cylinders. The outer cylinder, which has a diameter of 13 cm and a length of 31 cm, is connected to earth, while the inner cylinder, measuring 9 cm in diameter and 14 cm in length, is connected to the focussing voltage and suspended by perspex insulators. The lens support slides on rails, and the distance between lens system and ion source can be varied by means of a vacuum sealed screwing mechanism.

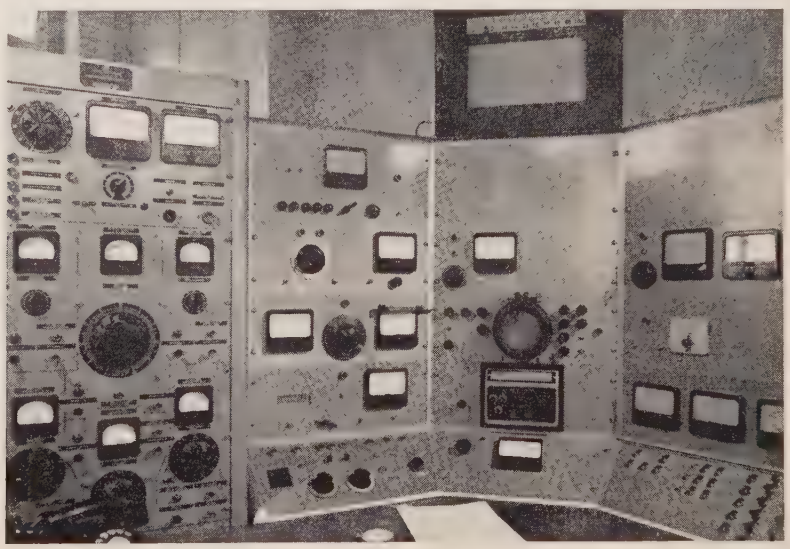

Fig. 9. Control board.

Axial focussing is obtained by an electrostatic cylinder lens, also similar to that used in the Stockholm separator[10]). It consists of three pairs of parallel horizontal aluminium plates. The two outer pairs are on earth potential and the middle pair is connected to the 2—20 kV double-focussing voltage. The plates measure 30×7 cm^2 and are 8 cm apart; the distance between each pair is about 1 cm.

Both the lens system and the axial focussing

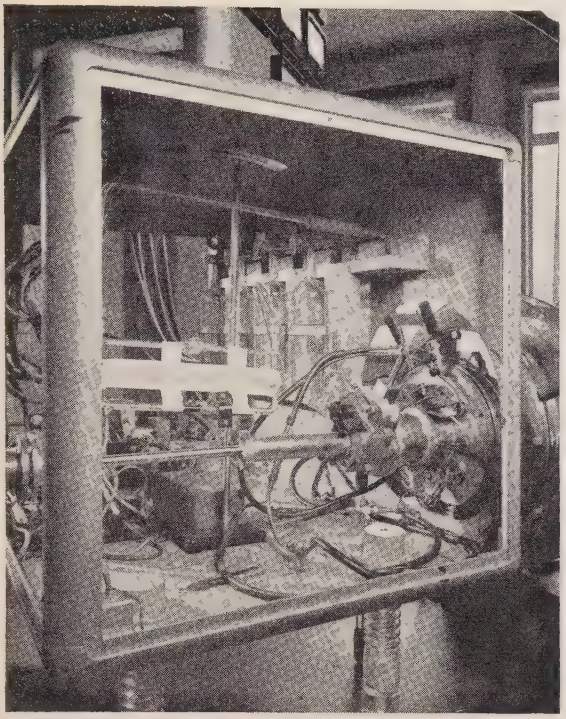

Fig. 10. Ion source and accessories.

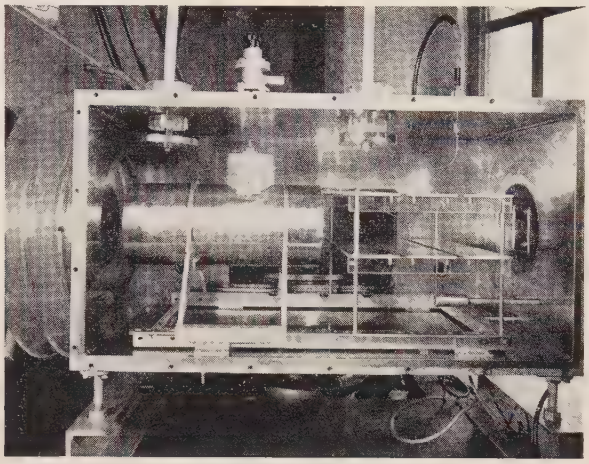

Fig. 11. Acceleration and focussing system.

system are mounted in a chamber made of mild steel to screen off the magnetic stray field. The chamber rests on jacking screws for lining-up. The front plate of the chamber has three glass windows for visual observation of the ion beam.

In fig. 11 the acceleration chamber is shown with the front plate removed. Inside on the left a part of the ion source can be seen, followed by the lens and axial focussing systems. On the right, the tube connecting the acceleration and deflection chambers is visible. In this tube the x- and y-deflection plates are mounted. On top of the chamber the vacuum sealed perspex insulators are situated through which the focussing systems are connected to the high voltage.

3.8. COLLECTOR SYSTEM

The collector chamber is made of mild steel and has a volume of 160 l. The collector and pump chambers, together with the fore vacuum pump for the collector system, are mounted on a stand running on wheels and are adjustable by jacking screws. The whole assembly can easily be disconnected from the separator.

The separated isotopes are collected by direct deposition. Different kinds of targets are used which can be mounted on a target holder by means of clamping screws to achieve good electrical and thermal contact. The width of the target holder is $D_c = 36$ cm, so that the number of mass lines which can be collected simultaneously is approximately given by

$$n = \frac{D_c}{R} A = \frac{1}{5} A .$$

The mass lines can visually be observed on a fluorescent screen mounted on the perspex front window of the collector chamber. The screen consists of a thin layer of luminescent material on a glass plate. A fine brass mesh, connected to earth, is pressed against the plate to prevent the glass from being electrically charged. The fluorescent screens are prepared in a simple way by spraying a mixture of paraffin oil and luminescent powder on glass plates. While observing the mass lines on the fluorescent screen, the target holder is lowered from outside the chamber by a rod operating through a sliding seal.

Ion currents are accurately measured by a device consisting of a collector placed in an auxiliary magnetic field which prevents secondary electrons from leaving the collector[5]). A

brass screen in front of the device permits only one mass line to reach the collector. The ion current measuring device remains in a fixed position, and the mass lines to be measured are

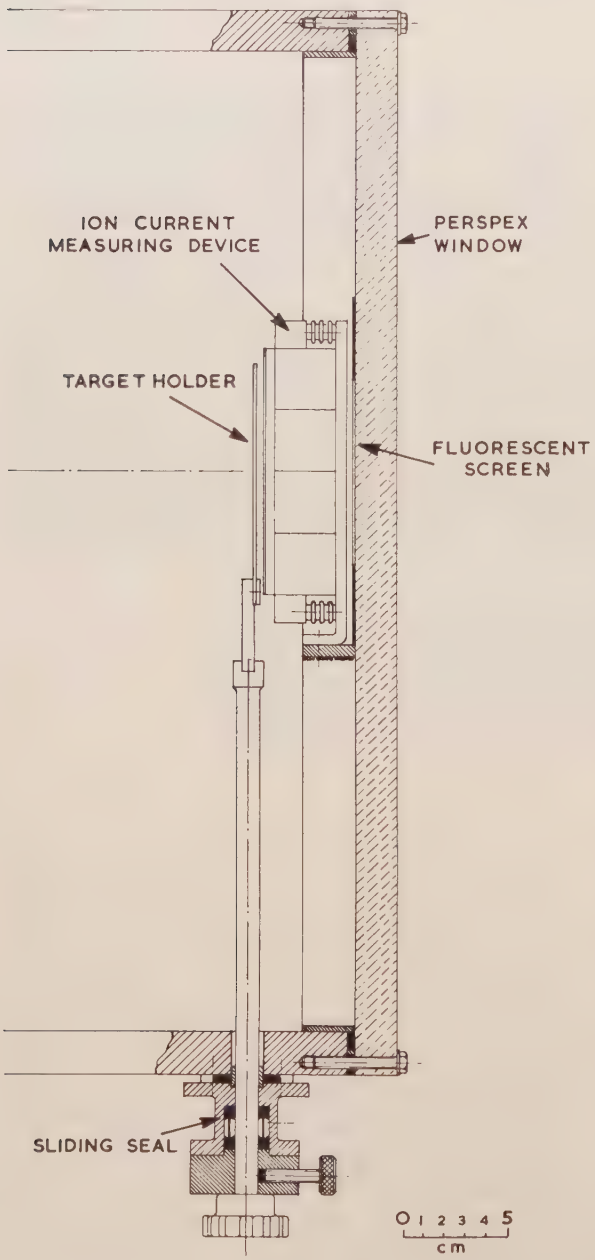

Fig. 12. Target arrangement.

brought to the collector by changing the magnetic field.

Fig. 12 shows the target holder in position, and the ion current measuring device in front of the fluorescent screen.

The collector chamber also contains a mechanical scanning device, an automatic recording system and the two feelers for the beam position stabilizer[20]). For the collection of short-lived radioactive isotopes, rapid mass assignment of the activities on the target is necessary. An automatic method of mass number determination has been developed and is at present being tested[23]).

4. Operational Characteristics

The separator has been tested first by means of a conventional gas ion source using mainly krypton and xenon, and later by means of the high temperature and sputtering ion sources. A minimum line width $b = 1.6$ mm, corresponding to a resolving power $P = 1100$ is obtained at small ion currents ($\approx 5\,\mu$A at the collector). The fluctuations in acceleration voltage and magnet current are reduced by beam position stabilization to $1:10^5$, corresponding to a line width contribution $b_1 + b_2 = 0.05$ mm. Thermal energy spread of the ions contributes $b_3 < 0.1$ mm. The geometry of the separator limits the beam divergence to $\alpha = 0.6°$, thus $b_4 = R\alpha^2 = 0.2$ mm. Since the beam diameters are smaller than 30% of the lens diameter, the spherical aberration contribution b_5 of the electrostatic lens system is also expected to be small. Therefore, the main contributions to the observed line width are given by b_6, b_7 and b_8. The high resolving power obtained proves these contributions to be sufficiently small in the region of low ion currents. For higher ion currents, the space charge broadening b_8, being the only current-dependent part of the line width, will increase and reduce the resolving power. By two-directional focussing, the line height can be reduced to 5 mm with negligible radial defocussing.

The special applications of the separator, discussed in 2.2, require total ion currents of about 100 μA. Currents of this magnitude can easily be obtained by increasing the filament

[23]) L. Wåhlin, to be published.

heating current of the ion source. However, the resolving power deteriorates rapidly with increasing current. This behaviour is caused by the combined action of plasma focussing and space charge repulsion. For smaller currents, the ions are emitted by a concave plasma boundary at the outlet of the ion source, and a "cross-over" region is formed from which the beam

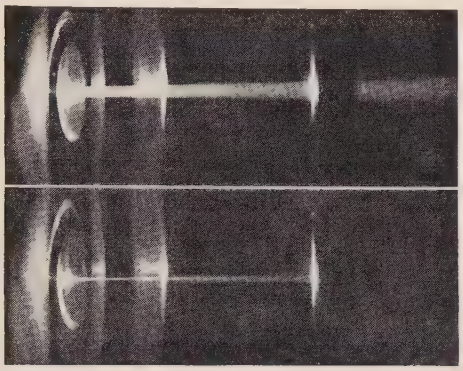

Fig. 13. Form of ion beam between ion source and acceleration electrode under different conditions of plasma focussing (krypton; acceleration voltage $V = 40$ kV, acceleration distance $L = 11$ cm): (a) Concave plasma boundary, $I = 40$ μA. (b) Convex plasma boundary, $I = 200$ μA.

diverges. With increasing ion current the plasma boundary becomes less concave, and the cross-over region moves further away from the outlet, resulting in a very narrow ion beam (fig. 13a). According to eq. (7), small beam diameters cause strong space charge broadening of the mass lines at the collector. However, if the ion current is still further increased, the plasma boundary becomes convex, and a diverging beam is formed which becomes wider with increasing intensity (fig. 13b). Thereby, space charge broadening of the mass lines is reduced and a region of good resolving power is again reached.

The dependence of the resolving power P on the total ion current I is shown in fig. 14. Also given in this figure is the "line transmission" T, defined as the percentage of total ion current present in all the mass lines on the collector.

It is seen that there exist two intensity regions, characterized by both high resolving power and good transmission. The existence of the second, high-intensity region is a novel feature which is necessary to obtain optimum working conditions at high ion currents in laboratory separators of fairly large size[15]).

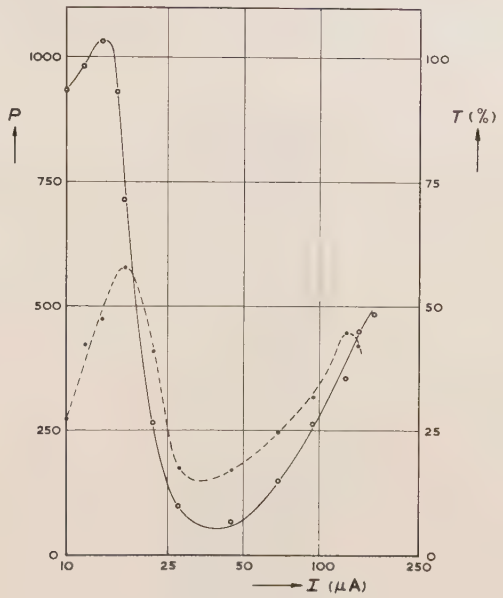

Fig. 14. Resolving power P and line transmission T as functions of the total ion current I. (krypton; acceleration voltage $V = 40$ kV, acceleration distance $L = 11$ cm.)

5. Application

In the course of the investigations on ion beam formation and the study of ion sources, the stable isotopes of various elements have been separated. For the beam formation studies mostly rare gases, Ne, A, Kr, Xe, were used. By means of the sputtering ion source, the mass lines of various metallic elements have been obtained, viz., Cu, Zn, Ag, Cd, Sb, Pb, Bi.

As an example of work with radionuclides, we describe a separation of the phosphorus isotopes. This separation was carried out to determine the P^{33}-content of a radiophosphorus (P^{32}) source which was to be used as a standardized internal source for radiolysis studies[24]).

The radiophosphorus which was obtained carrier-free by pile neutron irradiation of natural sulphur, was expected to contain about 1% P^{33}. In order to form a suitable charge material, a sample (1 — 2 mc) of the radioactive

[24]) M. Peisach and J. Steyn, J. S. Af. Chem. Inst., in course of publication.

solution was added to about 1 g of chemically pure phosphoric acid and heated in vacuum to about 300° C to remove most of the moisture. A small crucible containing the residue was placed near the filament of the gas ion source†. The bulk of the activity on the collector appeared

Fig. 15. Mass line at $A = 48$.

at mass numbers 47—50, and the mass lines were collected in this region by direct deposition on a Cu-foil. After a separation time of about six hours, the foil was cut into narrow strips which were measured by 2π-proportional counting. Beta absorption analysis of the target strips showed that the activity at mass number 48 contained only P^{32} in the form $(P^{32}O^{16})^+$, whereas the line at $A = 49$ contained P^{33} together with 44% P^{32}. The ratio P^{33}/P^{32} was found to be 1.6%. To obtain sources sufficiently small for 2π-proportional counting, two-directional focussing has been employed. The form of the mass line at $A = 48$ is shown in fig. 15. It contained an activity of 5.0×10^4 dis/min on a deposited area of 10×2.5 mm^2.

Acknowledgements

One of the authors (W. E. F.) gratefully acknowledges the stimulating discussions he enjoyed with leading physicists of several European separator groups, especially with Professor Jørgen Koch and Professor J. Kistemaker, Drs. Göran Andersson, Ingmar Bergström, René Bernas, Ch. Cassignol, Karl-Ove Nielsen, Sigvard Thulin, and Mr. T. Alväger. He is sincerely indebted to Professor Manne Siegbahn for the hospitality extended to him at the Nobelinstitutet för Fysik in Stockholm, and to Professor Niels Bohr at the Universitetets Institut for Teoretisk Fysik in Copenhagen.

The authors would like to thank Messrs. C. A. J. Kritzinger and J. J. Burgerjon for their valuable help with the technical design in the earlier stages of this work. We sincerely appreciate the skilful technical assistance of Messrs. J. M. Kuyl and J. J. Selier during construction of the separator, of Messrs. P. Koning and E. P. Blignaut who helped with the measurements, and of Messrs. G. F. Barclay, L. D. Bruins and J. J. Arnold of the drawing office. Our special thanks are due to Mr. G. O'Grady and the staff members of the laboratory workshop for their untiring assistance and high standard of work.

We are much indebted to Drs. S. J. du Toit and E. J. Marais for their interest in this work. It is a pleasure to thank the South African Council for Scientific and Industrial Research and its president, Dr. S. M. Naudé, as well as the South African Atomic Energy Board for supplying the necessary funds for this project.

† In the only previous separation of radiophosphorus isotopes, carried out with the Copenhagen separator (B. Elbek, K. O. Nielsen and O. B. Nielsen, Phys. Rev. **95** (1954) 96), phosphine was used as charge material, and $(P^{33}H_3)^+$-ions collected at mass number 36.

NUCLEAR INSTRUMENTS AND METHODS 7 (1960) 269–273; NORTH-HOLLAND PUBLISHING CO.

IMPROVEMENTS OF THE COLLECTOR SYSTEM FOR A LABORATORY ISOTOPE SEPARATOR

L. WÅHLIN

Nuclear Physics Division, National Physical Research Laboratory, C.S.I.R., Pretoria, South Africa

Received 20 November 1959

An improved beam position stabilizer, a new line scanning device and an automatic recording system are described. This equipment is used in the electromagnetic isotope separator in the Nuclear Physics Division of the National Physical Research Laboratory in Pretoria[1]).

1. Introduction

The beam position stabilizer described below eliminates the need for complex equipment for stabilizing the magnetic field. The line scanning system which is based on a new principle makes it possible to obtain high scanning amplitudes in a restricted space and to scan the line spectrum in both x and y coordinates simultaneously.

The last part of the paper deals with a method for recording the line spectrum on a chart recorder so that the resolving power of the isotope separator can be accurately measured.

2. Improved Beam Position Stabilization

All voltages for the ion source, as well as the acceleration voltage, are stabilized on the primary side by a Sorensen regulator to 1 part in 1000. This variation together with the voltage drop over the internal resistance, at different loads of the acceleration voltage, causes the beam to change position by about 3 mm at the collector.

Fig. 1 shows an electronic arrangement which stabilizes the ion beam in the desired position by feeding back a signal (which is caused by the beam drifting off position) to alter the magnetic field and the voltage over the two x-deflection plates. A line is held between the two pins at the collector and gives a signal to a balanced d-c amplifier.

The moment the line tends to drift, one of the pins collects a more intense ion current which induces a potential difference over the two pins. This potential difference is amplified and fed back to the magnet and to the two x-deflection plates. This has the effect of bending back the beam to its original position.

Indifferent results were obtained using only the magnetic field to compensate the drift as the time constant of the magnet was too high. By simultaneously stabilizing the beam with the x-deflection plates and the magnet, the feedback gain to the magnetic field can be considerably increased without any self-oscillation occurring.

Due to the high-gain feedback on the magnet the voltage and the disturbing field across the x-deflection plates is kept at a minimum. This system also has the advantage of eliminating the need for complex and expensive equipment for stabilizing the magnetic field separately. Measurement on mass number 28 has shown that a drift in one direction, corresponding to 40 cm at the collector, changes the field intensity from 800 gauss to 920 gauss and only changes the voltage across the x-deflection plates from 0 to 280 V.

3. Mechanical Two-Way Line Scanning System

A new mechanical scanning system has been developed to scan a line in both x and y directions simultaneously whilst the isotope is being collected. Furthermore, high scanning amplitudes

[1]) W. E. Frahn, W. L. Rautenbach and L. Wåhlin, Nuclear Instruments 7 (1960) 253.

can be obtained in the restricted space of the collector chamber. A different system of scanning was introduced by the author for the Stockholm separator in 1955, which was later improved by Nielsen and Skilbreid[2]).

output of an amplifier. A thin stainless steel cylinder (the feeler tube) is pushed over the rubber string and positioned centrally. A thin wire twisted around the string connects the feeler to an oscilloscope.

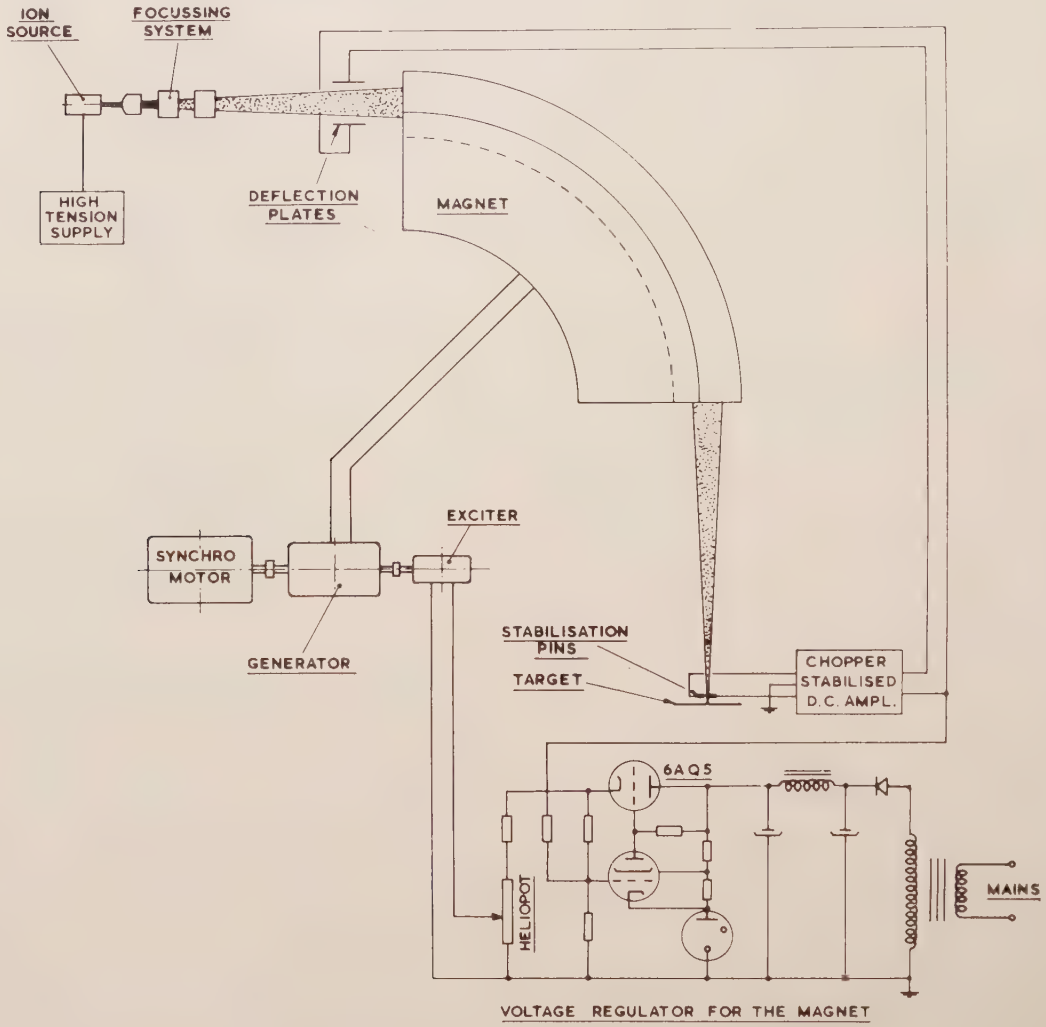

Fig. 1. Schematic diagram of the beam position stabilizer.

Fig. 2 shows a diagram of a rubber string held taut between an arm attached to a moving coil and a fixed point 30 cm away. The moving coil, which is placed in an auxiliary magnetic field, consists of two windings, one of which is connected to the input and the other to the

By giving the moving coil a small momentum in any direction, a voltage is induced in the input winding which is amplified and fed back to the output coil with a suitable phase shift. By this means the moving coil begins to oscillate at a frequency determined by the length, tension and weight of the rubber string assembly. The feeler, while remaining parallel to its

[2]) K. O. Nielsen and O. Skilbreid, Nuclear Instruments **1** (1957) 159.

original direction, oscillates in a plane with an amplitude of 3–15 cm depending on the amplification.

Fig. 3 shows how two vibrators are situated at the collector. One sweeps vertically over the line and the other one horizontally. One vibrator has only a single winding which is energized with the same frequency as the other, by simply

Fig. 4 shows the double trace on the oscilloscope screen of:

(a) The krypton spectrum detected by using the horizontal vibrator only,

(b) the line at mass number 28 detected by both vibrators,

(c) the same as (b) above after the line has been compressed by the double focussing plates.

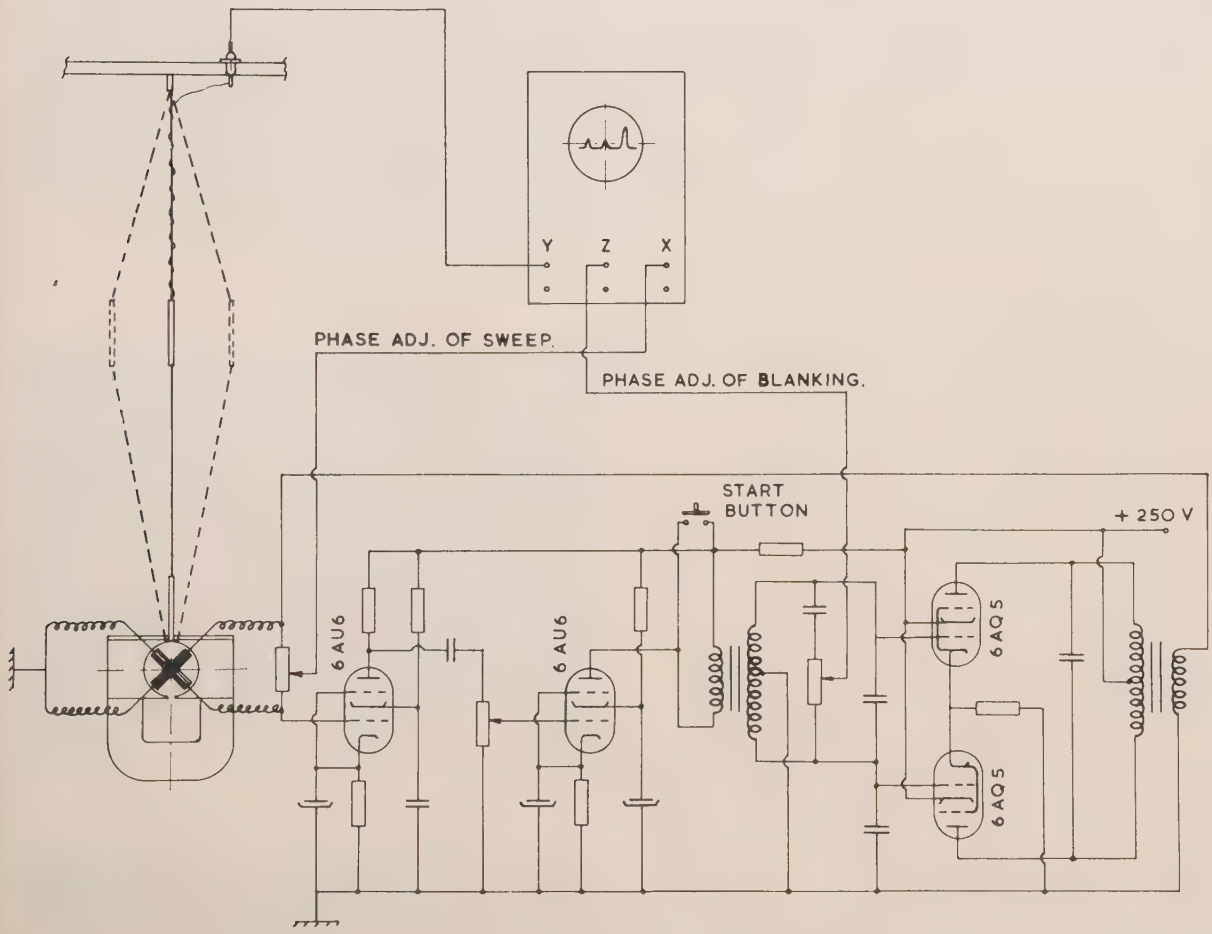

Fig. 2. Schematic diagram of the line scanning system.

connecting it to the output of the amplifier, and by adjusting the tension of the rubber string.

When the two feelers sweep over a line they pick up a signal corresponding to the ion distribution of the line in both coordinates. The signals are passed through a Dual Trace Preamplifier to an oscilloscope with x-sweep synchronized with the scanning frequency.

The vibrators are started under vacuum by a push button which gives a short electrical pulse to the amplifier.

4. Recording of the Line Spectrum

An automatic recording method has been designed to record a line spectrum and to measure accurately the resolving power

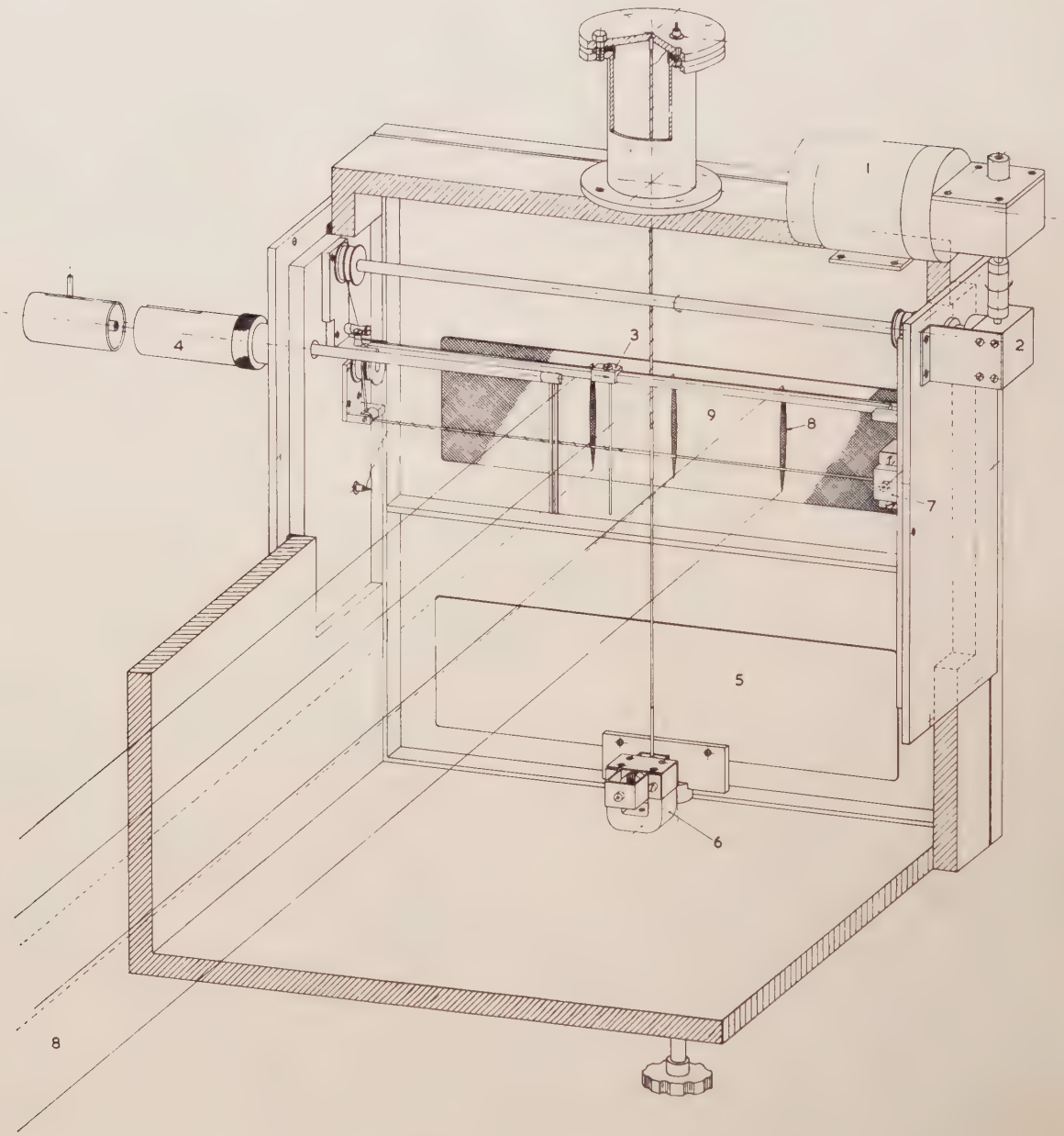

Fig. 3. Sketch showing the collector arrangement seen from inside the vacuum chamber. 1. Synchro-motor. 2. Gearbox. 3. Recorder electrode. 4. Beam stabilization pins. 5. Target holder in down position. 6 and 7. Vibrators. 8. Ion beam. 9. Fluorescent screen.

of the isotope separator during operation.

As fig. 3 shows, an electrode driven by a synchro-motor sweeps across the spectrum at the collector. The speed of the electrode is equal to the chart speed of the recorder in order to give a true reproduction of the line spectrum. The electrode is biased — 200 V to shield it from secondary electrons appearing in the collector chamber. The cadmium spectrum obtained by a sputtering ion source[3]) recorded in this way is shown in fig. 5.

[3]) W. L. Rautenbach, to be published.

The spectrum was stabilized in position by allowing the line at mass number 112 to pass between the two pins of the beam position stabilizer. The shadow of the pins appear on the recorded diagram.

Fig. 4 (a). Krypton spectrum detected by using the horizontal vibrator only.

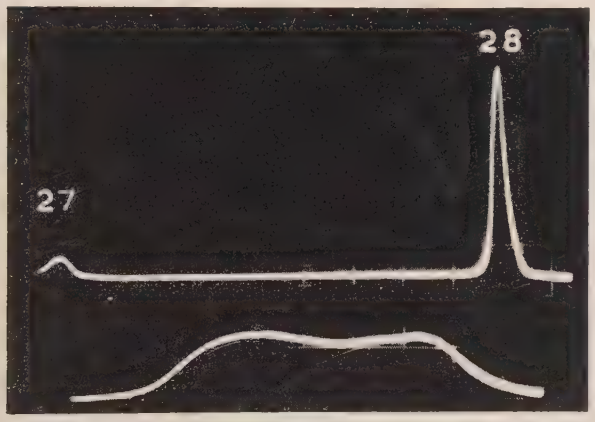

Fig. 4 (b). Mass number 28 detected by both vibrators.

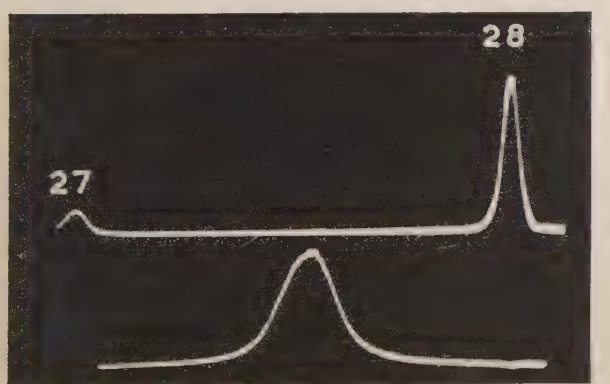

Fig. 4 (c) The same as (b) above after the line has been compressed by the double focussing plates.

Acknowledgements

It is a pleasure to thank Dr. S. J. du Toit and Professor W. E. Frahn for their continued interest in this work, and Mr. W. L. Rautenbach for valuable discussions. The enthusiastic assistance of Messrs. J. J. G. B. Selier, J. M. Kuyl, G. F. Barclay, G. O'Grady and A. Dekter is greatly appreciated. Finally I am indebted to the South African Council for Scientific and Industrial Research and to the South African Atomic Energy Board for making this work possible by supplying the necessary funds.

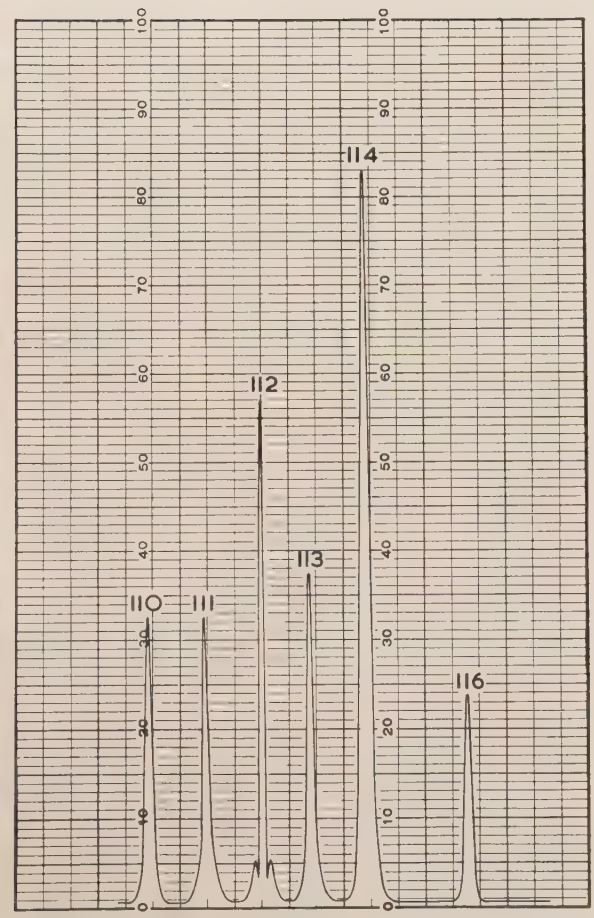

Fig. 5. Cadmium spectrum as traced by the recorder. The shadow of the stabilization pins can be seen on the line at mass number 112.

NUCLEAR INSTRUMENTS AND METHODS 7 (1960) 274–288; NORTH-HOLLAND PUBLISHING CO.

CYCLOTRON INSTRUMENTATION FOR NUCLEAR REACTION STUDIES BY MAGNETIC ANALYSIS

BO SJÖGREN

Nobel Institute of Physics, Stockholm 50, Sweden

Received 7 March 1960

An instrumentation for magnetic analysis work at a small cyclotron (7 MeV deuterons, 14 MeV α-particles) is described. The equipment consists of two quadrupole lenses and an analyzing magnet for the preparation of a beam spot on the target and of a magnetic spectrometer for investigation of the reaction particles. The magnetic analyzers have perpendicular bending planes. Angular distributions can be measured from 0° to 135°. The detectors, the adjustments, the experimental procedure and the performance of the system are discussed.

1. Introduction

When the individual particle groups from a nuclear reaction are to be investigated, it is in most cases necessary to have an apparatus with high energy resolution. This is, of course, the case in accurate determinations of energies. However, also when angular distributions are to be studied, close-lying groups must often be resolved. An example is given by reactions on the relatively light nuclei in the region around mass-number 25. Even between the low excited states there are fairly small level distances. These nuclei are of current interest with respect to the collective model[1]).

If the incident as well as the emerging particles are charged, a system of two magnetic analyzers is a suitable measuring arrangement when high resolution is desired. Sometimes, the second analyzer can be excluded and replaced by a detector with good resolution. Ionisation chambers, for instance, are used in such cases (see e.g. ref.[2])). However, a magnetic analyzer has several advantages. It discriminates between the particles and the resolution obtainable is higher.

When magnetic analysis work is performed, an accelerator giving a particle beam with well defined energy focused to a small spot is desirable. Accelerators suitable for this purpose are van de Graaff- and cascade-generators and the recently invented tandem-machines[3]). A cyclotron delivers a beam with a larger energy spread than these instruments. It is also difficult to focus a cyclotron beam to as small a spot as desired in front of the analyzing magnet without causing a large divergence of the particles. These two effects limit the part of the available external cyclotron beam which can be used. The first-mentioned effect, however, can be compensated fairly well if the analyzers are designed and combined in a suitable manner[4,5]). The second effect implies that a large mean radius of the first analyzer is favourable, as then a large object slit and thus a correspondingly large part of the total external beam, can be used for a certain resolution. The size of the analyzers is in most cases restricted by the available space or by the cost. There is also another feature of the beam from a standard cyclotron which implies a draw-back in reaction studies, namely the fixed energy†. It is possible to attain a variable energy by letting the particles pass through an

[1]) A. E. Litherland, H. McManus, E. B. Paul, D. A. Bromley and H. E. Gove, Can. J. Phys. **36** (1958) 378.

[2]) H. W. Fulbright, N. O. Lassen and N. O. Roy Poulsen, Mat. Fys. Medd. Dan. Vid. Selsk. **31**, No. 10 (1959).

[3]) Nucleonics **17**, No. 3 (1959) 116.

[4]) B. L. Cohen, Rev. Sci. Instr. **30** (1959) 415.

[5]) B. Sjögren, Nuclear Instruments **7** (1960) 76.

† As is well known it is possible to modify a cyclotron so that its frequency, and thus its energy, is variable. See e.g. ref.[6]).

absorber with variable thickness. However, this results in a severe loss of intensity behind the image slit of the beam analyzer, and the possible energy variation in this way is therefore limited.

An advantage of the cyclotron as compared with van de Graaff- and cascade-generators is that it generally has a higher energy. The tandem-machines[3]), however, seem to be comparable or superior to several cyclotrons in this respect.

In spite of the above-mentioned disadvantages of the standard cyclotron for high resolution measurements by magnetic analysis, it was considered desirable to build an instrumentation for such work at the small cyclotron of the Nobel Institute. This was done for several reasons. Much work is left to be done on light nuclei at the energy of this accelerator (7 MeV deuterons, 14 MeV α-particles). A double-focusing, heavy particle spectrometer[7]) was available at the 1 MeV cascade generator where it had been used for determinations of Q-values and angular distributions[8]). The spectrometer was designed for a maximum of about 20 MeV protons and it is thus suitable to be used at the cyclotron. A convenient experimental room was also available and the beam intensity was judged to be sufficient.

In the following the analyzing system, the target arrangements and the detectors are described and discussed in some detail. Except for the spectrometer, the components are newly constructed. Also some details of the experimental procedure in measurements of particle energies and angular distributions are briefly discussed. Some features of the system are given.

Cyclotron equipment for magnetic analysis has been described by Bender *et al.*[9]), Rasmussen *et al.*[10]), Green and Middleton[11]) and Bach *et al.*[12]).

2. Description of the instrumentation

2.1. FOCUSING AND ANALYZING OF THE BEAM

A view of the cyclotron layout is shown in fig. 1. The 80 cm-cyclotron is placed in a separate room shielded by a 0.9 m thick iron ore, concrete wall from the experimental room. By means of two small sector magnets (see ref.[13])), the electrostatically deflected particles are focused in the horizontal direction to a point just on the inside of the shielding wall. In the vertical direction the beam is nearly parallel, it diverges only very slightly. The sector magnets are adjusted so that the beam has a convenient direction into the experimental room. At the focusing point there is slit No. 1, defining the horizontal projection of the beam.

There are four experimental set-ups at the beam, namely, a time-of-flight equipment for fast neutron studies[13]) (not indicated in the figure), a trochoidal spectrometer recently devised by Malmfors and intended for γ-measurements[14]), an axial beta spectrometer for γ- and β-measurements[15]) and the heavy-particle spectrometer arrangement for investigations of charged particles. In this paper only this last-named set-up will be described. A 90°-analyzing magnet can bend the beam either to the trochoidal spectrometer or to the heavy particle spectrometer.

When the analyzing system in the experimental room was designed, it was considered important that the change-over between the different apparatuses could be made in a short time. The required flexibility is achieved by a pair of quadrupole magnets and the analyzing magnet, which is rotatable around the direction of the incoming beam.

[6]) I. Nonaka, H. Yamaguchi, T. Mikumo, I. Umeda, T. Tabata and S. Hitaka, J. Phys. Soc. Japan **14**, No. 10 (1959) 1260.

[7]) C. Mileikowsky, Ark. f. Fys. **4**, No. 16 (1952) 337; **7**, No. 3 (1953) 33.

[8]) K. Ahnlund, Ark. f. Fys. **10**, No. 27 (1956) 373.

[9]) R. S. Bender, E. M. Reilley, A. J. Allen, R. Ely, J. S. Arthur and H. J. Hausman, Rev. Sci. Instr. **23** (1952) 542.

[10]) V. K. Rasmussen, D. W. Miller and M. B. Sampson, Phys. Rev. **100** (1955) 181.

[11]) T. S. Green and R. Middleton, Proc. Phys. Soc. A**69** (1956) 16.

[12]) D. R. Bach, W. J. Childs, R. W. Hockney, P. V. C. Hough and W. C. Parkinson, Rev. Sci. Instr. **27** (1956) 516.

[13]) K. G. Malmfors, J. Kjellman and A. Nilsson, Nuclear Instruments **1** (1957) 186.

[14]) K. G. Malmfors, Nuclear Instruments **1** (1957) 251; Ark. f. Fys. **13**, No. 21 (1958) 237.

[15]) J. Kjellman and B. Johansson, Ark. f. Fys. **14**, No. 2 (1958) 17.

The quadrupole lenses (see below) can easily be moved about 4 m along the beam direction and their magnetizing currents can be varied independently. By choosing correct values of the position and strength of the lenses, it is possible to focus the beam to a machine would be minimized. The bending plane of the spectrometer is vertical. As to the target spot, this means that the radial direction of the analyzing magnet corresponds to the axial direction of the spectrometer (cf. ref.[5]).

The highest intensity of the deuteron beam

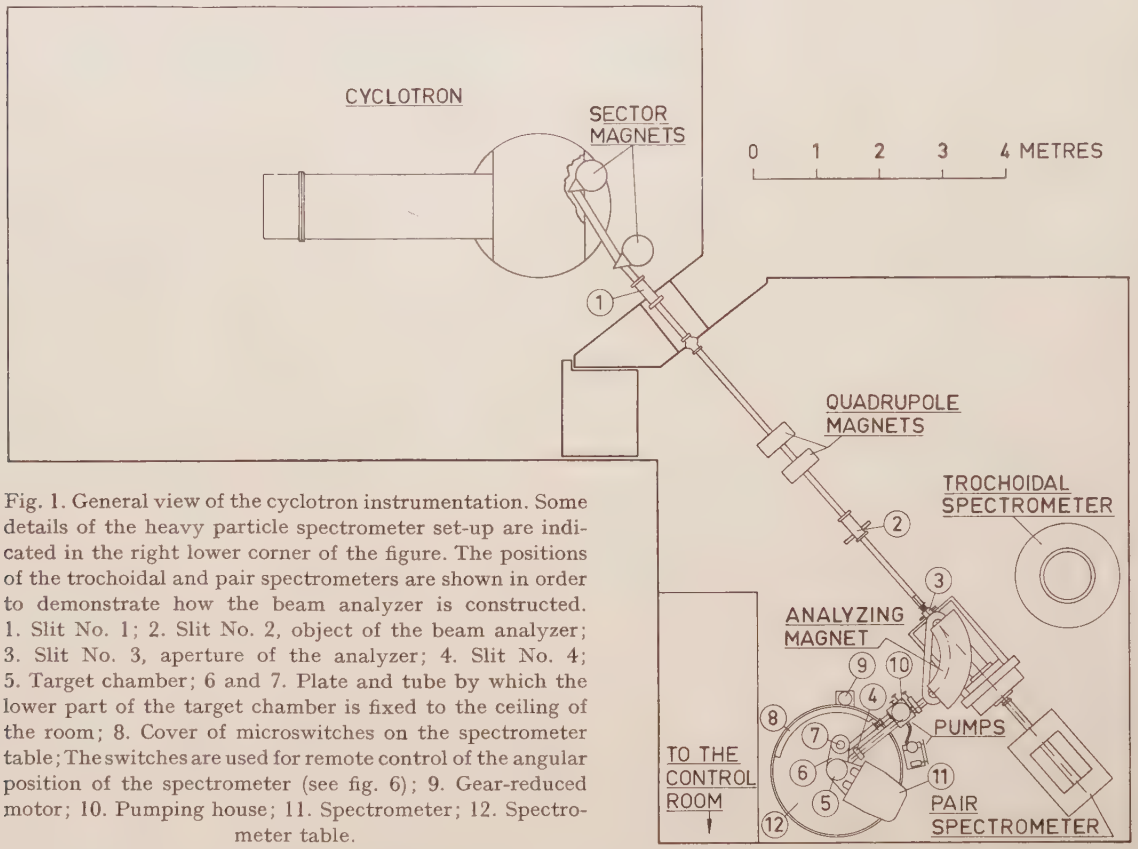

Fig. 1. General view of the cyclotron instrumentation. Some details of the heavy particle spectrometer set-up are indicated in the right lower corner of the figure. The positions of the trochoidal and pair spectrometers are shown in order to demonstrate how the beam analyzer is constructed. 1. Slit No. 1; 2. Slit No. 2, object of the beam analyzer; 3. Slit No. 3, aperture of the analyzer; 4. Slit No. 4; 5. Target chamber; 6 and 7. Plate and tube by which the lower part of the target chamber is fixed to the ceiling of the room; 8. Cover of microswitches on the spectrometer table; The switches are used for remote control of the angular position of the spectrometer (see fig. 6); 9. Gear-reduced motor; 10. Pumping house; 11. Spectrometer; 12. Spectrometer table.

stigmatic image at a desired point and with a desired angular spread. In the horizontal direction slit No. 1 at the shielding wall is imaged by the lenses.

When the beam is to be analyzed it is focused onto a slit system, No. 2 in fig. 1, at the object point of the analyzing magnet. The acceptance solid angle of this magnet, which is double-focusing is defined by the aperture slits No. 3. Finally, slits No. 4 (limiting the beam both horizontally and vertically) and No. 5 (horizontally, not shown in fig. 1) can determine the target spot size.

The magnetic spectrometer was put as far away from the cyclotron as possible so that the background caused by radiation from the obtainable in front of slit No. 2 is found to be approximately 10 μA concentrated within an area of about 50 mm^2. Slit No. 1 is then wide open so that the beam intensity is very little decreased there. When slit No. 2 is 4 $\times$ 4 mm^2, a maximum of 4—5 μA can be accepted by the analyzer. Of this current 0.5—1.0 μA can be focused onto the target when the spot width (slit No. 5) is 6 mm and the height is 2.5 mm. A striking feature of the beam is that its intensity distribution is strongly non-uniform.

The beam of α-particles is, for the present, approximately 10 times less intense than that of deuterons.

2.2. DESIGN OF THE QUADRUPOLE LENSES

The construction of the lenses is indicated in fig. 2. A photograph of the system is shown in fig. 3. It was considered convenient to make the

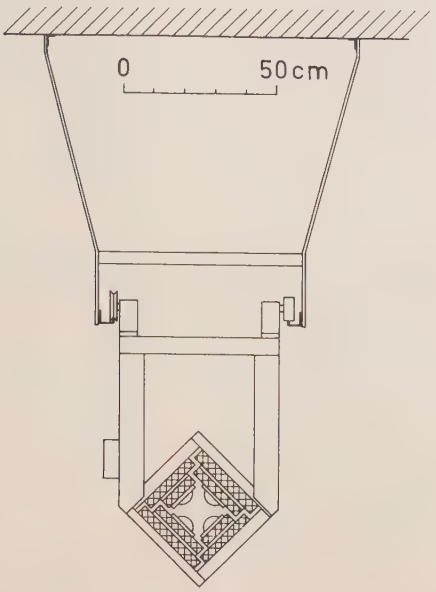

Fig. 2. Schematic view of the quadrupole lenses.

lenses relatively strong so that the beam could be focused about 1.5 m from the shielding wall if desired. The total pole gap is 8.2 cm and the length of the pole pieces is 25 cm. The pole tips, which can be exchanged so that, if necessary, a

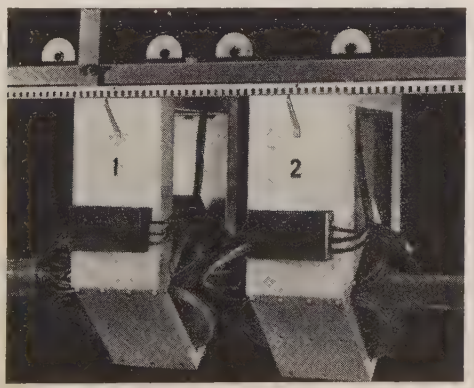

Fig. 3. Photograph of the quadrupole lenses.

different gap is obtainable are circular-cylindrical (radius 4.6 cm). This shape gives a satisfactory field[16]). The pole tips and pole pieces are made of forge iron (Surahammar 5A). Copper tubes for cooling water are soldered onto the bobbins of the coils. These coils have advantages over air-cooled ones. Apart from the fact that a higher magnetizing current can be used, also the

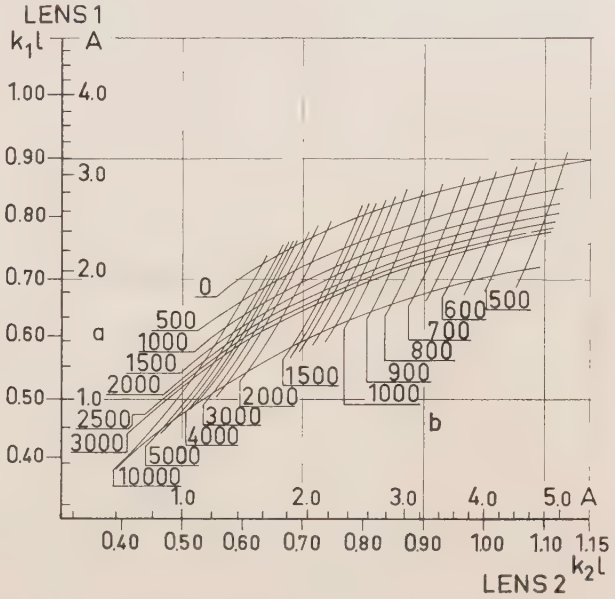

Fig. 4. Diagram from which the strengths of the quadrupole lenses and the corresponding magnetizing currents are obtained. a is the distance in mm from slit No. 1 (fig. 1) to the entrance of the first lens. b is the distance in mm from the exit of the second lens to the stigmatic image. l is the lens length and k_1 and k_2 are the values of the strength of the two lenses (see e.g. ref. [17])).

time-constant for the heating is smaller (the iron is screened). The coils are fed from two small generators and it has not been necessary to stabilize the currents.

The lenses are screwed in a framework which can roll along two bars on three small wheels. These bars are fixed with supports to the ceiling and are accurately adjusted to be parallel to the particle beam. The suitable placing of the lenses and the corresponding magnetizing currents which give a stigmatic image at a certain point are obtained from the diagram shown in fig. 4. This diagram has been determined with a graphical method suggested by Enge[17]). It is valid when the distance between the lenses is 25 cm.

[16]) P. Grivet et A. Septier, Les Lentilles Quadrupolaires Magnétiques, CERN PS-58-25 (1958); Nuclear Instruments **6** (1960) 126, 243.

[17]) H. Enge, Rev. Sci. Instr. **30** (1959) 248.

2.3. DESIGN OF THE ANALYZING MAGNET

The characteristics of the beam analyzer are assembled in table 1.

TABLE 1

Characteristic quantities of the analyzing magnet 7 MeV d, 14 MeV α

Mean radius, r_0	80 cm
Deflection angle	92.8°
Sector angle	87.2°
Average pole gap	5.7 cm
Pole-face width	18 cm
Average field, B_0	6900 gauss
Field gradient parameter $n = -\frac{r_0}{B_0}\left(\frac{\partial B}{\partial r}\right)_{r=r_0}$	0.47

Several factors influenced the choice of the mean radius, the transmission and the field shape.

(1) The energy definition of the particles hitting the target must be good. This implies, however, that the ratio between the object slit and the mean radius of the analyzer must be small. Therefore, a wide object slit provides a correspondingly large mean radius. The quadrupole lenses can concentrate the beam to quite a small image spot, but then the angular spread on the target will also be large. In the present case one has to use a fairly wide object slit.

(2) As the bending plane of the spectrometer is almost perpendicular to that of the analyzer (see 2.6) the width of the target spot does not directly influence the resolution of the measured particle groups. It is evident, however, that the resolution depends on the energy spread of the incoming particles (cf. 3.5) which is determined by the width. The height of the spot, on the other hand, must be small. The analyzer has therefore been made double-focusing.

(3) The geometry of the experimental room restricts the mean radius.

(4) It is possible to increase the useful beam intensity when one is measuring with a combination of magnetic analyzers[5]). From this point of view a relatively large mean radius is favourable in the present combination (see eq. (15) in ref.[5])).

When the analyzer was constructed, the n-value was chosen somewhat less than 0.50†, as it was considered suitable that there be a distance of about 30 cm between the radial and axial foci for an object distance of 190 cm. Thus the axial image is on the target and the radial image on slit No. 4. For the present, however, the object distance is 150 cm and the radial image is very near to the target (slit No. 5)††. Here $n = 0.50$ would be the optimal value. However, the effect of the value chosen is certainly not serious.

The construction of the analyzing magnet is shown by a photograph in fig. 5. It is also schematically indicated in fig. 1.

The magnet consists of five iron pieces—two pole pieces, two yoke sides and one yoke back with a thick axle-journal—which are cast in soft iron. Special attention was payed to the casting of the pole pieces so that the homogeneity would be satisfactory. The pole pieces were turned so that the pole faces have a conical shape (conicity $2 \times 0.97°$). The five pieces together weigh about 3000 kg. They are put together by $1\frac{1}{2}''$ and $2''$ screws and the fitting is attained by dowel pins. The journal is put in two ball-bearings fixed in a framework. In this way

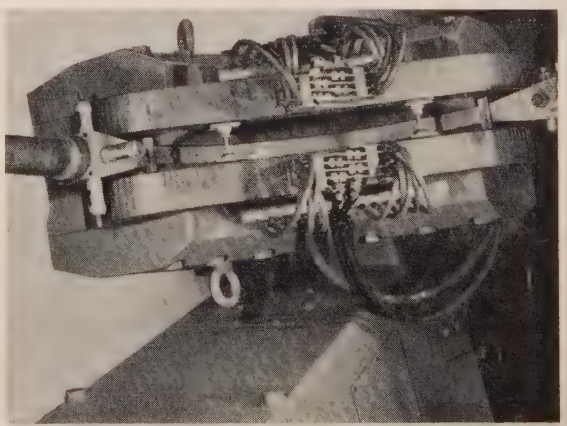

Fig. 5. Photograph of the beam analyzer. Its bending plane is inclined at 5.7° to the horizontal.

† A field with $n = 0.50$ is easily obtained if the gap is somewhat decreased. This is fairly simple to do with the present magnet design.

†† This is favourable when a wide target spot is used, see 3.5.

the magnet is hung up. On the journal a cogged wheel (⌀ 98 cm) is also fastened, which can be turned by a gear-reduced motor attached to the framework. By this motor the magnet is turned from one side to the other in a short time (4 min for half a turn). The journal has been accurately worked so that its axis, when the analyzer is adjusted, very nearly coincides with the incident beam direction and also lies in the bending plane, perpendicular to the entrance field boundary. The framework is made of welded iron plate (10 mm). It rests on four adjustable screws. In the journal centre an 8 cm hole is drilled in which it is possible to let the beam pass undeflected through the analyzer.

The two coils are made of copper tubes with a cross-section of 51 mm² (9 × 9 mm² with a central hole for cooling water) wound on brass frames. Each coil consists of 80 turns and is dimensioned for 22 500 ampere-turns (corresponding to a maximum pole gap of 6.5 cm).

The incident beam is somewhat deflected in the fringing field before it traverses the pole face boundary. The deflection angle has been determined to be 2.8°. The field was measured by means of a Hall-detector (In As, Siemens Fa 24) and ion paths were calculated by numerical integration. To compensate for this deflection, a corresponding part of the pole pieces at their entrance end has been cut off (39 mm at the mean radius). The sector angle of the analyzer is thus 87.2°.

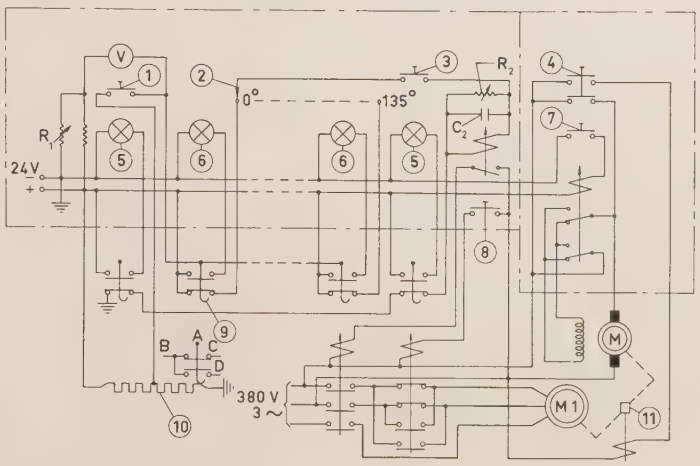

Fig. 6. Circuit-diagram of the remote control arrangement by which the spectrometer can be adjusted to a desired direction. M1 is the gear-reduced motor turning the spectrometer table and M is a small motor of a similar type for fine-adjustments. R_2 and C_2 define a suitable delay-time.

1. Switch used for the zero-setting of V (to be done with R_1).
2. Contact (19 positions) by which a fixed spectrometer angle is selected.
3. Operation of M1. 4. Operation of M.
5 and 6. Signal lamps indicating the limiting positions and angular values, respectively.
7 and 8. The rotating direction of M and M1, respectively.
9. Microswitches (21 in number) fixed onto the spectrometer table.
10. Wire-wound resistor mechanically operating the microswitches. It is fixed to the frame of M1.
11. Magnetic coupling. The instrument V indicates the deviation (within ± 2.0°) of the spectrometer direction from one of the fixed directions 0°, 7.5°, ··· 135°. The "dead" angles can be covered by moving the resistor 10 by an appropriate distance.
The components within the dashed lines are in the control room.

2.4. THE SPECTROMETER

The double-focusing spectrometer ($n = 0.50$) has previously been described[7]). Its mean radius is 40 cm, its deflection angle is 191.4° (2 × 5.7° caused by the fringing fields) and its energy range is about 8%. It rests on a table which can be rotated about a vertical axis through its centre by a gear-reduced motor. Its solid angle is defined by an almost rectangular window at $\varphi_a = 95.7°$ (see appendix 1).

During measurements it is often necessary to change the spectrometer to some approriate angular position. Therefore, a simple arrangement has been constructed by which this can be done from the control room. The device has turned out to be secure and easily handled in practice. It is indicated schematically in fig. 6.

The magnetic field of the spectrometer as well as that of the beam analyzer is kept constant by current stabilisation. The construction of equipment for proton resonance measurements of the fields is in progress†.

2.5. THE VACUUM SYSTEM

The cyclotron vacuum ductwork can be isolated from the system in the experimental room by a slide valve on the inside of the shielding wall (fig. 1). Another valve of the same type is mounted at the exit of the analyzing magnet. Because of this latter valve, the analyzer can be rotated with the vacuum preserved in its chamber. At the entrance there is a gasket tightening to the beam tube allowing this.

A baffled 6″ oil diffusion pump (forepump speed 450 l/min) is connected to a pumping house between the analyzer and the heavy-particle spectrometer. The pumping house is in connection with the target chamber through two tubes, one for the beam and the other (⌀ 100 mm inside) for evacuation. The opening to the analyzer can be closed by a valve inside the pumping house. Another valve on the detector side of the spectrometer makes it possible to change the detector arrangement without letting air into the target chamber. There is a separate connection to the forepump from the detector side.

In the pumping house a cooling trap is mounted which reduces the small amounts of oil leaking through to the target. From a container (≈ 2.5 l) of liquid air, suitably shaped metal plates surround the beam and point into the evacuation tube. A second cooling trap can be put into the target chamber.

† The author is much indepted to Mr. P. Hanssen at the University of Bergen, Norway, for submitting much valuable information about his fluxmeter construction.

Due to the large pumps, a satisfactory vacuum (better than 10^{-5} mm Hg) is obtained in the spectrometer system (≈ 80 l) very quickly. This is important as time can thus be saved when targets and detectors have to be changed.

2.6. TARGET CHAMBER

It is often of importance that one can measure the intensity of particle groups for very small scattering angles. Therefore the scattering chamber has been made so that angles in the region from 0° to about 135° are covered by the spectrometer (the upper limit is fixed by the magnet design). The particles from the target should enter the spectrometer in a direction 5.7° to the horizontal because of the fringing field. Also the incident particles must therefore have the corresponding direction. This is easily achieved with the analyzer.

The construction of the chamber and its supporting framework is indicated in fig. 7. The

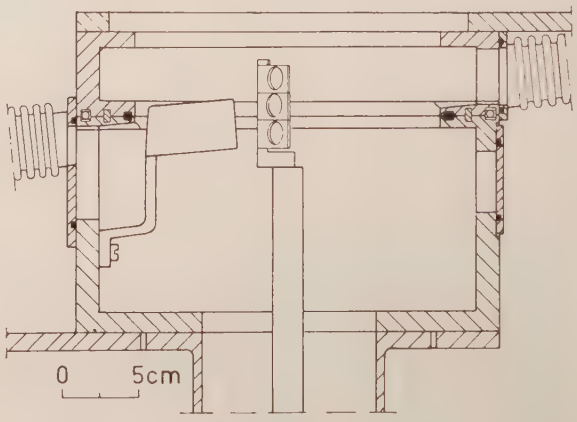

Fig. 7
Schematic view of the target chamber. In front of the targets a frame for slits (No. 5, see 2.1, and anti-scattering slits) is indicated. The spectrometer direction is assumed to be 0°.

chamber, being made of aluminium, is of the same type as was used previously[8]) but its dimensions are larger (⌀ 320 mm outside). It consists of two parts, one (the upper one) fixed to the spectrometer by a horizontal plate and the other fixed to the ceiling of the experimental room. Between these parts there are, a ball-bearing, a gasket tightening and a leading brass ring. In the lower part there are, apart from the

hole for the beam tube, four openings (⌀ 40 mm) on the side opposite to the spectrometer. These can be used, for instance, for a detector monitoring the beam which hits the target and for electrical connections from a faraday-cup. The pumping tube is connected to the bottom of the chamber.

As it is very convenient to have as much room as possible for the detector arrangement, the framework supporting the lower part of the chamber is fixed to the ceiling. The frame, also made of aluminium, consists of a horizontal plate (12 mm thick), mounted to the flange of a vertical tube (⌀ 125 mm outside, 115 mm inside). The plate is screwed to the underside of the chamber. There are dowel-pins at all the screwed joints so that one can remount the arrangement easily. The vertical axis of the chamber was carefully adjusted. This frame construction has appeared to be quite satisfactory for taking up the static momentum which arises when the spectrometer is rotated. The movement of any point on the chamber, when this one is rotated under vacuum, does not exceed 0.1 mm. If this rigidity will not be sufficient a further bellow-connection between the chamber and the frame of slit No. 4 can be applied. A target-support can then be fixed to the slit-frame within this connection.

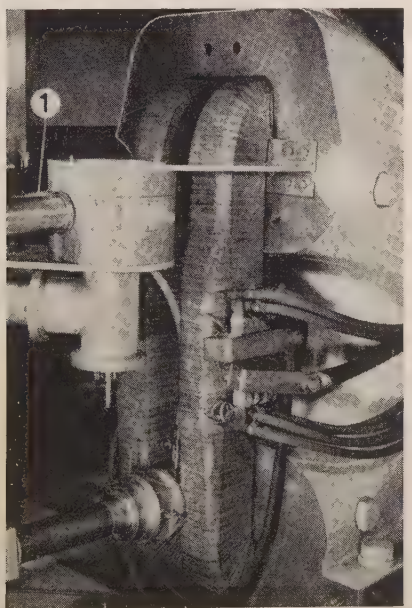

Fig. 8. Photograph of the target chamber and the spectrometer. Electronic detector behind the spectrometer and monitor detector are partially hidden. 1 is the tube for the incident beam.

A photograph of the target chamber and spectrometer is shown in fig. 8.

2.7. TARGETS

As it is desirable to have as pure targets as possible, electromagnetically separated isotopes will generally be used. The separated material is collected on thin foils of heavy metals. Au and Ta have been used for this purpose.

Another type of target is a volume of gas enclosed in a small chamber. Such a chamber has been constructed. It has two 1 mg/cm^2 Ni-foil windows through which the beam can pass and two larger mylar windows (about 1 mg/cm^2), one to the spectrometer and one to a detector for monitoring. It can be filled with a gas to a pressure of at least 1 atm. Its total volume is about 2.5 cm^3.

2.8. DETECTORS

If high energy resolution is wanted, a photographic plate is in many cases the best detector. It also has the advantage that it detects one or several groups at the same time. The running time is therefore shorter than it is when a movable, narrow slit in front of an electronic detector is used. However, the evaluation of the photographic plates is time-consuming work. Even if the reading of the particle tracks can be done by an automatic device[18]), the development procedure requires much time. This is serious, for example, in the preparation of an experiment when one generally needs the results at once. In addition, such a device is not very simple to construct. It has therefore been considered worth while to work out some simple arrangement of electronic detection which sometimes can replace the photographic plates. Such an arrangement, consisting of CsI(Tl)-pieces, will be described below. It is used in preliminary inspections of groups and in angular distribution measurements when its resolution is

[18]) P. V. C. Hough, Nuclear Instruments 6 (1960) 33.

sufficient. A more satisfactory arrangement will be constructed later. For the photographic plates a new camera has been made. It is described first.

(1) *A camera for nuclear emulsion plates*

The locus of the radial image of the spectrometer is a plane inclined at an angle of 41° to the optic axis[19]). The camera has therefore been made so that one can put plates (5″ × 1″) in this plane if desired. Thus the optimum resolution over the whole range is obtained. Often, however, shorter plates (3″ × 1″) perpendicular to the optic axis can be used. In the camera there is room for a maximum of 12 short or 6 long plus 6 short plates.

A photograph of the camera is given in fig. 9. The nuclear emulsion plates are symmetrically mounted to a frame which can be rotated about a vertical axis. In the opening of the surrounding cylindrical box there is a light-tight shutter by which the exposure time is defined. A couple of millimetres in front of the plates stopping foils can be placed. The shutter and the motor turning the plate-frame is operated from the control room. The position of those plates which are to be exposed is defined by a leading pin fitting into holes in the frame. By signal lamps in the control room one can see which plate is in the exposure position. The camera is easily removed for reloading without breaking of the vacuum in the target chamber (2.5).

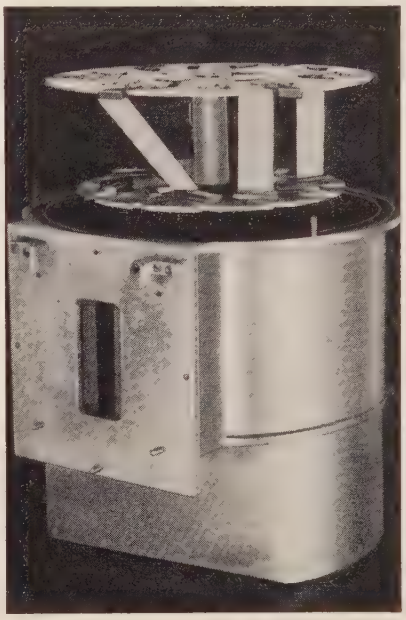

Fig. 9. Photograph of the camera for nuclear emulsion plates (1″ × 3″ or 1″ × 4.5″) with the plate-frame lifted up. The shutter is partially seen in the opening. The components necessary for the remote control are fixed to the under-side of the camera within a cover.

(2) *A multichannel position detector*†.

A simple version of the arrangement referred to above is shown in fig. 10. Thin strips of a CsI(Tl)-crystal are cemented†† to pieces consisting of coloured††† and uncoloured lucite. These pieces are cemented onto a lucite light-guide (⌀ 5.0 cm, length 20 cm), which, at the opposite end, is connected to the photomultiplier. Between the lucite pieces there are thin, light-tight Al-layers (evaporated). On the CsI(Tl)-surface, which is carefully polished, as well as on all sides of the pieces, there are thin

† The semiconductor detectors should be most convenient for this purpose. They can be made in very narrow strips (0.5—1 mm) so that a system might be constructed which in most cases could replace the photographic plates. Possible types of detectors are the Ge–Au layer[20]) and the Si p-n- junction[21]).

A system of small scintillation crystals with light-guides to each piece may also be a satisfactory arrangement. The number of photomultipliers can be reduced by means of an appropriate gatesystem[22]).

Another type of position detector[23]) consists of a scintillator viewed by two multipliers. The heights of the pulses in the two channels depend on where the particle hits the crystal because of the variation of the solid angles. A detector of this kind can be made in many ways. Maybe a combination with some pulse-reduction by absorption of the light would be favourable.

Note added in proof: See also Nuclear Spectroscopy, Part A, p. 41, editor F. Ajzenberg-Selove (Academic Press New York and London, 1960).

†† Epikote 812 with ethylenediamine (water-free) as a hardener. (See R. J. Omohundro, Rev. Sci Instr. **29** (1958) 893.)

††† It would have been convenient to make the pieces of gray lucite, had this material been available.

[19]) R. Pauli, Ark. f. Fys. **10**, No. 16 (1955) 175.

[20]) J. M. McKenzie and D. A. Bromley, Phys. Rev. Letters **2** (1959) 303.

[21]) S. S. Friedland, J. W. Mayer and J. S. Wiggins, Nucleonics **18**, No. 2 (1960) 54.

[22]) B. Johansson, private communication.

[23]) M. Deutsch, unpublished work.

reflecting Al-foils. The coloured parts of the lucite pieces have thicknesses which were fitted empirically. The amounts of light reaching the multiplier as a consequence of particles landing in the different pieces of CsI(Tl) vary in suitable

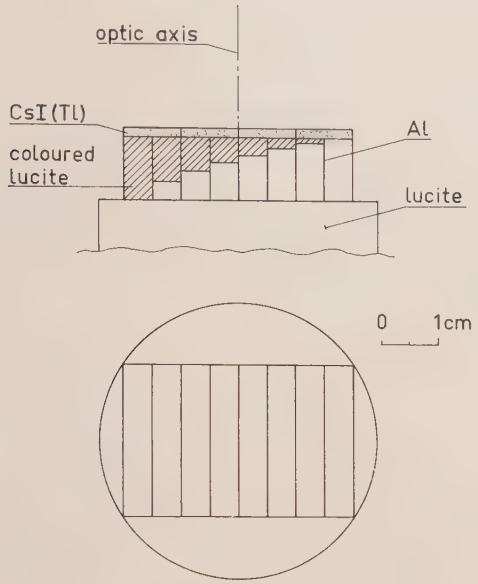

Fig. 10
Schematic view of the multichannel position detector.

steps. The pulses from the multiplier are fed to a multichannel, pulse-height analyzer. Which of the pieces is hit is thus seen by the corresponding pulse-heights.

The arrangement is independent of the particle energy. One has to adjust the amplification to obtain suitable pulse-heights.

It should be possible to cut down the widths of the CsI(Tl)-pieces. If the whole range is to be covered, two or more parallel systems can be used.

A light-guide is used as it is important to reduce the influence of the magnetic stray field from the spectrometer on the photomultiplier. The tube is enclosed in a shielding of mu-metal and ordinary iron.

In fig. 11 the pulse-height distribution from the detector indicated in fig. 10 is shown. It is seen that the distances between the peaks are not quite correct. An improved detector could be attained by trial and error. Under peak number 8 there is a fairly strong background when a deuteron beam is used.

3. Adjustments and Experimental Procedure

An accurate, mechanical adjustment of all the parts of the beam analyzing system was performed. The target chamber was carefully mounted. The suitable position of the object slit of the analyzing magnet with respect to the image slit position was experimentally determined. The 3.5 MeV proton beam was used as well as α's from ThC′ to expose photographic films at different positions. The object distance to the magnetic field boundary thus obtained, 150 cm for the present, agrees to within a few centimetres with the calculated value (147 cm), cf. refs. [12,24]).

3.1. MEASUREMENT OF THE REACTION ANGLE

The reaction angle θ is obtained from its projection ϕ on the horizontal plane by

$$\cos\theta = \cos^2\nu \cdot \cos\phi + \sin^2\nu\,, \qquad (1)$$

where $\nu = 5.7°$ is the inclination of the beam to the horizontal plane. The angle ϕ is determined

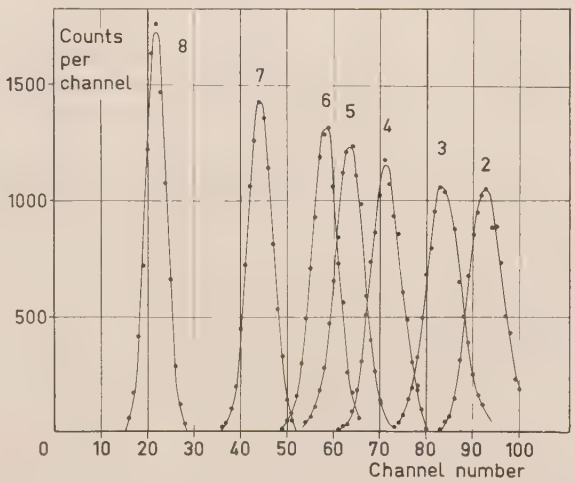

Fig. 11. Pulse-heights from the CsI(Tl)-pieces shown in fig. 10. The peaks were obtained by means of a 100-channel analyzer by imaging on the pieces the 8.78 MeV α-particles from a narrow ThC′-source. The same exposure time was used for each piece. Peak number 1 was detected in the surplus channel.

(i.e. the spectrometer setting is calibrated) by use of a narrow vertical slit mounted on a 100 mm long arm which is rotatable about the

[24]) J. Saudinos, These, Faculté des Sciences de l'Université de Paris, 1958.

central axis of the upper part of the target chamber. Elastically scattered protons were measured for several positions of this slit in front of the spectrometer opening and across the beam. The angular distance between the centres of mass of the window curves thus obtained was then determined. For a detailed discussion of the procedure see e.g. refs. [25]) and [26]). The probable error of the determination was $\pm$ 0.1°. It should be noted that an aperture slit setting $\varphi_a = \varphi_b = 127°$ (see fig. 13) should be convenient, as then a slight deviation of the target spot from the spectrometer rotation axis should not cause an error in the angular determination (appendix 1). The angle ν was previously determined in an analogous way[25]). ν varies slightly with the position of the peak on the detector plate, which follows from (5) ($\Delta\nu = \frac{1}{2}(\eta_1 - \eta_2)$). The change of θ due to this can at a maximum be a few tenths of a degree, but it is in general negligible.

3.2. ENERGY MEASUREMENTS

As mentioned above, the fields of the two magnetic analyzers are intended to be measured by proton resonance fluxmeters. The calibration can then be made with a standard α-source.

Before the fields can be accurately measured, it is necessary to determine the beam energy and the energy of the induced particles by comparison with well known Q-values. The determination has to be repeated every time accurate energy values are needed. As the changes of the fields are made carefully, the hysteresis effect is rather small†. Concerning the procedure of such comparisons and the calculation of the errors in the energy values obtained we refer to ref. [12]).

The deuteron beam energy has been measured by means of the reaction $N^{14}(d,p_0)\,N^{15}$ and the elastically scattered deuterons from Au. If the spectrometer is in the position $\phi \approx 90°$, the two peaks appear on the same photographic plate. From the distance between the peaks, the reaction angle and the Q-value of the (d,p)-reaction ($Q_0 = 8.615 \pm 0.007$ MeV[27])), the deuteron energy can be calculated. In a special case this energy was 7.154 ± 0.010 MeV. However, the beam energy is subject to small changes from time to time due to necessary adjustments of the cyclotron.

In energy measurements, corrections must be made for absorption in the target and for the variation of the dispersion and the line width (see [26])) along the plate. In a case where the angular distribution is strongly anisotropic, a displacement of the energy defining point (high energy edge, for instance) on the plate can be obtained and has to be corrected.

3.3. MONITORING

As a monitor detector, a thin CsI(Tl)-crystal (1 mm × ⌀ 20 mm) is used, mounted on a 30 cm × ⌀ 50 mm lucite light-guide. This detector seems to be satisfactory in several cases. There is also a current integrator available by means of which the charge from a faraday cup behind the target can be measured. The integrator is of the type described in ref. [28]). The cup is placed between the poles of a small permanent magnet and an electrostatic screening can also be applied. The contribution of secondary electrons is thus made very small.

A current integrator is often used when it is necessary to determine the beam intensity accurately. In relative measurements, however, the best way, where possible, is to use a fixed detector by means of which some group from a scattering or a reaction on the target nuclei can be resolved from other groups. The peak of elastically scattered particles is suitable if it can be distinguished from that coming from the backing.

The cross-section to be measured, $\sigma(\theta)$, is referred to the constant value of the "monitoring cross-section", σ_M. If the solid angles of the spectrometer and the monitor, ω and ω_M,

† *Note added in proof*: This effect is continously checked by a simple Hall-detector arrangement.

[25]) C. Mileikowsky, Ark. f. Fys. **7**, No. 8 (1953) 89.

[26]) R. T. Pauli, Ark. f. Fys. **9**, No. 36 (1955) 571.

[27]) F. Ajzenberg-Selove and T. Lauritsen, Nuclear Physics **11** (1959) 1.

[28]) I. A. D. Lewis and B. Collinge, Rev. Sci. Instr. **24** (1953) 1113.

respectively, can be considered constant for the whole target volume and for different θ, it follows that $\sigma(\theta)$ is proportional to the yield ratio $Y(\theta)/Y_M$.

$$\sigma(\theta) = \sigma_M \frac{\omega_M}{\omega} \frac{Y(\theta)}{Y_M}. \quad (2)$$

The measurement is independent of the numbers of bombarding particles and target nuclei and is therefore also independent of variations in these quantities. If the solid angles are not constant, it is necessary to integrate over the target volume. The density distributions of the beam and the target may then cause an uncertainty. Sometimes it may be necessary to correct ω and ω_M in (2) with respect to the angular derivatives of $\sigma(\theta)$ and σ_M (cf. appendix 2).

One has to be careful so that an error in the monitoring is not introduced when the angular position of the spectrometer is shifted. The detector may be influenced by the magnetic field, or the geometry may be changed. With the present screening such an influence is not troublesome.

If a group from the target itself cannot be distinguished by the monitor, it may be possible to use some group from the backing material. Then one must be careful and check that a reduction of the target thickness or a carbon deposition on the target during the exposure do not cause a large error in the measurement.

3.4. MEASUREMENT OF DIFFERENTIAL CROSS-SECTIONS

The absolute value of a cross-section may sometimes be obtained by reference to a known σ_M (see (2)), for example that for elastic scattering. In most cases, however, $\sigma(\theta)$ is to be determined independently. The numbers of bombarding particles and target nuclei within the reaction volume must be well known for such a determination. Also the density distribution of the beam and the target is in general of importance. A target consisting of a small volume of gas is suitable for measurements of absolute cross-sections. Apart from the geometry (see appendix 2), the gas temperature and pressure determine the number of target nuclei. A foil target of uniform thickness is, of course, also suitable.

In intensity measurements some corrections must be made besides those mentioned in the preceding section. The solid angle of the spectrometer has not an exactly constant value over the whole detector surface. The yield of a peak has therefore to be corrected with respect to this. The solid angle as a function of the distance across the image plane was reported in ref. [26]). The solid angle is independent of the type of reaction for the present combination of magnets (this is not always the case[5])). The influence of the finite opening angle and multiple scattering in the target on measurements of rapidly varying angular distributions is treated in ref. [12]). The corrections for these effects should generally be negligible for the present equipment.

3.5. ON THE RESOLUTION

One can increase the yield at a given resolution by reading the tracks on the photographic plate in an appropriate direction (see ref. [5])). It should then be possible to use a wider target spot than if the tracks are read in strips perpendicular to the length of the plate. If a different type of detector is used there is evidently a corresponding possibility. It was found that the optimum tilting angle φ_2 of the strips is given by

$$\operatorname{tg} \varphi_2 = \frac{F'}{F}. \quad (3)$$

Here

$$F' = K \frac{\partial E_2}{\partial E_1} \frac{E_1}{E_2},$$

where E_1 and E_2 are the energies of incident and emerging particles, respectively, and K is a parameter which is determined by the analyzing system[5]). For the present system $K = 0.52$ (object distance 150 cm). F is a function of the target orientation and the reaction angle. It can be chosen so that the energy spread caused by absorption in the target material is minimized. φ_2 is referred to the image plane perpendicular to the optic axis. In the present camera, the short plates are inclined at 45° to this plane (fig. 9).

The tilting angle φ on the plate is therefore given by

$$\operatorname{tg} \varphi = \frac{\operatorname{tg} \varphi_2}{\sqrt{2}}. \qquad (4)$$

A demonstration of this possibility to increase the yield is given in fig. 12. It is seen that the tilting of the target spot image is quite pronounced. The effect is evident even though the spot width is not very much larger than the image of the entrance slit. This may partly be due to the non-uniform intensity of the beam at slit No. 2 (fig. 1). That part of the beam width containing most of the current at slit No. 2 can be less than the slit opening.

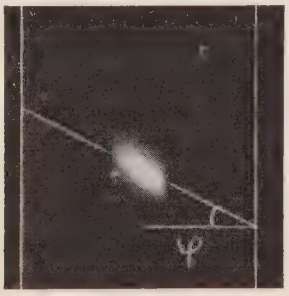

Fig. 12a. Photograph of a 1″ × 3″ nuclear emulsion plate, which was exposed in the image plane of the spectrometer to 7 MeV deuterons elastically scattered from an Au-foil (1 mg/cm²). The reaction angle was 90°. The width of the slit (No. 5) defining the target spot (4 cm in front of the target) was 6.0 mm. The height of the spot was about 2.5 mm. The object slit of the beam analyzer had a width of 3 mm. The tilting of the image depends upon the variation of the energy of the incident particles across the target. The tilting angle, $\varphi = 25°$, was obtained from (3) and (4).

It is possible to use a target spot with a width of at least 10 mm.

The total energy spread in the beam was measured with the analyzer. It was found to be about 1.0%. This corresponds to an approximate width on the target of 15 mm. It should be noted that the exposure was then made for a very short time and that the entrance slit was very narrow.

3.6. CONCLUDING REMARKS

Concerning a reduction of the beam energy by means of absorption, it should be noted that a material with low atomic number is favourable. When the particles pass the absorber they receive an angular spread due to multiple scattering and an increased energy spread due to straggling. Both effects mean a decrease of the intensity on the target. The former is most severe and depends on the atomic number of the absorber (see e.g. ref. [29])).

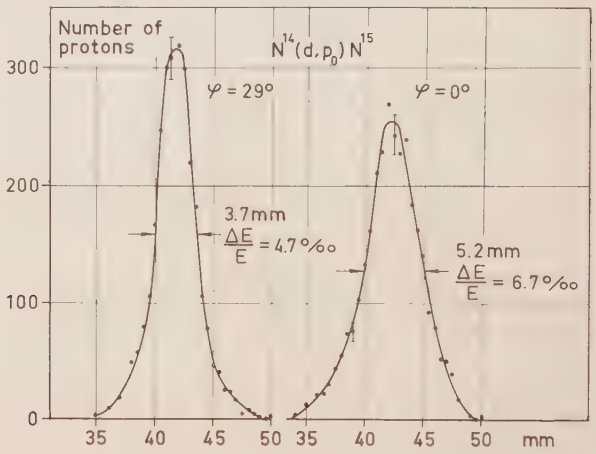

Fig. 12b. The proton group from a 7 MeV deuteron bombardment of N^{14}, corresponding to the ground state of N^{15}. The reaction angle was 90°. Target material: about 0.2 mg/cm² adenine ($C_5H_5N_5$) on 0.15 mg/cm² Al. The slit settings were the same as in fig. 12a. The scanning of the emulsion plate was done in two ways: (i) in strips which were inclined at an angle $\varphi = 29°$ (obtained from (3) and (4)); (ii) in the "ordinary" way ($\varphi = 0$).

The background from the cyclotron, the slits and the target backings has not yet been systematically investigated.

4. Measurements

The first measurement with the equipment described here is being made on the reaction $Ne^{22}(d,p)Ne^{23}$. Several other investigations of nuclei in the mass region 20—30 on separated targets are planned. Mainly the deuteron beam will be used, but also the α-particle beam when its intensity is sufficient.

Acknowledgements

The author wants to express his sincere thanks to Professor Manne Siegbahn for his stimulating

[29]) Experimental Nuclear Physics, editor E. Segrè (Wiley and Sons, Inc., New York, 1952).

interest throughout this work. Sincere thanks are also due to Docent Karl Gustav Malmfors for many valuable discussions and ideas, to Fil. Mag. Nils Johansson and Civ. Ing. Gunilla Hahn for their help in the final stages of the work, to Ing. Bo Höijer for his technical assistance, to Civ. Ing. Palne Mogensen for performing the adjustments of the quadrupole lenses, to Mr. Erik Abrahamsson for making many of the mechanical components, to Ing. Bengt Carlsson who has built a current stabilizer and a current integrator and to Ing. Tommy Appelqvist and Ing. Rolf Åkerlund who have operated the cyclotron.

Appendix 1

APERTURE SLIT POSITION AND SOLID ANGLE

It is assumed that the aperture of the spectrometer in its radial direction is defined by a $2a$-wide slit symmetrically placed at the angle φ_a, as in fig. 13. A first order calculation (cf. ref.[30])) of the aperture angles indicated in the figure results in the following expressions (index 1 corresponds to upper sign):

$$\eta_{1,2} = \frac{a \mp \left[\frac{\Delta \cdot r_0}{1-n} + \left(y_1 - \frac{\Delta \cdot r_0}{1-n}\right)\cos\varphi_a \sqrt{1-n}\right]}{l_0 \cos\varphi_a \sqrt{1-n} + \frac{r_0}{\sqrt{1-n}} \sin\varphi_a \sqrt{1-n}} . \tag{5}$$

Here r_0 is the mean radius, l_0 the distance from the object to the magnetic field boundary and n is the field gradient parameter. Δ indicates the deviation of the momentum of the particles from the mean value corresponding to the optic axis. y_1 is the distance of the object point from the optic axis.

The margin angles in the axial direction of the spectrometer, ϑ_1 and ϑ_2, are obtained from expressions corresponding to (5) ($\sqrt{1-n}$, y_1, and a are replaced by $\sqrt{n}$, z_1, and the axial slit width b, respectively) if the Δ-terms are first omitted.

It is seen that $\eta_1 = \eta_2 = \eta_0 = (a/r_0)\sqrt{1-n}$, if $\varphi_a \cdot \sqrt{1-n} = \frac{1}{2}\pi$ and that $\vartheta_1 = \vartheta_2 = \vartheta_0 = (b/r_0)\sqrt{n}$, if $\varphi_b \cdot \sqrt{n} = \frac{1}{2}\pi$ ($\Delta = 0$). This means that the angles are independent of y_1, z_1 and l_0. Thus, for this special slit setting, the aperture angles are constant for all points within a target volume. It should be noted that the size of this volume in the first order is restricted by the available field space in front of the aperture slits. When $n = \frac{1}{2}$, as for the present spectrometer, the radial and the axial slits should be placed at the same angle, $\varphi_a = \pi/\sqrt{2} = 127°$.

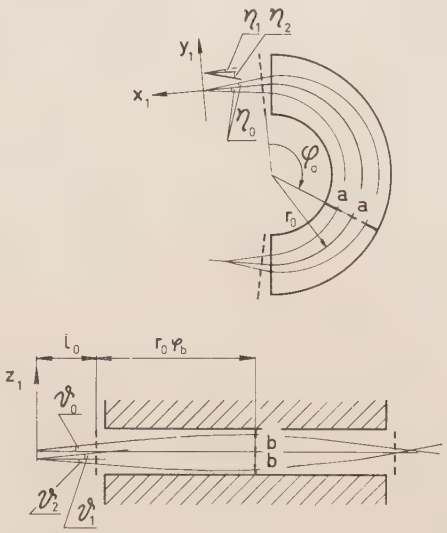

Fig. 13. Definition of the quantities determining the transmission through the spectrometer. The magnetic field boundaries are indicated by broken lines.

The solid angle ω is in the first order obtained from η_1, η_2, ϑ_1 and ϑ_2.

$$\frac{\omega}{A} = \left[\frac{l_0}{r_0}\cos\varphi_a \sqrt{1-n} + \frac{1}{\sqrt{1-n}} \sin\varphi_a \sqrt{1-n}\right]^{-1} \cdot \left[\frac{l_0}{r_0}\cos\varphi_b \sqrt{n} + \frac{1}{\sqrt{n}} \sin\varphi_b \sqrt{n}\right]^{-1} \tag{6}$$

where Ar_0^2 is the available cross-sectional area limited by the slits. For $n = \frac{1}{2}$ and $\varphi_a = \varphi_b = \pi/\sqrt{2}$

$$\omega/A = \tfrac{1}{2} . \tag{7}$$

As mentioned above (2.4), $\varphi_a = \varphi_b = 95.7°$ for the present. The aperture is 6.0×1.7 cm^2 (trapezoidal form), $l_0 = 30.0$ cm and $r_0 = 40.0$ cm. The solid angle obtained from (6) is

$$\omega_{\text{calc.}} = 2.50 \times 10^{-3} \text{ sterad} .$$

[30]) D. L. Judd, Rev. Sci. Instr. **21** (1950) 213.
N. Svartholm, Ark. f. Fys. **2**, No. 14 (1950) 115.

The solid angle was also determined by measuring the yields of an α-group from a ThC′-source both behind the spectrometer and within a known solid angle (the monitor). The result was

$$\omega_{\text{exp.}} = (2.49 \pm 0.09) \times 10^{-3} \text{ sterad}$$

where the total probable error is indicated (cf. ref. [7]).

Appendix 2

THE G-FACTOR FOR GAS SCATTERING

When a gas is used as a target, the effective volume is determined by a pair of slit systems, one defining the beam and the other defining the transmission to the detector. The yield Y from such a target is given by

$$Y = \frac{nNG \cdot \sigma(\theta)}{\sin \theta} . \tag{8}$$

Here n is the number of bombarding particles, N is the number of target nuclei per unit volume and $\sigma(\theta)$ is the differential cross-section for the reaction angle θ. G is the geometrical factor. Apart from the geometry, it depends in general on $\sigma(\theta)$, $\sigma'(\theta)$ (i.e. $\mathrm{d}\sigma(\theta)/\mathrm{d}\theta$), and the higher derivatives. It is convenient to express G as a series in the following way:

$$G = G_0 \left[1 + \Delta_0 + \Delta_1 \frac{\sigma'(\theta)}{\sigma(\theta)} + \Delta_2 \frac{\sigma''(\theta)}{\sigma(\theta)} + \cdots \right] . \tag{9}$$

The coefficients in (9) can be calculated by geometrical considerations. They are given in ref. [31]). The yield of the monitor detector (see (2)) is obtained by use of the applicable expressions.

[31]) E. A. Silverstein, Nuclear Instruments **4** (1959) 53.

As to the value of G for the spectrometer arrangement, we assume the type of aperture slit system treated in appendix 1. The target volume is defined by the cross-section of the incident beam, and by the aperture of the spectrometer and a vertical slit near to the target (see fig. 14). The slit is symmetric with respect to the mid-plane of the spectrometer. The factor is determined under the assumption that for all target

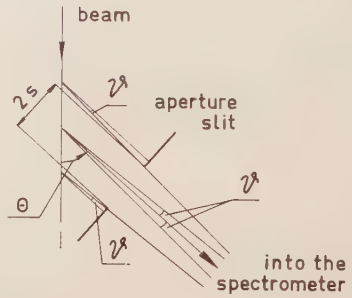

Fig. 14. Definition of the effective target volume when a gas sample is used.

points the angles ϑ and η (appendix 1) are constant. A simple modification of the expressions in ref. [31]) gives the following result:

$$\Delta_0 = (\tfrac{1}{3} \cot^2 \theta - \tfrac{1}{2}) \vartheta^2 - \tfrac{1}{2}\eta^2 , \tag{10}$$

$$\Delta_1 = \tfrac{1}{3} \cot \theta \, (\tfrac{1}{2}\eta^2 - \vartheta^2) , \tag{11}$$

$$\Delta_2 = \tfrac{1}{6}\vartheta^2 , \tag{12}$$

$$G_0 = 8 s \vartheta \eta = 2 s \omega . \tag{13}$$

It is seen that the correction terms in (9) are generally very small. They should in most cases be negligible.

NUCLEAR INSTRUMENTS AND METHODS 7 (1960) 289–292; NORTH-HOLLAND PUBLISHING CO.

THE SPECTRAL SENSIBILITY OF A MAGNETIC GAMMA-SPECTROMETER IN A PHOTOELECTRIC METHOD

E. P. GRIGORYEV and A. V. ZOLOTAVIN

Physics Dept., Leningrad University, Leningrad

Received 7 October 1959

It is shown that by using a cylindrically symmetric source one can compensate the influence of the angular distribution of photoelectrons on the determination of relative intensities of γ-rays in measurements with the help of a transversal magnetic spectrometer.

1. Introduction

The photoelectron method in combination with a magnetic spectrometer is often used to measure relative intensities of γ-rays I_γ in the region of energies higher than 50 keV. Since the photoelectrons are monochromatic, it is possible to gain very narrow photolines using this method. This is complicated by the circumstance, that the angular distribution of the photoelectrons depends on the energy of the γ-rays in a way, which cannot be exactly calculated. Because of this it is necessary to determine the spectral sensibility of a γ-spectrometer experimentally. This was done for a lens spectrometer in paper[1]). The spectral sensibility curve for a spectrometer with a transversal magnetic field "KOETRON" is shown in paper[2]), for a spectrometer with double focusing of the beam in paper)[3].

It is shown in this paper, that if one has a certain geometry of the source the angular distribution of the photoelectrons does not effect the transmission of relative intensities of γ-rays in a magnetic spectrometer with double focusing of the beam.

2. Choosing the Geometry of the Source

We will introduce several designements.

By the spectral sensibility of a γ-spectrometer we mean the dependence of the photopeaks, called forth by a given number of γ-quanta, on the energy of the γ-rays. Here the areas are reduced to equal intervals of impulse $H\rho$ and all necessary corrections (for background, decay, absorption of γ-rays and photoelectrons) are introduced into the measurements. This can be written (for a thin target):

$$S_\gamma = \Gamma \cdot \theta \cdot \tau_K \cdot N_\gamma = \varphi(h\nu) \cdot N_\gamma$$

S_γ = the area of the K-photoline (reduced to a unity interval of $H\rho$) in (impulses/minute gauss·cm].

Γ = a factor allowing for the geometry of the spectrometer (solid angle, source form etc.).

Θ = a factor allowing for the angular distributions of the photoelectrons.

τ_K = the photoelectron absorption cross-section for the rays on the K-shell of the target matter atome.

N_γ = the number of γ-quanta emited by the source of quanta in a time unit.

The function $\varphi(h\nu)$ determines the spectral sensibility of the instrument. We choose the area of one definite line as an area unit and then define the relative intensities of the γ-transitions:

$$I_\gamma = \frac{N_\gamma}{N_{\gamma_0}} = \frac{S_\gamma}{S_{\gamma_0}} \frac{\tau_{K_0}}{\tau_K} \frac{\Theta_0}{\Theta} = I_{\gamma e} \cdot f(h\nu)$$

[1]) P. A. Thiskin, Dissertation, Leningrad (1953).

[2]) N. M. Antonieva, A. A. Bashilov and E. K. Kulakovsky, Journ. Exptl. Theoret. Phys. (USSR) **37** (1959) 1497.

[3]) E. P. Grigoriev, A. V. Zolotavin, V. N. Klementiev and R. V. Sinitsin, Izv. Akad. Nauk SSSR (Ser. Fiz.) **23** (1959) 159.

The calibration of the spectrometer comes to determining the dependence $\Theta/\Theta_0 = f(h\nu)$. For this sake one uses sources, the I_γ of which are known (cascade transitions, a set of sources the intensities of which are determined calorimetrically, etc.)

Then, if one denotes

$$\frac{S_\gamma}{S_{\gamma_0}} \frac{\tau_{K_0}}{\tau_K} = I_{\gamma e}$$

the experimental not corrected value of the relative intensities, one determines the sought dependence

$$\frac{\Theta}{\Theta_0} = \frac{I_{\gamma e}}{I_\gamma} = f(h\nu) .$$

The arrangement of the photoelectron sources in this method is very important for the outlook of the function $f(h\nu)$. If the photoelectron source would be constructed as a spherical target in the centre of which a γ-ray source is placed, then the distribution of photoelectrons would be isotropic. In the case, when the γ-ray source is situated on the axis of a cylindrical target, the distribution of photoelectrons in a plane, perpendicular to the symmetry axis will be the same in all directions for all γ-ray energies. In the case of a plane target and a plane source of γ-rays filling a channel with a rectangular section behind the target, the distribution of photoelectrons in a plane, perpendicular to the target will not have such a feature. For such a source one can expect, that I_γ will be energy-dependent for the chosen volume beam.

In paper[4]) such a target was used. An experiment showed that the function $f(h\nu)$ grows when the energy of the quanta grows.

It follows from papers[2,3]) that for exactly symmetric photoelectron sources, when the diameter of the γ-ray source is larger than 1 mm or equal (see fig. 1) the function $f(h\nu)$ decreases when the energy of the quanta increases.

These experiments show that it is possible to choose such a geometry of the source that the angular distribution of the photoelectrons will not have an influence on the determination of I_γ. We succeeded in choosing such a geometry of an axially symmetric source for the volume beam used in the instrument.

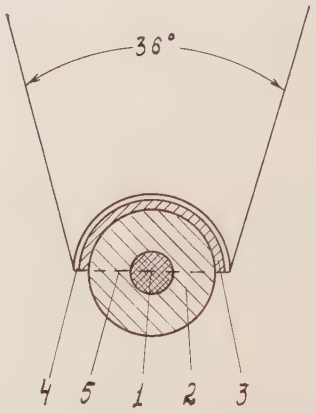

Fig. 1. Cross-section of the photoelectron source. 1. Radioactive preparation (diameter of the channel 0.3–0.5 mm). 2. Cylindrical ampoule. 3. Aluminium backing (outer diameter 1.2–3.0 mm). 4. Converter. 5. Position of the focus of the spectrometer. Divergence of the beam in the radial direction 36° in the axial direction to 9°.

In determining $I_{\gamma e}$ in the region $0.6 \leqslant h\nu \leqslant 2.1$ MeV the diameter of target was chosen equal 3 mm, the diameter of the channel filled with a radioactive preparation was 0.5 mm. The length of the target was 30 mm, length of the channel slightly more. In the energy region $0.05 \leqslant h\nu \leqslant 0.5$ MeV the diameter of the target was 1.2 mm and the diameter of the channel was 0.3 mm. The targets were made sufficiently thin, so that the halfwidth of the photoelectron lines did not top the instrumental halfwidth 0.5–0.8%.

A spectrometer with double focusing of the beam was used in the experiments[5]), which had the following characteristics: size of the focus 30 × 1 mm, aperture ratio 0.65%, radius of the equilibrium orbit 140 mm.

3. Results of Measuring

3.1. REGION 0.6–2.1 MeV

In this energy region we investigated the γ-spectrum of Sb^{124}[5]). With the chosen geometry of the source we obtained $I_{\gamma e} = 1.94$

[4]) P. P. Zarubin, Dissertation, Leningrad (1953).

[5]) A. V. Zolotavin, E. P. Grigoriev and M. A. Abroyan, Izv. Akad. Nauk SSSR (Ser. Fiz) **20** (1956) 289.

± 0.10 for the cascade transitions 603 and 1691 keV. The same value of the relation follows from an analysis of the decay scheme. Besides that it is possible to calculate I_γ by the intensities of the conversion lines and by the conversion coefficients for transitions, the multipole order of which is known. The $I_{\gamma e}$ which we determined, corresponded to the calculated values of the γ-ray intensities. All this gives us grounds to consider $f(h\nu) = 1$ in our experiments. Following determinations of I_γ for this isotope by the method of recoil electrons[6]) and by a scintillation spectrometer[7]) confirmed our conclusion. This can be seen in table 1.

TABLE 1

Comparing $I_{\gamma e}$ and I_γ for Sb^{124}

keV	$I_{\gamma e}$† our data 1956[5])	I_γ Recoil electrons 1957[6])	I_γ Scintillation spectrometer 1959[7])
603	100	100	100
714	3.9 } 14.2	14 ± 1	15 ± 1.5
723	10.3 }		
1691	51	51 ± 3	49 ± 4
2088	6.7	6.6 ± 1.0	6.3 ± 1.0

† Uncertainties in $I_{\gamma e}$ 5–10%.

3.2. REGION $0.05 < h\nu < 0.5$ MeV

In this region of energies we measured the γ-spectrum of Se^{75}. In this case, as we mentioned above, the dimensions of the source were reduced in the radial direction. Besides that we used very thin targets (0.03–0.25 mg/cm²). This made it possible to get photolines with the halfwidth 0.5%. It was found that for γ-transitions with $h\nu = 136$ keV even such thin heavy metal $Z = 83$) targets gave understated values of $I_{\gamma e}$. Because of this an Ag-target was used so as to reduce the energy loss of the photoelectrons, due to soft quanta. Simultaneously with $I_{\gamma e}$ the conversion spectrum of Se^{75} was measured and the internal conversion coefficients (α_K) of the transition were determined. The details about the measurements are stated in[3]). A criterion of the correctness of the obtained values of $I_{\gamma e}$ was the concurence of the values of $\alpha_{Ke} = I_K/I_{\gamma e}$ for the transitions 265, 280, 304, 401 keV determined by us with the α_K determined in paper[8]) by the graduated target method.

[6]) B. S. Dzhelepov, N. N. Zhukovsy and F. A. Predovsky, Izv. Akad. Nauk SSSR (Ser. Fiz) **21** (1956) 1614.

[7]) R. K. Girgis and R. Van Lieshout, Physica **25** (1959) 133.

[8]) A. A. Bashilov and V. V. Ilyn, Izv. Akad. Nauk SSSR (Ser. Fiz.) **23** (1959) 154.

TABLE 2

Comparing $I_{\gamma e}$ and I_γ for Se^{75}

$h\nu$† (keV)	$I_{\gamma e}$ our data 1959[3])	I_γ Recoil electrons 1959[9])	I_γ Scintillation spectrometer 1955[11])††	1959[10])
66.05	1.53 ± 0.15	—	1.8 ± 1.0	—
96.7	5.5 ± 0.3	—	6.6 ± 1.5	—
121.1	27.9 ± 1.3	—	28 ± 6	—
136.0	96 ± 5	—	94 ± 12	—
198.6	2.6 ± 0.2	< 6.4	3	
264.6	100.0	100.0	100.0	100.0
279.6	41.0 ± 2.5	44 ± 7	45.7 ± 4	47 ± 1
304.0	2.5 ± 0.3	3.2 ± 1.1	2.0 ± 0.5	2.1 ± 0.3
400.7	22.3 ± 2.3	23 ± 2	24.9 ± 2.3	19 ± 2

† The energies of the transitions are given in paper[12]).

†† The ratio of the intensities of near lines is determined with the help of a lens spectrometer.

[9]) N. A. Voinova, B. S. Dzhelepov and N. N. Zhukovsky, Izv. Akad. Nauk SSSR (Ser. Fiz.]) **23** (1959) 195.

[10]) F. R. Metzger and W. B. Todd, Nuclear Physics **10** (1959) 220.

[11]) M. W. Schardt and J. W. Welker, Phys. Rev. **99** (1955) 202.

[12]) W. E. Edwards, C. I. Gallagher and J. W. M. DuMond, Bull. Am. Phys. Soc. **4** (1959) 279.

Besides that α_{Ke} concure with the theoretical for the transitions 121, 136 and 401 keV, which belong to the type E1. The ratios α_{Ke}/α_K in both cases coincide with 1 in the range of 10%. From here it follows that if $f(h\nu)$ does change in the considered energy region in our experimental conditions, then it does not change for more then 15%.

Comparison with direct I_γ measurements for Se^{75} by other methods confirm this conclusion. The appropriate data are given in table 2.

4. Conclusion

Only one side of the problem of the spectral sensibility of γ-spectrometer is considered in this paper.

To get more exact and more reliable measurements of I_γ it is really necessary to know the precise form of the function $\varphi(h\nu)$. As a matter of fact, besides the influence of the angular distribution of the photoelectrons, an uncertainty is carried into $I_{\gamma e}$ because we do not know the quantity τ_K exactly. Here there is necessary work for theorists, so that $\tau_K(h\nu,Z)$ should be known with the same precision as internal conversion coefficients. One can of course avoid this difficulty, if one determines the form of $\varphi(h\nu)$ experimentally, using cascade quanta or other γ-rays, the relative intensities of which are known. One of the ways to solve this problem is the calibrated target method[8]). But in both cases one needs a large set of γ-rays standards.

The authors are deeply regarded to Prof. B. S. Dzhelepov for his useful advice and observations made when this paper was discussed.

NUCLEAR INSTRUMENTS AND METHODS 7 (1960) 293–296; NORTH-HOLLAND PUBLISHING CO.

A THIN LIQUID HYDROGEN OR DEUTERIUM TARGET

E. H. BELLAMY, W. R. HOGG and D. MILLER

Natural Philosophy Department, Glasgow University

Received 4 March 1960

The construction and performance of a low background double-walled flat liquid hydrogen or deuterium target of precisely known thickness is described.

Experimental studies of the elastic photoproduction of neutral pions from hydrogen and deuterium may be made by measuring the direction and energy of the recoil proton or deuteron. Because of the continuous nature of the bremsstrahlen spectrum, for low recoil energy the target must be thin if considerable uncertainty in the energy of the photon responsible for the reaction is to be avoided. Consider, for example, the reaction

$$\gamma + \mathrm{d} \rightarrow \pi^0 + \mathrm{d}\,.$$

Then with a target of liquid deuterium 0.07 g/cm² thick, a deuteron emerging at 31.5°, to the photon beam, with an energy of 10 MeV could be associated with a photon of energy from 180 MeV (90° c.m.s.) to 200 MeV (80° c.m.s.) depending on the position within the target of the production of the deuteron.

Thin solid targets of CH_2 or CD_2 have been used with a subtraction technique, (e.g.[1,2])). But the background of protons or deuterons from the photodisintegration of the carbon is excessive, and the low ratio of hydrogen or deuterium target material to stopping power in the target is also disadvantageous.

Gaseous targets can readily satisfy the requirement of small energy degradation in the reaction products, but when a sufficient density is achieved, by high pressure and cooling with liquid nitrogen, thick windows are necessary and the target is extended in space, making it unsuitable for use with external counters. This has been overcome by having photographic emulsions within the high pressure vessel[3]).

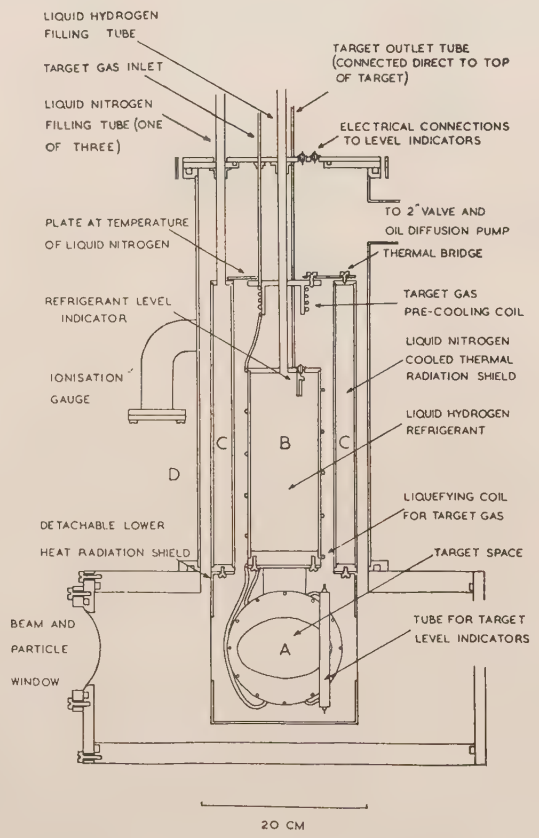

Fig. 1. Vertical section through cryostat.

A target of liquid hydrogen or deuterium can

[1]) G. Cocconi and A. Silverman, Phys. Rev. **88** (1952) 1230.

[2]) J. W. De Wire and A. Silverman, Phys. Rev. **99** (1955) 268.

[3]) Y. Goldschmidt-Clermont, L. S. Osborne and M. Scott, Phys. Rev. **97** (1955) 188.

be made of any thickness to suit experimental conditions, but if the walls are thin, to give low background, they bulge and absolute cross-sections are difficult to measure. A design has

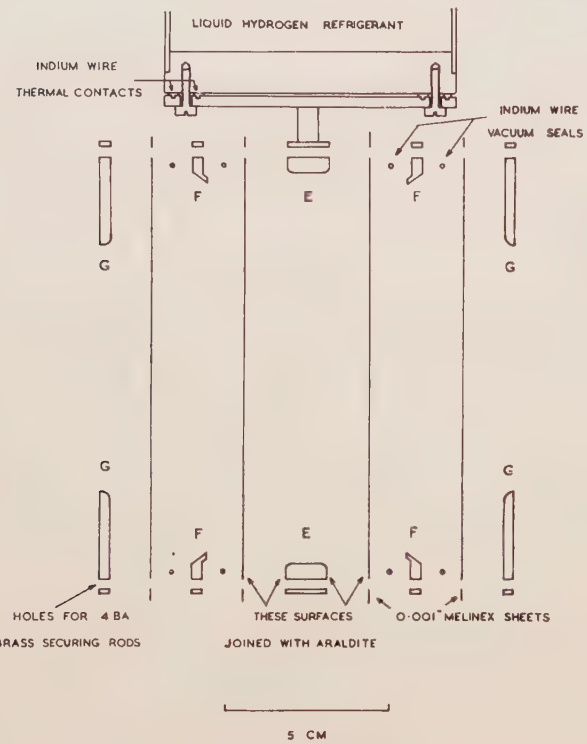

Fig. 2. Exploded vertical section through target chamber.

been developed in this laboratory which overcomes this, and models have been made from 2 mm to 1 cm thick and suitable for setting at angles up to 70° to the beam direction. In the following a typical target 1 cm thick is described.

The liquid target A (fig. 1) is contained in a liquid hydrogen cryostat of standard form[4,5,6]). The liquid hydrogen refrigerant at atmospheric pressure is contained in the 1 litre cylinder B, isolated by high vacuum and suspended by thin-walled copper-nickel tubing from the surrounding liquid nitrogen cooled radiation shield C. This shield and the inside surface of the vacuum jacket D are covered with aluminium foil to reduce transfer of heat by radiation. The vacuum is maintained at less than 10^{-6} mm Hg by an oil diffusion pump operating continuously. Typical evaporation rates for the refrigerants are 0.03 liter per hour of the liquid hydrogen and 0.25 litre per hour for liquid nitrogen, in agreement with calculations.

The detachable target chamber is shown in figure 2. It consists of a copper ring, E, $5\frac{1}{2}''$ o.d., $4\frac{3}{4}''$ i.d. and $\frac{1}{2}''$ thick. On each face of this, a 0.001″ thick sheet of "Melinex" (Mylar) (I.C.I. Ltd.) is cemented with "Araldite" (Ciba (A.R.L.) Ltd.). The hot (160° C) setting type is used and the process also serves to tension the foils. To increase this tension further the brass rings illustrated, F, are forced on to each side. The height of the step on the inside edge of the rings determines the target thickness. On the outside of this structure two more 0.001″ Melinex sheets are placed, held in position by the two brass plates, G. Since the beam goes through at an angle to the target (fig. 3) the hole in these plates is elliptical to give optimum clearance to the beam and support to the outer foils which sustain one atmosphere pressure difference. The whole structure described is held together by twelve 4 B.A. brass screws and the vacuum seals are achieved by ○-rings of welded loops of $\frac{1}{16}''$ indium wire in the positions indicated in fig. 2. Retaining grooves were found to be unnecessary and these seals have behaved satisfactorily under repeated temperature cycling.

The assembled target is drawn in fig. 3. The liquid hydrogen refrigerant and the target substance are separate. The target space H is filled with liquid hydrogen or deuterium condensed from a gas holder by cooling in the cryostat with liquid nitrogen and then circulating in a liquid hydrogen cooled coil. The vertical tube J is connected at the top and the bottom to the space H and contains two level indicators in the form of 68 ohm carbon resistances ($\frac{1}{2}$ W, 2% high stab.). Either may be connected in an external Wheatstone bridge and when balanced 0.3 watt is dissipated in the level indicator. If, on switching on, the resistance

[4]) D. Bodansky, A. M. Sachs and J. Steinberger, Phys. Rev. **93** (1954) 1367.

[5]) E. A. Whalin and R. A. Reitz, Rev. Sci. Inst. **26** (1955) 59.

[6]) D. E. Nagle, Phys. Rev. **97** (1955) 480.

is in vapour it heats up and gives a rapid shift in balance point; if in liquid, due to the greater thermal dissipation, negligible shift of balance occurs, indicating quite unambiguously whether the target is full or empty.

The spaces K, fig. 3, are connected together and are maintained at exactly the same pressure as H. To achieve this, tubes are led from both H and K out of the cryostat into the device L. This consists of two saucer shaped volumes separated by a slack cellulose acetate film. The position of the film can be observed through a glass window and any difference in pressure between H and K is compensated by the foil shifting and pumping gas into or out of K. Gas can be added to, or subtracted from, K manually through a needle valve. This has proved capable of compensating automatically for the slow changes in vapour pressure of the target material due to ortho-para conversion in it and in the refrigerant and due to changes in atmospheric pressure. The target thus remains flat. This has been checked by evaporating aluminium on to the walls to form a mirror and observing it through a hole in the radiation shield. A measure of its thickness at room temperature, by optical means to an accuracy of $\pm$ 0.03 mm in 1 cm, is used to determine the thickness of liquid hydrogen.

During the initial filling of the target, the gas to be liquefied is introduced into both H and K until a pressure a few centimetres below the liquefying pressure is reached. Some non-liquefying gas (helium for hydrogen targets and hydrogen for deuterium targets) is then let into K only, until the total pressure in K reaches approximately its working value. Target gas is then fed into H only, and liquefied at a few centimetres overpressure until the target is full. The pressure in K is adjusted with the needle valve to be the same as in H. The target is then plane and parallel sided, except for a tiny effect due to the hydrostatic pressure of a few centimetres of liquid hydrogen.

With this target, to measure the background counting rate from the walls, the main hydrogen refrigerant is allowed to boil off, when the target empties. Other designs incorporate a space to which the target liquid can be moved by closing a valve on the outlet tube and setting up a temperature, and hence pressure, difference with heat from the lower level measuring resistor.

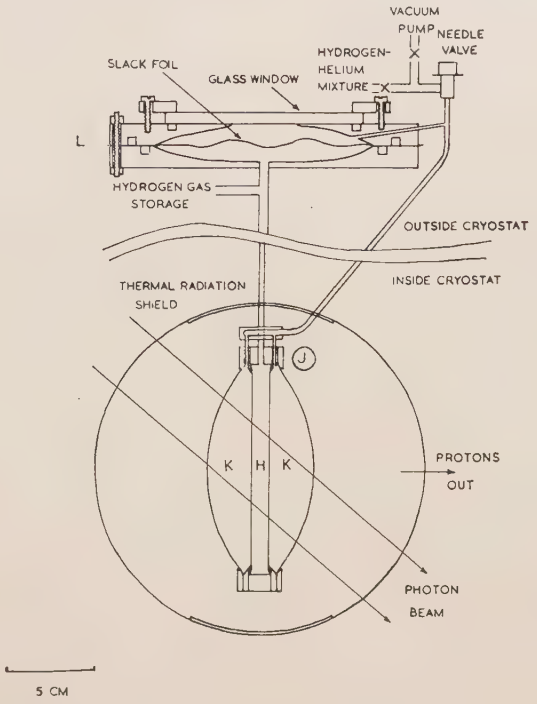

Fig. 3. Pressure compensator and horizontal section through target chamber.

To gain maximum target thickness to the beam and minimum thickness to the emerging particles the target is set at an angle to the beam as shown in fig. 3. Photon beam access to and particle emission from the target through the cryostat is by means of 0.004″ Melinex windows on the outer vacuum jacket and ports covered with 0.001″ aluminium foil on the radiation shield. Some trouble was experienced due to water vapour penetrating the Melinex and frost forming on the aluminium foil. This gave a slowly increasing background and higher liquid nitrogen loss rate (due to increased emissivity). This difficulty was overcome by making the vacuum jacket windows double with 0.0005″ Melinex outer wall and feeding the dry evaporated nitrogen gas through this space to sweep out water vapour.

This target has been used to obtain preliminary results on photoproduction of neutral pions at protons, and to measure the cross-section for positive pion production near threshold.

We are grateful to Professor J. F. Allen of the University of St. Andrews for much useful assistance and advice in the early stages of this work. We are indebted to the workshop staff under Mr. R. Irvine for assistance in construction. One of us (D. M. is indebted to D.S.I.R. for financial maintenance during this work.

NUCLEAR INSTRUMENTS AND METHODS 7 (1960) 297–305; NORTH-HOLLAND PUBLISHING CO.

DEPOLARISATION D'UN FAISCEAU DE PROTONS POLARISES DANS UN SYNCHROTRON

MARCEL FROISSART et RAYMOND STORA

Centre d'Etudes Nucléaires de Saclay, Gif-sur-Yvette (S. et O)

Reçu le 10 novembre 1959

An initially polarized proton beam, when injected in a synchrocyclotron, may suffer substantial depolarization effects, in view of magnetic field inhomogeneities "seen" by individual particles within the beam.

A semiquantitative study is made for the 3 GeV Saclay synchrocyclotron.

There, the combined effect of vertical betatron oscillations and passage through the straight sections fringing fields is critical. One finds indeed that a certain resonance condition is fulfilled for two values of the energy within the acceleration cycle, which entails a large depolarization in the present case. On the other hand, perturbations due to magnetic inhomogeneities inside the quadrants and the accelerating cavity as well as effects due to synchrotron oscillations prove to be small.

It is felt that the analysis presented here could be extended to other machines and other types of accelerated particles. In particular, it is easy to see whether the resonance condition implies the existence of "dangerous" energy regions or not.

Introduction

Diverses méthodes ont été proposées pour la construction de sources de protons polarisés. On a déjà songé à utiliser de telles sources sur des accélérateurs de moyenne énergie, pour lesquels les effets de dépolarisation à l'intérieur de la machine sont négligeables. Il serait également intéressant de pouvoir extraire d'une machine plus puissante un faisceau intense de protons polarisés; les phénomènes de dépolarisation durant le cycle d'accélération sont dans ce cas relativement plus complexes. Nous nous proposons dans ce travail de faire une étude semi-quantitative de la dépolarisation au cours d'un cycle d'accélération.

On sait qu'un ensemble de particules polarisée, dans un champ magnétique lentement variable en direction, garde par rapport à cette direction variable un taux de polarisation constant. Par suite, si on injecte des protons polarisés verticalement dans un synchrotron horizontal, le champ du synchrotron, qui reste sensiblement vertical en tous les points de l'orbite, maintiendra la polarisation verticale des protons, et l'on peut ainsi espérer que la polarisation se maintienne au cours du cycle d'accélération.

Cependant il y a des irrégularités du champ, et il faut examiner de près comment elles peuvent, dans certains cas, conduire à une dépolarisation plus ou moins complète du faisceau. En supposant connue la trajectoire exacte d'un proton, on pourrait toujours calculer la polarisation du proton à la sortie, mais cette polarisation dépendra d'abord de la position de cette trajectoire par rapport à l'orbite moyenne: il faudra donc chercher la polarisation moyenne de tous les protons du faisceau; et ensuite, nous verrons que de très petites variations entre les caractéristiques de deux cycles successifs peuvent conduire à des polarisations moyennes du faisceau notablement différentes: il faudra alors faire une moyenne de type probabiliste, en introduisant certaines phases à distribution de probabilité uniforme.

Dans la 1ère section nous rappellerons les équations de mouvement de spin et nous les linéariserons pour traiter simplement les petites dépolarisations. Nous verrons à ce moment qu'il existe des zones de "résonance" où la dépolarisation risque d'être forte. Dans la section 2, nous traiterons rigoureusement le phénomène de rèsonance, et nous verrons dans

la section 3 comment la résonance est un peu compliquée par des phénomènes secondaires tels que les oscillations synchrotron, sans toutefois changer profondément d'aspect. En conclusion nous indiquerons les voies possibles où rechercher un procédé pratique pour éviter les résonances.

1. Les petites dépolarisations

1.1. LES ÉQUATIONS DU MOUVEMENT. APPROXIMATION LINÉAIRE

Nous représenterons par un vecteur unité $\boldsymbol{s}$ la direction de polarisation, supposée totale, d'un proton. A ce moment, l'équation relativiste[1]) de mouvement de $\boldsymbol{s}$ dans le système de référence du laboratoire, dans un champ magnétique $\boldsymbol{B}$ est[1]):

$$\frac{\mathrm{d}\boldsymbol{s}}{\mathrm{d}t} = \frac{e}{M\gamma}\,\boldsymbol{s} \times \left[\boldsymbol{B} + \frac{g-2}{2}\,(\boldsymbol{B}_{\parallel} + \gamma \boldsymbol{B}_{\perp})\right]. \qquad (1)$$

Nous posons $c = 1$, β vitesse du proton, $\gamma = (1-\beta^2)^{-\frac{1}{2}}$. $\boldsymbol{B}_{\parallel}$ et $\boldsymbol{B}_{\perp}$ sont les composantes de $\boldsymbol{B}$ respectivement parallèle et perpendiculaire à la vitesse du proton. $\boldsymbol{g}$ est le facteur gyromagnétique du proton ($\frac{1}{2}\boldsymbol{g} = 2.8$). Pour simplifier l'écriture posons:

$$\frac{eB_0}{M\gamma} = \omega_{\mathrm{c}} \qquad \text{fréquence cyclotron}$$

$$\frac{eB_0}{M\gamma}\left(1 + \frac{g-2}{2}\gamma\right) = \omega_{\mathrm{p}} \qquad \text{fréquence de précession transversale}$$

$$\frac{g}{2}\frac{eB_0}{M\gamma} = \omega_{\mathrm{l}} \qquad \text{fréquence de précession longitudinale.} \qquad (2)$$

B_0 désigne ici la valeur de B sur l'orbite moyenne dans une partie circulaire du synchrotron. Pour linéariser l'équation (1) il convient de séparer du champ $\boldsymbol{B}_0$, constant sur l'orbite moyenne circulaire, la partie, seule importante au point de vue de la dépolarisation, de $\boldsymbol{B} - \boldsymbol{B}_0$ qui se trouve perpendiculaire à $\boldsymbol{B}_0$. Dénotons donc par $\boldsymbol{b}$ la projection sur le plan horizontal de $\boldsymbol{B} - \boldsymbol{B}_0$. Nous pouvons pratiquement, à l'approximation linéaire que nous allons faire, écrire $\boldsymbol{B} = \boldsymbol{B}_0 + \boldsymbol{b}$. L'équation (1) s'écrit donc:

$$\frac{\mathrm{d}\boldsymbol{s}}{\mathrm{d}t} = \frac{e}{M\gamma}\,\boldsymbol{s} \times \left[\boldsymbol{B}_0 + \boldsymbol{b} + \frac{g-2}{2}\,(\boldsymbol{b}_{\parallel} + \gamma \boldsymbol{B}_0 + \gamma \boldsymbol{b}_{\perp})\right]$$

$$\frac{\mathrm{d}\boldsymbol{s}}{\mathrm{d}t} = \frac{e}{M\gamma}\left[1 + \frac{g-2}{2}\gamma\right]\boldsymbol{s}' \times \boldsymbol{B}_0 + \frac{e}{M\gamma}\,\boldsymbol{s} \times \left[\boldsymbol{b} + \frac{g-2}{2}\,(\boldsymbol{b}_{\parallel} + \gamma \boldsymbol{b}_{\perp})\right]. \qquad (2)$$

Pour linéariser cette équation, il suffit de poser que b/B_0 est un infiniment petit du premier ordre, par conséquent $\boldsymbol{s}$ diffère du vecteur unité vertical $\boldsymbol{k}$ par une quantité $\boldsymbol{s}'$ infiniment petite. En négligeant les termes d'ordre supérieur, il vient:

$$\frac{\mathrm{d}\boldsymbol{s}'}{\mathrm{d}t} = \frac{e}{M\gamma}\left[1 + \frac{g-2}{2}\gamma\right]\boldsymbol{s}' \times \boldsymbol{B}_0 + \frac{e}{M\gamma}\,\boldsymbol{k} \times \left[\boldsymbol{b} + \frac{g-2}{2}\,(\boldsymbol{b}_{\parallel} + \gamma \boldsymbol{b}_{\perp})\right]. \qquad (3)$$

Représentons les vecteurs horizontaux $\boldsymbol{s}'$ et $\boldsymbol{b}$ par des nombres complexes:

$$s = s'_x + is'_y\,; \qquad b = b_x + ib_y$$

l'équation (3) devient:

$$\frac{\mathrm{d}s}{\mathrm{d}t} = +\,i\omega_{\mathrm{p}}s - i\omega_{\mathrm{l}}b_{\parallel} - i\omega_{\mathrm{p}}b_{\perp}\,. \qquad (4)$$

Cette équation se résout, en posant

$$\varphi = \int_0^t \omega_{\mathrm{p}}\,\mathrm{d}t\,,$$

par:

$$s = -\,i\,\mathrm{e}^{i\varphi(t)}\int_0^t \mathrm{e}^{-i\varphi(\tau)}\left[\omega_{\mathrm{l}}\frac{b_{\parallel}(\tau)}{B_0} + \omega_{\mathrm{p}}\frac{b_{\perp}(\tau)}{B_0}\right]\mathrm{d}\tau\,. \qquad (5)$$

1.2. ANALYSE DES CHAMPS PERTURBATEURS

Nous ferons l'analyse des champs perturbateurs pour le synchrotron Saturne supposé parfaitement réalisé. Toute imperfection dans la réalisation du champ magnétique pourra être considérée comme susceptible d'engendrer une dépolarisation supplémentaire, que l'on pourra analyser par les mêmes méthodes que celles que nous développons ici.

Saturne consiste en quatre quadrants magnétiques séparés par quatre sections droites sans

[1]) Case et Mendlowitz, Phys. Rev. **97** (1955) 33;
Case, Phys. Rev. **106** (1957) 175;
L. Michel, communication privée;
V. Bargmann, L. Michel et V. L. Telegdi, Phys. Rev. Lett. **2** (1959) 435.

champ. Par conséquent, il existe aux limites de ces régions des champs de fuite qui ont des composantes parallèles à l'orbite. C'est une première cause de dépolarisation. D'autre part le champ dans les quadrants n'est pas homogène, pour assurer la stabilité de l'orbite. Le proton, s'il oscille verticalement par rapport à l'orbite moyenne, subira donc des champs radiaux également dépolarisants.

D'autre part, on peut penser à la présence des champs électromagnétiques dans la cavité où se produit l'accélération.

Nous allons calculer ces différentes dépolarisations dans l'approximation linéaire. Désignons par α l'angle polaire repérant la position de la particule dans un quadrant, par rapport au centre du quadrant. Pour les sections droites, $\alpha = {}^{\prime}\frac{1}{2}n\pi$, est constant, pour les quadrants $\mathrm{d}\alpha/\mathrm{d}t = \omega_c$.

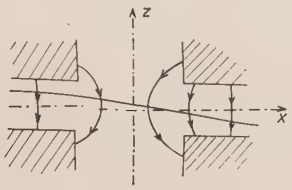

Fig. 1. Schéma en coupe d'une section droite.

Au passage d'une section droite (fig. 1), le proton est en général en train d'osciller verticalement, ce qui fait qu'il ne verra pas les mêmes champs de fuite longitudinaux à la sortie d'un quadrant et à l'entrée du suivant. Par suite, il faut évaluer la quantité (φ reste constant dans la section droite):

$$\int |\, \boldsymbol{b}_{\parallel} \,|\, \mathrm{d}t = \int b_{\parallel} \frac{\mathrm{d}x}{\beta} \simeq \frac{1}{\beta} \int \boldsymbol{B} \cdot \mathrm{d}\boldsymbol{x} \,.$$

Mais $\boldsymbol{B}$ dérive d'un potentiel, par suite:

$$\int b_{\parallel} \,\mathrm{d}t \simeq \frac{1}{\beta} B_0 \Delta z \,. \tag{6}$$

Si R est le rayon d'un quadrant, et L la longueur d'une section droite, on a:

$$\Delta z = L \frac{\mathrm{d}z}{\mathrm{d}x} = \frac{L}{R} \frac{\mathrm{d}z}{\mathrm{d}\alpha} \,.$$

Donc, nous pourrons écrire l'équation (5) sous la forme:

$$s = \mathrm{e}^{i\varphi} \sum_{\alpha = \frac{1}{2}n\pi} \mathrm{e}^{-i\varphi}\, \omega_1\, \mathrm{e}^{i\alpha} \frac{L}{\beta R} \frac{\mathrm{d}z}{\mathrm{d}\alpha} \,.$$

Le facteur $i\mathrm{e}^{i\alpha}$ tient ici compte du changement de direction des sections droites successives. Si nous posons $\mathrm{d}z/\mathrm{d}\alpha = \lambda a \sin \lambda\alpha$, a amplitude des oscillations bêtatron verticales (on verra App. A la forme exacte de $\mathrm{d}z/\mathrm{d}\alpha$), il vient:

$$s = \mathrm{e}^{i\varphi} \sum_{\alpha = \frac{1}{2}n\pi} \omega_1\, \mathrm{e}^{-i\varphi + i\alpha} \sin \lambda\alpha \frac{L\lambda a}{\beta R} \,. \tag{7}$$

S se présente donc comme la somme d'une suite de petites dépolarisations se produisant à des angles différents, à cause du terme $\mathrm{e}^{-i(\varphi-\alpha)}$. Si ces angles sont effectivement différents, il est à prévoir que la somme de ces petites dépolarisations dans toutes les direction sera faible. Si par contre il se trouve que ces angles soient multiples d'un tour, les petites dépolarisations s'ajouteront de façon cohérente et peuvent devenir importantes. Il s'agit ici en quelque sorte d'un phénomène stroboscopique: interaction entre petites impulsions brèves et mouvement de rotation.

Pour voir cela clairement, utilisons une propriété des séries de Fourier:

$$\sum_{\alpha = \frac{1}{2}n\pi} f(\alpha) = \frac{2}{\pi} \sum_{p=-\infty}^{p=+\infty} \int_{-\infty}^{+\infty} \mathrm{e}^{4pi\alpha} f(\alpha)\, \mathrm{d}\alpha \tag{8}$$

$$s = \frac{2}{\pi} \mathrm{e}^{i\varphi} \sum_{p} \int_0^{\alpha(t)} \mathrm{e}^{i(4p+1)\alpha - i\varphi} \sin \lambda\alpha \frac{\omega_p L\lambda a}{\beta R} \,\mathrm{d}\alpha$$

$$s = \frac{\mathrm{e}^{i\varphi}}{\pi i} \sum_{p,\, \varepsilon = \pm 1} \int \mathrm{e}^{(4p+1+\varepsilon\lambda)i\alpha - i\varphi} \frac{\omega_p L\lambda a}{\beta R} \,\mathrm{d}\alpha \,. \tag{9}$$

Le coefficient $\omega_p L\lambda a/\beta R$ est lentement variable. Par conséquent, nous pourrons séparer les termes où le terme oscillant n'a pas de point stationnaire; ils sont très faibles, du même ordre de grandeur que l'intégrand, soit:

$$\frac{1}{\pi} \frac{g}{2} \frac{L\lambda a}{R^2} \simeq 5 \times 10^{-4} \,.$$

Par contre, si le terme oscillant admet un point stationnaire, soit, en dérivant par rapport au temps, si:

$$(4p + 1 + \varepsilon\lambda)\, \omega_c - \omega_p = 0 \tag{10}$$

il faut appliquer la méthode du col au calcul de l'intégrale (9). Posant:

$$\Gamma = -\frac{\mathrm{d}}{\mathrm{d}t}\left[(4p + 1 + \varepsilon\lambda)\,\omega_c - \omega_p\right] \qquad (11)$$

on trouve:

$$s = \frac{e^{i\varphi}}{\pi} \sum_{\text{cols}} \frac{\omega_1 L \lambda a}{\beta R}\, e^{i\chi} \sqrt{\frac{2\pi}{i\Gamma}}, \qquad (12)$$

les cols, ou résonances, étant déterminés par la condition (10).

Pour calculer Γ, on remarque, en utilisant (10) que:

$$\Gamma = \omega_c \frac{\mathrm{d}}{\mathrm{d}t}\frac{\omega_p}{\omega_c} = \omega_c \frac{\mathrm{d}}{\mathrm{d}t}\left(\frac{d-2}{2}\gamma\right). \qquad (13)$$

Mais $\mathrm{d}\gamma/\mathrm{d}t = (1/\beta)\,\mathrm{d}(\beta\gamma)/\mathrm{d}t$, et $\beta\gamma$ croît linéairement (proportionnel à B_0). Donc

$$\Gamma = \frac{1.8\,\omega_t}{\beta T}\,[\beta\gamma]_i^f,$$

T étant la durée de l'accélération.

Comme il s'introduit dans s une phase $e^{i\chi} \equiv e^{i(4p+\varepsilon\lambda)\alpha - i\varphi}$ qui dépend beaucoup des irrégularités de montée du champ, il faut considérer que les résonances sont indépendantes, et n'ont pas de relation de phase bien déterminée (c'est ici que s'introduit la notion de moyenne probabiliste dont nous avons parlé dans l'Introduction).

Pour Saturne, il se produit deux cas de résonance: $p = 1$, $\varepsilon = 1$ aux valeurs

$$\gamma = \frac{4 \pm \lambda}{1.8} = \begin{cases} 2.7 \\ 1.7 \end{cases}.$$

On trouve pour les protons d'oscillation maximum des valeurs de $|s|$ de l'ordre de 2, qui sont nettement en dehors du cadre des petites dépolarisations.

Examinons maintenant l'effet du champ focalisant radial qui existe dans les quadrants, en dehors du plan équatorial. Ce champ est

$$b_\perp = nB_0\, e^{i\alpha}\frac{z(\alpha)}{R}.$$

Or, (cf. Appendice A)

$$z(\alpha) = \frac{a}{2\pi}\frac{L}{R}\sqrt{n}\,\frac{\sin\sqrt{n}\pi/2}{\sin\lambda\,\pi/2}\sum_{p,\varepsilon}\varepsilon\, e^{(4p+\varepsilon\lambda)i\alpha}\frac{4p+\varepsilon\lambda}{(4p+\varepsilon\lambda)^2 - n}.$$

Par conséquent, le même phénomène de résonances que ci-dessus aura lieu, pour les mêmes valeurs de γ. Mais une comparaison des coefficients des développements de Fourier montre aisément que ce dernier effet est inférieur à un dixième du précédent. Comme d'autre part, il lui est perpendiculaire, il se traduit simplement par une rotation du plan de basculement de la polarisation qui n'a aucune conséquence pratique.

On peut également se demander si les oscillations bêtatron horizontales ne peuvent pas induire de dépolarisation. Ceci aura lieu uniquement si elles induisent un déplacement vertical, c'est-à-dire si elles sont couplées avec les oscillations verticales. Or le couplage est très faible entre les deux types d'oscillations. Il introduit simplement une légère déviation du plan d'oscillation, les fréquences n'étant pratiquement pas modifiées. Par conséquent les déplacements verticaux qui correspondraient à une résonance avec la fréquence d'oscillation bêtatron horizontale sont très faibles et n'introduisent pas sensiblement de dépolarisation.

Traitons rapidement l'effet des champs qui règnent au sein de la cavité accélératrice.

On a d'abord un effet dû au champ magnétique circulaire qui accompagne le champ électrique variable dirigé le long de l'orbite, puis un effet dû au champ électrique lui-même, qui agit sur la polarisation si la particule n'est pas animée d'un mouvement parallèle au champ électrique.

La fréquence circulaire du champ accélérateur est, dans Saturne $2\omega_c/1 + k$; $(k = 2L/\pi R)$. Par suite, le champ magnétique $\boldsymbol{b}$, à la hauteur Z au dessus de l'orbite moyenne, est

$$b_E = z\frac{\mathrm{d}\,E(t)}{\mathrm{d}t} = zE\cos\phi\,\frac{2\omega_c}{1+k},$$

ϕ phase du champ accélérateur

$$E(t) = E\sin\left(\frac{2\omega_c t}{1+R} + \phi\right).$$

Par suite, on doit prendre pour l'expression (5) l'intégrale:

$$\int b_\perp\,\mathrm{d}t = \frac{2\omega_c\cos\phi}{\beta\,(1+k)}\,z\int E\,\mathrm{d}x. \qquad (14)$$

De même l'expression analogue à (3) de l'influence du champ électrique est:

$$\frac{d\boldsymbol{s}}{dt} = \frac{e}{M\gamma}\,\boldsymbol{k} \times (\boldsymbol{\beta} \times \boldsymbol{E})\left[\frac{1}{\gamma+1} + \frac{g-2}{2}\right].$$

Par suite, l'intégrale qu'il faut ajouter à (14) est:

$$\frac{dz}{dx}\left[\frac{1}{\gamma+1} + \frac{g-2}{2}\right]\int E\,dx\,. \qquad (15)$$

Posant $z = -a\cos\lambda\alpha$, l'effet total est, pour un passage:

$$s = \frac{a\omega_c}{B_0}\left[-\frac{2\omega_c\cos\phi}{\beta(1+k)}\cos\lambda\alpha + \right.$$

$$\left. + \frac{\lambda}{R}\left[\frac{1}{\gamma+1} + \frac{g-2}{2}\right]\sin\lambda\alpha\right]\int E\,dx\,.$$

Il est clair que

$$e\int E\,dx = \Delta(M\gamma)\,.$$

Par suite, en négligeant la phase qui figure dans (5), on obtient une majorante:

$$s = \frac{a}{R}\,[\gamma]_1^f\left[2\,\frac{\cos\phi}{1+k} + \lambda\frac{g}{2}\right] \approx 1\%\,. \qquad (16)$$

Par suite cet effet est négligeable, puisque nous avons majoré la somme entière, au lieu de nous borner à la sommation dans les zones de résonance.

2. Étude détaillée d'une résonance idéale

Nous allons résoudre l'équation (1) sans nous borner à l'approximation des petites dépolarisations, pour le cas de l'influence des champs de fuite des sections droites.

Analysons de près ce qui se passe au cours d'une résonance. Pour cela, plaçons-nous dans un système d'axes tournant avec une vitesse $\omega_R = (4p + 1 + \varepsilon\lambda)\,\omega_c$. L'équation (2) devient:

$$\frac{d\boldsymbol{s}}{dt} = -\omega_R\,(\boldsymbol{k} \times \boldsymbol{s}) + \omega_p\,(\boldsymbol{k} \times \boldsymbol{s}) + \boldsymbol{\omega} \times \boldsymbol{s}\,. \qquad (17)$$

$\boldsymbol{k}$ est le vecteur unité vertical, et $\boldsymbol{\omega} = (ge/M\gamma)\,\boldsymbol{b}_\parallel$, est constitué par une suite d'impulsions très courtes:

$$\int\omega\,dt = \frac{L\lambda a}{\beta R}\,\omega_1\sin\lambda\alpha\,, \qquad \text{(cf. Eq. (7))} \qquad (18)$$

de direction faisant un angle $\alpha - (4p + 1 + \varepsilon\lambda)\,\alpha$ avec un des axes tournants. Etant donné, par suite, que ces impulsions sont très courtes, elles correspondent à des rotations d'angle petit

$$\frac{L\lambda a\omega_1}{\beta R} \simeq 1.5 \times 10^{-3}\,,$$

et on peut par conséquent, en négligeant des rotations d'ordre supérieur, faire la moyenne sur quelques impulsions successives, ce qui revient, si l'on représente

$$\int\boldsymbol{\omega}\,dt$$

par le nombre complexe

$$\frac{L\lambda a}{\beta R}\,\omega_1\sin\lambda\alpha\,e^{-i\alpha(4p+\varepsilon\lambda)} =$$

$$= \frac{L\lambda a}{\beta R}\,\frac{\omega_1}{2i}\,e^{-i\alpha(4p+\varepsilon\lambda)}\,(e^{i\lambda\alpha} - e^{-i\lambda\alpha})$$

à négliger le terme tournant et à garder:

$$\frac{L\lambda a\omega_1}{2i\beta R}\,\varepsilon\,e^{-4pi\alpha} = \frac{\varepsilon L\lambda a\omega_1}{2i\beta R} \qquad \text{puisque} \qquad \alpha = \tfrac{1}{2}\,n\pi\,.$$

Par suite, nous avons ramené le champ perturbateur à un champ constant dans le système d'axes tournants, correspondant à une valeur moyenne de $\boldsymbol{\omega}$:

$$\omega = \frac{L\lambda a\omega_1\omega_c}{\pi\beta R} = \frac{\lambda}{\pi}\,\frac{aL}{R^2}\,\omega_1 \qquad (19)$$

$$\left(\frac{2\omega_c}{\pi} = \left[\int_{\alpha=0}^{\frac{1}{2}\pi} dt\right]^{-1}\right)\,.$$

Pour la résolution de l'équation (17), on suppose que $\omega_p - \omega_R$ croît linéairement avec le temps, $\omega_p - \omega_R = \Gamma(t - t_0)$. (Voir l'appendice B pour la résolution de cette équation.) Le résultat est que le vecteur de polarisation tourne, sa composante verticale étant multipliée par:

$$S_z = 2\,e^{-\pi\omega^2/2\Gamma} - 1\,. \qquad (20)$$

Pour les résonances envisagées, on trouve $S_z = -0.4$ pour une amplitude d'oscillation bêtatron verticale de 1 cm.

On peut se demander ce que signifie le résultat (20). Si la résonance est peu importante, $\omega^2/\Gamma \ll 1$, la polarisation S_z reste ≈ 1. Mais si la résonance est importante, $\omega^2/\Gamma \gg 1$, il y a simplement retournement de la polarisation.

Ceci peut se comprendre de la façon suivante[2]). Le vecteur rotation instantané de la polarisation (dans les axes mobiles) est $\Gamma t\, \boldsymbol{k} + \boldsymbol{\omega}$. Il peut être ramené à un champ magnétique équivalent qui lui est proportionnel. Si ce champ est suffisamment fort (ω grand) et varie lentement (Γ petit) alors $\boldsymbol{s}$ va suivre le champ dans son mouvement et par conséquent va se retourner. Si par contre ω est petit et Γ grand, il y a renversement rapide du champ, la polarisation $\boldsymbol{s}$ ne suit pas le mouvement, il n'y a pas changement de polarisation.

3. Perturbations de la résonance

Dans la réalité, la résonance n'est pas si simple; la présence des oscillations synchrotron fait que les différents paramètres ω_c, γ, etc. ne varient pas régulièrement en fonction du temps, mais oscillent autour d'une position moyenne qui croît régulièrement, et pour laquelle seulement on peut utiliser l'approximation linéaire. Il faut donc poser:

$$\omega_p - \omega_R = \omega_c\,(1.8\gamma - 4p - \varepsilon\lambda) = \Gamma t + \theta \cos\,(\Omega t + \varphi)$$

Ω étant la pulsation des oscillation synchrotron. Cela complique le calcul de la résonance, que nous ne ferons pas ici. Mais on peut se rendre compte de l'ordre de grandeur du terme additionnel par rapport au champ perturbateur représenté par $\bar{\omega}$.

$$\bar{\omega} = \frac{\lambda a L \omega_1}{\pi R^2} = 1.6 \times 10^4 \text{ rad/sec}\,.$$

$$\Omega \cong 1.6 \times 10^4 \text{ rad/sec}\,.$$

Le calcul de θ se fait simplement de la façon suivante. Désignons par Δx l'amplitude de la partie oscillante de x:

$$\theta = \Delta\,(\omega_p - \omega_R) =$$

$$= \Delta\,(\omega_c\,(1.8\gamma - 4p - \varepsilon\lambda)) = 1.8\,\omega_c \Delta\gamma$$

or

$$\frac{\Delta\omega_c}{\omega_c} = \frac{\Delta B_0}{B_0} - \frac{\Delta\gamma}{\gamma} = -\left[1 + \frac{n}{(1-n)\,\beta^2\gamma}\right]\frac{\Delta\gamma}{\gamma}\,.$$

[2]) Les auteurs ont profité d'une fort intéressante discussion sur ce point avec Mr. P. de Gennes.

Mais $\Delta\omega_c = \Omega\Delta\alpha$, donc:

$$\theta = 1.8\gamma\left[1 + \frac{n}{(1-n)\,\beta^2\gamma}\right]^{-1} \Omega\Delta\alpha \simeq 1.5\Omega\,.$$

Par conséquent, le vecteur polarisation, au lieu de suivre un vecteur de champ effectif en mouvement uniforme, suivra un vecteur qui oscille à une vitesse comparable à la vitesse de ce mouvement uniforme. Il est à prévoir que les résultats ne seront guère modifiés par les oscillations synchrotron. La largeur de la résonance, en particulier, ne sera pas affectée par les oscillations synchrotron.

Conclusions

En conclusion, nous voyons qu'il apparaît deux résonances susceptibles de produire une dépolarisation du faisceau. Ces résonances sont données par la relation $\gamma = (4p \pm \lambda)/1.8 = \frac{2.7}{1.7}$, ce qui correspond à des énergies du proton respectivement de 0.7 GeV et 1.7 GeV.

La dépolarisation produite par une résonance a lieu dans les régions extrêmes, haute et basse du faisceau, et elle est d'autant plus importante que l'on traverse lentement la résonance (elle dépend de $\bar{\omega}^2/\Gamma$).

Il en découle deux procédés éventuels pour atténuer ces effets: soit diaphragmer le faisceau dans le sens vertical à l'approche des résonances, soit "sauter" la résonance en déplaçant soudainement l'orbite par augmentation rapide de l'énergie des protons.

ORDRES DE GRANDEUR NUMERIQUES

Coefficient de dépolarisation à 1 cm de l'orbite moyenne: — 0.4 pour une résonance. Largeur de la résonance $\tau = 2/\sqrt{\Gamma} = 10^{-4}$ sec soit 0.5 MeV en énergie du proton. Durée d'un tour

$$\frac{2\pi\,(1+k)}{\omega_c} = 2 \times 10^{-7} \text{ sec}\,.$$

Les auteurs tiennent à remercier Monsieur le Professeur A. Messiah qui leur a proposé le sujet de cette étude, et qui s'est constamment intéressé à son développement.

Appendice A

OSCILLATIONS BETATRON VERTICALES

Dans un quadrant:

$$0 < \alpha' = \alpha - \alpha_0 < \tfrac{1}{2}\pi\,; \quad \alpha_0 = \tfrac{1}{2}k\pi$$

les oscillations bêtatron verticales sont données par:

$$z = \xi \cos \sqrt{n}\,\alpha' + \frac{\xi'}{\sqrt{n}} \sin \sqrt{n}\,\alpha'$$

n est l'indice de gradient du champ.

A l'extrémité du quadrant

$$z\ (\alpha' = \tfrac{1}{2}\pi) = \xi \cos \sqrt{n}\ \tfrac{1}{2}\pi + (\xi'/\sqrt{n}) \sin \sqrt{n}\ \tfrac{1}{2}\pi$$

$$z'\ (\alpha' = \tfrac{1}{2}\pi) = -\xi \sqrt{n} \sin \sqrt{n}\ \tfrac{1}{2}\pi + \xi' \cos \sqrt{n}\ \tfrac{1}{2}\pi\,.$$

Les conditions initiales ξ_1, ξ'_1 à prendre pour le mouvement dans le quadrant suivant sont:

$$\xi_1 = z\ (\alpha' = \tfrac{1}{2}\pi) + (L/R)\, z'\ (\alpha' = \tfrac{1}{2}\pi)$$

$$\xi'_1 = z'\ (\alpha' = \tfrac{1}{2}\pi)\,.$$

Soit

$$\begin{pmatrix}\xi_1\\ \xi'_1\end{pmatrix} = \begin{pmatrix}\cos \sqrt{n}\ \tfrac{1}{2}\pi - (L/R)\ \sqrt{n} \sin \sqrt{n}\ \tfrac{1}{2}\pi & \\ -\sqrt{u} \sin \sqrt{n}\ \tfrac{1}{2}\pi & \end{pmatrix}$$

$$(1/\sqrt{n})\ (\sin \sqrt{n}\ \tfrac{1}{2}\pi + (L/R)\ \sqrt{n} \cos \sqrt{n}\ \tfrac{1}{2}\pi \quad \cos \sqrt{n}\ \tfrac{1}{2}\pi) \begin{pmatrix}\xi\\ \xi'\end{pmatrix}.$$

Les valeurs propres de la matrice de transfert sont données par:

$$s^2 - (2 \cos \sqrt{n}\ \tfrac{1}{2}\pi - (L/R)\ \sqrt{n} \sin \sqrt{n}\ \tfrac{1}{2}\pi)\, s + 1 = 0\,.$$

Nous posons:

$$2 \cos \sqrt{n}\ \tfrac{1}{2}\pi - (L/R)\ \sqrt{n} \sin \sqrt{n}\ \tfrac{1}{2}\pi = 2 \cos \lambda\ \tfrac{1}{2}\pi$$

alors les modes propres sont donnés par:

$$s = \mathrm{e}^{\frac{1}{2}\varepsilon i\lambda\pi} \quad ; \quad \varepsilon = \pm 1$$

$$\xi \propto \cos \sqrt{n}\ \tfrac{1}{2}\pi - \mathrm{e}^{\frac{1}{2}\varepsilon i\lambda\pi}$$

$$\xi' \propto \sqrt{n} \sin \sqrt{n}\ \tfrac{1}{2}\pi\,.$$

On a donc deux solutions propres pour z:

$$z^{(\varepsilon)} = \mathrm{e}^{\varepsilon i\lambda\alpha_0}\,[(\cos \sqrt{n}\ \tfrac{1}{2}\pi - \mathrm{e}^{\frac{1}{2}\varepsilon i\lambda\pi}) \cos \sqrt{n}\,\alpha + \\ + \sin \sqrt{n}\ \tfrac{1}{2}\pi \sin \sqrt{n}\,\alpha']\,.$$

Donc:

$$z = \rho_+ z^+ + \rho_- z^- = \rho_+ \mathrm{e}^{i\lambda\alpha_0}$$

$$[(\cos \sqrt{n}\ \tfrac{1}{2}\pi - \mathrm{e}^{+\frac{1}{2}i\lambda\pi}) \cos \sqrt{n}\,\alpha' + \sin \sqrt{n}\ \tfrac{1}{2}\pi \sin \sqrt{n}\,\alpha']$$

$$+ \rho_+{}^* \mathrm{e}^{-i\lambda\alpha_0}$$

$$[(\cos \sqrt{n}\ \tfrac{1}{2}\pi - \mathrm{e}^{-\frac{1}{2}i\lambda\pi}) \cos \sqrt{n}\,\alpha' + \sin \sqrt{n}\ \tfrac{1}{2}\pi \sin \sqrt{n}\,\alpha']\,.$$

Avec les conditions initiales $z(0) = a$,

$$\frac{\mathrm{d}z}{\mathrm{d}\alpha}(0) = 0$$

on trouve

$$\rho_+ = \frac{ia}{2 \sin \tfrac{1}{2}\lambda\pi}$$

d'ou

$$z = \frac{ai}{2 \sin \tfrac{1}{2}\lambda\pi}\,(z^+ - z^-)\,.$$

(Pour $L/R \to 0$, $\lambda \to \sqrt{n}$ et $z \to a \cos \lambda\alpha$.)

Comme $\mathrm{e}^{-\varepsilon i\lambda\alpha}\, z^{(\varepsilon)}$ ne dépend que de α', nous pouvons écrire le développement en série de Fourier:

$$\mathrm{e}^{-\varepsilon i\lambda\alpha}\, z^{(\varepsilon)} = \sum_p c_p{}^{\varepsilon}\, \mathrm{e}^{4pi\alpha}\,,$$

$$c_p{}^{\varepsilon} = \frac{2}{\pi}\int_0^{\frac{1}{2}\pi} \mathrm{e}^{-4pi\alpha' - \varepsilon i\lambda\alpha'}$$

$$[(\cos \sqrt{n}\ \tfrac{1}{2}\pi - \mathrm{e}^{\varepsilon i\lambda\frac{1}{2}\pi}) \cos \sqrt{n}\,\alpha' + \sin \sqrt{n}\ \tfrac{1}{2}\pi \sin \sqrt{n}\,\alpha']$$

$$= \frac{1}{i\pi}\left[(\mathrm{e}^{-i\sqrt{n}\frac{1}{2}\pi} - \mathrm{e}^{\frac{1}{2}\varepsilon i\lambda\pi})\ \frac{\mathrm{e}^{-\frac{1}{2}\varepsilon i\lambda\pi + i\sqrt{n}\frac{1}{2}\pi} - 1}{-4p - \varepsilon\lambda + \sqrt{n}}\right.$$

$$\left. + (\mathrm{e}^{i\sqrt{n}\frac{1}{2}\pi} - \mathrm{e}^{\frac{1}{2}\varepsilon i\lambda\pi})\ \frac{\mathrm{e}^{-\frac{1}{2}\varepsilon i\lambda\pi - i\sqrt{n}\frac{1}{2}\pi} - 1}{-4p - \varepsilon\lambda - \sqrt{n}}\right]$$

$$= \frac{1}{i\pi}\left[\frac{\mathrm{e}^{-\frac{1}{2}\varepsilon i\lambda\pi} + \mathrm{e}^{\frac{1}{2}\varepsilon i\lambda\pi} - \mathrm{e}^{\frac{1}{2}i\sqrt{n}\pi} - \mathrm{e}^{-\frac{1}{2}i\sqrt{n}\pi}}{-4p - \varepsilon\lambda + \sqrt{n}}\right.$$

$$\left. + \frac{\mathrm{e}^{-\frac{1}{2}\varepsilon i\lambda\pi} + \mathrm{e}^{\frac{1}{2}\varepsilon i\lambda\pi} - \mathrm{e}^{-\frac{1}{2}i\sqrt{n}\pi} - \mathrm{e}^{\frac{1}{2}i\sqrt{n}\pi}}{-4p - \varepsilon\lambda - \sqrt{n}}\right]$$

$$= -\frac{4}{i\pi}\,(\cos \tfrac{1}{2}\lambda\pi - \cos \sqrt{n}\ \tfrac{1}{2}\pi)\ \frac{4p + \varepsilon\lambda}{(4p + \varepsilon\lambda)^2 - n}$$

$$= \frac{2}{i\pi}\,\frac{L}{R}\ \sqrt{n} \sin \sqrt{n}\ \tfrac{1}{2}\pi\ \frac{4p + \varepsilon\lambda}{(4p + \varepsilon\lambda)^2 - n}\,.$$

Ainsi,

$$z = \frac{a}{\pi}\,\frac{L}{R}\ \sqrt{n}\ \frac{\sin \sqrt{n}\ \tfrac{1}{2}\pi}{\sin \lambda\ \tfrac{1}{2}\pi} \sum_{p,\varepsilon} \varepsilon\, \mathrm{e}^{4pi\alpha + \varepsilon i\lambda\alpha}\ \frac{4p + \varepsilon\lambda}{(4p + \varepsilon\lambda)^2 - n}$$

$$\frac{\mathrm{d}z}{\mathrm{d}\alpha} = i\,\frac{a}{\pi}\,\frac{L}{R}\ \sqrt{n}\ \frac{\sin \sqrt{n}\ \tfrac{1}{2}\pi}{\sin \lambda\ \tfrac{1}{2}\pi} \sum_{p,\varepsilon} \varepsilon\, \mathrm{e}^{4pi\alpha + \varepsilon i\lambda\alpha}\ \frac{(4p + \varepsilon\lambda)^2}{(4p + \varepsilon\lambda)^2 - n}\,.$$

Extrayons la partie discontinue (terme indépendant de p):

$$\left.\frac{\mathrm{d}z}{\mathrm{d}\alpha}\right|_{\text{disc.}} = i\,\frac{a}{\pi}\,\frac{L}{R}\ \sqrt{n}\ \frac{\sin \sqrt{n}\ \tfrac{1}{2}\pi}{\sin \lambda\ \tfrac{1}{2}\pi} \sum_{p,\varepsilon} \varepsilon\, \mathrm{e}^{4pi\alpha + \varepsilon i\lambda\alpha}$$

$$= +\frac{iaL}{2R}\ \sqrt{n}\ \frac{\sin \sqrt{n}\ \tfrac{1}{2}\pi}{\sin \lambda\ \tfrac{1}{2}\pi}\,(e^{i\lambda\alpha} - \mathrm{e}^{-i\lambda\alpha}) \sum_n \delta(\alpha - \tfrac{1}{2}n\pi)$$

$$= -\frac{aL}{R}\ \sqrt{n}\ \frac{\sin \sqrt{n}\ \tfrac{1}{2}\pi}{\sin \lambda\ \tfrac{1}{2}\pi} \sin \lambda\alpha \sum_n \delta\,(\alpha - \tfrac{1}{2}n\pi)\,.$$

Par suite

$$\Delta z = -\frac{L}{R}\, a\, \sqrt{n}\, \frac{\sin \sqrt{n}\, \frac{1}{2}\pi}{\sin \lambda\, \frac{1}{2}\pi} \sin \lambda\alpha$$

ce qui justifie l'approximation faite dans l'équation (7) $\Delta z = (L/R)\, a\lambda \sin \lambda\alpha$ si l'on prend $\lambda \approx \sqrt{n}$.

Appendice B

CALCUL D'UNE RESONANCE ISOLEE

Nous partons de l'équation (17):

$$\frac{\mathrm{d}\boldsymbol{s}}{\mathrm{d}t} = (\omega_\mathrm{p} - \omega_\mathrm{R})\, \boldsymbol{k} \times \boldsymbol{s} + \boldsymbol{\omega} \times \boldsymbol{s}$$

ω est un vecteur fixe de longueur $\overline{\omega}$ (équ. 19).

Posons $(\omega_\mathrm{p} - \omega_\mathrm{R})\, \boldsymbol{k} = \boldsymbol{\Omega}_\mathrm{p}$ $(\boldsymbol{\omega} \cdot \boldsymbol{\Omega}_\mathrm{p} = 0)$. Dans les systèmes d'axes tournant à la vitesse angulaire Ω_p,

$$\frac{\mathrm{d}\boldsymbol{s}'}{\mathrm{d}t} = \boldsymbol{\omega}'_\mathrm{R} \times \boldsymbol{s}'$$

où $\boldsymbol{\omega}'_\mathrm{R}$ est un vecteur de longueur

$$|\, \omega_1 \boldsymbol{b}_\parallel + \omega_\mathrm{p} \boldsymbol{b}_\perp \,| = \omega$$

et faisant un angle $(4p + 1 \pm \lambda)\, \alpha - \varphi = \chi$ avec une direction fixe de ce repère.

On peut introduire le spineur $\mu = \binom{f}{g}$ et écrire $\boldsymbol{s}' = u^* \boldsymbol{\sigma} u$, ou $\boldsymbol{\sigma}$ sont les matrices de Pauli. Alors u obéit à l'équation de Schrödinger

$$i\frac{\mathrm{d}u}{\mathrm{d}t} = \tfrac{1}{2}\, \boldsymbol{\omega} \cdot \boldsymbol{\sigma} u\,.$$

Soit:

$$\frac{\mathrm{d}f}{\mathrm{d}t} = -\tfrac{1}{2} i\omega\, \mathrm{e}^{-i\chi}\, g$$

$$\frac{\mathrm{d}g}{\mathrm{d}t} = -\tfrac{1}{2} i\omega\, \mathrm{e}^{i\chi}\, f\,.$$

Eliminons f:

$$\frac{\mathrm{d}}{\mathrm{d}t}\left(\mathrm{e}^{-i\chi}\frac{\mathrm{d}g}{\mathrm{d}t}\right) + \tfrac{1}{4}\omega^2\, \mathrm{e}^{-i\chi}\, g = 0\,.$$

Soit:

$$\frac{\mathrm{d}^2 g}{\mathrm{d}t^2} - i\dot{\chi}\frac{\mathrm{d}g}{\mathrm{d}t} + \tfrac{1}{4}\omega^2 g = 0 \qquad \left(\dot{\chi} = \frac{\mathrm{d}\chi}{\mathrm{d}t}\right).$$

Posons:

$$\dot{\chi} = \omega_\mathrm{p} - \omega_\mathrm{R} = \Gamma t$$

on a alors

$$\frac{\mathrm{d}^2 g}{\mathrm{d}t^2} - i\Gamma t\frac{\mathrm{d}g}{\mathrm{d}t} + \tfrac{1}{4}\omega^2 g = 0$$

avec les conditions initiales

$$g(-\infty) = 0\,,\quad g'(-\infty) = -\tfrac{1}{2} i\omega f(-\infty) = -\tfrac{1}{2} i\omega\,.$$

Nous cherchons plus précisément $g(+\infty)$; alors on a:

$$\cos\theta_f = 1 - 2\,|\, g(+\infty)\,|^2\,.$$

Le changement de variable $z = i\chi = \frac{1}{2} i\Gamma t^2$ transforme l'équation en une équation hypergéométrique confluente[3]) de paramètres $c = \frac{1}{2}$, $a = i\omega^2/8\Gamma$:

$$z\frac{\mathrm{d}^2 g}{\mathrm{d}z^2} + (\tfrac{1}{2} - z) - \frac{i\omega^2}{8\Gamma} = 0\,.$$

Deux solutions asymptotiques sont pour $z = i\infty$:

$$F = \Gamma(c - a)\,|\, z\,|^{a-c}\, \mathrm{e}^{\frac{1}{2} i\pi(a-c)}\, \mathrm{e}^{z} + \\ + \Gamma(a)\,|\, z\,|^{-a}\, \mathrm{e}^{\frac{1}{2} i a\pi} \qquad (\mathrm{M}.5.3.51)$$

$$G = \sqrt{z}\,(\Gamma(1 - a)\,|\, z\,|^{a-1}\, \mathrm{e}^{\frac{1}{2} i\pi(a-1)}\, \mathrm{e}^{z} + \\ + \Gamma(a + \tfrac{1}{2})\,|\, z\,|^{a-\frac{1}{2}}\, \mathrm{e}^{\frac{1}{2} i(a+\frac{1}{2})\pi}) \quad (M.5.3.57).$$

Asymptotiquement:

$$F \to f \sim \frac{1}{\sqrt{a}}\,\Gamma(\tfrac{1}{2} - a)\,|\, z\,|^{a}\, \mathrm{e}^{\frac{1}{2} i a\pi};$$

$$g \sim \Gamma(a)\,|\, z\,|^{-a}\, \mathrm{e}^{\frac{1}{2} i a\pi}$$

$$G \to f \sim \frac{1}{\sqrt{a}}\,\Gamma(1 - a)\, \mathrm{e}^{\frac{1}{2} i a\pi}\,|\, z\,|^{a}\,;$$

$$g \sim i\Gamma(a + \tfrac{1}{2})\,|\, z\,|^{-a}\, \mathrm{e}^{\frac{1}{2} i a\pi}\,.$$

La présence de $\sqrt{z}$ dans G indique que si t passe de $-\infty$ à $+\infty$, z passe de $i\infty$ à $i\infty$ en passant par 0 et G change de signe, alors que F ne change pas.

Les conditions initiales $|f| = 1$, $g = 0$ donnent

$$g = \frac{i\Gamma(a + \frac{1}{2})\, F - \Gamma(a)\, G}{i\Gamma(a + \frac{1}{2})\,\Gamma(\frac{1}{2} - a) - \Gamma(a)\,\Gamma(1 - a)}\,\sqrt{a}$$

d'où

$$g(+\infty) = \frac{2i\Gamma(a)\,\Gamma(a + \frac{1}{2})\,|\, z\,|^{-a}\,\sqrt{a}}{i\Gamma(a + \frac{1}{2})\,\Gamma(\frac{1}{2} - a) - \Gamma(a)\,\Gamma(1 - a)}$$

et

$$s_z = \cos\theta_f = 1 - 2\,|\, g(+\infty)\,|^2 = 1 - 8\,|\, a\,| \\ \frac{|\,\Gamma(a)\,|^2\,|\,\Gamma(a + \frac{1}{2})\,|^2}{|\, i\Gamma(a + \frac{1}{2})\,\Gamma(\frac{1}{2} - a) - \Gamma(a)\,\Gamma(1 - a)\,|^2}\,.$$

[3]) Cf. Morse et Feshbach, Methods of Theoretical Physics T.I p. 604. Equ. (5.3.44) et suivantes.

Utilisant la formule $\Gamma(x)\,\Gamma(1-x) = \pi/\sin \pi x$ et le fait que a est imaginaire pur, on trouve:

$$s_z = 2\,e^{-4\pi|a|} - 1 = 2\,e^{-\pi\omega^2/2\Gamma} - 1\,.$$

Si l'on veut calculer la dépolarisation du faisceau de densité $\rho(z)\,dz$, on doit intégrer:

$$< s_z > = \int_0^{z_{max}} \rho(z)\,dz\,(2\,e^{-\pi\omega^2/2\Gamma} - 1) \quad \left(\int_0^{z_{max}} \rho(z)\,dz = 1\right).$$

Comme ω^2 est quadratique en z, pour $\rho(z) = z/z_{max}$ on a (fig. 2):

$$< s_z > = \frac{\sqrt{\pi} - 2\,\mathrm{Erfc}\,(\pi\omega^2/2\Gamma)^{\frac{1}{2}}_{max}}{(\pi\,\omega^2/2\Gamma)^{\frac{1}{2}}_{max}} - 1\,.$$

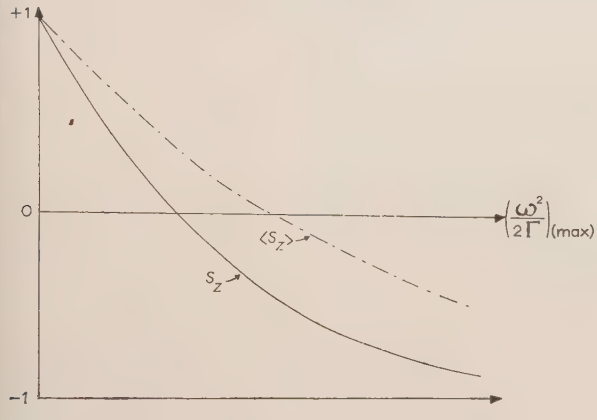

Fig. 2. Courbes de dépolarisation.

Appendice C

DONNEES NUMERIQUES, ORDRES DE GRANDEUR†

$$R = 8.42\,m\,.$$

$$L = 4\,m\,.$$

† Les données numériques concernant Saturne sont extraites du rapport O.C. 35 "Oscillations Synchrotron" par M. Salvat et G. Gendreau.

$$300 \text{ gauss} \leqslant B_0 \leqslant 12\,000 \text{ gauss}\,.$$

$$\beta\gamma = \frac{eB_0R}{M} = 0.0924 + 5.423\,t$$

$$0.017 < t < 0.7 \text{ sec}\,.$$

$$(\beta\gamma)_i = 0.0924 \qquad (\beta\gamma)_f = 3.7966$$

$$\omega_c = \frac{eB_0}{M\gamma} = \frac{e}{M\gamma}\frac{Mc^2\beta\gamma}{ecR} = \frac{c\beta}{R} = 3.56 \times 10^7 \text{ sec}^{-1}$$

$$n = 0.6\,.$$

Résonances

$$4 \pm \lambda = 1.8\gamma \qquad \gamma = \frac{2.7}{1.7} \qquad \beta = \frac{0.93}{0.81} \qquad \lambda = 0.887$$

$$\Gamma = \omega_c \frac{d}{dt} 1.8\gamma \approx 3.47 \times 10^8 \text{ sec}^{-2}$$

$$\tau = \frac{1}{\sqrt{\Gamma}} = 0.54 \times 10^{-4} \text{ sec}$$

$$a \approx 1 \text{ cm}\,.$$

$$|s_{\parallel}| = 2.1 \qquad \theta_{\parallel} = 111°,5$$

$$|s_{\perp}| = 0.25 \qquad \theta_{\perp} = 19°\,50'\,.$$

Oscillations synchrotron

ϕ_s = phase de la particule synchrotron $\approx 30°$.

V = maximum de la tension accélératrice $\approx 2\,000$ volts.

A = Amplitude selon α des oscillations synchrotron ≈ 0.8 radians.

NUCLEAR INSTRUMENTS AND METHODS 7 (1960) 306–314; NORTH-HOLLAND PUBLISHING CO.

THE PROBLEM OF MEASURING THE ABSOLUTE YIELD OF 14-MeV NEUTRONS BY MEANS OF AN ALPHA COUNTER

J. BENVENISTE, A. C. MITCHELL, C. D. SCHRADER and J. H. ZENGER

Lawrence Radiation Laboratory, University of California, Livermore, California

Received 23 February 1960

The assumptions used to derive the total neutron yield per detected alpha particle (from the D–T reaction) which were derived in an earlier report are re-examined in the light of additional experimental information. It is concluded that, for an alpha counter at 90° to the incident beam direction, the assumptions introduce practically no difficulties. Therefore, for precise monitoring in the absence of certain target information, it is recommended that this configuration be used. For counters at angles different from 90°, non-uniformity of target loading contributes the most serious error to the computed yield.

1. Introduction

In UCRL-4266[1]), an expression was derived for the total neutron yield per detected α particle.

$$N = \frac{4\pi \int_0^E \frac{\sigma_{cm}(\theta, \varepsilon)}{\frac{d\varepsilon}{dx}} d\varepsilon}{\Delta\Omega_\alpha \int_0^E \frac{\sigma_{cm}(\theta,\varepsilon)}{\frac{d\varepsilon}{dx}} \left(\frac{d\omega_{cm}}{d\omega_{lab}}\right)_\alpha d\varepsilon} \equiv \frac{4\pi}{\Delta\Omega_\alpha} R_\alpha , \qquad (1)$$

where

$\Delta\Omega_\alpha$ is the solid angle subtended by the α counter,

$\sigma_{cm}(\theta,\varepsilon)$ is the differential cross section for the D–T reaction in the center-of-mass system,

$d\varepsilon/dx$ is the rate of energy loss of deuterons in the target material,

$d\omega_{cm}/d\omega_{lab}$ is the solid angle conversion factor from the center-of-mass to the laboratory system for the detected α particles, and

E is the incident deuteron energy.

Implicit in the derivation of this expression are the following assumptions:

1. The reaction products are isotropically distributed in the cm system for the incident deuteron energies to 500 keV.

2. $d\varepsilon/dx$ is fairly well known in the region $0 < \varepsilon < E$.

3. Uniform loading of tritium atoms to a depth at least equal to the range of incident deuterons.

4. No scattering of incident deuterons.

Subsequent experience in measuring absolute cross sections for 14-MeV neutron interactions has cast some doubt on the reliability of this calculated calibration. This report presents the results of the investigation to determine the validity of the expression and the factors that contribute to it.

2. Discussion of the Assumptions

1. Data available at the writing of UCRL-4266[1]) led to the assumption of isotropy, in the cm system, of reaction products for incident deuteron energies up to 500 keV. More recent information, however, shows a measurable anisotropy above 200 keV. In fig. 1 are presented the data of Bame and Perry[2]) on the angular distribution of neutrons in the cm system for

[1]) J. Benveniste and J. Zenger, Information on the Neutrons Produced in the H^3(d,n)He^4 Reaction, University of California Radiation Laboratory (Livermore) Report UCRL-4266 (Internal) (Jan. 1954).

[2]) S. J. Bame, Jr., and J. E. Perry, Jr., Phys. Rev. **107** (1957) 1616.

several bombarding energies. The angular dependence may be represented as

$$①^{\dagger}\ \frac{\sigma_n(\theta)}{\sigma_n(0)} = 1 \qquad E < 200 \text{ keV}$$

$$②^{\dagger}\ \frac{\sigma_n(\theta)}{\sigma_n(0)} = 0.998 + 0.0213\cos\theta_n - 0.0190\cos^2\theta_n \qquad E = 350 \text{ keV}$$

$$③^{\dagger}\ \frac{\sigma_n(\theta)}{\sigma_n(0)} = 0.992 + 0.0382\,\theta_n - 0.0303\cos^2\theta_n \qquad E = 500 \text{ keV}\ .$$

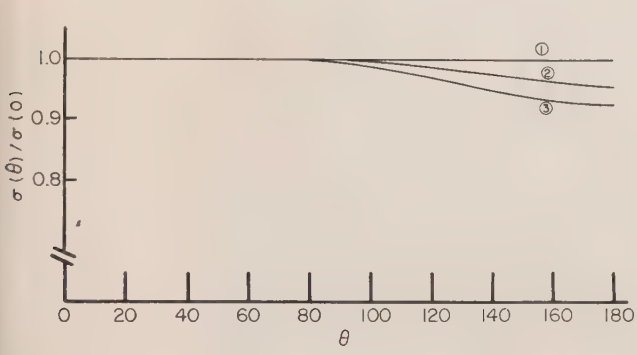

Fig. 1
Angular distribution of neutrons from T(d,n)He^4 reaction.

Since, in the cm system, $\theta_n = \pi - \theta_\alpha$ the α-particle distribution is given by

$$\frac{\sigma_\alpha(\theta)}{\sigma_\alpha(0)} = 0.998 - 0.0213\cos\theta_\alpha - 0.0190\cos^2\theta \qquad E = 350 \text{ keV}$$

$$\frac{\sigma_\alpha(\theta)}{\sigma_\alpha(\theta)} = 0.992 - 0.0382\cos\theta_\alpha - 0.0303\cos^2\theta_\alpha \qquad E = 500 \text{ keV}\ .$$

This lack of isotropy does not affect the value obtained for the numerator of eq. (1) since it represents the total yield of neutrons. The denominator, however, can be affected because it is evaluated at a particular angle. Calculation shows that the observed anisotropy would affect the contribution of 500 keV deuterons to the integral by about 1% and of 350-keV deuterons by about 0.5%. Since the yield of α particles by deuterons in the 300—500 keV range is about one-seventh of the total, it is clear that the assumption of isotropy in calculating R has contributed an error no larger than a small fraction of 1%.

† The circled numbers refer to similarly numbered curves in fig. 1.

2. The rate of energy loss of deuterons in the titanium-tritium target material was calculated from the expression

$$\frac{d\varepsilon}{dx} = \frac{48}{48 + 3\mathcal{N}}\left(\frac{dE}{dx}\right)_{Ti} + \frac{3\mathcal{N}}{48 + 3\mathcal{N}}\left(\frac{dE}{dx}\right)_{T},$$

where $(dE/dx)_{Ti}$ and $(dE/dx)_T$ refer to deuterons in normal titanium and tritium, and $\mathcal{N}$ represents the number of tritium atoms per titanium atom.

The rate of energy loss of protons in hydrogen was used to derive $(dE/dx)_T$, down to a deuteron energy of about 25 keV. $(dE/dx)_{Ti}$ was derived by interpolating between proton data for aluminum and copper and, assuming dE/dx was only a function of the velocity of the particle, changing the energy scale to apply to deuterons. Since proton data was available only down to 50 keV, deuteron data could be derived only to 100 keV. Since the peak yield of the D–T reaction occurs near 100 keV, it might be feared that an extrapolation below 100 keV would be a little risky. This is not quite the case because $d\varepsilon/dx$ appears in both the numerator and denominator of R. Calculation shows that a 50% error in $d\varepsilon/dx$ below 100 keV yields a 2% change in R.

$d\varepsilon/dx$ also depends on the loading factor, the ratio of tritium to titanium atoms. In early calculations a loading factor of 1 was assumed. Later experience showed that it was not unusual to have loading factors of $\frac{1}{2}$ or less. It is easy to compute that a change of a factor of 3 in the loading factor will yield a 10% change in $d\varepsilon/dx$, while an infinite change (no tritium at all) will yield but a 15% change. It is clear, however, that, because $d\varepsilon/dx$ appears in both the numerator and denominator of R, a change in the magnitude of $d\varepsilon/dx$ affects R not at all. Only a change in the shape, that is, the energy dependence of $d\varepsilon/dx$, is important. Since the energy dependence of $d\varepsilon/dx$ is a very weak function of the loading factor, and since even a 50% change in $d\varepsilon/dx$ in a sensitive part of the yield curve gave only a 2% change in R, the loading

factor can be expected to have an unimportant influence on R.

3. The tritium distribution with depth in the target was assumed constant in the absence of any other information. It is possible to imagine, however, a surface layer lacking in tritium

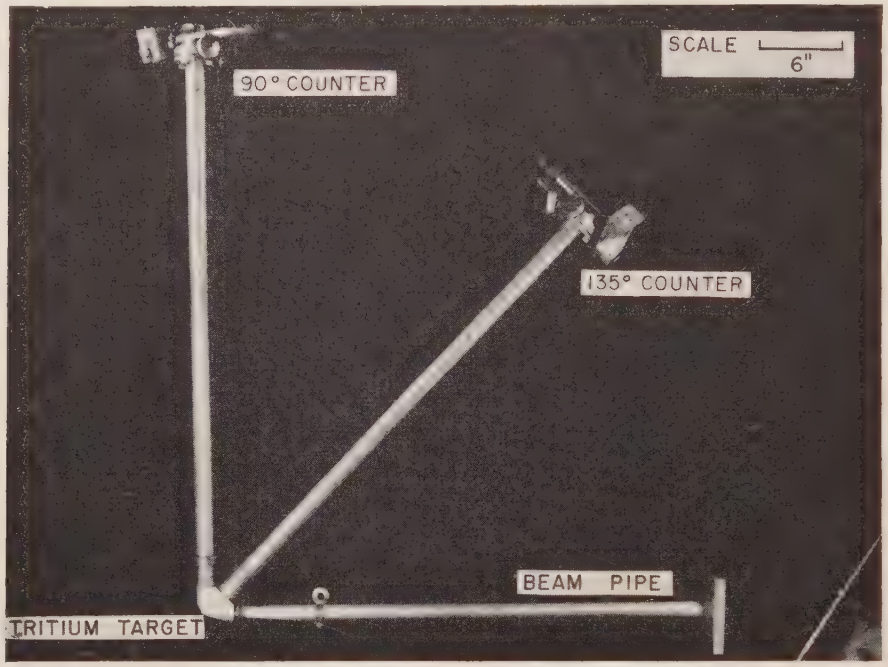

Fig. 2. 90—135° alpha counter assembly.

atoms existing on fresh targets or being built up with bombardments. The existence of a surface layer would have the effect of lowering the value of the upper limit on the integrals and reducing the value of R.

4. Thomas[3]) has calculated that for deuterons of 400 keV incident on a zirconium-tritium target the rms multiple scattering angle will be 20 degrees after a loss of 300 keV in the target material. Since the factor $d\omega_{cm}/d\omega_{lab}$ in the denominator of eq. (1) is derived from kinematical considerations in which the reacting deuteron direction is taken to be that of the beam, neglect of multiple scattering can be expected to affect the accuracy of this term. $d\omega_{cm}/d\omega_{lab}$ is a cosine-like term which is given approximately by

$$\frac{d\omega_{cm}}{d\omega_{lab}} \approx \left(\frac{\cos\phi + K}{K}\right)^2,$$

where ϕ is the angle which the α particle makes with the incident deuteron direction and K is a constant ($>>1$) determined by the kinematics. Multiple scattering would yield a scatter of ϕ's about the α observation angle. This suggests that no correction for multiple scattering would be necessary for an α observation angle about which this function is closely linear. Such an angle is 90 degrees. For α's observed at 135 degrees the correction due to this effect has been estimated as less than 0.5 %.

3. Measurements

If we drop the assumption of uniform loading of the target, the expression for R becomes

$$R' = \frac{\int_0^E n(x)\,\frac{\sigma_{cm}(\theta,\varepsilon)}{\frac{d\varepsilon}{dx}}\,d\varepsilon}{\int_0^E n(x)\,\frac{\sigma_{cm}(\theta,\varepsilon)}{\frac{d\varepsilon}{dx}}\left(\frac{d\omega_{cm}}{d\omega_{lab}}\right)_\alpha d\varepsilon}. \qquad (2)$$

Now, it turns out that for an α detector at 90 degrees, $d\omega_{cm}/d\omega_{lab}$ is a very slowly varying

[3]) R. G. Thomas, Private communication.

function of energy (e.g., from 0 to 500 keV the ratio goes from 1 to 0.9775, and the weighted average of $d\omega_{cm}/d\omega_{lab}$ in the denominator integral, if $n(x)$ is constant, is 0.9911 at 500 keV and 0.9926 at 350 keV). Thus for a 90-degree α detector we may write

$$R'_{90^\circ} \equiv \frac{\int_0^E n(x)\,\frac{\sigma_{cm}(\theta,\varepsilon)}{\frac{d\varepsilon}{dx}}\,d\varepsilon}{\left(\overline{\frac{d\omega_{cm}}{d\omega_{lab}}}\right)_{90^\circ}\int_0^E n(x)\,\frac{\sigma_{cm}(\theta,\varepsilon)}{\frac{d\varepsilon}{dx}}\,d\varepsilon} \equiv \frac{1}{\left(\overline{\frac{d\omega_{cm}}{d\omega_{lab}}}\right)_{90^\circ}}, \tag{3}$$

practically independent of our knowledge of the loading factor and of $d\varepsilon/dx$. This feature makes it possible to devise a rather sensitive experimental method for evaluating R and testing the assumptions on which the calculations were based.

To this end a target assembly was designed with two α arms (see fig. 2) so that α particles could be detected simultaneously at 90 and 135 degrees. The ratio of the number of α's observed at 90 degrees to those observed at 135 degrees is

$$\frac{N_\alpha(90^\circ)}{N_\alpha(135^\circ)} = \frac{\Delta\Omega_{90^\circ}}{\Delta\Omega_{135^\circ}} \frac{\left(\overline{\frac{d\omega_{cm}}{d\omega_{lab}}}\right)_{90^\circ}\int_0^E n(x)\,\frac{\sigma_{cm}(\theta,\varepsilon)}{\frac{d\varepsilon}{dx}}\,d\varepsilon}{\int_0^E n(x)\,\frac{\sigma_{cm}(\theta,\varepsilon)}{\frac{d\varepsilon}{dx}}\left(\frac{d\omega_{cm}}{d\omega_{lab}}\right)_{135^\circ}d\varepsilon}$$

$$= \frac{\Delta\Omega_{90^\circ}}{\Delta\Omega_{135^\circ}}\left(\overline{\frac{d\omega_{cm}}{d\omega_{lab}}}\right)_{90^\circ} R'_{135^\circ}\,. \tag{4}$$

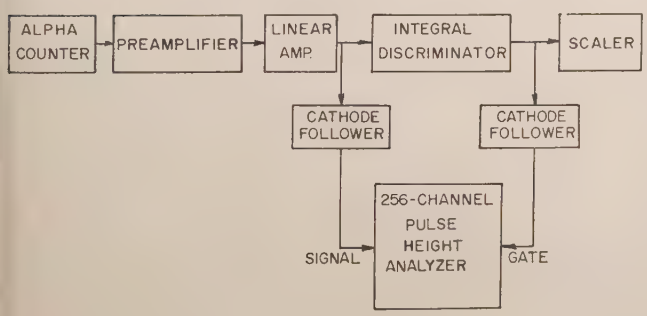

Fig. 3. Alpha-monitoring electronics.

Thus, a fundamentally simple measurement of the ratio of two numbers leads to a rather precise test of the calibration constant R'_α.

The 90—135 degree assembly was mounted on the 26-degree port of the Cockcroft-Walton. A collimator in the beam pipe insured that only the active part of the target was exposed to the beam. The α particles were detected in argon-CO_2 gas proportional counters after passing through 1 mg/cm² aluminum-coated Mylar foils. A remotely controlled shutter in each α arm made it possible to measure background contributions to the α spectrum. Background corrections were customarily less than 3%.

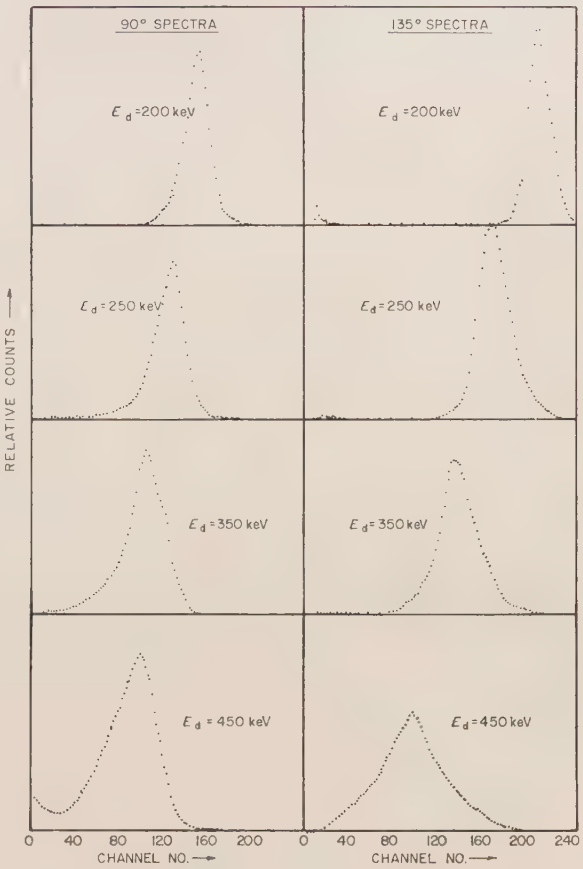

Fig. 4. Change in shape and channel position of alpha spectrum as E_d is varied.

A schematic diagram of the α-monitoring electronics is shown in fig. 3. The multichannel analyzer served primarily as a visual means for setting amplifier gains and discriminator levels quickly and accurately.

Fig. 4 shows the pulse-height distributions of the alpha particles in the two counters for

several different deuteron bombarding energies. The shift of the peak toward lower energies as the incident energy increases is due to the fact that's from the most prolific deuterons (those in the neighborhood of 100 keV) are being formed deeper in the target material. Furthermore, it is suggested that the larger low-energy tail observed in the 90° counter is due to the fact that, in our geometry, 90° alphas had to travel through 40% more target material before being detected. Scattering could increase this considerably with consequent appreciable losses of energy. Below about 400 keV this behavior of the spectrum gave no difficulty in setting the discriminator level for precise monitoring of the yield. Above 400 keV, however, the separation between significant portions of the alpha spectrum and noise was not as clean and the same degree of confidence could not be held for the measured number.

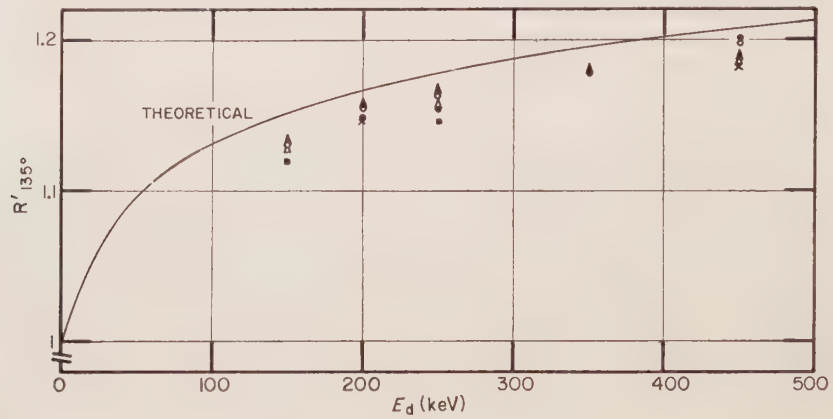

Fig. 5a. $R'_{135°}$ vs E_d for normal targets.

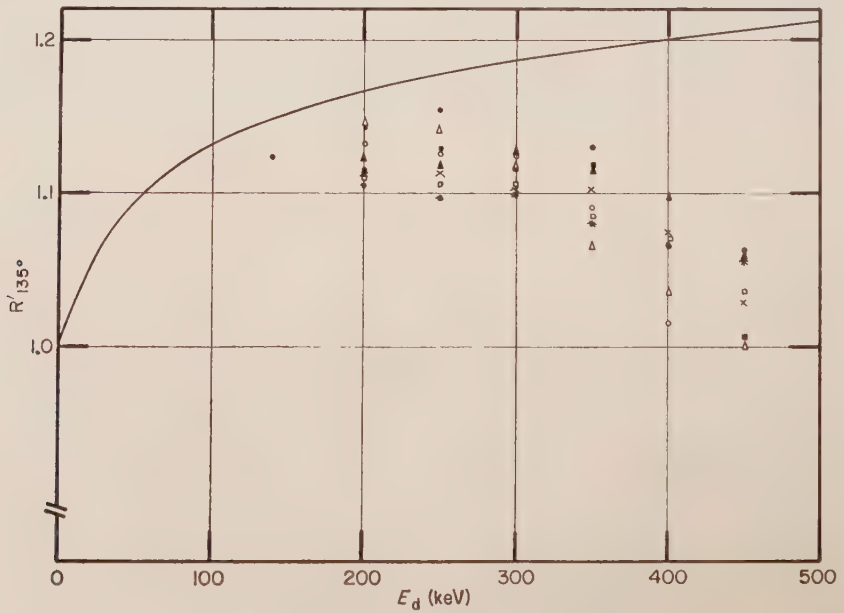

Fig. 5b. $R'_{135°}$ vs E_d for anomalous targets.

In the course of a run, counts were observed in the 90° and 135° alpha counters simultaneously. Then the shutters were inserted and, using a neutron detector as monitor, background

counts were observed. Net alpha counts were deduced after both observations had been corrected for dead-time in the system.

4. Results

In order to determine whether target parameters were important, a rather broad selection of targets was studied, with stress laid on obtaining a good sampling of loading parameters and dates of preparation. Table 1 presents the target data.

For each target, observations of the 90—135° ratio were made at several deuteron bombardment energies in the range $150 \leqslant E \leqslant 450$ keV. These ratios appear in table 2.

Figs. 5a and 5b are graphical representations of these ratios after having been converted to R's by means of eq. (4). The data have been displayed separately for those targets that behaved as expected theoretically and those that behaved anomalously. The precision of the measurements is $\pm 1\%$ as determined by the measurements of the solid angles and counting statistics and verified by their reproducibility.

Fig. 5a shows that one group of targets yields an energy dependence for $R'_{135}{}^{\circ}$ very similar to that expected from the evaluation of the integral in eq. (1). However, the magnitude of R'_{135° turns out to be consistently 1.5% to 2.5% lower than that calculated. Within the precision of the measurements, this lowering could be understood in terms of the existence of a surface layer, about 50 keV thick, depleted in tritium.

TABLE 1

Characteristics of targets.

Target No.	Tritium (cc)	Titanium (mg)	Loading factor Tr/Ti	Zeus meter reading of β activity
818	1.13	11.7	0.414	240
1037	1.55	7.7	0.861	350
1018	1.52	5.9	1.102	1100
813	1.22	12.7	0.432	235
1012	2.58	10.9	1.014	1000
1015	3.47	13.5	1.100	1000
1010	1.94	7.9	1.052	600
993	2.14	8.5	1.078	600
1008	2.56	13.7	0.800	600
1016	4.12	16.0	1.102	900
815	1.22	12.6	0.414	250
742	4.25	24.4	0.746	1200
807	1.23	12.1	0.436	—
705	1.61	12.5	0'551	700
814	1.23	12.8	0.412	240
822	1.80	11.4	0.676	450
809	1.73	14.3	0.518	700
823	1.90	12.0	0.678	500

TABLE 2

Ratio $N_\alpha(90^\circ)/N_\alpha(135^\circ)$ for various targets and E_d's.

Target No.	Incident deuteron energy E_d (keV)						
	150	200	250	300	350	400	450
818	1.355	1.341	1.384		1.349		1.266
1037		1.302	1.357		1.403		1.406
1018		1.392			1.407		1.431
1010	1.365	1.380	1.40		1.412		1.417
813		1.342	1.374		1.321		1.234
1012	1.363	1.388	1.395		1.408		1.427
1015	1.350	1.391	1.373		1.407		1.407
993	1.360		1.390		1.411		1.415
1008	1.358		1.385		1.410		1.409
742		1.380	1.370	1.340	1.274	1.237	1.194
814		1.3750	1.355	1.337	1.314	1.274	1.20
705		1.362	1.351	1.346	1.304	1.212	1.172
807		1.351	1.342	1.350	1.333	1.309	1.264
815		1.330	1.318	1.318	1.292	1.272	1.258
822		1.338	1.336	1.320	1.318	1.282	1.226
823		1.336	1.328	1.325	1.298	1.279	1.236

The assumption of isotropy also yields a discrepancy in the right direction; however, it is expected to be about 1% at 500 keV and to decrease rapidly with decreasing energy. Likewise, the effect of scattering of the incident deuterons is to give a smaller value to $R'_{135°}$. The correction was estimated to be less than 0.5% at 500 keV and one would expect this to decrease with decreasing energy. The possibility that counts were lost from the 90° detector by absorption or scattering of the alpha particles emerging from the target has been ruled out on the basis of our observations of alpha pulse-height distributions. Important effects of this sort would be made obvious by the ragged appearance of the lower edge.

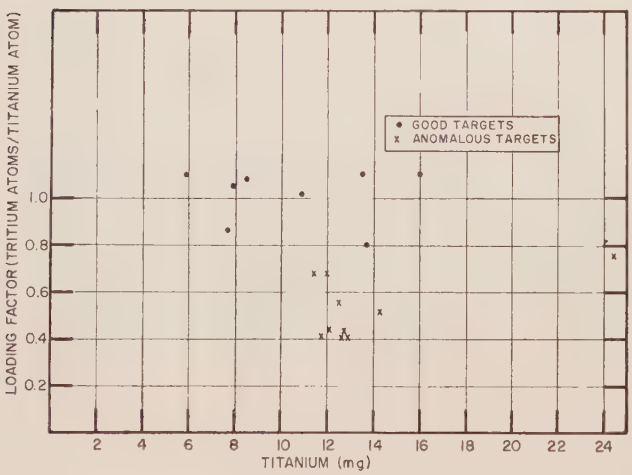

Fig. 6. Loading factor vs weight of Ti.

The behavior of the targets displayed in fig. 5b is understandable in terms of nonuniform loading with the tritium concentration increasing rapidly with depth. A simple test for uniformity of loading would be to plot the loading factor N_T/N_{Ti} vs the weight of titanium. Uniform loading would show N_T/N_{Ti} = constant, while if the tritium were concentrated in a relatively thin layer one would expect N_T/N_{Ti} to decrease monotonically with the weight of titanium.

Fig. 6 shows that the "good" targets, those that behave as expected with regard to the energy dependence of $R'_{135°}$ do indeed indicate that the loading is uniform. Unfortunately, there is not a sufficiently large range of titanium weights for the "anomalous" targets to show conclusively that the tritium was not uniformly distributed. We may only conclude that the average loading was relatively low and the best evidence for nonuniform loading remains the observed energy dependence of $R'_{135°}$.

5. Conclusions

In examining the assumptions made for calculating the calibration constant for an alpha counter monitor, it is concluded that:

1. For an alpha counter at 90° to the incident beam direction, the assumptions introduce practically no difficulties; therefore, for precise monitoring in the absence of certain target information, it is recommended that this configuration be used. Above an incident deuteron energy of about 400 keV, however, the alpha spectrum degenerates on the low side so that one must take considerable care to insure proper monitoring conditions.

2. For alpha monitors at angles different from 90°, it was shown experimentally that nonuniformity of target loading contributed the most serious error to the computed calibration constant.

3. For the targets investigated, those having a loading factor of at least 0.8 T atom per Ti atom were sufficiently uniformly loaded to yield calibration constants that behaved normally.

4. For uniformly loaded targets, a discrepancy in the observed and computed $R'_{135°}$ amounting to (2.0 ± 1)% was noted.

Acknowledgment

It is a pleasure to acknowledge the very helpful participation in this study of the Cockcroft-Walton crew under the direction of L. M. Erickson and R. V. Cedarlund.

Appendix

CALIBRATION OF THE 174° α ARM

In our study of γ rays from 14-MeV-neutron interactions with various nuclei in ring geometry, it is desirable to use a target assembly that can be completely shielded from the view of the detector. To this end, a target assembly was constructed for monitoring alpha particles which were emitted in a direction making an angle of 174° with the incident beam (see fig. 7).

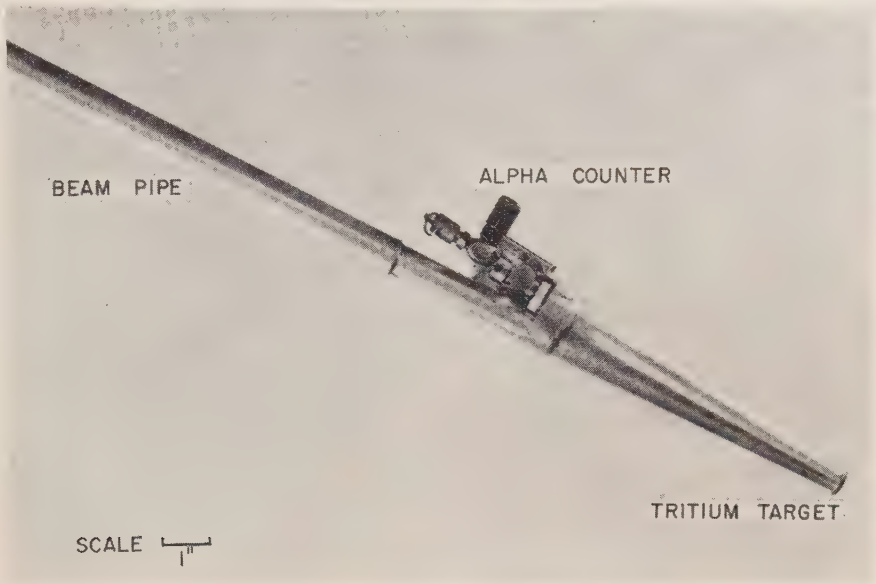

Fig. 7. 174° alpha counter assembly.

Since the difficulties encountered with the calculation of the calibration constant for the 135° alpha counter are expected to be aggravated at 174°, no attempt was made to calculate R (174°). Rather the 174° assembly was calibrated against the 90° assembly using a neutron detector as intermediary.

Neutrons were detected in a $\frac{1}{2}$ in. $\times$ $\frac{1}{2}$ in. cylindrical plastic scintillator placed directly in line with the incident deutron beam. To achieve insensitivity to gain shifts in the electronic amplifiers, the signals were passed through a differential discriminator set to select pulses in the flat region of the knock-on spectrum. The behaviour of this system is displayed in fig. 8. Long-term tests of this system showed that the ratio of neutron counts to alpha-particle counts was constant well within statistics.

The experimental procedure was to measure the number of alpha counts per detected neutron for first the 90° assembly, and then for the 174° assembly. In each case corrections were made for dead time. The ratio of the two measurements and knowledge of the 90° assembly calibration gives us the 174° assembly calibration.

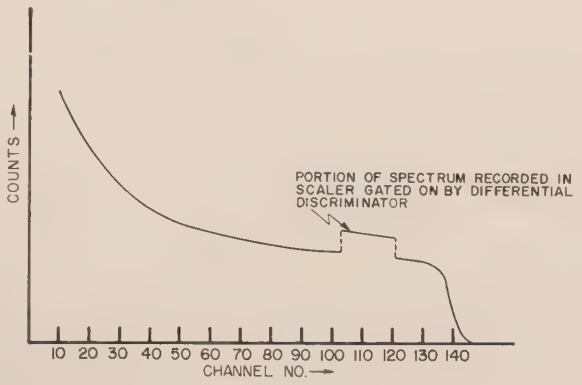
COUNTS
PORTION OF SPECTRUM RECORDED IN SCALER GATED ON BY DIFFERENTIAL DISCRIMINATOR
10 20 30 40 50 60 70 80 90 100 110 120 130 140
CHANNEL NO.

Fig. 8. Neutron spectrum produced by knock-on protons in plastic scintillator.

Different targets were observed, in order to determine the extent of variation among them.

Several completely separate runs were conducted to assure ourselves that our measurements were reliable and meaningful. All observations were made at a bombarding energy of 350 keV because it is at this energy that the gamma-ray work is being done.

Table 3 displays the results of our measurements. It appears that all but target No. 813 gave a ratio $N_\alpha\,(90°)/N_\alpha\,(174°) = 0.127$ within 1%. This is not at all surprising since target No. 813 is the only one in the list which was previously revealed to behave anomalously.

TABLE 3

Ratio $N_\alpha(90°)/N_\alpha\,(174°)$ for various targets and $E_\alpha = 350$ keV.

Target No.	$\frac{N_\alpha(90°)}{N_\alpha(174°)}$
813	0.115
993	0.1263
1008	0.126
1016	0.128
1010	0.128
1018	0.1283
1012	0.127

NUCLEAR INSTRUMENTS AND METHODS 7 (1960) 315–319; NORTH-HOLLAND PUBLISHING CO.

ON THE AUTOMATIC CONTROL OF SCINTILLATION SPECTROMETERS

H. W. TAYLOR and R. McPHERSON

Physics Dept., Queen's University, Kingston, Canada

Received 15 February 1960

A simple control circuit is described which permits the automatic control of a scintillation coincidence spectrometer used for directional correlation studies and coincidence measurements. Automatic sequential pulse height analysis is obtained by coupling to the control unit a 100-position stepper which advances the bias on a single channel analyser.

1. Introduction

The multichannel pulse-height analyser is one of the most useful tools available to the nuclear spectroscopist. The device has two inherent drawbacks, however; one is the high initial cost, the other is the servicing problem which is often expensive in both money and time. One electronic alternative to the use of multichannel analysers is manual operation of a single channel analyser. Unfortunately this technique is costly in man-hours. A compromise between these two alternatives is obtained, however, if one employs automatic control of a single channel analyser accompanied by a display of the experimental data on paper tape. A simple control unit developed in this laboratory permits the automatic recording of data in this way from directional correlation experiments as well as coincidence and single counting experiments with scintillation counters. The unit is reliable and inexpensive. Furthermore, only standard electronic units (scalers, etc.) are needed to realize the automatic operation offered by the control system.

2. The Coincidence Spectrometer

As an introduction to the control unit, the coincidence spectrometer itself will be discussed in some detail.

The control system was designed to operate a coincidence spectrometer built in this laboratory for directional correlation studies of successive gamma-rays. Fig. 1 shows a block diagram of this spectrometer. The detectors which have been used to date are standard scintillation counters employing NaI(Tl) crystals ranging in size from the $3'' \times 3''$ cylinder down to the $1\frac{1}{2}'' \times 1''$ cylinder. Standard linear amplifiers and single channel pulse-height analysers complete the two single spectrometers which form a

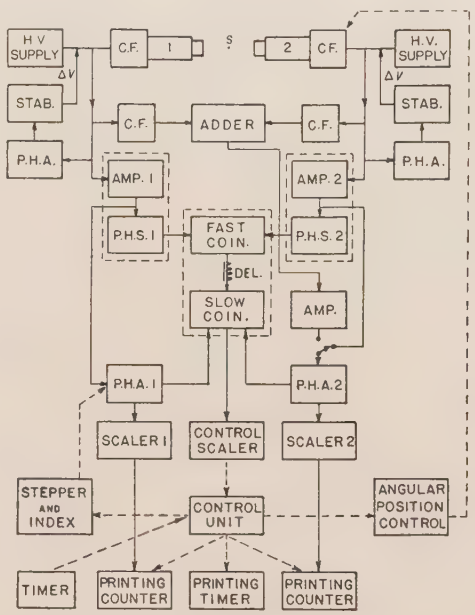

Fig. 1.

Block diagram of the fast-slow coincidence spectrometer. S = radioactive source; 1 and 2 = scintillation counters; C. F. = cathode follower; H. V. = high voltage supply; P. H. A. = "pulse-height" analyser; STAB. = de Waard stabiliser; ΔV = feedback voltage; AMP. = linear amplifier; P.H.S. = integral pulse-height selector; COIN. = coincidence unit; DEL. = delay line.

Note added in proof: Each stabilization feedback loop should include an amplifier.

part of the coincidence set-up. The gain of each of these is stabilised against drift following the method of de Waard[1]). Pulses from integral pulse-height selectors are fed into a fast-slow coincidence unit ($\tau = 40$ mμsec). The output pulses from the fast section are delayed by a time equal to the delay time of the analysers, and then fed into a slow section ($\tau = 2$ μsec) along with the output pulses of the two analysers. The triple coincidence pulses from the slow section are recorded with a decade scaler, called the control scaler, and the pulses from the analysers are recorded by two decade "singles" scalers (1 and 2). Each scaler has a built in "preset count"-"preset time" circuit. One additional feature of the spectrometer is the adder circuit which is patterned after the one employed by Hoogenboom[2]). "Gated" coincidence spectra obtained with this circuit exhibit a substantial reduction in the intensities of the Compton distributions present.

The control of the spectrometer and the recording of the data are accomplished through the combined use of the control scaler, the control unit, an electrical timer, printing counters and a printing timer. With the exception of the control unit, all of these items are available commercially in considerable variety. When the spectrometer is used for directional correlation studies an angular position control advances the movable counter from one angular position to the next. The counting interval is determined by the preset-count setting on the control scaler. Rotational motion is achieved through the use of a motor mounted at the free end of the arm which supports the movable counter. The arm is pivoted about a point source located on a post at the center of a circular table. The motor advances the arm by means of a friction drive which bears on the edge of the table. Angular positions are defined by studs placed along a circular arc on the upper surface of the table. For coincidence experiments, a stepper (precision rheostat) which advances the gate of one of the single-channel analysers is substituted for the angular position control. In this case the spectrometer may be set to operate on either a preset-time or preset-count basis, with the pulses being recorded on either mechanical registers (manual operation) or printing counters (automatic operation). Of course, each single-channel spectrometer may be used independently for single counting experiments.

The operating sequence for the spectrometer is as follows: If directional correlation studies are to be undertaken, the control scaler is set to turn off automatically after a predetermined number of coincidence counts have been collected at the angular position θ_i. (θ_i is the angle between the axes of the counters; $90° \leqslant \theta_i \leqslant 180°$.) Upon receiving the last pulse of this preset number, the control scaler also turns off the singles scalers, which have recorded all the pulses received by the pulse-height analysers. The accumulated count on the register of each printing counter is printed on to paper tape, as is the time required to collect the coincidence counts. The control unit switches on the advancing motor of the directional correlation gear, and the movable counter is advanced to the next angular position θ_{i+1} at which point a stud fixed in the table top actuates a microswitch mounted on the arm supporting the movable counter. The switch, operating through the control unit, resets all the scalers and stops the motor. After a brief delay, the scalers and the printing timer again become operative and the collection of the next set of coincidence counts proceeds. After the predetermined number are collected, the scalers are again turned off and the sequence of events begins anew. After both the 90° and 180° positions, the direction of rotation of the movable counter is reversed by changing the direction of rotation of the advancing motor.

If the apparatus is being used to scan coincidence or singles spectra, the stepper is substituted for the angular advance gear. The sequence of events is similar to that outlined above, with the stepping of the gate of the scanning analyser replacing the change of angular position. The counting interval may be

[1]) H. de Waard, Nucleonics **13** (1955) 36.
[2]) A. M. Hoogenboom, Nuclear Instruments **3** (1958) 57.

established on the basis of a preset count or by an electrical timer which resets automatically after each counting period.

3. The Control Unit

The automatic operation of either a single spectrometer or the complete coincidence system is realized through the use of the control unit and a control scaler. The latter must have a number of values of "preset count" available if a wide range of counting rates is to be handled successfully.

The circuit diagram of the control unit is shown in fig. 2 together with sections of those units forming the spectrometer which are essential to automatic operation. The unit is designed to run off a 110 V. A.C. main with a simple half-wave rectifier supplying the D.C. voltages required. (All control voltages are isolated from ground.) The controls are simple, consisting of an off-on switch (SW1), a motor control switch (SW2) and a selector switch (SW3) which indicates the mode of operation (position 1: preset count, position 2: preset time). The motor control switch operates either the angular-advance motor or the motor which steps the analyser bias.

Scalers 1 and 2 and the printing timer are

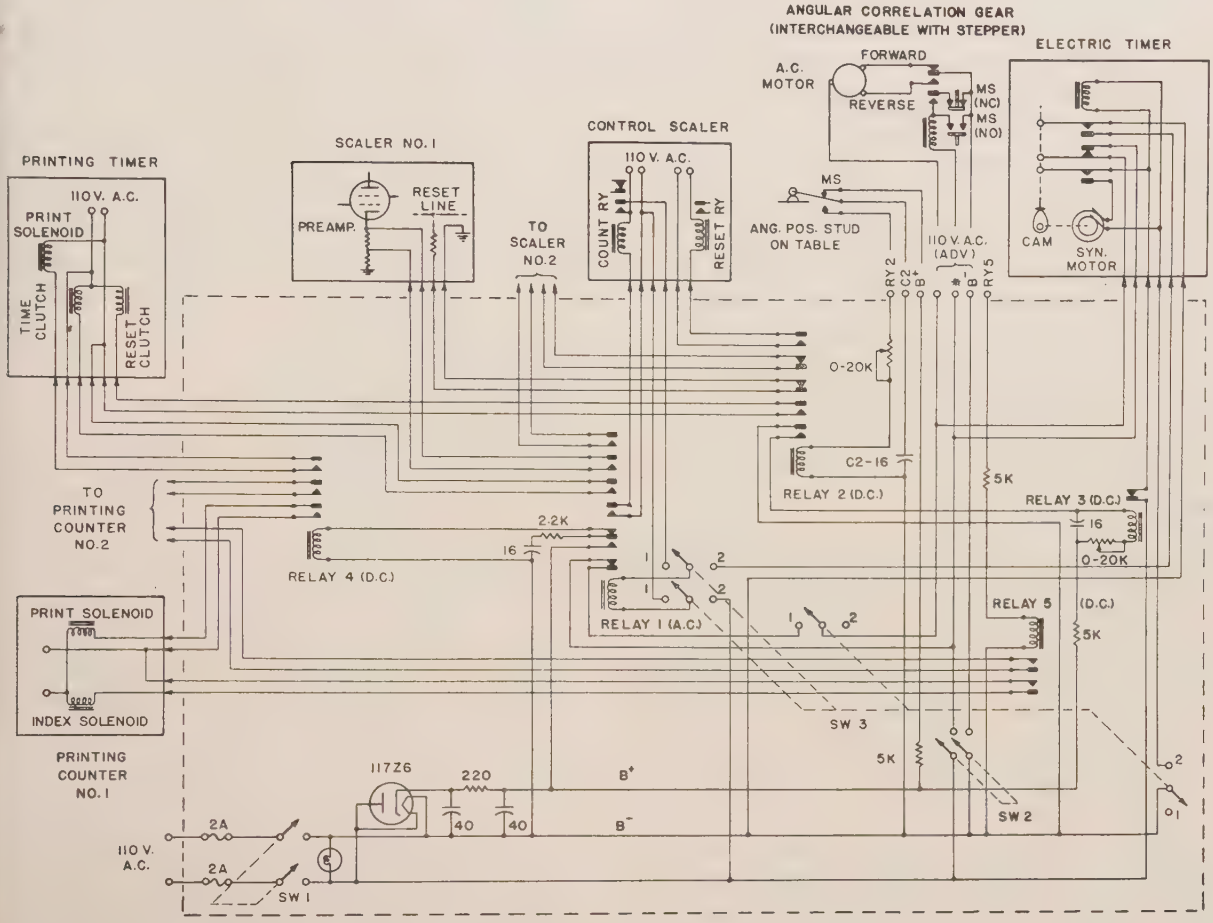

Fig. 2. Schematic diagram of control unit showing interlocking electronic units. All capacitances in mFd. SW-1: on-off switch; SW-2: motor control switch; SW-3: position 1-preset count, position 2-preset time; M.S.: precision (micro-) switch; RY 1: count relay (110 V A.C.; 6 P.D.T.); RY 2: reset relay (15 mA; 5 P.D.T.); RY 3: delay relay (1 mA; S.P.S.T.); RY 4: print relay (15 mA; 3 P.D.T.); RY 5: index relay (15 mA; D.P.S.T.).

* Not in use when stepper is coupled to control unit.

controlled by the count relay (RY1) in the control unit. With the selector switch in position 1 (preset count), relay 1 is operated by a switch (not shown) ganged to the register of the control scaler. This switch actuates the count relay in the scaler; it opens when the register indicates a predetermined number of counts and closes when the register is reset to zero. With SW3 in position 2 (preset time), relay 1 is closed by a switch in the electric timer which opens when the preset time interval is terminated. The timer itself is reset by interruption of its line voltage. The count relay (RY1) is closed for the next counting interval by restorting the timer line voltage. When RY1 is opened at the end of a counting interval, the print relay (RY4) is actuated by condenser discharge, which results in the printing of the accumulated count of the singles scalers on paper tape. At the same instant 110 V A.C. is applied to either the angular-advance motor or the stepper motor. (This voltage is applied by a switch in the timer which closes at the end of the count cycle when the selector switch is in position 2.) If the correlation apparatus is in use, the moving counter proceeds to the next position, where a microswitch closes the reset relay (RY2) momentarily by condenser discharge. If the stepper is in use, a motor drives two cam-actuated switches, one to alter the analyser bias, the other, 3.7 seconds later, to trip the reset relay. The 110 V A.C. motor driving voltage can be interrupted in one of two ways: for preset count operation, this is accomplished by the closing of the count relay when the control scaler register is reset to zero; for preset time operation, the interruption occurs as the timer resets when the timer voltage line is opened.

The method of resetting the control scaler depends upon its make. Our control scaler is a Baird-Atomic Model 1090 which features preset-count operation through the use of a switching circuit in the electrically resetting register. When the reset relay (RY2) of the control unit closes, the reset relay of the control scaler is also actuated. For our singles scalers 1 and 2 it is sufficient for the reset relay to open the reset lines of the scaling strips. Since the resetting of the scaler registers takes one second, the resetting period for the electrical timer used (Microflex Reset Timer) must be lengthened to about two seconds by means of the holding relay (RY3). The index relay (RY5) is used only when spectral analysis is undertaken with the stepper.

It is evident from the above description that the design of the control unit is determined not only by the basic functions it must perform, but also by the circuits in the scalers, timers, etc. coupled to it. These, of course, will vary from laboratory to laboratory. However, a number of variations of the control circuit should be possible so that the basic simplicity of the device will not be lost when scalers with circuits different from ours are employed.

4. The Stepper

As mentioned above, the automatic advancing of the bias on a pulse-height analyser supplies a compromise between manual operation of the analyser and the use of a multichannel unit. The device we have used for this purpose is shown in fig. 3. A chain of precision resistors is substituted for the 50 kΩ bias potentiometer in the analyser. The bias is altered by means of a 100-position stepping relay built in this laboratory. The toothed wheel of this relay shares a

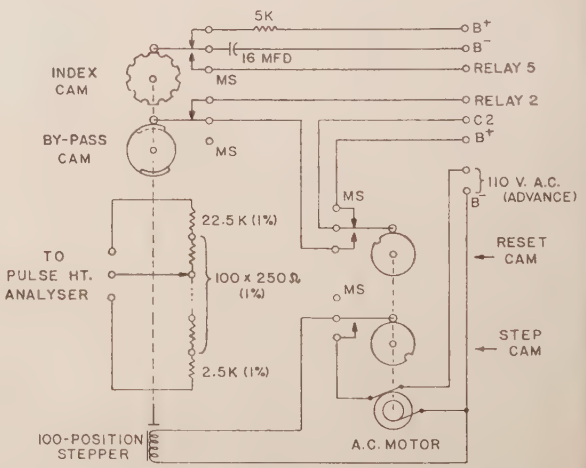

Fig. 3.
Schematic diagram of stepper which decreases bias on pulse-height analyser. (M.S. = precision (micro-) switch).

common shaft with the index cam, the by-pass cam and the movable contact of the rheostat. One hundred precision resistors form a circular chain with the shaft collinear with the symmetry axis. The result of this arrangement is that the 100 gate positions are spread uniformly over an angle of rotation of 360°. To facilitate analysis of the data the recorded count for every tenth gate position is accompanied by an identifying number on the paper tape. This indexing of the data is accomplished through the use of the index cam (one indentation every 36°) and the indexing relay (RY5) which is coupled to printers 1 and 2.

The step and reset cams are mounted on a common shaft with the 8 r.p.m. advancing motor. The reset cam lags behind the step cam by 180°. With the motor speed used, an operational interval of 7.5 seconds is realized, during which the gate is advanced and the scaler registers reset to zero. Since the choice of counting interval is determined in general by the nature of the experimental problem, it should be noted, that for counting periods shorter than one minute, the efficiency of automatic operation is somewhat reduced because a rather large fraction of the time is consumed in the recording and resetting operations.

A gate width of 0.5 volt is usually employed for pulse-height analysis, with the spectrum confined to the voltage range 5—55 volts. This combination of gate width and operating range has been found to be satisfactory for most purposes. If a 1.0 volt gate is desired, it is not difficult to arrange for the stepper to advance twice in succession upon receiving 110 V A.C. from the control unit. This mode of operation is effected by replacement of the usual step cam with one having two indentations spaced a few degrees apart.

Should only a part of the full pulse-height spectrum be of interest, the by-pass cam may be adjusted so that only the section under study will be scanned by the spectrometer. The cam keeps the advancing motor running continuously by interrupting the reset pulse while the analyser gate is outside the region of interest. This feature of the stepper is particularly useful if the counting rates over the spectrum differ by large factors. One can adjust the by-pass cam so that high counting rate regions are avoided when weak photopeaks are being studied. The overworking of the scaler registers and printing counters is thereby avoided.

No provision has been made for automatic shut-down of the spectrometer after the 100 gate positions have been used. As a consequence, the stepper works on a repetitive scan basis only.

The spectrometer described above has been used in a number of different experiments. Directional correlation measurements, coincidence counting (both gated and ungated) and single counting experiments have been successfully carried out, with the spectrometer being operated on a 24-hour basis in each case. No chronic failures have appeared in either the control unit or the stepper mechanism during the time these units have been in service.

The authors wish to thank W. R. Frisken for designing the prototype of the directional correlation apparatus. This work has been supported by the National Research Council of Canada and the Atomic Energy Control Board.

NUCLEAR INSTRUMENTS AND METHODS 7 (1960) 320–324; NORTH-HOLLAND PUBLISHING CO.

A MULTIPLE EVENT ANALYSER

W. G. GORE

AWRE, *Aldermaston*

Received 1 February 1960

A circuit is described that produces an output pulse, the height of which is proportional to the number of input pulses received in a given time interval after an input gate pulse. This circuit, when used with a pulse height analyser, enables the distribution of the number of pulses per burst to be analysed. The maximum number of pulses per burst that can be counted is ten.

1. Introduction

For certain nuclear physics experiments it is necessary to analyse the number of events that are counted after the occurrence of a certain event, for example, the number of neutrons detected after a fission. This paper describes a circuit developed for such purposes. The action of the circuit is started by a gate pulse, which causes a gate to open for a period of 10, 15, 25 40 or 100 μs, as chosen by the operator. The number of signal pulses passed through the gate during this time determines the amplitude of the output pulse, which varies from 4 V to 23 V for input counts from zero to ten. Provision is also made to veto any output from the circuit by means of a negative input pulse in another channel, if desired.

2. Block Diagram

The block diagram of the unit, with idealised waveforms, is given in fig. 1. The positive gate input pulse operates two trigger circuits, the gate pulse generator and the reset pulse generator. The gate pulse generator produces a pulse to open the gate, the length of which is selected by a switch to give the time intervals mentioned above. The reset pulse generator produces a 110 μs pulse that makes the step circuit operative. The positive signal input pulses fire the discriminator and, if the gate is open, cause a current pulse to pass to the step circuit. The step circuit produces an output of amplitude proportional to the number of events counted. However, this waveform is not suitable for operating a kicksorter.

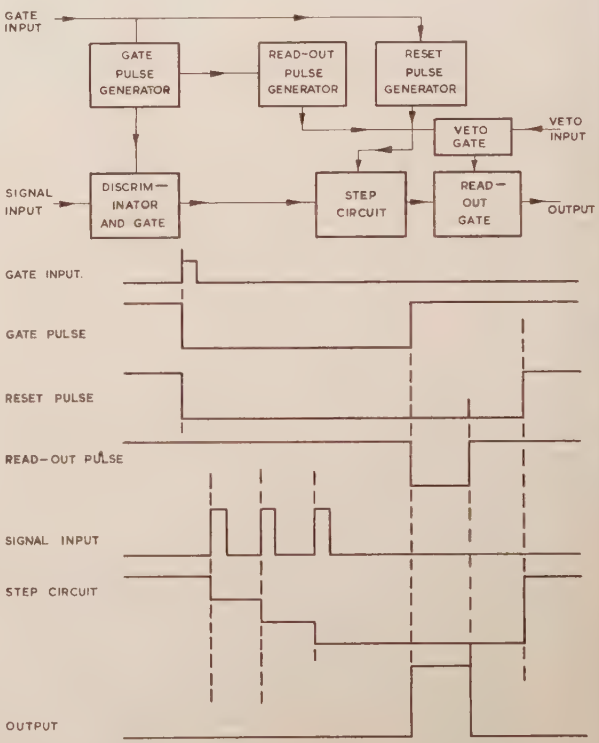

Fig. 1. Block diagram and idealised waveforms.

An output is taken from the gate pulse generator and triggers the read-out pulse generator at the end of the gate pulse. The 5 μs pulse produced passes through the veto gate, if no veto pulse is present, and opens the

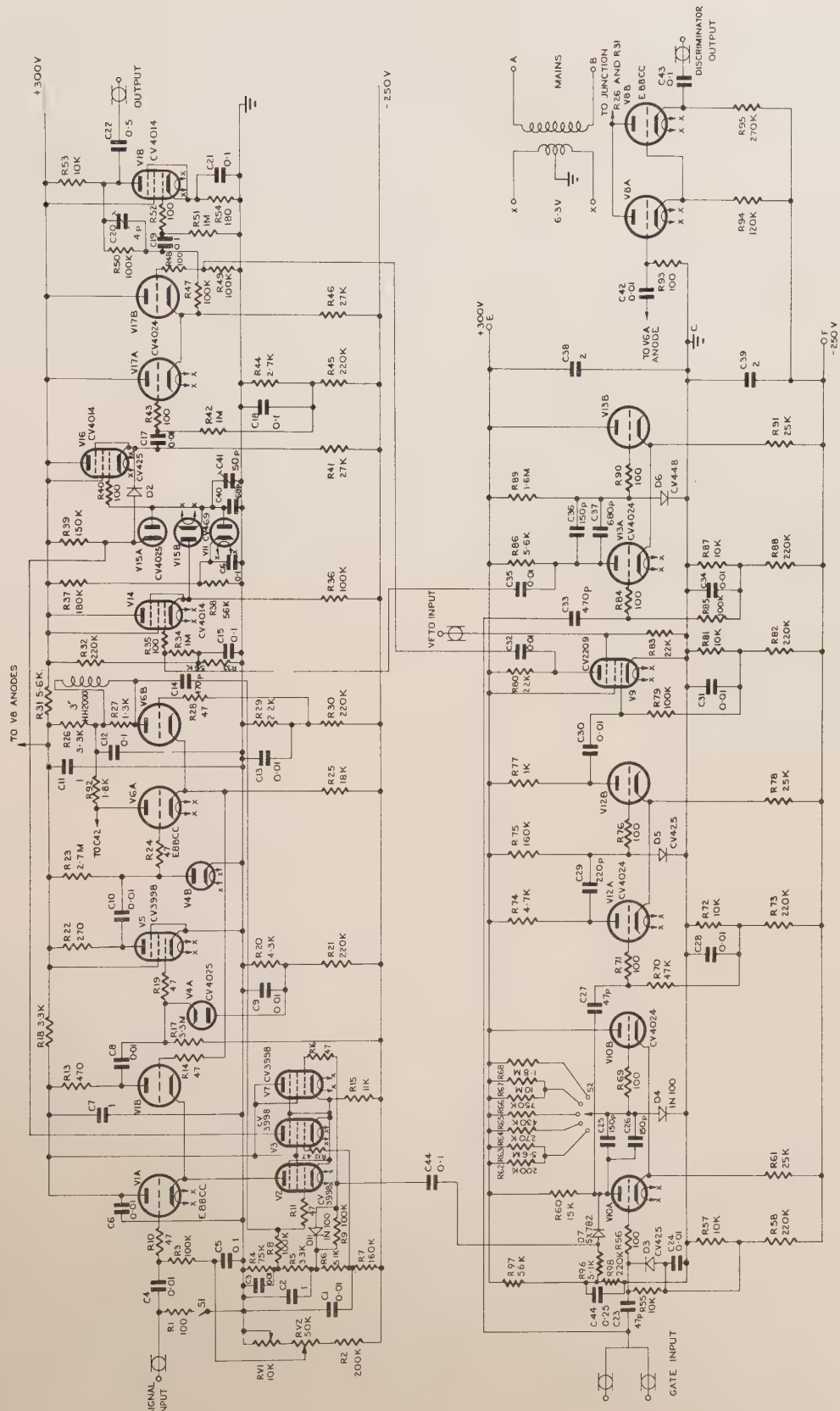

Fig. 2. Circuit diagram.

read-out gate, which passes a portion of the step waveform, after it has reached its maximum value, to the output. At the end of the reset pulse, the step circuit is returned to its quiescent condition.

3. Circuit Action

The circuit diagram is given in fig. 2. The gate input is differentiated and fed to the grid of V10A and fires the trigger circuit formed by V10, which is the gate pulse generator. The length of the pulse produced can be varied by selecting different values of grid leak by the switch S2. The pulse is taken from V10A anode through the series clamping diode D7 so that it has short rise and fall times. The diode D3 removes the negative part of the differentiated waveform, which would cause the circuit to trigger off. The gate input also fires the trigger circuit formed by V13, which is the reset pulse generator.

A negative pulse is taken from V10A anode and differentiated by C27 and R60. The positive pulse formed at the lagging edge of the original pulse fires the trigger circuit V12, which is the read-out pulse generator. A positive pulse from V12B anode is passed to the veto gate valve V9, which is a short suppressor base pentode. This valve is normally cut off at its control grid and the positive input pulse causes it to conduct and produces a negative pulse at its anode. A negative veto pulse would cut V9 off at the suppressor grid and stop any pulse appearing at the anode. The negative pulse at V9 anode is fed to the read-out gate valve V17.

The discriminator and gate consists of the valves V1 to V7. The circuit is similar to that described by Lewis and Wells[1]). Provision is made for the input to be terminated with 100 Ω by the switch S1. The bias on the discriminator is adjustable by the potentiometer RV2. In the quiescent condition, the grid of the triode V6A is held at earth potential by the diode V4B and the resistor R23. The grid of the triode V6B is held negative, by resistors R29 and R30, so that V6A passes all the current flowing through R25. The cathode of V6 is a volt or two above earth potential and determines the grid potential of the triode V1B. The triode V1A is held cut off by the discriminator bias. The cathode current of V1 flows from V2, and V3 and V7 are cut off, the bias on V3 being more than twice that on V7. The valve V5 is also cut off, as its grid is held negative by the diode V4A and resistor R17.

When a positive input pulse that exceeds the discriminator bias is received, V1A will start to conduct. This causes the current in V1B to decrease and a positive pulse to be formed at its anode. This pulse is amplified by V5 and a negative pulse fed back to V1B grid through the cathode follower V6A. The action is cumulative and the circuit snaps over, all the current flowing in V1B being transferred to V1A. The grid of V6A is driven sufficiently negative for V6B to take all the cathode current. Since the grid potential of V6B is fixed, the negative voltage step fed to V1B grid is limited. When V6B conducts, a negative pulse about 0.1 μs long is developed across the shorted delay line at its anode. This pulse cuts off V2 and removes the current from V1 for the duration of the pulse. At the end of the delay line pulse, V2 again conducts and if the input pulse has ended the circuit returns to its quiescent condition. When V2 is cut off, the current will be switched to V7 or V3. If the gate pulse is not present, V7 has the smallest bias and takes the current, but when the negative gate pulse increases the bias on V7 the current is passed through V3 to the stepping circuit. A positive pulse is taken from V6A anode and fed out through the double cathode follower V8 to give an output pulse each time the discriminator fires.

The stepping circuit consists of V11 and V14 to V16. The step waveform is formed by feeding the pulse of current from the discriminator into the capacity from V16 grid to earth. Initially, the grid of V14 is held at 60 V and its cathode is slightly more positive. The grid of V16 is held at about 60 V by the diode V11. When a gate

[1]) I. A. D. Lewis and F. H. Wells. Millimicrosecond Pulse Techniques (Pergamon Press, 1954) p. 236.

input pulse arrives, the reset pulse generator is triggered and feeds a negative pulse to V14 grid that reduces its potential to zero. Thus the diodes V11 and V15B are cut off and the voltage at V16 grid is no longer held, but because of the high impedance at this point the voltage will be almost constant for a time longer than 110 μs. Initially, the diode V15A is held cut off, as its anode is connected to the grid of the cathode follower V16 and its cathode to V16 cathode through the diode D2. The current pulse from V3 in the discriminator causes V15A to conduct and feed the current into the capacity between V16 grid and earth. At the end of the current pulse, the voltages at V16 grid and V15A cathode remain steady at a value lower than their initial value. Of the current from the discriminator, a small amount flows through R39 to replace the current originally flowing through D2, and the rest is used to charge the capacity between V16 grid and earth and gives an almost equal voltage step at V16 grid for each input pulse. At the end of the reset pulse, V14 grid is returned to 60 V, its cathode follows and V15B conducts. This quickly raises the potential of V16 grid until it is caught at its initial value by V11. The amplitude of the steps can be adjusted by the variable capacitor C41. The output from the step circuit is taken from V16 cathode to the read-out gate V17.

When the step waveform is fed to V17A grid, it will have little effect on V17 cathode potential, because of the clamping action of the cathode follower V17B. When the negative read-out pulse arrives at V17B grid, the potential of V17 cathode will fall by an amount equal to the sum of the standing bias on V17A and the value of the step waveform applied to the grid of V17A. As the read-out pulse occurs after the gate has closed, the step waveform will be at its final value. A standing bias is applied to V17A so that an output pulse will appear at V17 cathode, even if no pulses have been counted during the gate period. The negative output from V17 cathode is inverted by the anode follower V18 and fed to the kicksorter.

4. Results

The unit was tested with a multiple pulse generator and the amplitude of the output pulse for various numbers of input pulses was as follows.

No. of pulses	0	1	2	3	4	5	6	7	8	9	10
Output (V)	4	6	8.2	10	12	13.6	15.3	17.3	19	21	23

The unit was also tested with a double pulse generator[2]) type 1147 using two 50 mμs input pulses and varying the separation between them. The variation of output pulse height with input pulse separation is shown in fig. 3. When the separation is less than 150 mμs, the two pulses are recorded as one and when the separation is greater than 275 mμs, the step has reached its full value. With separations between these limits, the output varies between that for one pulse and that for two. The dead time with respect to gate input pulses is 120 μs.

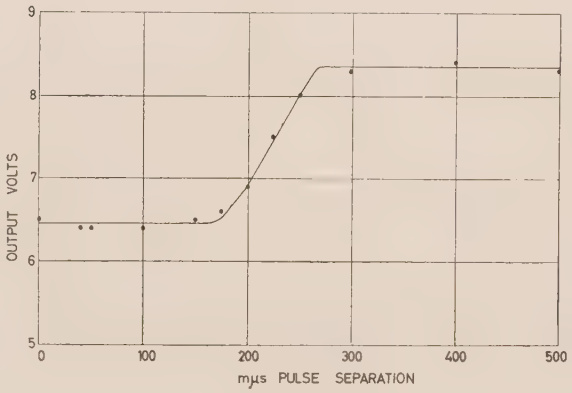

Fig. 3.
Variation of output with separation of two input pulses.

[2]) Pulse Generator Type 1147, Instruction Manual (Specifications and Manuals Section, AERE, Harwell).

5. Conclusions

This circuit provides a satisfactory means of counting the number of pulses in a burst. It incorporates a suitable discriminator for the input pulses and has a time resolution of about 0.25 microseconds between consecutive pulses. The count is started by a gate-opening pulse in another channel, and a veto pulse may be applied to a third channel, if desired, to inhibit any output from the circuit for the vetoed events. Up to ten pulses may be counted in each burst. In conjunction with a suitable kicksorter, the unit may be used to record the distribution of the numbers of pulses in the bursts.

Acknowledgement

The author's thanks are due to the Director of the Atomic Weapons Research Establishment, Aldermaston, for permission to publish this paper. He wishes to acknowledge the assistance of Mr. T. Ring, who built the prototype and assisted in testing it, and the encouragement of Dr. C. H. Vincent, who was in charge of this work.

NUCLEAR INSTRUMENTS AND METHODS 7 (1960) 325–337; NORTH-HOLLAND PUBLISHING CO.

A HIGHLY ACCURATE CONTINUOUSLY VARIABLE FREQUENCY CONTROL SYSTEM

C. H. VINCENT

United Kingdom Atomic Energy Authority, A.W.R.E., *Aldermaston, Berks.*

Received 30 December 1959

A method is described for controlling the frequency of an oscillator with crystal accuracy and at the same time permitting effectively continuous adjustment of the frequency required. A selected multiple of the oscillator period is obtained by counting the oscillator cycles with a fast binary scaler followed by a special scaler with a widely variable scaling factor. The resulting time interval is accurately compared, in a suitable circuit, with a fixed time interval, derived from a crystal oscillator. A signal is thus obtained which drives a differential motor system in the appropriate direction to correct the adjustment of the oscillator tuning condenser.

1. Introduction

In general, electronic oscillators (of frequencies up to 60 Mc/s or so) may be divided into two classes, those which are crystal-controlled and those which are capable of being set at any frequency over a wide band by a tuned circuit or otherwise. The crystal-controlled oscillators cannot normally be set over a wide range of frequencies, while the other types lack the accuracy of frequency control possessed by the crystal oscillators. The development of an oscillator with its frequency both continuously variable over a wide range and capable of being held with crystal accuracy is a problem of considerable interest. This is particularly so in view of its possible application to the accurate automatic control of magnetic fields by proton resonance and thereby (by standard methods) to the control of particle accelerator energies.

In this Establishment, the energy of the emergent beam of each Van de Graaff accelerator in use is continuously monitored and automatically corrected by reference to the degree of bending of the beam in the field of an electromagnet. The current of each such electromagnet is held constant to about 1 part in 10^5 by a suitable current stabilizer, and the value of the field is checked at intervals to about the same accuracy by an operator using a proton resonance magnetometer. Equipment has already been developed here which enables the field to be controlled automatically by the proton resonance signal and the last step required for completely automatic control of the

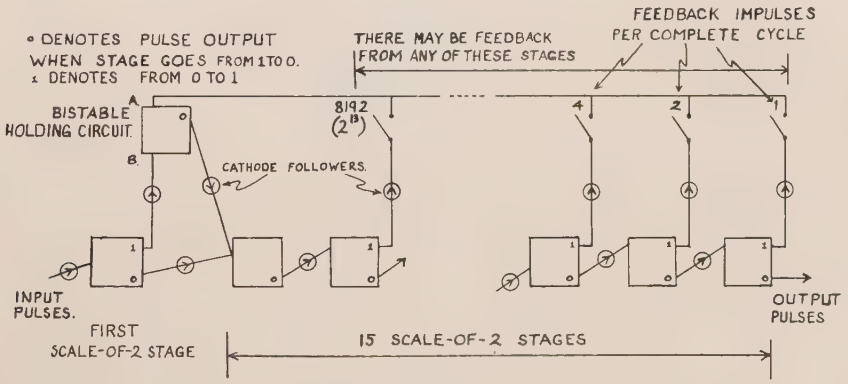

Fig. 1. Variable scaler block diagram.

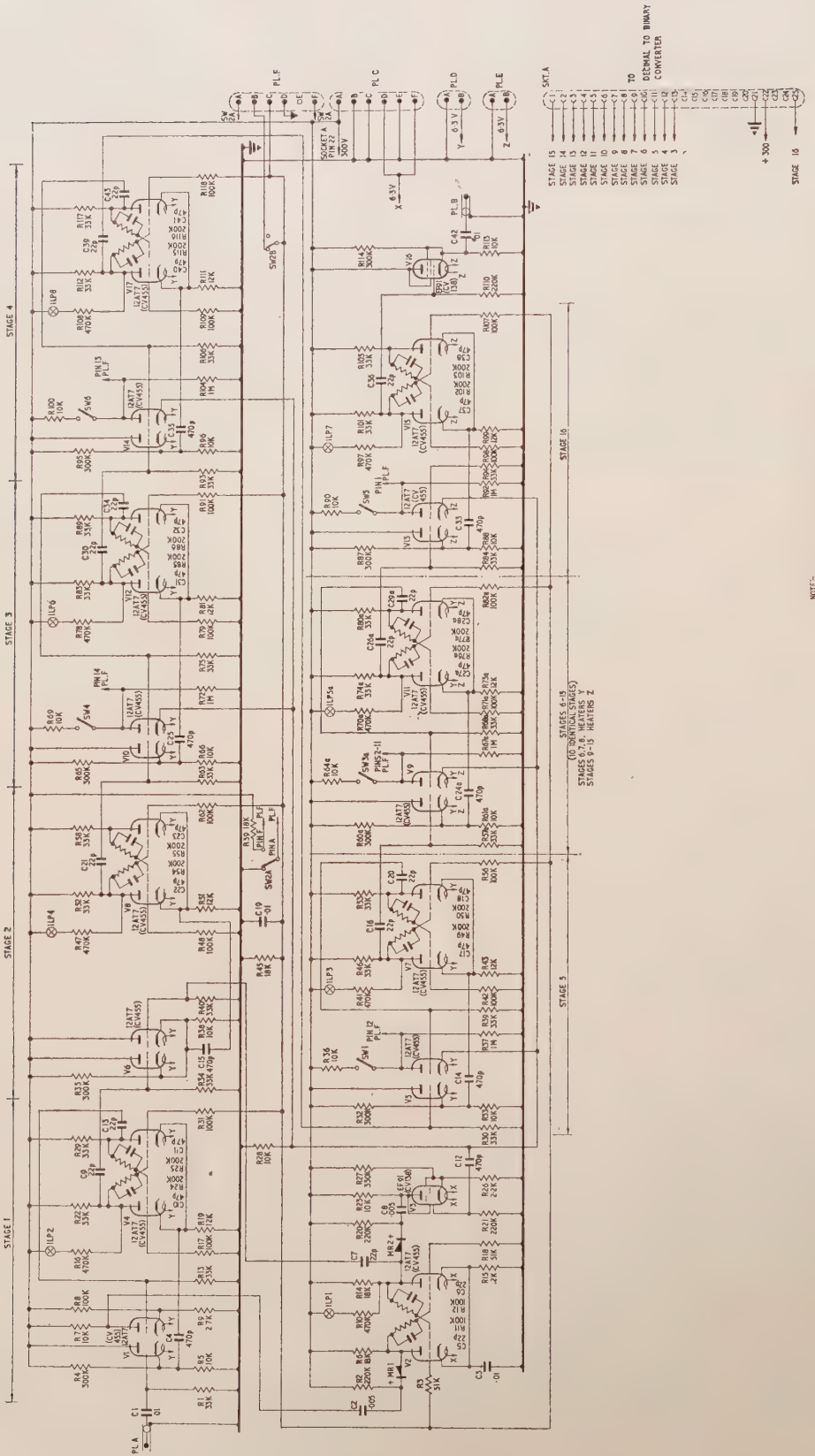

Fig. 2. Circuit diagram of the variable scaler.

magnet field and the accelerator energy is an accurate control of the proton resonance oscillator frequency. Direct control of the magnet field in this way would give reliable and accurately reproducible setting of the particle energy required, whereas a current setting does not provide this, owing to hysteresis and other effects in the magnet. This paper describes a suitable system of oscillator frequency control which is being tried out experimentally.

2. Principle of Control

This system depends on a comparison between two nearly equal time intervals. One interval is a binary multiple of the period of a crystal-controlled oscillator (at a frequency of 16 kc/s) and is 0.512 s. The other interval is a multiple of the period of the oscillator of which the frequency is to be controlled. This multiple is obtained by means of a sequence of binary scalers and also a special scaler which may count any number $2n$, where n is any number from 16 385 to 32 768, inclusive. In this way, the controlled frequency may be set to any value required, over a wide range. The controlled frequency may be 16.385 to 32.768 Mc/s or may be set to a binary multiple or submultiple of this by changing the number of binary stages used in the sequence. It follows that the controlled frequency can always be set to within about 3 parts in 10^5 of any desired value. However, if this setting is not fine enough, a finer control may be obtained by adjustment of the crystal frequency by means of a trimming condenser in series with the crystal. If the two frequencies are not in the set ratio, the two time intervals are not equal and a signal is obtained which turns the output shaft of a differential motor system in the appropriate direction to correct the error by readjusting the tuning condenser of the controlled oscillator.

3. Variable Scaler

Since the variable scaler is a vital component of this system, it will be described briefly here. The first account of it was published by the author in 1947[1]). A block diagram showing the principle of its action is given in fig. 1. Basically, the scaler is a binary one of 16 stages. Feedback pulses which effectively add to the total count of input pulses are obtainable at will from all the stages except the first two. These pulses are generated when the stage concerned changes from the 0 setting to the 1 setting. (Normal carry pulses are, of course, generated at the change from 1 to 0.) It is apparent that the last stage generates 1 such pulse per complete cycle, and the successively preceding stages 2, 4, 8, – – – –, 8192 (2^{13}). These pulses are not fed directly into the input but are used to trigger a bistable circuit into its alternative state. It is triggered back from this state by the next pulse from the first stage, as the latter passes from 0 to 1 . As the bistable circuit returns, it passes a pulse into the second stage, thus adding 2 to the total count recorded. This method has the outstanding advantage that it enables the feedback to be introduced while still ensuring that no circuit in the scaler receives more than one input pulse for each input pulse to the first stage. This avoids undesirable interactions, provided, of course, that the input pulses are not at an excessively high frequency which does not permit complete recovery of the circuit before the next input pulse. Fig. 2 shows the circuit used.

A switch is provided which controls the passing or inhibition of the feedback pulses from each stage. It is evident that by suitable adjustment of these switches the total number of feedback pulses per cycle may be varied from 0 to $2^{14} - 1$. Since each of these counts as 2 input pulses, and the total cycle of the scaler is 2×2^{15}, it follows that the overall cycle of the scaler may be varied from $2 \times (2^{15})$ input pulses down to $2 \times (2^{14} + 1)$ input pulses, the figure in the brackets being adjustable in steps of unity. The next step down, corresponding to $2 \times (2^{14})$, is obtained, of course, by removing one of the binary scaler stages which are in sequence with the variable scaler, so that in this way an almost continuous coverage is

[1]) C. H. Vincent, Proc. Roy. Soc. N. Z. Science Congress 1947, p. 50.

obtained. The fixed factor of 2 is allowed for, without any inconvenience, by using one less external binary stage than would be required without it. A small relay-operated decimal to binary convertor has been designed which will enable the required frequency to be set up on decade dials (see fig. 3). Once the correct setting has been obtained, it may be held by latching the output relays or by setting the hand switches on the variable scaler, enabling the convertor to be switched off, if the same frequency is to be held for some time.

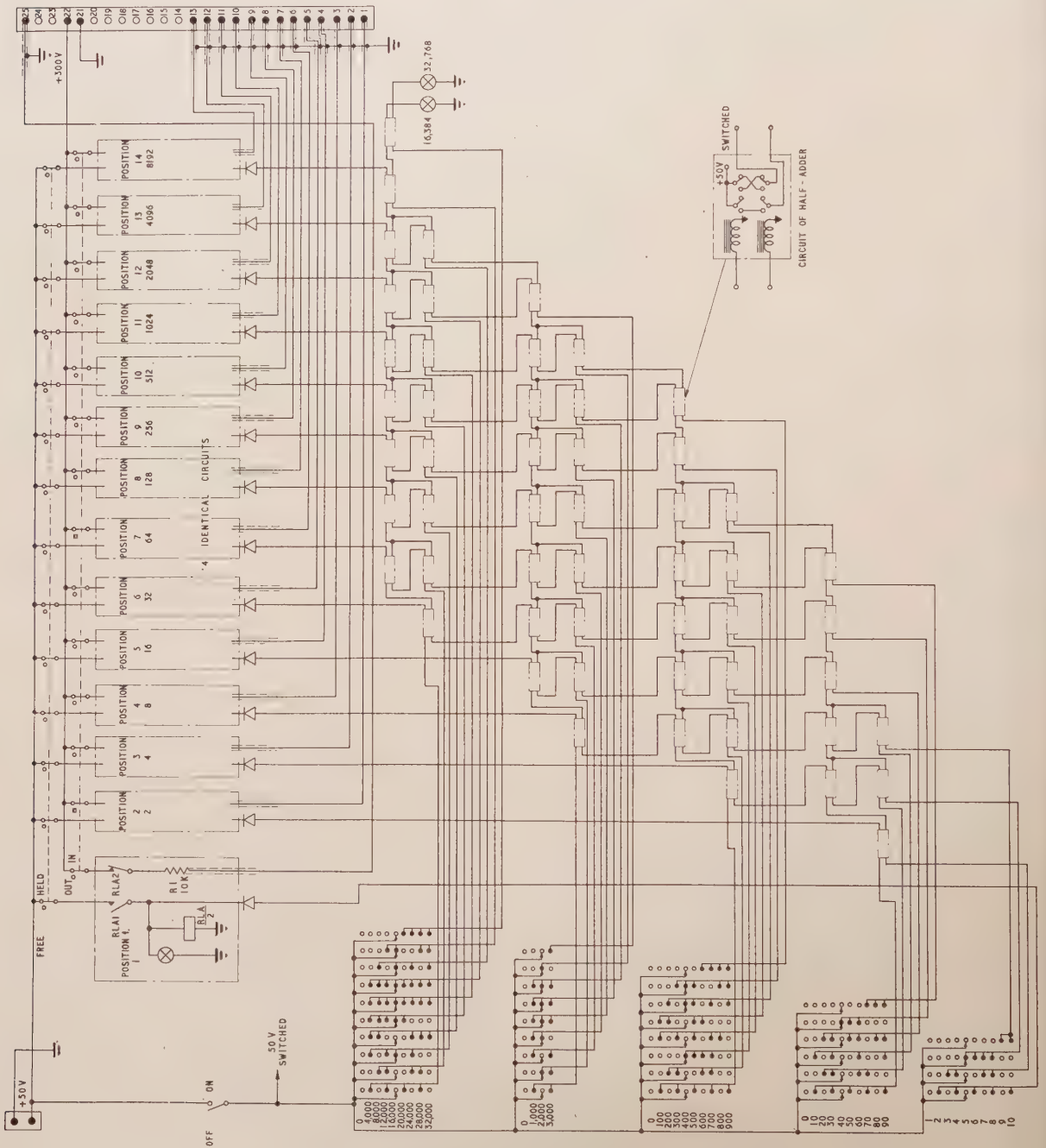

Fig. 3. Circuit diagram of the decimal to binary convertor.

The maximum input pulse rate at which all input pulses are dependably counted by the variable scaler depends to some extent on the feedback switch settings. The present scaler is capable of working, with any switch setting, at any input frequency up to 150 kc/s or more.

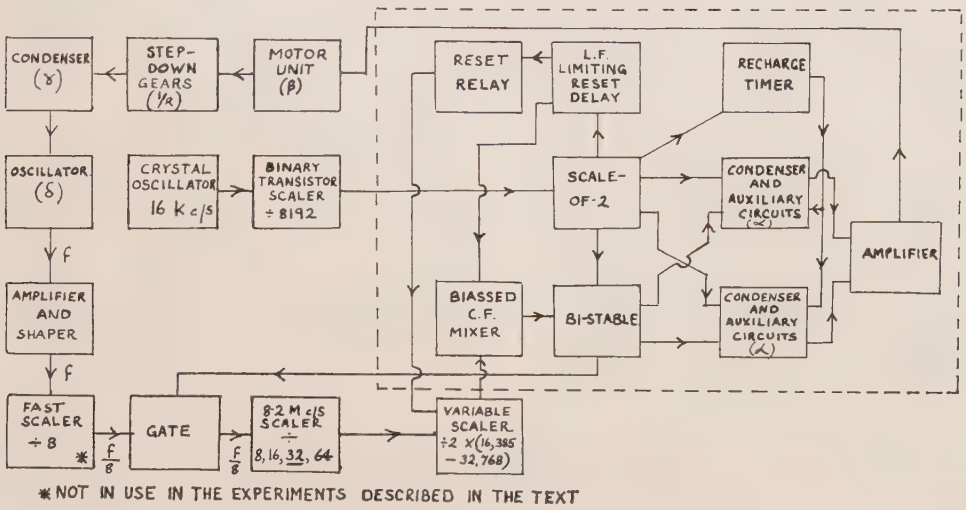

Fig. 4. General schematic of the frequency control system.

128 kc/s is the maximum frequency at which the variable scaler is required to work under any conditions in the present frequency control equipment. The arrangement of switching the anode supply to the cathode follower in each feedback path, as shown in the circuit diagram, is more convenient and reliable than direct interruption of the paths. The resistors shown in the anode circuits are placed close to their respective switches and are to suppress switching transients, which would otherwise cause temporary but inconvenient changes in the count registered, whenever a switch was operated.

4. Method Used

The time intervals referred to above are marked by changes of state in two bistable circuits. One of these (see fig. 4) is a normal scaling circuit and it is operated by input pulses with a period of 0.512 s which are derived from the 16 kc/s crystal oscillator followed by 13 binary scaling stages. We shall refer to this as "the scale-of-2" to distinghuish it from the other bistable circuit. The comparison of the frequencies is repeated every 1.024 s, this period being controlled by the cycle of the scale-of-2. The two states of each bistable circuit may be distinguished by means of a neon lamp connected to it. On the scale-of-2, this lamp is off for the first half of the cycle and on for the second, as the start of the cycle is defined, for convenience of reference (see fig. 5b). The other bistable circuit is normally in the off state at the end of the previous cycle. When the scale-of-2 circuit goes off at the beginning of each cycle, it produces a pulse which turns the second bistable circuit on. As it goes on, this circuit opens a gate circuit in the sequence of scalers from the controlled oscillator and permits pulses to pass through to the variable scaler (see figs. 5, c and d). When the latter returns to zero at the count which has been preset on it, it produces a pulse which turns the bistable circuit off and closes the gate again. The variable scaler starts counting from zero, as it is left at zero by the previous operation (due to the rapidity with which the gate closes). Since the scale-of-2 circuit comes on at the midpoint of the cycle, it follows that the scale-of-2 circuit and the bistable circuit may both be on together or off together for a short time in the middle of each cycle, according as the

variable scaler period is greater than or less than the crystal binary scaler period (see figs. 5; a, c, e and f).

During the time that the two circuits are both on together, if that is the case, the condenser C'_s is being discharged to earth through a series resistor and switching tube (see fig. 6). This switching tube is controlled by two control tubes, one from each of the bistable circuits,

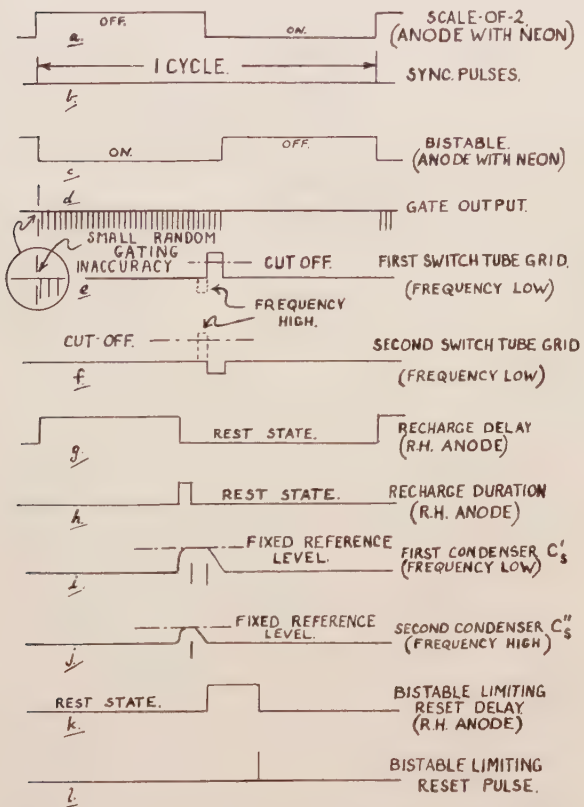

Fig. 5. Voltage waveforms of frequency control system. The smallest time intervals in this figure have been shown greatly exaggerated in order to make them visible.

with a common anode load. The condenser C'_s is charged to a potential of about 75 V by a recharging circuit, which comes into operation just before the discharge commences. The recharging is timed by a delay flip-flop from the pulse from the scale-of-2 at the beginning of the cycle .The voltage left on the condenser after the discharge is stored there for the rest of the cycle and applied to a differential direct-current amplifier which controls the relative speed of the motors. If the two circuits are off together, on the other hand, another similar condenser C''_s is discharged instead, this being connected to the opposite grid of the amplifier input. In either case, the storage condenser that is not affected retains its recharge voltage, while the other stores a lower voltage, the fall in voltage being proportional to the discharge time, unless the condenser voltage is below a certain value. (It eventually limits, towards earth potential.) The motor output turns in one direction or the other to correspond to the difference of the condenser voltages.

5. Motor Unit and Amplifier

The two motors used are small direct-current motors of the split field type. The two field coils of each motor carry currents to give fields of the same polarity, so that their effects always add. One field coil of each motor carries a fixed current of about 15 mA. This current ensures that the field never falls into the stalling region (see fig. 7a) but remains in the normal region, where the motor speed is approximately inversely proportional to the field strength. The second coil of each motor carries a current which is controlled by the differential amplifier. This is a long-tailed pair, and the cathode current is the total current of these two field coils (about 30 mA). When the signal grid voltages from the two storage condensers are equal, neither condenser having been discharged at all, the cathode current is equally divided between the two anodes and therefore between the two motors. A zero adjustment is provided here to compensate for any small differences between nominally indentical components. As one grid voltage falls, more current is transferred to the opposite motor.

The two motors are lightly loaded by step-down gear trains (200 to 1) and therefore run at close to their zero torque speeds. The two outputs are put into a differential, which gives an output speed for small errors proportional to the frequency error and of corresponding direction. If the error is increased, the variable field current of one motor is finally completely

cut off and the motor runs at a maximum speed on its fixed current field coil only, while the other runs at a minimum speed determined by the total cathode current plus the fixed current. It follows that when the difference of frequencies is followed by further step-down gearing, the ratio of which may be varied to suit conditions, but may be of the order of 1000 to 1 or higher. The considerations determining the choice of this ratio are discussed later.

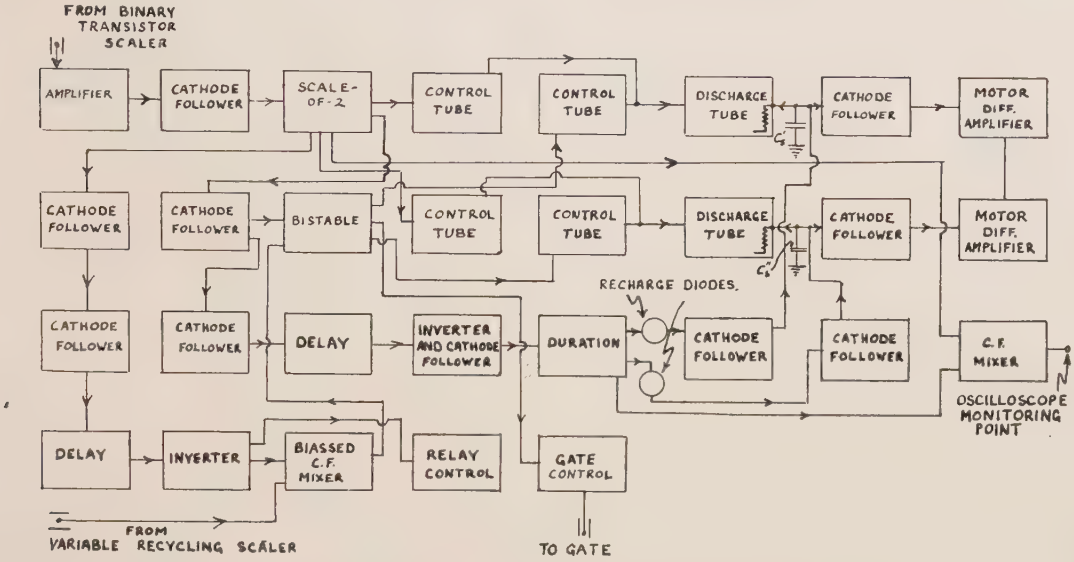

Fig. 6. Valve by valve block diagram of frequency control system.

is so great as to be outside the region of proportional control, the motors simply continue to turn the output shaft at a fixed limiting speed

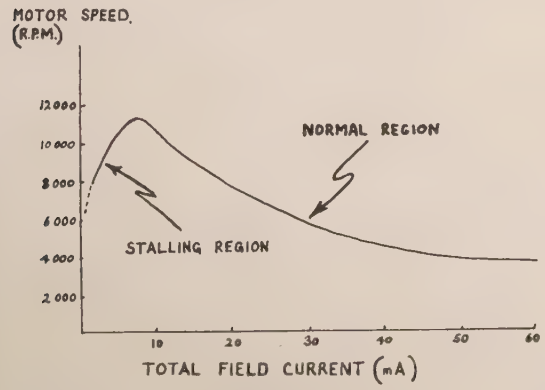

Fig. 7a. Motor speed characteristic at zero torque of frequency control system.

6. General Features of Operation

If the controlled oscillator frequency is less than half the frequency set for control, the

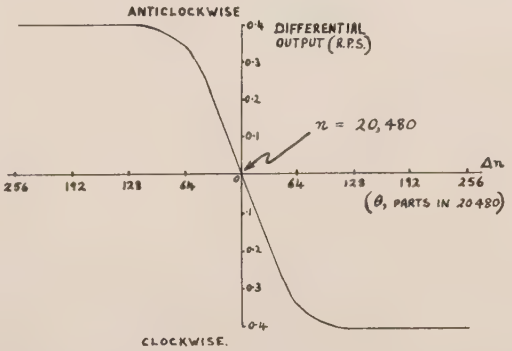

Flg. 7b. Overall control system characteristic of frequency control system. (Sensitivity reduced by increase of C'_s and C''_s to 0.5 μF.).

in the appropriate direction (see fig. 7b). This is a very necessary and desirable condition to ensure that a satisfactory correction or indication is obtained when the frequency adjustment is a long way out. The output of the differential variable cycle scaler will not reach the end of its count before the end of the scale-of-2 cycle at all. As this could lead to confusing results, a limiting pulse is put into the bistable circuit from a delay circuit triggered from the scale-of-2

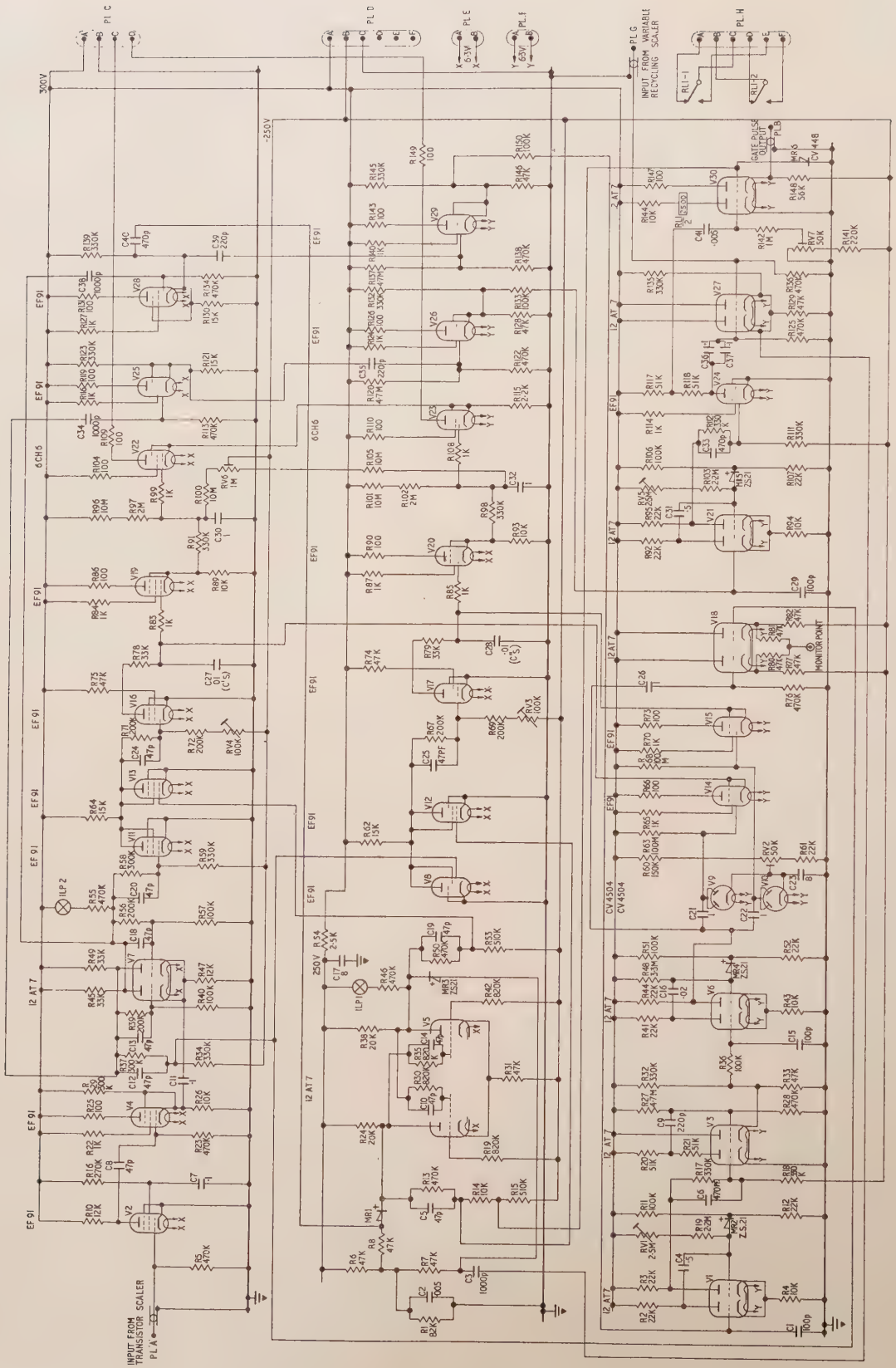

Fig. 8. Circuit diagram of the frequency control unit.

which ensures that it is turned off at a set time during the second half-cycle, if not before (see fig. 5*l*). A relay circuit which resets the variable scaler to zero, in this case, is also provided. (This relay circuit is superfluous, under normal circumstances, as the variable scaler then stops at zero after counting, as previously mentioned.) This limiting pulse and the reset action ensure that the output signal should always have the correct sign, however great the initial error may be.

The condenser used for tuning in the experimental oscillator is one with semi-circular rotor plates, giving a linear increase of capacity over one half-turn and a similar decrease over the other. If the frequency set is within its range, the servo will find the correct point of adjustment and come to rest. Over one half of the condenser rotation, the direction of the capacity change with rotation is obviously wrong, but this does not matter, as the servo automatically turns the condenser into the correct region. There is a point of unstable equilibrium where the correct frequency is obtained in the wrong region. The correct frequency range of the oscillator must be selected by the operator. If the frequency set is outside the range of the tuning condenser, the servo just continues to turn it in the appropriate direction.

The output of the motor unit may show a slight oscillation or intermittency due to the recharging pulse reaching the motors through the amplifier. Integrating circuits are placed between the storage condenser cathode followers and the amplifier, to reduce this effect. The width of the pulse between the recharge and the discharge should be kept as small as practicable, to reduce the effect also (see figs. 5, i and j). A special monitoring circuit is provided to facilitate this adjustment (see fig. 6). The recharge duration waveform is added to the scale-of-2 waveform for display on an oscilloscope, to permit a precise relative timing adjustment. A complete circuit diagram of the frequency control unit is given in fig. 8.

7. Sensitivity Adjustment

The sensitivity of the circuit to small time differences may be adjusted conveniently, in accordance with the accuracy of frequency control called for, either by changing the equal storage capacities C'_s and C''_s or by changing the step-down gear ratio following the differential. A decrease in the former increases the rate of fall of voltage when either switching tube conducts, and has the advantage that it increases the sensitivity of the circuit and at the same time decreases the relative importance of any effects due to drift in the direct-current amplifier or the motors. A decrease of the step-down gear ratio, on the other hand, does not decrease the relative importance of such effects, but has the advantage that it increases the rate of rotation of the final output shaft when the limiting motor speeds have been reached, as well as increasing the sensitivity. It therefore increases the rate of change of frequency under limiting conditions correspondingly.

The overall sensitivity of the circuit must not be so great as to give an excessive over-correction which would lead to hunting. (This question is discussed in more detail below.) It follows that a compromise must be reached between the requirement of accurate response to small errors, achieved by the use of low storage condenser values, and the requirement of sufficiently rapid correction of errors large enough to involve the limiting motor speed, achieved by keeping down the final stepdown gear ratio. The main emphasis in the present work is on the former, as the servo is normally only required to compensate for very slow drifts occurring over hours. (An approximate manual adjustment should be made where a large frequency change is required quickly.)

8. Inherent Accuracy Limitation in Gating

Since there is no direct adjustment of the phase of the controlled oscillator by reference to the crystal oscillator, it follows that the latter may open the gate at any phase with respect to the sequence of pulses going through

(see fig. 5d). The closing of the gate, on the other hand, is timed by reference to one of these pulses, the one which completes the cycle of the variable scaler and any other scalers between it and the gate. Since the time interval measured is that between the opening and closing

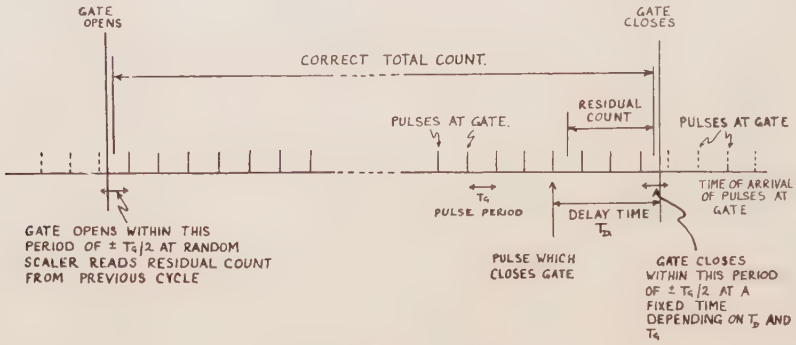
GATE OPENS
GATE CLOSES
CORRECT TOTAL COUNT.
RESIDUAL COUNT
PULSES AT GATE.
PULSES AT GATE
TIME OF ARRIVAL OF PULSES AT GATE
T_G PULSE PERIOD
DELAY TIME T_D
GATE OPENS WITHIN THIS PERIOD OF $\pm T_G/2$ AT RANDOM SCALER READS RESIDUAL COUNT FROM PREVIOUS CYCLE
PULSE WHICH CLOSES GATE
GATE CLOSES WITHIN THIS PERIOD OF $\pm T_G/2$ AT A FIXED TIME DEPENDING ON T_D AND T_G

Fig. 9. Gate timing diagram.

of the gate, it follows that there is an uncertainty in the time measurement of $\pm \frac{1}{2} T_G$ in 0.512 s, where T_G is the period of the pulses passing through the gate. This corresponds to an error of $\pm T_G/1.0124$. Hence, it is desirable that the gating should be carried out at a sufficiently high frequency to ensure that this source of error is kept to negligible proportions. However, even in the worst possible case, when the gate immediately precedes the variable scaler, and the latter is set for the minimum possible input frequency for the system of 64 004 c/s, this error amounts to only $\pm$ 16 part in 10^6.

9. Effects of Delay in the Operation of the Gate

It has already been mentioned that the variable scaler is always found to be at zero after the gate has been closed, under normal conditions of operation. It is the output pulse at the count of zero which closes the gate, and the operation of the circuits involved is sufficiently rapid to ensure that the gate is closed in time to prevent another input pulse reaching the variable scaler. The same is not true, however, of the faster scaler, counting at up to 8 Mc/s or so, which precedes the variable scaler and follows the gate in the present experimental system. This scaler shows a small count after the gate has closed. The existence of this count is evidence of a delay in the loop formed by the gate, 8 Mc/s scaler, variable scaler, and bistable circuit (see fig. 4). Consideration of the action of the loop shows that a delay at any point of it may cause such a count. The significance of this delay with respect to the accuracy of timing depends on its exact nature and origin.

Consider, for example, an absolutely fixed delay. If such a delay is inserted at any point in the loop, the scaler following the gate will show the same fixed count, corresponding to the delay, when the gate has closed. However, if the operation of the circuit is allowed to continue, the time that the bistable remains on will be correct for all operations after the first. This is because the scalers count precisely the set number of pulses (from the residual count number, through zero and back to the residual count number again) and the gate is therefore open for precisely the correct time (apart from the error of $\pm \frac{1}{2} T_G$ discussed above and a similar error, also less than $\pm \frac{1}{2} T_G$, but constant for given T_G, which arises from the fact that the delay may not be an exact integral multiple of T_G). (See fig. 9.) Since the gate operation bears a constant time relationship to the operation of the bistable circuit, the latter must be on for the correct interval also. However, if there were any difference between the delays in the opening and closing of the gate by the bistable circuit, this would lead to a

small zero error at this point (causing a small fixed percentage error in the frequency obtained). For this reason, in the present equipment, precautions are taken to ensure that the opening and closing of the gate are as precisely simultaneous as possible with the changes of state of the bistable circuit, thus minimizing any such error. The reading showing on the 8 Mc/s scaler, after the gate has closed during each operation, is a useful monitoring indication of the functioning of the system.

10. Theoretical Aspects of Stability against Hunting

The most important single factor here is the correction factor $C = \Delta\theta/\theta$, where $\Delta\theta$ is the correction which the circuit makes over its period of 1.024 s, when it has measured an error θ. We define θ as $(f - f_0)/f_0$, where f is the actual frequency and f_0 is the required frequency. C is a numerical measure of the sensitivity previously discussed. Values of C of about 0.1 to 0.44 appear to be suitable. The highest of these values would be necessary to secure maximum accuracy, if the controlled oscillator were liable to relatively rapid changes, but this is not so in the present application. It is obvious that C must not be too large, as this would cause a greater error of opposite sign after each cycle, leading to hunting.

The value of C may be determined by measurements and calculations made with the servo loop open. It is given by

$$C = \frac{\Delta\theta}{\theta} = \frac{T_m T_c \alpha\beta\gamma\delta}{R}$$

where

T_m = Measuring time (0.512 s)

α = Rate of fall of condenser voltage (adjusted by capacities)

β = Rate of change of differential output speed with condenser voltage

T_c = Time shaft turns per cycle (1.024 s)

γ = Capacity change per revolution. (This is twice the total capacity, for a semicircular rotor condenser.)

δ = Fractional frequency change ($\Delta\theta$) per unit capacity change.

R = Ratio of final step-down gearing from differential output.

Since the frequency is measured over a time interval of half a cycle and since the frequency may be changing linearly with time over this interval, due to a previous error signal, the frequency that is effectively measured is that at the mid-point of the interval, which is quarter way through the total cycle. The correction is then made over an interval of one complete period extending from the middle of that cycle to the middle of the next. The delay between the time of measurement and the commencement of the correction introduces a minor complication in that the successive steps towards the correct adjustment, when an error has been introduced, obey a second order difference equation rather than a first order one.

If θ_n is the value of θ at the nth measuring time (quarter way through the cycle), then we have

$$\theta_{n+1} - \theta_n = -\Delta\theta_n$$
$$= -\tfrac{3}{4} C\,\theta_n - \tfrac{1}{4} C\,\theta_{n-1}\,.$$

This is evident, because the motor speed is controlled by θ_{n-1} for $\frac{1}{4}$ of the period concerned and by θ_n for the remaining $\frac{3}{4}$ of the period. Rearranging this into its normal form, we have

$$\theta_{n+1} - (1 - \tfrac{3}{4} C)\,\theta_n + \tfrac{1}{4} C\,\theta_{n-1} = 0\,.$$

Such an equation may be solved by putting $\theta_n = AX^n$, where A is a constant, when it reduces to

$$X^2 - (1 - \tfrac{3}{4} C)\,X + \tfrac{1}{4} C = 0$$

giving

$$X = \frac{(1 - \tfrac{3}{4} C) \pm \sqrt{(1 - \tfrac{3}{4} C)^2 - C}}{2}\,.$$

Provided that the discriminant is positive, this means that the answer consists of 2 terms, each an exponential function of n, instead of one as for a simple first-order difference equation (which would be obtained if the correction followed the measurement immediately). For small values of C, the solutions for X approximate to $1 - C$ and $\frac{1}{4} C$ respectively. The second term then represents a very rapid decay of the error and may be neglected. The first term is the same as for a simple correction

system without a delay, having a first-order difference equation, for the same value of C. Putting $C = 0.4$, for example, gives $X = 0.5$ $(1 - C = 0.6)$ or 0.2. We may therefore conclude that for values of C of 0.4 or less the behaviour of the system is little affected by the quarter cycle of delay between the measurement and the commencement of the new correction.

For values of C above 0.444 ($X = 0.333$), the solutions for X become complex and the two terms contain periodic factors. The decay factor becomes the same for both terms, in this case, being the common modulus of the complex solutions, which is $\sqrt{\frac{1}{4}C}$. This factor therefore increases as C increases, and it is not desirable to increase C further, although a condition of actual instability would not be reached until $C = 4$, according to this result. The occurrence of hunting with values of C above 4 has been verified experimentally. The amplitude of the oscillations was small, presumably owing to the limitation on the differential output speed. It would therefore appear that the optimum value of C is 0.44, although lower values are acceptable provided that it is not necessary for the equipment to compensate for the fastest possible sources of frequency drift. At the optimum condition stated, the error is reduced by a factor of 0.33 per cycle (provided, of course, that it is not so great as to involve the limiting motor output speed). Since the system may be operated with a value of C at or below the optimum of 0.44, and since instability does not occur unless $C > 4$, the equipment can always be designed to have a good safety factor against instability.

11. Typical Experimental Conditions and Results

The following table summarizes the conditions used and the results obtained in a typical experiment. The controlled frequency was monitored by beating the output with that from a crystal-controlled oscillator at nearly the same frequency. The beat frequency was measured by means of a ratemeter and recorded continuously by means of a recording milliammeter

Reference crystal frequency = 16.000 00 kc/s

Crystal scaler dividing ratio = 2^{13}

Period of crystal scaler output $T_m = 0.512$ s

Period of complete cycle $T_c = 1.024$ s

Storage capacity value (nominal) = 0.01 μF

Initial current switched on = 0.9 mA

Rate of voltage fall $\alpha = 9 \times 10^4$ V/s

Transconductance of amplifier tubes $g_m = 12$ mA/V

Rate of change of difference of currents $(2 \times \frac{1}{2} g_m) = 12$ mA/V

Motor armature supply voltage = 50 V

Series resistance used in motor armature circuit = 68 Ω

Total field current at balance = (15 + 15) mA = 30 mA

Rate of change of output speed with current = 2.0 (R/s)/mA

Step-down gear ratio to differential output = 200

Rate of change of output speed with condenser voltage $\beta = (12 \times 2.0/200)$ $(R/s)/V$ $= 0.12$ $(R/s)/V$

Differential output speed per fractional frequency error $(T_m \alpha \beta)$ at an increased storage capacity $(C_s = 0.5) = 0.512 \times 1800 \times 0.12$ $R/s = 111$ R/s

Measured value of this quantity (at $C_s = 0.5$) = 122 R/s

Step-down gear ratio from the differential output $R = 625$

Semicircular tuning condenser capacity = 12.5 pF

Rate of change of capacity with rotation $\gamma = 25$ pF/R

Rate of oscillator fractional frequency change $\delta = 0.0016$ $(pF)^{-1}$

Correction factor $C = 0.512 \times 1.024 \times 9 \times 10^4 \times 0.12 \times 25 \times 0.0016/625 = 0.36$

Total value of variable scaler feed-back switches in use = 8192 + 4096 + 256 + 128 + 64 + 4 = 12 756

Number of external scales-of-2 used with variable scaler = 6

Frequency set = $16 \times 2^6 \times 2 \times (32\,768 - 12\,756)/2^{13} = 20\,012/4$ kc/s $= 5003$ kc/s

Crystal-controlled comparison frequency = 4999.950 kc/s

Expected beat frequency (controlled oscillator high) = 3.050 kc/s

The measured beat frequency showed small fluctuations, departing from the correct value for the oscillator frequency set by not more than $\pm$ 50 c/s.

Fractional discrepancy. Within $\pm$ 1 in 10^5. Under the conditions of this experiment, the smallest steps by which the frequency could be adjusted were 250 c/s or 1 part in 20 000 and the successive frequency values thus obtained were clearly distinguishable from each other with the degree of control available. Both the reference crystal and the comparison crystal need to be used in thermostatically controlled ovens to avoid small drifts in frequency due to ambient temperature changes.

12. Application to the Proton Resonance Magnetometer

The present experimental system has been tried out at frequencies in the region of 4 to 8 Mc/s, using an initial binary scaler capable of counting at 8 Mc/s or more. Modern developments in fast binary scalers[2]) permit counting at rates up to or greater than the 60 Mc/s or so which is the maximum frequency likely to be required for a proton resonance magnetometer used on a normal iron-cored electromagnet. (The conversion factor for proton resonance is approximately 235 Gauss per Mc/s.) The present system can therefore be extended to cover these frequencies by the addition of the appropriate number of such fast binary scaling stages. (An alternative method, but a less convenient one, requiring tuning controls, would be to make use of beats with harmonics of a crystal-controlled frequency to reduce the frequency range required.) The oscillator in the present standard proton resonance equipment used in this Establishment is remotely controlled by the operator by means of a synchro and this system is quite suitable for automatic control, provided that sufficient of the step-down gearing is incorporated at the oscillator end, in order to ensure that the effects of backlash in the synchro transmission system are kept to negligible proportions. The frequency control equipment could also be used to stabilize an oscillator by means of a reactance tube. This method would also be suitable for remote control of the oscillator. The present system may be used without any modification, other than the addition or removal of binary stages, to control any oscillator frequency from 64.004 kc/s up to the highest frequencies at which a binary scaler may be operated.

[2]) G. W. Hutchinson, H. W. Wells and D. H. White, Nuclear Instruments and Methods **4** (1959) 228–233.

Acknowledgements

The author wishes to acknowledge the valuable assistance of J. F. Marriott and D. Buckley, apprentices, of this establishment, who have carried out a large part of the constructional and experimental work described and have prepared most of the diagrams for this paper.

NUCLEAR INSTRUMENTS AND METHODS 7 (1960) 338–349; NORTH-HOLLAND PUBLISHING CO.

LOW ENERGY PARTICLE ACCELERATORS FOR PRECISION NUCLEAR PHYSICS RESEARCH

FRED L. NIEMANN

High Voltage Engineering Corporation, Burlington, Mass.

Received 15 November 1959

The three types of particle accelerators presently available for precision research in the nuclear binding energy range are positive-ion linear accelerators, azimuthally-varying-field cyclotrons, and multi-stage Van de Graaff accelerators. The state of development of these accelerators is reviewed and their relative advantages and disadvantages are compared on the basis of performance capabilities, approximate costs and availability.

1. Introduction - Types of Accelerators

In the present state of particle accelerator technology there are three types of accelerators which may be considered for precision nuclear physics research with proton energies in the 10 to 20 MeV range and correspondingly higher total energies for heavier ions. In order of increasing versatility and flexibility, these are positive-ion linear accelerators (linacs), the azimuthally varying field (AVF) cyclotron (sometimes referred to as the "variable energy" cyclotron) and the Tandem Van de Graaff accelerator.

For work in this energy range perhaps only two of these types of accelerators need be considered in any detail. Because of limitations inherent in the nature of positive-ion linacs, it is unlikely that these machines would be proposed for diversified research in this energy range. However, some discussion of these accelerators and their capabilities will be included for completeness. The suggested use of a proton linac as an injector for a Tandem Van de Graaff will also be considered briefly.

Since there appears to be some uncertainty in regard to cyclotron terminology, particularly the term "variable energy", perhaps a short review of cyclotron types is warranted. In its original form with fixed frequency (FF) and uniform magnetic field, the cyclotron was limited in the maximum particle energies attainable by the relativistic increase of particle mass with energy. Since the angular frequency of the particle in orbit decreases as the particle mass increases, this frequency falls below that of the fixed frequency oscillator as the particle energy increases and the proper phase relations for acceleration cannot be maintained.

In the frequency modulated (FM) or synchrocyclotron this relativistic effect is compensated for by changing the oscillator frequency. This machine produces particles with much higher energies than those from FF cyclotrons, but are limited to pulsed operation at the modulation frequency since particles can be accelerated only during a portion of each FM cycle. They therefore produce considerably lower average currents than the FF machines.

Since the particle orbit radius in a cyclotron increases with particle energy, the relativistic effect can also be compensated for by a magnetic field which increases in intensity with radius. Unfortunately such a field has gradients which cause defocussing of the beam[1]). However, this defocussing effect can be counteracted by a magnetic field which varies periodically with azimuth angle about the center[2]). Machines utilizing these principles are known as fixed-frequency, azimuthally varying field (AVF)

[1]) H. A. Bethe and M. E. Rose, Phys. Rev. **52** (1937) 1254.

[2]) L. N. Thomas, Phys. Rev. **54** (1938) 580.

cyclotrons. Alternating gradient (AG) or "strong focussing" synchrotrons are based on essentially the same principle.

The particle energies produced by any of these three types of cyclotrons can be varied within limits by utilizing different magnetic field intensities and a variety of rf oscillator tuning schemes. Nearly all new cyclotrons now under construction or being planned are AVF machines and many of these are designed to provide for variation in particle energy over a considerable range[3]). Because of this there has been a tendency of late to refer to the AVF cyclotron as a "variable energy cyclotron". In fact, however, a number of standard cyclotrons have been built with special provision for particle energy variation and several AVF machines have been or are being built with no such special provisions[3]). Thus, an AVF cyclotron need not be a variable energy cyclotron and vice versa.

Since the AVF cyclotron has several advantages over other types that are particularly important at the lower energies considered here, further discussion will be limited to this type of cyclotron with provision for variation in particle energy.

The principle of energy doubling by charge exchange in an electrostatic accelerator, on which the Tandem Van de Graaff is based, was first proposed more than 20 years ago[4]) and demonstrated nearly 9 years ago[5]). It is only comparatively recently that the successful operation of such machines first in this country and later in England has drawn considerable attention to this method of extending the range of particle energies obtainable with a Van de Graaff accelerator. Because of this fact, a brief review of the principles of operation of these machines in their present and proposed forms may be in order.

The Tandem and other multi-stage Van de Graaff accelerators utilize the fact that hydrogen and a number of heavier elements can form negative ions in sufficient quantity such that useful beams of high energy particles can be obtained by acceleration involving a charge exchange process. Fig. 1 illustrates the operation of the Tandem or two stage accelerator. Negative ions are formed by passing positive ions through a low pressure gas. After analysis these ions are accelerated to a positive high voltage terminal at the center of the insulating column. Stripping occurs in this terminal and the resulting positive ions are accelerated a second time by the same terminal potential. For protons the maximum energy is $2\,eV$ where V is the terminal potential. For heavier ions, the total particle energy depends upon the charge

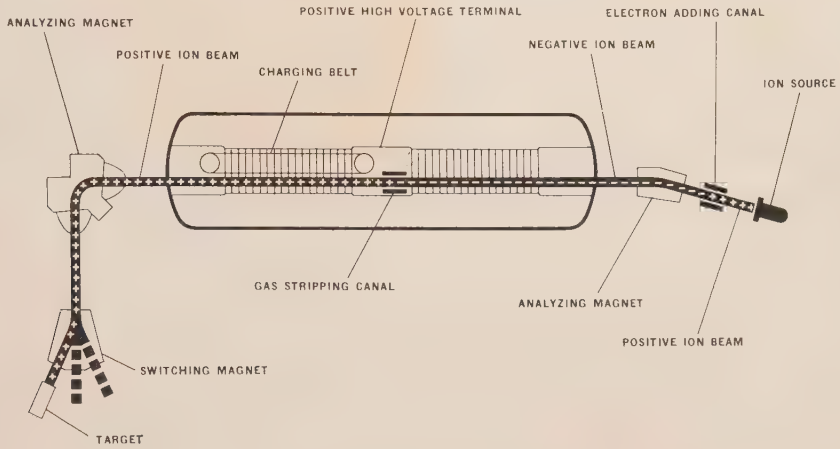

Fig. 1. The Two-Stage Tandem Van de Graaff Accelerators.

[3]) F. T. Howard, ORNL-2644.
[4]) W. H. Bennett, U.S. Patent No. 2, 206, 558 (1937).
[5]) L. W. Alvarez, Rev. Sci. Instr. **22** (1951) 705.

states involved. Though higher total particle energies can be obtained with the heavier ions, the maximum energy per nucleon, even with complete stripping, will always be less than with protons.

The Three-Stage Tandem illustrated in fig. 2 uses neutral particles produced in the same manner as the negative ions. In this case, analysis before neutralization ensures a monoenergetic beam of neural particles of the correct mass. A small magnet (not shown in the diagram) is used to remove charge particles from the neutral beam.

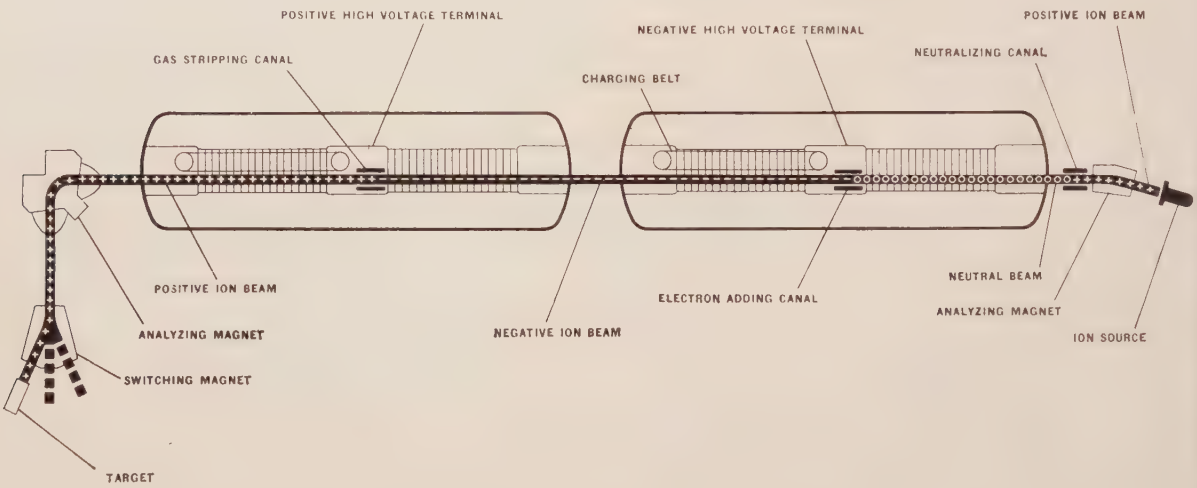

Fig. 2. The Three-Stage Tandem Van de Graaff Accelerator.

Negative ions are formed in the first (negative) terminal and accelerated through the potential difference between the first and the second (positive) terminals. After stripping in the second terminal the particles receive a third acceleration. Thus, the Three-Stage Tandem can achieve proton energies up to $3\,eV$ where V is the potential of each terminal and correspondingly higher energies with heavier ions.

This system can, in principle, be extended to provide a fourth stage of acceleration. To do this the accelerated positive ions from the output of the second section are fed back by means of magnets to the input of the first section. In a second acceleration tube parallel to that through which the neutral beam passes, these positive ions are accelerated to the negative terminal. However, this scheme poses rather serious problems in obtaining sufficient intensity, and requires that the target be inside the terminal which greatly limits the utility of such an arrangement.

It has been suggested that a proton linac could be used as an injector for a Tandem to provide the convenience and flexibility of the Van de Graaff type of accelerator at energies beyond the range of the Tandem itself. For example, using a 10 MeV linac as an injector for a 12 MeV Tandem would permit continuous variation of particle energy from 12 to 22 MeV.

Such an arrangement has two additional advantages. One is that the linac can be operated at optimum performance as a single energy accelerator, which it essentially is. The other advantage is that the current efficiency of the Tandem would be quite high, i.e.; since the injected beam would already be well collimated and at high energy a very large fraction of it would be accelerated further by the Tandem.

However, this combination of accelerators would still have many of the limitations of the linac. In particular the low duty cycle of the pulsed linacs together with the comparative inefficiency of the negative ion formation process would result in average beam intensities so low as to be of questionable utility. This suggested arrangement will be discussed further in the next section.

2. Present Status of Accelerator Development

2.1. POSITIVE ION LINACS

Outside of Russia there are eight proton linacs built or under construction in the world, five of which are single energy machines intended as injectors for proton synchrotrons[3]). All but one of the eight are designed for considerably higher proton energies than those considered here. The exception is also an injector operating at 10 MeV. There are also three heavy ion linacs capable of producing particles with energies up to about 10 MeV per nucleon. Thus, all six of the positive ion linacs, not intended as injectors for larger machines, are designed for considerably higher total particle energies than those considered here. No new positive ion linacs are presently being planned.

Proton linacs are essentially single energy machines and can operate at peak effectiveness over a very small energy range about the design energy[6,7]). They can be used in sections, and by certain tuning adjustments can be made to produce particles over a considerable energy range[8]). However, this is generally accomplished at the sacrifice of appreciable beam intensity and energy resolution which, at best, is considerably less than can be obtained with the Van de Graaff type of accelerator.

Linacs are capable of pulsed operation only, and, because of duty-cycle limitations on the rf power sources and the long accelerator cavity filling times required, low repetition rates (60 pps or less) and long pulse lengths (several hundred microseconds) are used. As a result, the maximum average beam currents obtained are fractions of a microampere.

These accelerators also have an energy spread of 10 to 100 times that obtainable with the Van de Graaff type and the average currents obtainable from a linac after definition to the same energy spread are two to three orders of magnitude less than those obtainable with a Tandem.

Heavy-ion linacs can accelerate a few heavier nuclei but only those with certain charge-to-mass ratios. These machines are subject to the same or more stringent limitations with regard to energy spread, variability and beam intensity as the proton linacs. Thus, positive-ion linacs in general are considerably less flexible and versatile than other types of accelerators.

However, any linear accelerator has one very great advantage over the circular types and that is in the angular definition which may be achieved with linear machines. Beam divergences in proton linacs and Van de Graaff accelerators are of the order of milliradians whereas those of the external beams from cyclotrons are the order of degrees. Precision low-angle scattering studies can be done best with linear machines, and, at energies above the range of the Three-Stage Tandem the positive-ion linac may be the most satisfactory accelerator for such studies.

In addition to those given above, there are other less-fundamental disadvantages of the positive-ion linac over the Tandem type of accelerator. These are factors such as the complexity and power requirements of the rf system, the prodigious size of the vacuum system, and the injector which is a separate accelerator in itself and requires that the source be at a high potential.

It also appears, from what little information is available, that the initial equipment and installation costs of a 20 MeV proton linac would not be significantly different from those of an AVF cyclotron or a Three-Stage Tandem producing the same proton energy[3]). A heavy ion linac would very likely have an even higher initial cost, and any comparable linac would be considerably more expensive to operate and maintain than a Three-Stage Tandem. In view of these considerations, it does not seem reasonable to propose the extensive use of positive-ion linear accelerators at energies available to the Van de Graaff type of accelerators.

The idea of using a linac as an injector to a Tandem was mentioned briefly in the last section. This could provide flexibility and convenience of energy variation at energies above the range of the Tandem. However, this

[6]) L. W. Alvarez *et al.*, Rev. Sci. Instr. **26** (1955) 111.
[7]) Bruce Cork, Rev. Sci. Instr. **26** (1955) 210.
[8]) E. A. Day *et al.*, Rev. Sci. Instr. **29** (1958) 457.

arrangement would still be subject to most of the limitations inherent in linacs discussed in this section. In particular, it would be limited to the use of a few different particles and would have the same energy resolution as the linac. The source would have to be at a high potential, which is a particular disadvantage in the case of the complex source equipment required to produce negative ions.

Perhaps the most serious limitation in this proposed combination of accelerators would be in the maximum beam currents that could be obtained. This limitation arises because of the low duty cycle and current efficiencies of the linac combined with the comparative inefficiency of the negative-ion forming process. On the basis of the best performance yet achieved by these machines, it is unlikely that peak currents of more than a few tenths of a microampere and average currents of more than a few thousandths of a microampere could be achieved with a linac-tandem combination of machines based on present designs. Considerable refinement of these designs could probably improve the output by not more than about one order of magnitude.

In the energy range of which it is capable, the Three-Stage Tandem appears to be a much more promising instrument than a linac-tandem combination. On the other hand, at energies beyond the range of the multi-stage Van de Graaff accelerators, the combined linac-tandem may eventually prove the most satisfactory method of conducting precision nuclear physics research. However, since the energy range under consideration here is essentially covered by the Tandem and Three Stage Tandem accelerators, further discussion will be limited to a comparison of this type of accelerator with the variable energy AVF cyclotron.

2.2. VARIABLE ENERGY FF-AVF CYCLOTRONS

It is now well established from work in the field that the FF-AVF Cyclotron, first proposed in the early papers of Thomas on focussing[2]), is the most promising version of the cyclotron yet devised. It is capable of producing considerably higher particle energies and beam intensities than other types of cyclotrons with the same magnetic field strength and pole diameter[3]). Further, this can be done with much lower Dee voltages and rf power[9]).

Operating as a fixed frequency machine, the AVF cyclotron does not require the complex modulation system of the FM or synchrocyclotron, and need not be pulsed (at other than the oscillator frequency), thereby providing many times the average current of these earlier machines. By the use of oscillator harmonics and various tuning schemes it appears possible to provide continuous energy variation over a considerable range as well as to accelerate particles with a variety of charge-to-mass ratios[10]).

However, these accelerators are still subject to many of the limitations characteristic of cyclotrons which have long made them considerably less satisfactory for precision measurements than electrostatic machines. Among these are the fact that only a fraction of the internal beam can be obtained outside the magnetic field. The energy spread in the external beam is the order of several percent, and beam divergences of several degrees are characteristic. Even after magnetic analysis the energy resolutions obtainable are no better than one part in 1000[3,11]). Analyzed beam currents are less than one percent of the internal currents so that more than 99% of the beam at full energy must be stopped by something other than the target. This creates considerable background and radiation hazard and requires extensive shielding. These factors limit the accuracy and sensitivity of the measurements which can be made using these accelerators as particle sources.

Energy variation is a complex procedure and the adjustments involved radically alter beam intensities. Sources must be small in size and located in strong magnetic fields. Only a limited

[9]) F. A. Heyn and Khoe Kong Tat, Rev. Sci. Instr. **29** (1958) 662.
[10]) The Oak Ridge Isochronous Cyclotron, ORNL-2648.
[11]) R. S. Bender *et al.*, Rev. Sci. Instr. **23** (1952) 542.

number of different particles having the appropriate charge-to-mass radio can be accelerated. These factors limit the versatility and flexibility of these sources of accelerated particles.

There are some eight AVF cyclotrons built or under construction in the world, about which information is available[3]). All but two of these are modifications of existing cyclotrons. One exception is a small test model[9]), and the other is designed to operate at particle energies considerably above 20 MeV. There are, in addition, eight more of these cyclotrons in the design or study phase and all of these are intended for operation at higher energies. Thus, the trend in new AVF cyclotron construction is toward machines intended to produce particles with energies well above 20 MeV.

2.3. TANDEM VAN DE GRAAFF ACCELERATORS

Tandem Van de Graaff accelerators have accelerated protons to nearly 14 MeV and heavier ions to higher energies, such as stripped oxygen nuclei up to 60 MeV total energy. Recent results in the acceleration of negative ions produced in the terminal by an accelerated neutral beam from the source have assured the success of the Three-Stage Tandem machine which should eventually produce protons with energies up to nearly 20 MeV. Studies are also underway to increase the maximum terminal voltage without appreciable modification of the present design. It is very likely that in the near future proton energies of 16 MeV with a Tandem and 24 MeV with a Three-Stage Tandem may be achieved.

Analyzed beam currents of several microamperes with an energy resolution of one part in 10 000 have been obtained. Beam divergences are of the order of a milliradian and beam diameters of a millimeter are not difficult to achieve. Since cyclotrons and positive-ion linacs at best produce analyzed currents somewhat smaller than those from a Tandem and have beam diameters of about a square centimeter, the Tandem can provide current densities at the target about two orders of magnitude greater than the other two types of accelerators. The following sections will compare the performance of the Tandem type of accelerator with the AVF cyclotron in more detail.

Twelve Tandem Van de Graaffs have now been ordered commercially. Some have been completed and others are in various stages of test or construction. It is known that a number of others are being planned for the near future. Two laboratory-built Tandems have recently been put into operation in England. In view of recent results obtained in a study of the Three-Stage Tandem principle, several organizations are seriously considering the acquisition of these larger machines. A number of Tandem purchasers have made or are making provision for the addition of a second section at some later time.

3. A Comparison of Multi-Stage Van de Graaff Accelerators with AVF Cyclotrons

3.1. PERFORMANCE CAPABILITIES

A. Particle Energies. Excluding the Four-Stage Tandem Van de Graaff (described in Section 1) because of its limited utility, the maximum proton energy obtainable in the near future with multi-stage Van de Graaff accelerators is probably between 20 and 25 MeV using a Three-Stage Tandem. It is conceivable that this upper limit could be extended to as high as 30 MeV by a major redesign of the present horizontal model. On the other hand, most new AVF cyclotrons being built or planned are intended to produce protons at somewhat higher energies.

In a cyclotron the maximum particle energy depends upon the charge-to-mass ratio of the accelerated particle. In an electrostatic accelerator, this energy depends only on the charge. Comparing cyclotrons and Three-Stage Tandems which give the same maximum proton energy, it is easy to show that the Tandem, by utilizing the appropriate charge state can always accelerate the heavier ions to higher total energies, and therefore greater energies per nucleon, than can the cyclotron. Or conversely, the energy per nucleon achievable with heavy ions in a Three-Stage Tandem can compare favorably with that

produced in a cyclotron capable of somewhat greater proton energies.

B. Particle Intensities: The limitations imposed on Tandem performance by the comparative inefficiency of the negative ion forming process have, in large measure, been compensated for by the very large currents obtainable with the recently developed Von Ardenne or Duoplasmatron ion sources[12]). Currents of more than a hundred milliamperes of positive ions have been produced by sources of this type; so that, at present, the limitations on the current obtainable with Tandem accelerators are in the ion optics, which, it is believed, can be improved considerably.

Analyzed beam currents of a few microamperes are readily attainable, and unanalyzed currents of 10 microamperes have been observed. It is expected that in the near future analyzed currents of the order of ten microamperes will be standard with the Tandem and somewhat smaller currents will be obtained with the Three-Stage Tandem. Refinements in ion optics are expected to improve the output somewhat. However, there is, at present, no apparent way in which the currents produced by these machines could be increased as much as an order of magnitude.

AVF cyclotrons can produce internal beam currents as high as one or two milliamperes[3]) and for experiments which can be performed using the internal beam, such as isotope or neutron production with an internal target, this is clearly the superior tool. However, it is seldom possible to obtain more than 20 to 30% of the internal beam outside the cyclotron and the beam emerges with an angular divergence of several degrees so that in a comparatively short distance the current is spread over considerable area[3,11]).

After the external beam has been focussed and further defined to improve the energy resolution the remaining current is of the order of a microampere with a density of a few microamperes per square centimeter[3,11]). Thus, only about 0.1% of the internal beam is available with good resolution at the target. The other 99.9% is at full energy and causes considerable background and radiation hazard as it strikes vacuum chamber walls and defining slits.

By comparison, the Tandem can produce currents of the order of several microamperes with most of the beam inside a spot about one millimeter in diameter. Thus, current densities are one or two orders of magnitude larger than what has been achieved with a well defined external beam from a cyclotron. Further, under normal operating conditions the total current accelerated to high energy by a Tandem is at most ten times the analyzed beam current at the target. Consequently, the background and radiation problems are much less serious.

C. Resolution: The energy spread in beams from Van de Graaff accelerators is determined almost entirely by the stability of the terminal voltage. Stabilities of less than $\pm$ one kilovolt have been demonstrated on the terminal of a Tandem, so that no more than $\pm$ three keV energy spread is to be expected in the beam from a Three-Stage Tandem. The stabilities quoted are for 95% of elapsed time with occasional manual adjustment of the stabilization system controls.

For a Three-Stage Tandem operating at 20 MeV, a $\pm$ three keV spread in energy represents $\pm$ 0.015% of the particle energy. The smallest energy spread yet reported for an analyzed external cyclotron beam is 0.10% of the maximum particle energy[3,13]). Beam currents remaining in this case were only a few tenths of a microampere or about 0.10% of the internal beam. Thus, the Tandem should be capable of an energy resolution about one order of magnitude smaller than has been obtained with analyzed cyclotron beams, and with this smaller resolution the Tandem should provide approximately ten times the beam current obtainable with the cyclotron.

D. Flexibility: A number of factors are involved in judging the applicability of these types of particle accelerators to a diversified

[12]) M. Von Ardenne: Tabellen der Electronenphysik, Ionenphysik und Ubermikroskopic (VEB, Deutscher Verlag der Wissenschaften, Berlin, 1956).

[13]) W. J. Henderson *et al.*, J. Frank Inst. **228** (1939) 563.

nuclear research program in the range of particle energies considered here. Some, such as particle energies, beam intensities, resolution, and radiation and background problems have been considered previously. Some additional factors, perhaps less fundamental but none-the-less significant in planning a research program, are outlined briefly in this section.

One of the more important characteritsics of an accelerator is the energy range over which it can operate. The larger Van de Graaff machines can function with excellent stability with terminal potentials of one million volts or less. This means that a Three-Stage Tandem can produce protons with continuously variable energy from three to 20 MeV. Further, this energy is variable with simple adjustments that do not affect the beam intensity.

The lower energy, variable energy cyclotrons on the other hand, can operate over energy ranges of only three or four-to-one for protons and generally smaller energy ranges for the heavier ions[3]). An elaborate machine has been proposed to provide considerably wider energy ranges by means of an rf system tuneable over a wide range[10]). This machine, which would also accelerate a wider variety of particles, is now under construction. In addition, adjustment of energy in a cyclotron is quite complex and affects radically the beam intensity. For a large range of energy variation and convenience in changing energy, the variable energy cyclotron is not to be compared with the Van de Graaff type of accelerator.

Table 1

Observed atomic negative ions (Taken from Ref. 14)

Period	Group							
	I	II	III	IV	V	VI	VII	VIII
1	H							He(1)
2	Li		B	C	(2)	O	F	
3	Na		Al		P	S	Cl	
4	K					Cr		
	Cu				As	Se	Br	
5	Rb							
	Ag				Sb	Te	I	
6	Cs							
	Au		Tl		Bi			

(1) He^- formed in an excited state.
(2) N^- presumed unstable, often looked for.

With regard to the variety of heavy ions which can be accelerated, each type of accelerator has one limitation and they both share a third. A Tandem is limited to those elements which can form negative ions. A cyclotron is limited to the use of particles having only certain charge-to- mass ratios. Both are limited by the efficiency with which a given charge state can be produced by stripping.

There are some 27 elements between hydrogen and bismuth that are known to form negative ions[14]). These are listed in Table I. It is expected that there are a great many more. Nitrogen apparently does not form negative ions. Helium in an excited state can form such ions but whether in sufficient quantity for use in a Tandem is still under study. The same may be true of the other noble gases, but this is also not known at present.

[14]) L. M. Branscomb, Advances in Electronics and Electron Physics **9** (The Academic Press, N.Y., 1957) 43.

Most variable energy cyclotrons intended for use with more than one particle have been used to accelerate only a few of the lighest nuclei such as protons, deuterons, tritons, helium three and alpha particles[3]). A very few machines are used to accelerate one or two heavier ions. A very elaborate machine now under construction is expected to accelerate ten different ions in the appropriate charges states and ranging from hydrogen to krypton in mass[10]).

Difficulties in producing a given charge state by stripping, which is a problem only for the heavier nuclei, may constitute limitations for both types of accelerators. In the Tandem the total particle energy depends directly on the charge state produced in the stripping canal. In the cyclotron these difficulties may limit the number of different ions which can be produced with the appropriate charge-to-mass ratio for use with the available oscillator frequencies and magnetic field combinations.

Although much is yet to be learned about which elements can form negative ions in sufficient number to be useful in a Tandem accelerator, and many variations of the AVF cyclotron concept are possible, it appears that at present the cyclotron is more limited as to the number of different particles it can accelerate than is the Tandem. The cyclotron, however, can achieve, for about the same cost as that of a Three-Stage Tandem, considerably higher particle energies and higher energies per nucleon, especially for the lighter nuclei among those particles which it can accelerate.

Another advantage of the Tandem type of accelerator, which is likely to become of increasing importance as research at these energies becomes more subtle and complex, is the fact that the source is external to the accelerator. This means that source equipment is not limited by factors involving size, heat dissipation or operation in strong electric or magnet fields so that considerably more elaborate equipment may be used.

In particular, a variety of pulsing schemes can be utilized. Auxiliary equipment is available commercially for providing pulsing in both the microsecond and millimicrosend range with Tandem accelerators. Also, it is now believed that polarized particles may be accelerated by the charge exchange process and maintain polarization. It is not likely that equipment to provide a source of polarized particles could be built into the terminal of a conventional Van de Graaff accelerator or be made to work effectively in the magnetic field of a cyclotron, even if there were space for it.

The fact that both source and terminal equipment are outside of the accelerator in a Tandem makes for much greater reliability and ease of maintenance. Because nearly all of the complex equipment and components can be maintained without removing the pressure tank or opening more than a portion of the vacuum system, the down time involved in maintenance should be greatly reduced. Further, since spare parts and components are available commercially, it is not necessary for the user to stock such equipment or maintain extensive shop facilities for its fabrication.

To summarize, it appears that the Tandem type of accelerator is a more versatile and reliable research machine than the cyclotron in terms of range of energy variation, simplicity of operation, variety of particles which can be accelerated, and ease of maintenance.

3.2. COSTS

A. Equipment: Since virtually all accelerators other than the Van de Graaff type have been built in universities and national laboratories in this country and no two are alike, estimates of the total initial equipment costs differ widely for machines operating in approximately the same energy range. As mentioned in the last section nearly all of the AVF cyclotrons, now being built to operate at proton energies less than 20 MeV, are modifications of existing cyclotrons, and all completely new machines are designed for higher energies. All these factors make price comparisons between cyclotrons and the Tandem Van de Graaffs difficult.

However, as near as can be determined from the incomplete information available the initial

equipment cost for a variable-energy AVF cyclotron to accelerate protons to 30 or 40 MeV is between one and two million dollars[3]). It would probably not be economical to build such an accelerator limited to appreciably lower energies.

The Three-Stage Tandem Van de Graaff is expected to produce protons with energies up to 20 MeV and possibly as high as 25 MeV. It is expected to sell for between $ 1.5 and $ 2.0 million. Thus, the two types of accelerators should have roughly the same initial equipment cost, and no good case can be made for either on the basis of this cost alone.

B. Building and Installation: Buildings, laboratories' facilities, and auxiliary equipment for accelerators operating in this energy range generally cost from 50% up to 100% of the cost of the machines themselves. Because of its considerable length (upwards of 100 feet) the Three-Stage Tandem requires considerably more space than the equivalent energy cyclotron.

However, the cost of the larger building area for a Three-Stage Tandem is somewhat offset by the cyclotrons requirement for much more shielding and auxiliary equipment necessary for precision work. At best only 10% to 20% of the internal beam current can be obtained outside the cyclotron vacuum chamber and generally less than one percent of the original beam remain after the definition required for optimum energy resolution[31,1]). The remainder of this current is at full energy and creates a sizeable radiation hazard and a major background problem as it strikes the defining slits and chamber walls. Elaborate and extensive shielding structures are required to protect personnel and to permit use of sensitive measuring equipment. The Tandem accelerators do not require such extensive shielding outside the target area. The overall building and installation costs for the two types of accelerators are not likely to differ greatly.

C. Operation and Maintenance: The cost of operating and maintaining a cyclotron is likely to be considerably greater than that for a Three-Stage Tandem. First, the cyclotron requires literally an order of magnitude more power. For example, a complete Three-Stage Tandem accelerator would have a maximum power consumption of less than 50 kW; whereas the rf and magnet systems alone of the Livermore variable energy cyclotron (15 MeV protons) use up to a maximum of 650 kW.

Another reason that the cyclotron is more costly to operate is that it is considerably more complex. Spare components and maintenance service are not available commercially. This means that a larger staff of more highly trained personnel as well as more elaborate shop facilities are necessary.

In the case of the Tandem machines, spare parts and major maintenance service are available from the manufacturer. Further, because of its simplicity of operation, highly trained technical personnel are not required to run the accelerator.

3.3. PROCUREMENT

Tandem Van de Graaff accelerators are available commercially with a delivery time of about 24 months from receipt of order. A Three-Stage Tandem would require perhaps six months longer. Both delivery times are expected to be shorter in the near future when new manufacturing facilities, now nearing completion, are put into operation. In addition, installation, maintenance service and spare components are available from the manufacturer.

For accelerators of this general magnitude constructed in and largely by university and other laboratories, the time from the beginning of the study phase to first operation is at least three and generally four years[3]). Further, such projects occupy, nearly full time, much of the research staff who could more effectively and would rather be conducting research with existing facilities.

This form of procurement tends to be considerably more costly to the institution involved than it generally appears. Since cost accounting is not so thorough as it has to be in a commercial organization, the institution frequently absorbs much overhead and many hidden costs such

that the total cost to the institution is very likely to be equal to or greater than the cost of the machine built commercially. All AVF cyclotrons built or under construction represent projects of this sort. This, plus the fact that all the machines are different, are reasons why there exists no good estimate for the cost of such machines.

No AVF cyclotron has yet been built commercially, although one is now on order from an European manufacturer. At this stage the delivery and performance of the first commercially built AVF cyclotron are uncertain. Thus, the Tandem type of accelerator is the only one now readily available commercially, and it almost certainly can be obtained sooner than any other type of accelerator can be built. This includes modifications of existing cyclotrons which appear to require two years or more[3]).

4. Summary

The three types of particle accelerators available today for nuclear physics research at energies below 20 MeV have been discussed and numbers of each type built, under construction, or planned, have been reviewed. Reasons have been given to show that the positive-ion linear accelerator is less satisfactory for such work than either the azimuthally varying field cyclotron or the Tandem Van de Graaff type of accelerator. The last two accelerators have been compared in some detail.

From this comparison it appears that the cyclotron has clearly only two advantages over the Tandem, and one of these is significant only for certain applications. The first of these is in the particle energy which may be obtained for a given cost. It appears possible to build an AVF cyclotron to produce 40 MeV protons for about the same cost as that of a 20 MeV Three-Stage Tandem. It would probably not be economical to construct a 20 MeV cyclotron for less than the cost of a Three-Stage Tandem. The saving would be principally in the magnet, which comprises only about 20% of the total cost, and it would be small.

The other advantage of the AVF cyclotron is that it can achieve internal beam currents far in excess of any currents that are reasonable to anticipate with a Tandem. For work where an internal cyclotron beam can be used and where currents as high as several hundred microamperes or a milliampere are required, the cyclotron is clearly the superior instrument.

For accelerators operating at energies below 20 MeV, neither type has significant advantages over the other in terms of initial equipment or installation costs. A Three-Stage Tandem can probably be obtained commercially sooner than an AVF cyclotron can be built or obtained commercially. It should also be significantly less expensive to operate and maintain. However, the major advantages of the Tandem over the AVF cyclotron are in its performance capabilities, versatility and reliability. To summarize these advantages:

1. Higher total energy and more energy per nucleon, with nuclei which can be highly ionized, than provided by an AVF cyclotron giving the same proton energy.

2. Up to ten times the total current and 100 times the current density obtainable with analyzed external beams from cyclotrons.

3. Energy spread one-tenth that obtained with cyclotrons.

4. Angular divergences 100 to 1000 times smaller than obtainable with circular machines.

5. Considerably wider range of energy variation.

6. Energy continuously variable without change in beam intensity.

7. A wider variety of ion masses and charge states may be used.

8. External source and terminal equipment permit greater flexibility, reliability and ease of maintenance.

9. Commercial availability of accelerators, spare components and installation and maintenance service.

10. Available sooner than any other type of accelerator.

To conclude, it seems apparent that for a program of nuclear physics research concerned chiefly with precision studies at energies of

20-MeV and lower, that the Three-Stage Tandem Van de Graaff accelerator is more suitable than a variable-energy AVF cyclotron.

The following institutions have built, purchased, or ordered Tandem Van de Graaff accelerators. All but the two British machines have been ordered commercially. Those institutions also having low-energy cyclotrons built or under construction are indicated by asterisks.

1. Argonne National Laboratory, Lemont*
2. Atomic Energy of Canada Ltd., Chalk River
3. Atomic Energy Research Establishment, Harwell
4. Associated Electrical Industries. Ltd., Aldermaston
5. Australian National University, Canberra*
6. California Institute of Technology, Pasadena
7. University of Copenhagen*
8. Eidgenossische Technische Hochschule, Zurich*
9. Florida State University, Tallahassee
10. University of Liverpool*
11. Oak Ridge National Laboratory*
12. Max Plank Institute, Heidelberg*
13. Rice Institute, Houston
14. University of Wisconsin, Madison.

Acknowledgement

For much information and many helpful discussions, the writer would like to express his appreciation to Professors Robert J. Van de Graaff and John G. Trump, Dr. Denis M. Robinson, Mr. E. Alfred Burrill, Mr. J. C. Nygard, Mr. A. John Gale, Dr. Peter Rose and Mr. Richard Connor.

NUCLEAR INSTRUMENTS AND METHODS 7 (1960) 350–354; NORTH-HOLLAND PUBLISHING CO.

ALPHA-PULSE ANALYSIS BY SCINTILLATION DETECTORS

G. BERTOLINI, A. M. DEL TURCO and G. RESTELLI

C.N.R.N., *Ispra, Italy*

Received 4 January 1960

The light output of CsI(Tl), NaI(Tl) and plastic crystals to alpha-particles of 4.68, 5.3, 5.8, 6.05 and 8.78 MeV was investigated and the resolutions for the 5.3 MeV line of Po^{210} were respectively found to be 4.5, 5 and 5.5%. The relative efficiency to alpha and beta particles and the pulse height as a function of the energy is given. The branching ratio $\alpha/(\alpha+\beta)$ of Th-C was determinated by the CsI(Tl) and found equal to 0.358 ± 0.003.

1. Introduction

Many authors[1–10]) have investigated the response of organic and inorganic phosphors to alpha-particles of different energies. Their results show generally a non-linearity[4,5,9,10]) at low energies of the particles, that is due to a saturation effect. (Scintillation efficiency decreased with increasing specific ionization.)

The purpose of this work has been to investigate the limits and the possibilities of CsI(Tl), NaI(Tl) and plastic scintillators as tools in alpha-spectroscopy, regardless to the general problem of the fluorescence.

2. Apparatus

The CsI(Tl) purchased from the Harshaw Chemical Co., 0.15 mm thick and 38 mm in diameter, was mounted on a lucite light pipe, 38 mm in diameter and 20 mm high.

The NaI(Tl) supplied also by Harshaw Chemical Co., 3 mm thick and 38 mm in diameter, was rubbed with Silicon Carbide paper N.500, carefully polished and mounted on a light-pipe like that of CsI(Tl). Obviously every operation on this phosphor was performed in a dry-box.

The plastic NE-102 purchased from the Nuclear Enterprises Ltd., 0.4 mm thick and 38 mm in diameter, was mounted on a light-pipe like that of CsI(Tl) and NaI(Tl).

Each phosphor was covered with aluminum-sheet of 0.23 mg/cm² and the surface sensitive to alpha-particles reduced to 0.8 cm² with a brass collimator. Correction has been made for the energy absorbed in the aluminum.

The output from the 6292 Dumont photomultiplier was fed into an amplifier clipped to 1.6 μsec and then to a 256-channel pulse-height analyzer.

The assembly is reported in fig. 1, where is shown the possibility of changing in vacuum the sources and the distance source-phosphor with an external knob. It is also possible to place another phototube for coincidence measurements. The chamber is evacuated to 100 μ with a rotary pump to prevent the absorption of alpha-particle energy and the moisture damage to the NaI(Tl) surface.

[1]) W. Franzen, R. W. Peelle and R. Sherr ,Phys. Rev. **79** (1950) 742.
[2]) S. A. Johansson, Arkiv Fys. **2** (1950) 171.
[3]) E. G. Michaelis, Helv. Phys. Acta **23** (1950) 155.
[4]) R. Lovberg, Phys. Rev. **84** (1951) 852.
[5]) C. N. Chou, Phys. Rev. **87** (1952) 903.
[6]) Beat Hahn, Phys. Rev. **91** (1953) 772.
[7]) S. K. Allison and H. Casson, Phys. Rev. **90** (1953) 879.
[8]) A. Galonsky, C. H. Johnson and C. D. Moak, Rev. Sci. Inst. **27** (1956) 58.
[9]) H. Albert, Phys. Rev. **107** (1957) 647.
[10]) S. Pashkin, R. R. Carlson, R. A. Douglas and J. A. Jacobs, Phys. Rev. **109** (1958) 434.

SOURCES

Four alpha-particles thin sources were used for this work:

Th^{230} †	prepared by vacuum sublima-
$E_\alpha = 4.68$ MeV	tion at 168° C of Th-acetil-
	acetonate
Po^{210}	prepared by electrolytic depo-
$E_\alpha = 5.3$ MeV	sition
Cm 244 ††	prepared by vacuum sublima-
$E_\alpha = 5.8$ MeV	tion of Cm nitrate
Bi^{212}, Po^{212}	obtained by collecting the decay
$E_\alpha = 6.05$ MeV	products of Rn^{220} on a stainless
$E_\alpha = 8.78$ MeV	steel disc, kept at a potential
	of — 350 V respect to a source
	of Th^{228} [11]).

† Supplied by the Chem. Div. of the A.E.R.E., Harwell.
†† Supplied by the Res. Chem. of the A.E.C.L., Chalk River.

[11]) F. E. Senftle, T. A. Farley and N. Lazar, Phys. Rev. **104** (1956) 1629.

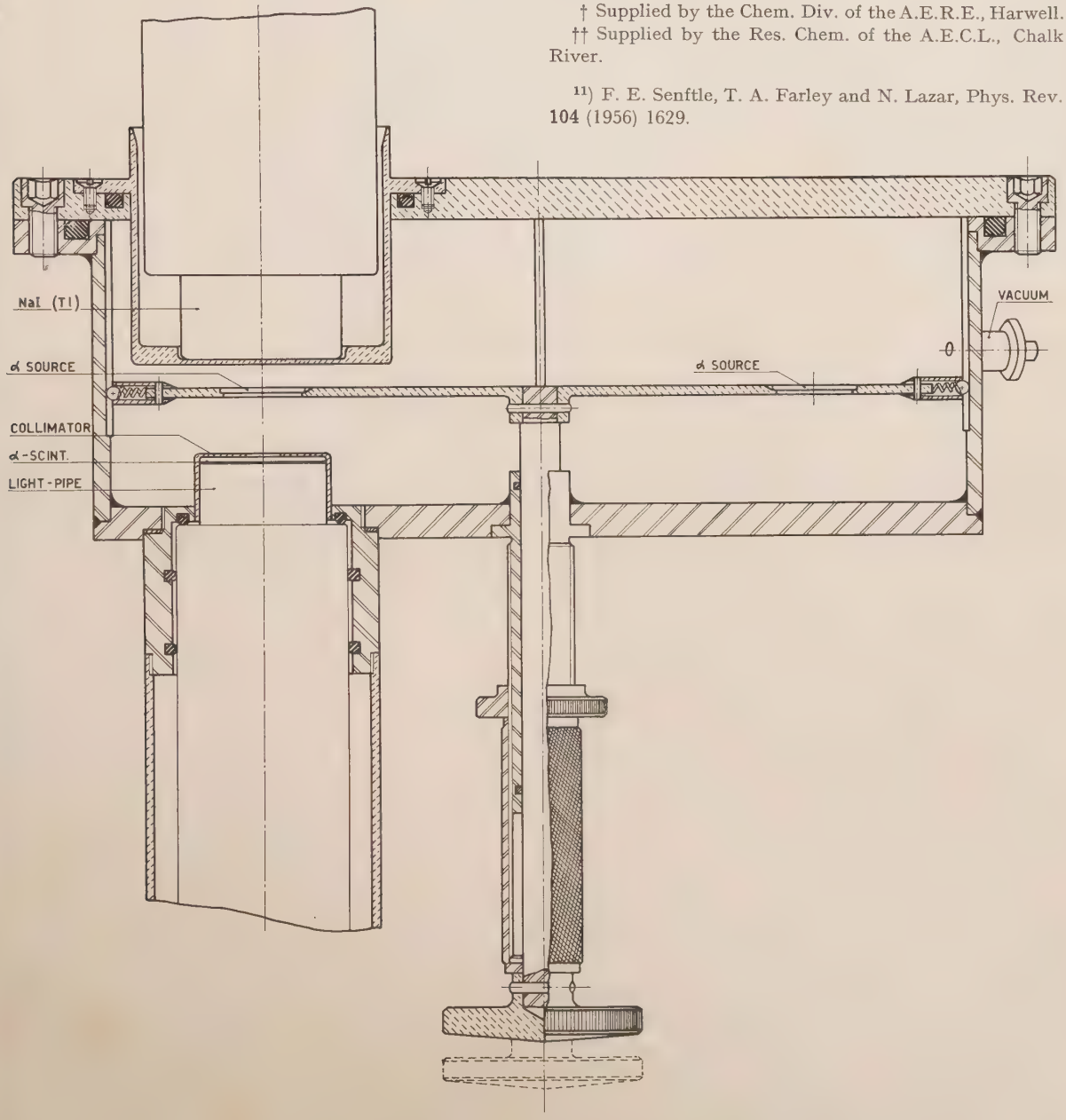

Fig. 1. Apparatus for α-detection.

3. Experimental Results

CsI(Tl)

This crystal seems for its mechanical and chemical characteristics, not brittle and non hygroscopic, and for its performances, suitable for alpha spectroscopy.

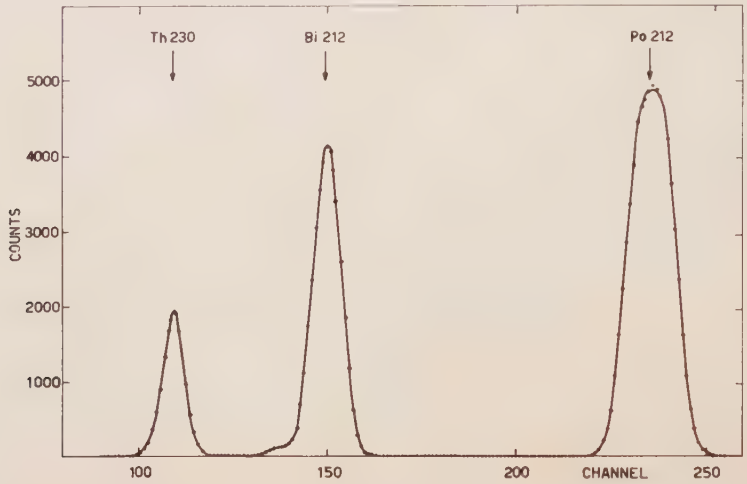

Fig. 2. α-spectra from CsI(Tl). Spectra from different sources (Th^{230} and $Bi^{212}Po^{212}$) have been superposed.

It is possible to obtain very thin sheets of this phosphor, that is very desirable for detection of alpha particles in presence of high beta and gamma background.

A typical pulse spectrum is shown in fig. 2.

The energy resolution is the higher of the three phosphors investigated and the best result for the 5.3 MeV alpha line of Po^{210} is 4.5% (defined as the full width at half maximum of the pulse height distribution expressed as the percentage of the pulse height associated with the peak of the distribution). CsI(Tl) shows a saturation effect but lower in proportion to NaI(Tl) and plastic phosphors.

The pulse-height/energy relation seems to have a good linearity in the range 4.5 MeV–9 MeV approximately, as from fig. 5. Relative efficiency, calculated from the light response to alpha and beta particles, has been measured comparing the pulse height of Po^{210} alpha-line and the 88 keV gamma-line of Cd^{109}. For this measurement it must be marked that the clipping time (1.6 μsec) of the amplifier takes into account only the shortest decay time (0.55 μsec) of the phosphor[12]), regardless to the long-lived phosphorescence decay time (220 sec)[13]).

The ratio E_α/E_β has been found equal to 0.8.

From this result it is apparent the reason why the alpha-lines of Bi^{212} and Po^{212} are far from the continuous pulse spectrum due to internal conversion and to beta-decay electrons.

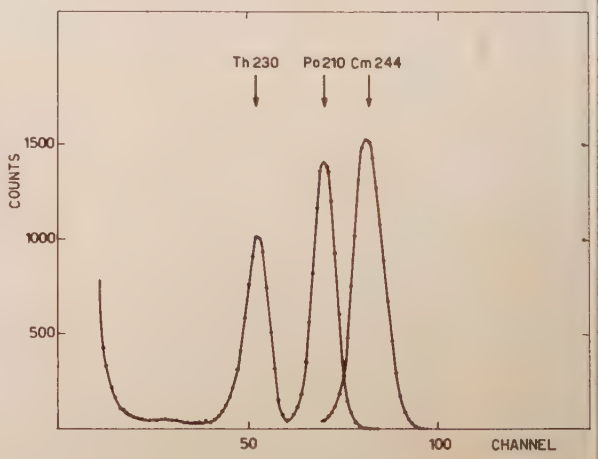

Fig. 3. α-spectra from NaI(Tl) of Th^{230}–Po^{210} and Cm^{244}

We have been allowed by this to perform a careful determination of the branching ratio $(\alpha/\alpha+\beta)$ of Bi^{212}, which has been found equal

[12]) Handbuch der Physik, Band 45, Sect. 11, 138.

[13]) Measurement reported in Handbuch der Physik, Band 45, Sect. 11, p. 138 from an unpublished work of J. E. Francis and P. R. Bell, O.R.N.L. Rep. 1975 (1955).

to 0.358 ± 0.003 in agreement, among the previous determinations[11,14,15]), with that of Senftle and Co-workers[11]).

energy, also plotted in fig. 5 shows non linearity, especially for the higher energy where a saturation effect is more evident.

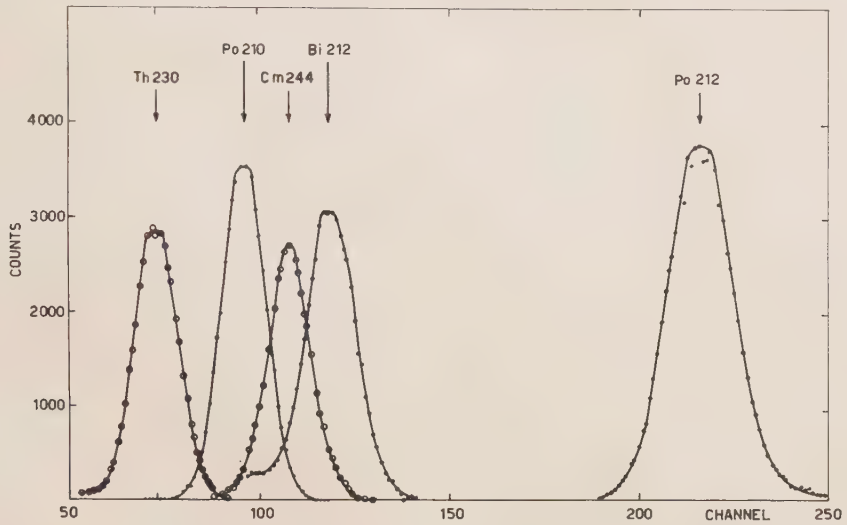

Fig. 4. α-spectra from NE-102 plastic scintillator.

NaI(Tl)

Although it has a shorter fluorescence decay time[12]) and higher light response to alpha particles than crystals of CsI(Tl), NaI(Tl) it is not very satisfactory for normal work.

In effect it is not possible to obtain very thin crystals. Furthermore their hygroscopicity makes its use more difficult because of the very critical state of its surface.

A rather good resolution is obtainable in pulse spectra as in fig. 3. For Po^{210} alpha-line 5.3 MeV, the energy resolution is 5%.

The pulse-height curve as a function of particle

The light output of this phosphor is the highest as from table 1, but the relative efficiency of the response to alpha and beta particles is lower than CsI(Tl) and equal to 0.5. This ratio has been measured comparing the pulse height of 5.3 MeV alpha-line of Po^{210} and 0.661 MeV gamma of Cs^{137}.

Table 1

Phosphor	NaI(Tl)	CsI(Tl)	Plastic NE-102 Nucl. Ent. Ltd.
Size	3 × 38 mm	0.12 × 38 mm	0.4 × 38 mm
Relative pulse height to α-particles	100	86	3.5
E_α/E_β	0.5	0.8	0.084†
Resolution Po^{210} 5.3 MeV α-line	5%	4.5%	5.5%
$h_{ThC}/h_{ThC'}$ h = pulse height	0.59	0.63	0.55

† Measurement performed with a plastic NE-102–2.56 cm in diameter and 1.26 cm thick.

PLASTIC

It is very difficult to draw a conclusion on plastic phosphors owing to the great deal of the phosphors of this type commercially available.

[14]) A. Kovarik and N. Adams, Phys. Rev. **34** (1938) 413.
[15]) D. Prosperi and S. Sciuti, Nuovo Cimento **4** (1958) 734.

The results are reliable for NE-102 supplied from the Nuclear Enterprises Ltd. employed in this work. A typical pulse spectrum is shown in fig. 4.

as alpha-particle detector. This suggests its use in alpha-gamma coincidence work, as detector replacing the ionization chamber. In effect this does not allow high counting rates, although it

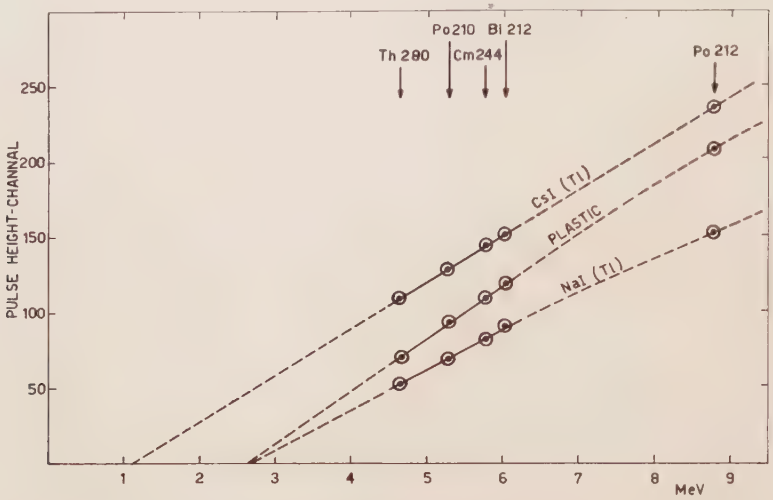

Fig. 5. Scintillation pulse height as a function of α-particles energy for CsI(Tl), NaI(Tl) and NE-102 plastic.

The resolution obtained is 5.5% for the 5.3 MeV alpha-line of Po^{210}. The energy/pulse-height curve shows nonlinearity in the range investigated (fig. 5). The relative efficiency to alpha and beta particles has been measured with a thicker plastic of the same type previously used, comparing the 5.3 MeV alpha-line of Po^{210} and the 624 keV electron conversion line of Ba^{137}.

The ratio E_α/E_β has been found equal to 0.084.

From the above results surveied in table 1 and fig. 5, it is possible to draw, in agreement with other workers, a good behaviour of CsI(Tl) has a resolution in energy far better than CsI(Tl).

Notwithstanding the ratio E_α/E_β equal to about 0.08, plastic scintillators can be useful when very high counting rates are necessary and for measurements of half-lives of excited levels in heavy elements.

Acknowledgements

The authors wish to thank Mr. C. B. Amphlett of the Chemistry Division A.E.R.E., Harwell for the supply of Th^{230} and Mr. Alec Eastwood of the Research Chemistry A.E.C.L. Chalk River for the Cm^{244} supplied.

AUTHOR INDEX

Akimov, Yu. K., V. I. Komarov, O. V. Savchenko and L. M. Soroko, The separating of particles according to their ionization value in several scintillation counters 37

Anderson, Carl E., Arthur R. Quinton, William J. Knox and Robert Long, Apparatus for the investigation of heavy ion induced reactions . . . 1

Andersson, G., G. Rudstam and T. Stenström, Recoil technique in cyclotron bombardments using powder targets 73

Bar-David, Israel, *see* A. F. Fischmann-Arbel

Barna, Arpad, J. Howard Marshall and Matthew Sands, A nanosecond coincidence circuit using transistors 124

Bellamy, E. H., W. R. Hogg and D. Miller, A thin liquid hydrogen or deuterium target 293

Benveniste, J., A. C. Mitchell, C. D. Schrader and J. H. Zenger, The problem of measuring the absolute yield of 14-MeV neutrons by means of an alpha counter 306

Bertolini, G., A. M. Del Turco and G. Restelli, Alpha-pulse analysis by scintillation detectors 350

Brownell, Gordon L., *see* William H. Ellett

Burge, Edward J., Further comments on errors in polarization measurements (Letter to the Editor) 221

Burke, Edward A. and Lester F. Lowe, Derivation of thermal neutron spectra from transmission data 193

Burman, Robert L. and Avivi I. Yavin, Multipurpose magnetic particle analyzer 101

Butler, J. W., Neutron-absorbing bricks made from CaB_6 201

Chaplin, G. B. B. and A. J. Cole, A linear gate of 10 to 100 mμsec duration 45

Chapman, K. R. and S. Gowariker, A convenient method of constructing accelerator sections 215

Cole, A. J., *see* G. B. B. Chaplin

De Croës, M., W. Parker and K. Sevier, Jr., Thin film thickness distribution by alpha absorption 160

De Croës, M., *see* W. Parker

Del Turco, A. M., *see* G. Bertolini

Deruytter, A., A 4π-fission detector 145

Doran, G. A., E. A. Finlay, H. R. Shaylor and M. M. Winn, Extraction of protons from the Birmingham 1000-MeV synchrotron 225

Dowell, J. D., W. R. Frisken, G. Martelli and B. Musgrave, The propane bubble chamber used with the Birmingham proton synchrotron 184

Dymanus, A., *see* F. P. G. Valckx

Edwards, D. N. and B. Rose, An extension of the transfer matrix method to a beam transport system containing a solenoid 135

Ellett, William H. and Gordon L. Brownell, A total absorption gamma ray spectrometer combining sodium iodide and plastic scintillators 56

Finlay, E. A., *see* G. A. Doran

Fischmann-Arbel, A. F. and Israel Bar-David, A method of linear pulse amplifier design 153

Forsén, S. and J. Rydberg, End-window proportional flow counter tube 204

Fowler, T. K. and W. M. Good, A theory on obtaining short bursts of ions from a beam of ions 245

Frahn, W. E., W. L. Rautenbach and L. Wåhlin, The electromagnetic isotope separator in Pretoria 253

Frisken, W. R., *see* J. D. Dowell

Froissart, Marcel et Raymond Stora, Dépolarisation d'un faisceau de protons polarisés dans un synchrotron 297

Fuchs, H. and K. H. Lindenberger, Loss of activity from betatron irradiated samples by diffusion (Letter to the Editor) 219

Good, W. M., *see* T. K. Fowler

Gooding, T. J. and H. G. Pugh, The response of plastic scintillators to high-energy particles 189

Gore, W. G., A multiple event analyser 320

Gorodetzky, S., R. Richert, R. Manquenouille et A. Knipper, Convertisseur temps-amplitude à pouvoir de résolution élevé 50

Gowariker, S., *see* K. R. Chapman

Grigoryev, E. P. and A. V. Zolotavin, The spectral sensibility of a magnetic gamma-spectrometer in a photoelectric method 289

Henneberke, G., An electron accelerator in pressurized tank for 3 mA at 1.5 MV direct voltage . 89

Hogg, W. R., *see* E. H. Bellamy

Hutchinson, G. W., R. Rubinstein and W. H. Wells, A transistorized ring scaler of resolving time 0.3 μs 167

Karlsson, Erik and Kai Siegbahn, A new design for a beta-ray spectrograph for relative measurements 113

Kesseler, G. und Ch. Schlier, Blasendichtemessungen in einer Diäthyläther-Blasenkammer 210

Knipper, A., *see* S. Gorodetzky

Knox, William J., *see* Carl E. Anderson

Komarov, V. I., *see* Yu. K. Akimov

Kuchela, K. S. and L. H. Peshori, Application of bidirectional Dekatron tubes in low level beta activity measurements by cancellation technique 180

Lindenberger, K. H., *see* H. Fuchs

Long, Robert, *see* Carl E. Anderson

Lotz, W. und A. Sittkus, Elektronische Geräte hoher Konstanz für die Registrierung der Nukleonenkomponente der kosmischen Strahlung 237

Lowe, Lester F., *see* Edward A. Burke

Manquenouille, R., *see* S. Gorodetzky
Marshall, J. Howard, *see* Arpad Barna
Martelli, G., *see* J. D. Dowell
McPherson, R., *see* H. W. Taylor
Miller, D., *see* E. H. Bellamy
Mitchell, A. C., *see* J. Benveniste
Mitrofanov, Nicolai and J. J. van Loef, Detection of neutron and photon induced fission by ZnS(Ag) mixed with uranium and thorium compounds 63
Mladjenović, Milorad, Recent developments of beta spectrometers 11
Musgrave, B., *see* J. D. Dowell

Newson, H. W. and R. M. Williamson, High resolution neutron spectroscopy 67
Niemann, Fred L., Low energy particle accelerators for precision nuclear physics research 338

Parker, W., M. de Croës and K. Sevier, Jr., Some methods in the preparation of radio-active materials for use in beta-spectroscopy 22
Parker, W., *see* M. de Croës
Peshori, L. H., *see* K. S. Kuchela
Pugh, H. G., *see* T. J. Gooding

Quinton, Arthur R., *see* Carl E. Anderson

Rautenbach, W. L., *see* W. E. Frahn
Restelli, G., *see* G. Bertolini
Richert, R., *see* S. Gorodetzky
Rose, B., *see* D. N. Edwards
Rozenstein, S., An anti-coincidence circuit for randomly delayed pulses 213
Rubinstein, R., *see* G. W. Hutchinson
Rudstam, G., *see* G. Andersson
Rydberg, J., *see* S. Forsén

Sands, Matthew, *see* Arpad Barna
Savchenko, O. V., *see* Yu. K. Akimov
Schlier, Ch., *see* G. Kesseler
Schrader, C. D., *see* J. Benveniste
Septier, Albert, Lentilles quadrupolaires sans fer à gradient constant (Letter to the Editor) 217
Sevier, Jr., K., *see* M. de Croës
Sevier, Jr., K., *see* W. Parker
Shaylor, H. R., *see* G. A. Doran
Sicard, F., Analyse d'impulsions en régime statistique 207
Siegbahn, Kai, *see* Erik Karlsson
Sittkus, A., *see* W. Lotz
Sjögren, Bo, Combination of magnetic analyzers in nuclear reaction experiments 76
Sjögren, Bo, Cyclotron instrumentation for nuclear reaction studies by magnetic analysis 274
Soroko, L. M., *see* Yu. K. Akimov
Stenström, T., *see* G. Andersson
Stora, Raymond, *see* Marcel Froissart

Taylor, H. W. and R. McPherson, On the automatic control of scintillation spectrometers 315

Valckx, F. P. G. and A. Dymanus, A fast linear gate circuit 197
Van Loef, J. J., *see* Nicolai Mitrofanov
Vincent, C. H., A highly accurate continuously variable frequency control system 325

Wåhlin, L., Improvements of the collector system for a laboratory isotope separator 269
Wåhlin, L., *see* W. E. Frahn
Waters, J. R., A "time expander" for precision neutron time-of-flight experimentation 174
Wells, W. H., *see* G. W. Hutchinson
Williamson, R. M., *see* H. W. Newson
Winn, M. M., *see* G. A. Doran

Yavin, Avivi I., *see* Robert L. Burman

Zenger, J. H., *see* J. Benveniste
Zolotavin, A. V., *see* E. P. Grigoryev

BOOK REVIEWS

Goldstein, Herbert, Fundamental aspects of reactor shielding (E. K. Sokolowski) 99
Proceedings of the international symposium on nuclear electronics Part I Nuclear Electronics (P. A. Tove) 99
Directory of nuclear reactors. Vol. II: Research, test and experimental reactors (E. K. Sokolowski) 100
Who's who in atoms. 1960. An international reference book (Olov Bergman) 223
Sharpe, J., Nuclear radiation measurement (Ingrid Olsson) 223

SUBJECT INDEX

Accelerators and Reactors

Recoil technique in cyclotron bombardments using powder targets, G. Andersson, G. Rudstam and T. Stenström 73
Combination of magnetic analyzers in nuclear reaction experiments, Bo Sjögren 76
An electron accelerator in pressurized tank for 3 mA at 1.5 MV direct voltage, G. Henneberke 89
A convenient method of constructing accelerator sections, K. R. Chapman and S. Gowariker 215
Extraction of protons from the Birmingham 1000-MeV synchrotron, G. A. Doran, E. A. Finlay, H. R. Shaylor and M. M. Winn 225
The electromagnetic isotope separator in Pretoria, W. E. Frahn, W. L. Rautenbach and L. Wåhlin 253
Improvements of the collector system for a laboratory isotope separator, L. Wåhlin 269
Cyclotron instrumentation for nuclear reaction studies by magnetic analysis, Bo Sjögren 274
Dépolarisation d'un faisceau de protons polarisés dans un synchrotron, Marcel Froissart et Raymond Stora 297
Low energy particle accelerators for precision nuclear physics research, Fred L. Niemann 338

Detectors

Detection of neutron and photon induced fission by ZnS(Ag) mixed with uranium and thorium compounds, Nicolai Mitrofanov and J. J. Van Loef 63
A 4π-fission detector, A. Deruytter 145
The propane bubble chamber used with the Birmingham proton synchrotron, J. D. Dowell, W. R. Frisken, G. Martelli and B. Musgrave 184
The response of plastic scintillators to high-energy particles, T. J. Gooding and H. G. Pugh 189
Neutron-absorbing bricks made from CaB_6, J. W. Butler 201
End-window proportional flow counter tube, S. Forsén and J. Rydberg 204
Blasendichtemessungen in einer Diäthyläther-Blasenkammer, G. Kesseler und Ch. Schlier 210
The problem of measuring the absolute yield of 14-MeV neutrons by means of an alpha counter, J. Benveniste, A. C. Mitchell, C. D. Schrader and J. H. Zenger 306

Errata

J. A. Dattilo and J. van Bladel, Fields in gap-excited circular ducts (Nuclear Instruments 6 (1960) p. 283) . . 224
K. A. Dolmatova and V. M. Kelman, A longitudinal β-spectrometer with compensated spherical aberration (Nuclear Instruments 5 (1959) p. 269–279 224

Instruments and Methods for Nuclear Spectroscopy

Apparatus for the investigation of heavy ion induced reactions, Carl E. Anderson, Arthur R. Quinton, William J. Knox and Robert Long 1
Recent developments of beta spectrometers, Milorad Mladjenović 11
Some methods in the preparation of radio-active materials for use in beta-spectroscopy, W. Parker, M. De Croës and K. Sevier, Jr. 22
A total absorption gamma ray spectrometer combining sodium iodide and plastic scintillators, William H. Ellett and Gordon L. Brownell 56
High resolution neutron spectroscopy, H. W. Newson and R. M. Williamson 67
Multi-purpose magnetic particle analyzer, Robert L. Burman and Avivi I. Yavin. 101
A new design for a beta-ray spectrograph for relative measurements, Erik Karlsson and Kai Siegbahn 113
An extension of the transfer matrix method to a beam transport system containing a solenoid, D. N. Edwards and B. Rose 135
Thin film thickness distribution by alpha absorption, M. De Croës, W. Parker and K. Sevier, Jr. 160

A "time expander" for precision neutron time-of-flight experimentation, J. R. Waters 174
Derivation of thermal neutron spectra from transmission data, Edward A. Burke and Lester F. Lowe 193
The spectral sensibility of a magnetic gamma-spectrometer in a photoelectric method, E. P. Grigoryev and A. V. Zolotavin 289
A thin liquid hydrogen or deuterium target, E. H. Bellamy, W. R. Hogg and D. Miller 293
Alpha-pulse analysis by scintillation detectors, G. Bertolini, A. M. Del Turco and G. Restelli 350

Instruments and Methods for High Energy Physics

The separating of particles according to their ionization value in several scintillation counters, Yu K. Akimov, V. I. Komarov, O. V. Savchenko and L. M. Soroko 37
A theory on obtaining short bursts of ions from a beam of ions, T. K. Fowler and W. M. Good 245

Letters to the Editor

Lentilles quadrupolaires sans fer à gradient constant, Albert Septier 217
Loss of activity from betatron irradiated samples by diffusion, H. Fuchs and K. H. Lindenberger 219
Further comments on errors in polarization measurements, Edward J. Burge 221

Nuclear Electronics

A linear gate of 10 to 100 mμsec duration, G. B. B. Chaplin and A. J. Cole 45
Convertisseur temps-amplitude à pouvoir de résolution élevé, S. Gorodetzky, R. Richert, R. Manquenouille et A. Knipper 50
A nanosecond coincidence circuit using transistors, Arpad Barna, J. Howard Marshall and Matthew Sands . . 124
A method of linear pulse amplifier design, A. F. Fischmann-Arbel and Israel Bar-David 153
A transistorized ring scaler of resolving time 0.3 μs, G. W. Hutchinson, R. Rubinstein and W. H. Wells 167
Application of bidirectional Dekatron tubes in low level beta activity measurements by cancellation technique, K. S. Kuchela and L. H. Peshori 179
A fast linear gate circuit, F. P. G. Valckx and A. Dymanus 197
Analyse d'impulsions en régime statistique, F. Sicard 207
An anti-coincidence circuit for randomly delayed pulses, S. Rozenstein 213
Elektronische Geräte hoher Konstanz für die Registrierung der Nukleonenkomponente der kosmischen Strahlung, W. Lotz und A. Sitikus 237
On the automatic control of scintillation spectrometers, H. W. Taylor and R. McPherson 315
A multiple event analyser, W. G. Gore 320
A highly accurate continuously variable frequency control system, C. H. Vincent 325

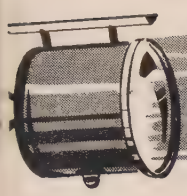

Spotlight on Industry

This section appears each month and features various happenings of interest in the nuclear industrial world and objective information on products of the nuclear manufacturers. It is offered entirely as a service and all nuclear manufacturers are cordially invited to submit clearly objective and descriptive material on their endeavours and product developments for consideration for use in this section.

LOW LEVEL COUNTING FACILITY

Nuclear Enterprises,
Bankhead Medway, Sighthill,
Edinburgh, 11, Scotland

For measurement of very low levels of radioactivity in large samples and assessment of lean content of animals the low level counting facility NE 8015 is announced.

Performance

1. Energy resolution (half width at half height) for the Potassium-40 1.46 MeV gamma ray is 27% with optimum photomultiplier balancing. This figure refers to the multiple scattering peak at the edge of the Compton distribution.

2. The detection sensitivity (3 times standard deviations) of any radioisotope emitting gamma rays in the energy range 0.5—2.0 MeV is 500 micromicrocuries per 60 lb. sample in a 1 minute count of sample activity and of background, or 50 micromicrocuries in a 20 minute count.

3. Detection efficiency of Potassium-40 gamma rays in potassium channel (10 volts wide) is 25% for a standard small source.

4. Detection efficiency of Caesium-137 gamma rays in caesium channel (5 volts wide) is 22% for a standard small source.

5. Less than 1% of activity in Potassium-40 channel is due to equivalent amount of Caesium-137 activity.

6. Potassium content of 60 lb. meat sample can be measured to 5% standard deviation in 40 seconds or 1% standard deviation in 15 minutes counting of sample.

7. Variation of count rate with position of small standard sample is less than 10% over length of chamber.

8. Self-absorption factor of sample can be calibrated with a sugar phantom. Typically, the decrease in count rate for animal tissue is about 10% when the sample weight is increased from 20 lb. to 60 lb.

9. Complete equipment can operate from a mains input of 110 or 210 to 250 volts, 50 to 60 cycles per second.

Specifications

Control unit:

Amplifier NE 5202: Non-overloading Fairstein double differentiated amplifier with gain 50 000. (See Bulletin 14.)

Single Channel Discriminator NE 5102(B): Both integral and differential facilities. Pulse heights 3 to 100 volts. Gate width 0 to 20 volts continuously variable. (See Bulletin 18).

Single Channel Discriminator NE 5103: As above, but with independent power supply.

E.H.T. Supply NE 5302: 500 to 1500 volts continuously variable output with stability of 0.01%. (See Bulletin 16.)

Mains Voltage Stabiliser 1000S: Sorenson—supplying A.C to all units. Scalers—(2) PW 4032: Phillips—suitable for counting positive and negative pulses. Maximum total count 400 000. Five decade counting tubes.

Pre-set Count Units (2) PW 4052: Phillips–automatic timing of five preset count values. Pulses may be positive or negative. Clock is spring driven thus independent of mains frequency.

Photomultiplier Adjusting Panel NE 6101: Each photomultiplier independently adjustable for optimum resolution.

Rack: Twin cabinet with two VentAxia cooling fans.

Cabling: All necessary cable interconnections and mains supply leads.

Overall Dimensions: 48 ins. long by 60 ins. high by 25 ins. wide.

Detector unit:

Lead Shield: Minimum thickness $3\frac{1}{2}$ ins.

Plastic Phosphors NE 102: Four quadrant sections—$23\frac{5}{8}$ ins. long; inner radius $7\frac{3}{16}$ ins.; outer radius $12\frac{5}{16}$ ins.

Photomultiplier-Preamplifier Units (8): E.M.I. Type 9530 A (Specially selected for high resolution). White cathode follower pre-amplifiers.

Pre-Amplifier Power Supply and Adding Circuit NE 6102: Stabilised H.T. supply for Pre-amplifiers. Circuit for adding pre-amplifier signals giving one signal out.

Stainless Steel Cradle and Drive Mechanism: Accepts samples up to $12\frac{3}{8}$ ins. dia. by $21\frac{1}{4}$ ins. long. Rate of travel 75 ins./minute; duration of travel approximately 20 seconds. Twin push-button operation for safety.

Overall dimensions: 74 ins. long by $66\frac{1}{2}$ ins. high by 45 ins. wide.

Weight of Complete Equipment: Approximately 6 tons.

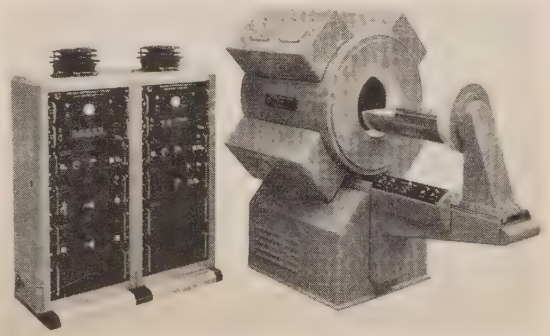

FIVE-OUNCE TRANSISTOR GEIGER COUNTER

Gelman Instrument Company of Chelsea Michigan, U.S.A.

A very small warming-giving Gelman-Wallace "Sparrow" is announced with the following specifications:

Dimensions: 4.96″ × 1.89″ × 0.94″
Weight: 5.302 ounces with batteries
Power: 2 self-contained 1.5 volt flashlight batteries 0.6″ × 2″

Energy Response:
0.1–2 MeV gamma sensitivity
Background: 20 counts/minute
0.1 mR/hr: 2 counts/second
1 mR/hr: violent crackle
10 mR/hr: smooth buzz 150 cycles/sec.
100 mR/hr: high whine 500 cycles/sec.

SUB-CRITICAL REACTOR WITH PULSED NEUTRON GENERATOR

Miles Hivolt Ltd., Shoreham Airport, Sussex, England

SUB-CRITICAL REACTOR TYPE BU 10. SPECIFICATION

Fuel: Natural uranium bars $43\frac{1}{4}$″ long, 1.22″ diameter, encased in plain aluminium cans 0.04″ thick.

The full loading of fuel consists of 324 bars giving a total mass of about 5 tonnes (11 000 lbs.). Smaller amounts can, of course, be used in reflected assemblies.

Moderator: Light water of high purity, supplied by demineralising plant which is part of the main equipment. The high purity is required to avoid corrosion.

Reflector: Two water-tanks made of stainless steel are supplied. One, 44″ × $34\frac{1}{2}$″ × $36\frac{1}{2}$″ high, fits closely around the lattice to give essentially an unreflected system. The second, 60″ × 54″ × 51″ high, provides a minimum of 8 inches of water on the sides of the lattice: the amount above and below depends on the lattice position selected but need not be less than 6 inches.

The smaller tank holds 200 gallons (2000 lbs.) of water and the larger one 650 gallons (6500 lbs.) without uranium being present. The full loading of uranium is equivalent to 68 gallons.

Lattice: The uranium bars are supported horizontally by an aluminium lattice plate at each end to form a square lattice of pitch 1.9″. The pitch is constant over the whole lattice plate to an accuracy better than 0.005″. Different lattice pitches can be obtained by using different plates.

Lattice Support Structure: The lattice plates are suspended from a gantry structure, to remove any problems of buckling, and spacing pieces enable the whole lattice structure to be placed at any of the three heights associated with the different positions of the source tube in the lattice.

Neutron source: A source tube 1″ in diameter passes horizontally through the system and is coupled to a deuteron accelerator. The deuteride or tritide target for neutron production can be placed at any position in the tube. Holes in the tank and the lattice plate allow four possible positions for the source tube. An accelerator source of neutrons enables measurements to be made with both constant and time-dependent fluxes. Radioactive sources can be used for constant flux measurements and the system can be used for orthodox exponential experiments by having sources in graphite placed outside the lattice.

Neutron Detectors: For constant fluxes, foils or electrical detectors (BF_3 counters, scintillation counters) can be used, but for time-dependent measurements the electrical detectors only can be used. A traversing head is supplied for accurate location of the detector at any point in the moderator.

Keff and Neutron Multiplication: For the lattice arrangement quoted, and with a full loading of uranium, k_{eff} for the unreflected case is about 0.88 and hence the neutron multiplication is about 8. With the reflected assembly the values are approximately 0.9 and 10.

PLASTIC SCINTILLATION FLUORS

Semi-Elements Inc., Saxonburg Boulevard Saxonburg, Pa., U.S.A.

The Single Crystal Division of Semi-Elements, Inc. has entered full scale production and announces that it is successful in polarizing and producing the largest Plastic Scintillation Fluors ever made. The Plastic Scintillation Fluors, before machined, weigh approximately 400 lbs., it is possible to get 16″ or more in diameter out of them and 24″ in length. Due to the size of these Scintillation Fluors, Semi-Elements, Inc. are selling the casting in the rough. It is now possible that more efficient human body count can be performed with this and also for high energy radiation detection.

DATE DUE

GAYLORD

PRINTED IN U.S.A.